Studies on reusabilities of cold-formed steel square hollow section columns after fire
(冷間成形角形鋼管柱の火害後再利用性能に関する研究)

Kai Ye
(葉　凱)

Doctor of Engineering
Graduate School of Environmental Studies, Nagoya University
（名古屋大学大学院環境学研究科　博士（工学））

2022

Contents

Chapter 1. Introduction

1.1 Research background

In recent years, a new concept referred to as a sustainable and resilient society has become increasingly significant. In the field of civil engineering, the reuse of steel structure after fire accidents is an important topic; the research on which, however, is still in the early stages. In Japan, according to the Recommendations for the Diagnosis and Repair Methods of Fire-damaged Buildings [1.1], the reuse of steel structures after fire is based on empirical judgment, because there is insufficient scientific data on it. As a result, it is very difficult to judge whether the steel structures could be reused and how to reuse them after fire. Especially, in Japan, not only the basic structural capacity (useable, strength, and beauty) but also the seismic-resistance capacity needs to be considered when a steel structure is reused after fire. Therefore, it is more important to judge whether a steel structure could be reused after fire based on the scientific data of its structural capacity after fire.

In this research, the reusabilities of the cold-formed steel square hollow section column, which is generally used in the steel structures, was investigated. Fig.1.1 shows a steel building, and Fig.1.2 shows the details of a steel-structure column. As shown in Fig.1.2, both the steel welded connections and the cold-formed steel square hollow section constitute the column. To comprehensively study the reusability of a steel-structure column after fire, both the welded connections and cold-formed steel square hollow section column need to be considered, on the basis of a comprehensive experimental investigation of the column after fire, including the material properties of both welded connections and cold-formed steel square hollow section members as well as the post-fire mechanical properties of the cold-formed steel square hollow section column. In the view of material properties, a Charpy impact test was employed to study the fracture performance, on the contrary, for mechanical properties, a coupon tensile test, an axially loaded compressive test and a stub-column test were employed. Furthermore, a residual displacement prediction equation of the cold-formed steel square hollow section column after fire based on the structural mechanics was proposed, considering the safety of fire damage diagnosis and repair work for reuse.

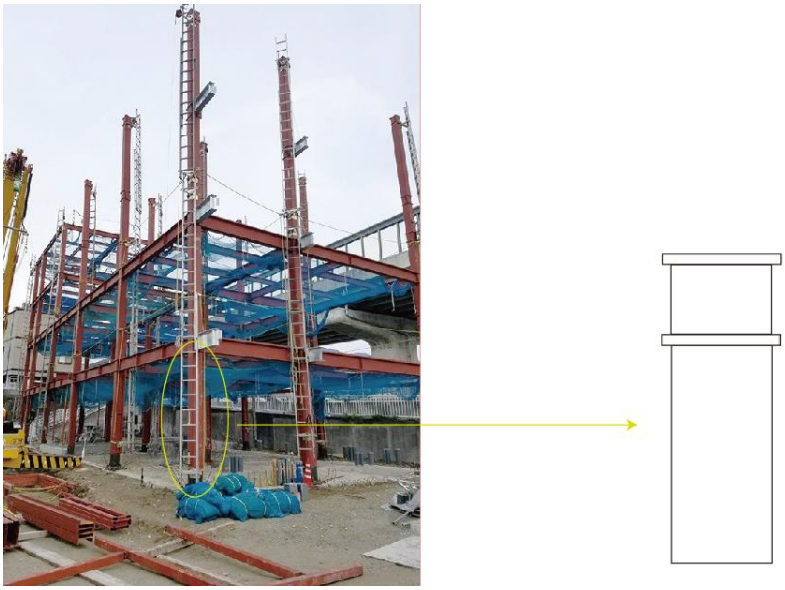

Figure 1.1 A steel structure and its column

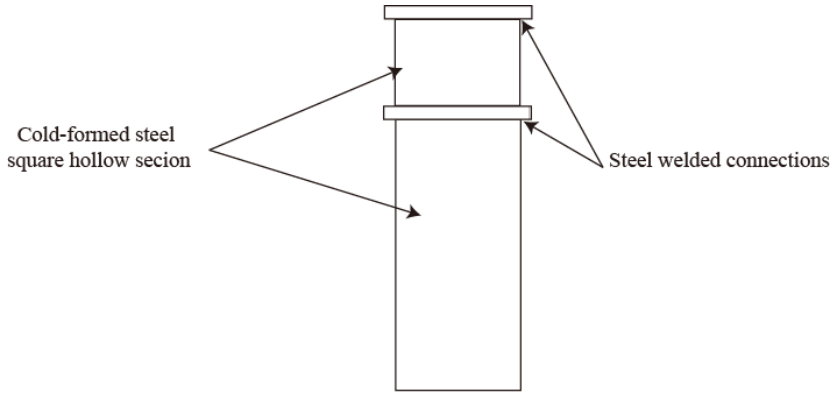

Figure 1.2 Composition of a steel structure column

1.2 Studies and the previous researches

1.2.1 Charpy impact test on steel welded connections after fire

Many welded connections in steel buildings have exhibited brittle fractures at the welded connections after brittle cracks are developed during severe earthquakes, such as the Kobe earthquake in 1995 and Northridge Earthquake in 1994 [1.2-1.4]. When cold-formed steel square hollow section column was reused as the seismic-resistance members after fire, it needs to study the reusabilities of both the steel welded connections and cold-formed steel square hollow section. Much work has been conducted to examine the post-fire mechanical behavior of steel members. Nikolaou et al. [1.5] investigated the mechanical properties of 500MPa class weldable steel after heating. This research suggests that the fracture toughness and mechanical properties of steel members might be altered after fire. Azhari et al. [1.6] studied the post-fire properties of the UHSS (grade 1200), HSS (grade 800) and MS (grade 350) steel, and indicated that their

tensile strength would be altered by the maximum heating temperature and cooling rate. Additionally, Hirohata et al. [1.7] investigated the Charpy impact energy of steel members in bridges cooled after fire. The test specimens were heated to 600 and 900 ºC, and cooled by quenching with water and leaving at the ambient temperature, respectively. After this, a Charpy impact test was carried out at the ambient temperature and it was reported that the quenched specimens possessed a very low Charpy impact energy. In addition, Koufu et al. [1.8, 1.9] investigated the Charpy impact energy of three steel grades: Japan Industrial Standard (JIS) SN400B (standard value of yield point at the ambient temperature, Fy = 235 MPa and tensile strength at the ambient temperature, Fu = 400 MPa), JIS SA440B (Fy = 400 MPa and Fu = 590 MPa), and JIS SN490B (Fy = 325 MPa and Fu = 590 MPa). The specimens were heated to 500 and 800 ºC, then cooled by quenching with water. Charpy impact tests conducted on these specimens under 60, 0, −30, and −60 ºC. These results showed that the quenched specimens had a lower Charpy impact energy compared to the untreated specimens. However, the post-fire fracture performance of steel welded connections after the heating and cooling processes has not been investigated.

Furthermore, in fire resistance, it is assumed that brittle fractures are not developed in steel members and their connections when subjected to fire because the fracture toughness increase with the temperature. The capacity of steel welded connections at elevated temperature is studied in many works, such as [1.10-1.12]. On the other hand, according to the previous experimental research on real-scale steel welded connections at elevated temperature, it has been reported that brittle fractures occur in the heat-affected zones of beam-to-column welded connections when they were heated to 400 ºC [1.13]. In addition, steel exhibits a "blue brittleness phenomenon" under the temperature range of 100–300 ºC, and the total elongation under this range is smaller than that at the ambient temperature [1.14]. Therefore, the possibility of brittle fractures must be investigated for steel members at relatively low fire temperature, including the blue brittleness temperature. The possibility of brittle fracture in steel members and welded connections is verified in some studies such as [1.15-1.17]. However, the grades of the steel in the abovementioned research are not the generally steel used as structural members of steel buildings and the welded connections subjected to fire are also not considered in these studies. Therefore, except for the brittleness fracture capacities investigation for the steel welded connections after fire, it also needs to measure the brittleness fracture capacities of the steel welded connections at elevated temperature.

In Chapter 2, three specimens were quarried out for the steel welded connections, they a base metal, welding materials, and heat-affected zone. To investigate the fracture properties of the steel welded connections after fire, specimens were treated by quenching with water and air-cooling in a furnace, and a Charpy impact test was conducted at the ambient temperature and a low temperature below 0 ºC. Furthermore, the fracture properties of steel welded connections at elevated temperatures, including the blue brittleness temperature, were also investigated by the Charpy impact test; because there is no data of the Charpy impact energies of the steel welded connection member at elevated temperature.

1.2.2 Charpy impact test on cold-formed steel square hollow section after fire

Cold-formed steel hollow section members are widely applied to steel buildings because they have many advantages, such as cost efficiency, high strength, and high torsional stiffness and strength [1.18]. However, owing to the cold-formed manufacturing process, including the roll-forming, seam welding, and sizing in an ambient temperature environment, large residual stresses and plastic strains remain in the cross sections [1.19]. Considering the reusability of cold-formed steel square hollow section used as a seismic-resistance member, it is also very important to verify the possibility of brittle fractures after fire, because steel square hollow section column subjected to the strong plastic processing during cold-formed manufacturing. However, there is no existing study investigating the possibility.

Many studies have also been conducted on the material properties of cold-formed steel hollow section members at elevated temperatures, such as [1.20-1.22]. However, the possibility of a brittle fracture must also be investigated on a steel member at a relatively low fire temperatures, including the blue brittleness temperature.

In Chapter 3, the fracture energy of the cold-formed steel square hollow section during and after fires has been experimentally investigated through a Charpy V-notch impact test. Regarding the previous research on Charpy V-notch impact tests without taking into account a fire effect, Li et al. [1.23, 1.24] performed Charpy V-notch impact tests on Q420 grade steel (Chinese standard GB50017-2017 [1.25]) at both sub-zero and ambient temperatures. Sun et al. [1.26] performed Charpy V-notch impact tests on cold-formed hollow section members at a low temperature. Száraz et al. [1.27] performed a Charpy V-notch impact test on SA508-III (ASME standard [1.28]) and MA956 ODS steels, which is widely used in nuclear plants. For the Charpy impact test on cold-formed steel square hollow section, Charpy V-notch impact specimens were cut-out from the flat part (FP) and corner part (CP) of the cold-formed steel hollow cross section. Furthermore, the fracture energy after fire was investigated at both the ambient temperature and a low temperature below 0 ºC for specimens treated through water quenching and air cooling respectively.

1.2.3 Post-fire mechanical properties and buckling strength of cold-formed steel square hollow section columns

The Charpy impact fracture properties of steel welded connections and steel square hollow section columns after fire are studied in Chapters 2 and 3. However, the Charpy impact fracture properties are the performance of steel used as a material, while for the reuse of steel structure, more investigation is needed on the performance of steel used as a structural member. When a steel building suffers from a fire, some protected steel members might be heated to 100–400 °C, the lower and upper limits of which correspond to the low- and medium-temperature, respectively, at post-flashover fire conditions. It is well known that both the strength of steel members does not change significantly in low- and medium-temperature regions. However, according to previous research [1.29,1.30], the post-fire mechanical properties will change when steel members are cooled from the above temperature. Although steel members may not exhibit obvious

deformation in their exterior after low- and medium-temperature heating, their residual mechanical properties may be altered. For some steel members without fireproofing materials, the temperatures at post-flashover fire conditions may exceed 600 °C (high-temperature regions). Owing to the strength degradation of steel members at high-temperatures, severe damage (plastic deformation) may be observed in these members after fire. When considering the reuse of steel structures, these members must be replaced with new ones. Therefore, to ensure the safety of the repair work, it is crucial to examine the residual strength at the post-fire stage. Some studies have been conducted on the post-fire mechanical properties of cold-formed steel members. Huang et al. [1.31] and Kesawan et al. [1.32] evaluated the post-fire mechanical behaviours of cold-formed ferritic stainless steel and steel hollow sections. The specimens were heated to high temperatures and cooled through an air-cooling process. They performed coupon tensile tests at the ambient temperature and confirmed that the specimens had sufficient residual strength for reuse after fire. However, these studies are focused on the post-fire material properties of cold-formed steel members, but the stability of cold-formed steel columns after fire has been examined in few studies. Okabe. et al. [1.33] performed stub-column compression tests after the heating and cooling processes and reported the elasto-plastic behaviours and load-bearing capacities. The stub-columns were heated to 400-700°C, and cooled in the furnace. According to their results, the yield strength of the stub-column that were heated to 400°C presented the similar or larger value than the untreated specimen, but it decreased with the heating temperature increased. However, they focused only on the local buckling behaviours of cold-formed steel columns, and the mechanical properties, local buckling, or flexural buckling at the post-fire stage have not been comprehensively examined in any study.

Therefore, the mechanical properties as well as flexural and local buckling strength of Japan Industrial Standard (JIS) STKR400 steel columns are reported in experimental studies in Chapter 4, which are widely used in Japan, after the heating and cooling processes. Three types of tests were conducted: coupon tensile test, axially loaded compressive test, and stub-column test. Furthermore, the flexural buckling strengths were calculated based on the Eurocode design equations [1.34,1.35], and the validity was examined from the test results. For the local buckling strength, the design equations of both Eurocode [1.34,1.35] and AS/NZS 4600:2005 [1.36] were verified.

1.2.4 Prediction equations of the residual displacement of the cold-formed steel square hollow section column after fire

According to the Recommendations for the Diagnosis and Repair Methods of Fire-damaged Buildings [1.1], when columns of a steel structure were reused after fire, the residual drift angle of column needs to be checked. Three limited values of the residual drift angle were suggested, namely 1/200 (A rank in the temporary risk evaluation), 1/700 (the tolerance limit of accuracy inspection standard), and 1/1000 (the tolerance limit of management standard), for which the residual drift angle is calculated through the equation of δ_r/h where δ_r is the residual displacement of the column after fire, h is the height of the

column. However, when a steel structure suffers a fire, the displacement of the columns or beams need to be measured during the fire diagnosis. According to the recommendation, a steel column could be reused after repair work if the residual drift angle is lower than 1/200; however, while it exceeds 1/200, it is considered to be very dangerous for reusing. To measure the residual drift angle or to repair the building, skilled workers need to enter the building, which makes these skilled workers in danger because the residual structure properties are unknown.

In Chapter 5, a simple prediction equation of the residual displacement of the cold-formed steel square hollow section columns after fire is proposed to calculate the residual displacement for a column after fire based on its structural mechanics. The calculation result is compared with the FEM analysis, which simulated a whole process in a 1-storey steel frame in case that subjected to heating and the cooling process in the fire and fire extinguishing proceed. The accuracy of the FEM analysis was confirmed in the previous research [1.37].

1.3 Organization of thesis

This thesis is organized into six Chapters. A brief description of the content of each Chapter is listed as follow:

In Chapter 2, the result of a Charpy impact test on steel welded connections at low- and ambient-temperature as well as high-temperature, including the blue brittleness temperature range (100-300) ºC, is reported. Then, the Charpy impact test result of steel welded connections after heating and cooling treatment (water-cooling and furnace-cooling) is also investigated at ambient temperature. Furthermore, the Vickers hardness and microstructure observation were conducted to confirmed the microstructural change in steel members after the heating and cooling treatment.

In Chapter 3, Charpy impact test result of cold-formed steel square hollow sections at low- and ambient-temperature as well as high-temperature, including the blue brittleness temperature range (100-300) ºC, is reported. Then, the Charpy impact test result of the above steel after the heating and cooling treatment (water-cooling, furnace-cooling, and air-cooling) is also investigated at ambient temperature. Furthermore, the Vickers hardness and microstructure observation were conducted to confirmed the microstructural changes in the steel members after the heating and cooling treatment.

In Chapter 4, the mechanical properties as well as flexural and local buckling strength of cold-formed steel square hollow sections after heating and cooling treatment (water-cooling and furnace-cooling) were measured at ambient-temperature though three types of tests, which included coupon tensile tests, axially loaded compressive tests, and stub-column tests. Furthermore, the flexural and local buckling strength was examined and calculated based on the existing design equations, and the validity was examined based on the test results.

In Chapter 5, a prediction equation of the residual displacement of cold-formed steel columns after fire is proposed. Three kinds of models, namely a basic model, a model subjected to axial load and a model considering the local buckling were used to simulate the whole proceeding for the buildings suffer to fire and then cooled by fire extinguishing, and the residual displacement of these three kinds of models was obtained through a FEM analysis. The FEM analysis result of these models was compared to the calculation results of the prediction equation, so as to examine the validity of the prediction equation.

In Chapter 6, the research is summarized. Conclusions from the study are stated and directions for further research are suggested.

Reference

[1.1]. Recommendation for diagnosis and repair Methods of fire-damaged Buildings, 2015 (in Japanese)

[1.2]. K. Horikawa and Y. Sakino. Review of Damage in Welded Joints Caused by the Kobe Earthquake. Trans. JWRI, Vol.24 (1995), No.2, pp.1-10

[1.3]. H. Kuwamura. Fracture of steel during an earthquake—state-of-the-art in Japan. Engineering Structures. Vol.20 (1998). Issues 4-6, pp310-322.

[1.4]. S. A. Mahin. Lessons from damage to steel buildings during the Northridge earthquake. Engineering Structures. Vol.20 (1998). Nos 4-6, pp261-270.

[1.5]. J. Nikolaou and G.D. Papadimitriou. Microstructures and mechanical properties after heating of reinforcing 500 MPa class weldable steels produced by various processes. Constr. B. Mater. 18 (2004), pp. 243-254.

[1.6]. M. Koufu, K. Mika, I. Fuyuki (2017). A Study on Steel Mechanical Property Considering Heating History Temperature and Cooling Method Part Ⅴ Effect of Steel Type on Impact properties. Summaries of Technical Papers of Annual Meeting Architectural Institute of Japan, Fire Safety, pp.171-172 (in Japanese).

[1.7]. K. Sugimoto, S. Kintou, M. Koufu, J. Haruhata, K. Nishimura, J. SUZUKI (2017). A Study on Steel Mechanical Property Considering Heating History Temperature and Cooling Method. PartⅥ Effect of Steel Type on Microstructure. Summaries of Technical Papers of Annual Meeting Architectural Institute of Japan, Fire Safety, pp.173-174 (in Japanese).

[1.8]. A. Ghosh and M. Ghosh. Tensile and impact behaviour of thermo mechanically treated and micro-alloyed medium carbon steel bar. Constr. B. Mater. 192 (2018), pp. 657-670.

[1.9]. B.K. Panigrahi. Microstructure-mechanical property relationships for a Fe/Mn/Cr rocks bolt reinforcing steel. J. Mater. Eng. Perform., 19 (2010), pp. 885-893.

[1.10]. G. Zhang, M.-C. Zhu, V. Kodur, G.-Q. Li. Behavior of Welded Connections after exposure to elevated temperature. J. Constr. Steel Res., 130(2017) pp. 88-95.

[1.11]. F. Ozaki and Y. Kawasaki. Fire resistance of steel beams including beam-column welded connections with through diaphragms. J. Structural and Construction Engineering (Transaction of AIJ) .82(2017.10), No.740, pp.1687-1694. (in Japanese).

[1.12]. A.S. Daryan and M. Yahyai. Behaviour of welded top-seat angle connections exposed to fire. Fire Saf. J., 44 (4) (2009), pp. 603-611.

[1.13]. I. E. Dolzhenkov, "Nature of blue brittleness of steel," Metal Science and Heat Treatment., Vol.13, Issue 3, (March 1971), pp.220-224.

[1.14]. C.-H. Lee, H.-S. Shin, K.-T. Park, K.-H. Chang. Impact fracture energy of structural steel welds constructed at low ambient temperatures. Constr. B. Mater. 50 (2014), pp. 394-400.

[1.15]. D. Zhang, Z. Li, H. Wu, F. Huang. Experimental study on fatigue behavior of Q420 high-strength steel at low temperature. J. Constr. Steel Res. 145 (2018), pp.116-127.

[1.16]. L.-J. Jia, T. Ikai, K. Shinohara, H. Ge. Ductile cracj initiation and propagation of structural steel under cyclic combient shear and normal stress loading. Constr. B. Mater. 112 (2016), pp. 69-83.

[1.17]. X. Li, Y. Song, Z. Ding, S. Bao, Z. Gao, A modified correlation between KJIC and Charpy V-notch impact energy of Chinese SA508-III steel at the upper shelf, J. Nucl. Sci. Vol. 505 (2018), p.22-29.

[1.18]. R. Puthli and J.A. Packer, Structural design using cold-formed hollow section, Steel Constr. Des. Res., 6 (2) (2013), pp. 150-157.

[1.19]. S.H. Li, G. Zeng, Y.F. Ma, Y.J. Guo, X.M. Lai, Residual stresses in roll-formed square hollow sections, Thin-Wall Struct. 47 (2009), pp. 505-513.

[1.20]. Y. J. Guo, A. Z. ZHU,Y. L. Pi and F. Tin-Loi, Experimental study on compressive strengths of thick-walled cold-formed sections, J. Constr. Ste. Res. 63 (2007), pp. 718-723.

[1.21]. S. V. Devi, T.G. Singh and K. D. Singh, Cold-formed steel square hollow members with circular perforations subjected to torsion, J. Constr. Ste. Res., 162, (2019), pp. 400-411.

[1.22]. T. G. Singh and K. D. Singh, Structural performance of YSt–310 cold–formed tubular steel stub columns, Thin-Walled Struct. 121 (2017), pp.25-40.

[1.23]. Z. Li, D. Zhang, H. Wu, F. Huang, Wan Hong, X. Zang. Fatigue properties of welded Q420 high strength steel at room and low temperatures. Constr. B. Mater. 189 (2018), pp. 955-966.

[1.24]. D. Zhang, Z. Li, H. Wu, F. Huang. Experimental study on fatigue behavior of Q420 high-strength steel at low temperature. J. Constr. Steel Res. 145 (2018), pp.116-127.

[1.25] National standard of the people's republic of China, GB 50017-2003, https://kupdf.net/download/gb-50017-2003-code-for-design-steel-structure-chinese-national-standard_58fec5eddc0d60a342959e7b_pdf, Apr. 2nd, 2021, pp.13.

[1.26]. M. Sun and J.A. Packer, Charpy V-notch impact toughness of cold-formed rectangular hollow sections, J. Constr. Ste. Res. 97 (2014), 114-126.

[1.27]. Z. Száraz, P. Hähner, J. Stráská, S. Ripplinger, Effect of phase separation on tensile and Charpy impact properties of MA956 ODS steel, Materials Science and Engineering: A, Vol 700(2017), p.425-437.

[1.28]. W. Zhang, M. Li, D. Guo, D. Jiao. Y. Zhang, Study on progress of SA508-3 steel for nuclear power, Nuclear and Radiation Safety Center, MEP, Beijing 100082, China. (in Chinese).

[1.29]. D. Rasouli, S. Khameneh, A. Akbarzadeh, G.H. Daneshi. Effect of cooling rate on the microstructure and mechanical properties of microalloyed forging steel. J. Mater. Process. Technol., 206 (2008), pp. 92-98.

[1.30]. L. Ceschini, A. Marconi, C. Martini, A. Morri, A.D. Schino. Tensile and impact behaviour of a microalloyed medium carbon steel: effect of the cooling condition and corresponding microstructure. Mater. Des., 45 (2013), pp. 171-178.

[1.31]. Y. Huang, and B. Young, Post-fire behaviour of ferritic stainless steel material. Constr. B. Mater. 157 (2017), pp. 654-667.

[1.32]. S. Kesawan, and M. Mahendran, Post-fire mechanical properties of cold-formed steel hollow

sections. Constr. B. Mater. 161 (2018), pp. 26-36.

[1.33]. Y. Kuroiwa, T. OKABE, T.AVE, and T. OZAKi, Compression behavior of cold-formed steel box stub-columns at cool-down temperature after heating. J. Struct. Constr. Eng., AIJ, 78(2013), pp.1159-1166. (In Japanese)

[1.34]. EN 1993-1-1, Eurocode 3 - Design of steel structures – Part 1-1: General rules and rules for buildings, May. 2005.

[1.35]. EN 1993-1-5, Eurocode 3 - Design of steel structures – Part 1-5: Plated structural elements, Oct. 2006.

[1.36]. AS/NZS 4600, cold-formed steel structures, AS/NZS 4600:2005 AIJ, 8(2013), pp.701-702. (In Japanese).

[1.37]. Y. Iwai and F. Ozaki, Collapse temperature of steel plane frames considering fire spreads, Japanese society of steel structure: Steel Construction Engineering, Vol 28(109), (March 2021), pp.79-88. (In Japanese).

Chapter 2. Impact fracture energy of steel welded connections after fire

2.1 Introduction

In this Chapter, the result of a Charpy impact test on steel welded connections at low- and ambient-temperature as well as high-temperature, including the blue brittleness temperature range (100-300) ºC, is reported. Then, the Charpy impact test result of steel welded connections after heating and cooling treatment (water-cooling and furnace-cooling) is also investigated at ambient temperature. Furthermore, the Vickers hardness and microstructure observation were conducted to confirmed the microstructural change in steel members after the heating and cooling treatment.

2.2 Charpy impact test

Charpy impact tests is a standardized high strain-rate test to investigate the absorbed energy for a metal material during fracture. This absorbed energy is a measure of a given material's notch toughness and acts as a tool to study temperature-dependent ductile-brittle transition. In this Chapter, Charpy impact tests results of steel welded connections (JIS SN400B and YGW-11) has been reported, and previous research [2.1] which is regarding the Charpy impact value of JIS SN400B steel, JIS SN490B steel, and JIS SA440B steel is investigated, and compared the result in the previous study with the result in this research.

Fig. 2.2.1 shows the Charpy impact test machine used in the test, the maximum capacity of the Charpy impact machines used in this study is 300J. Fig. 2.2.2 is the mechanical of the Charpy impact energies measured by the Charpy impact machine. In principle, a Charpy impact value of the specimens is calculated from the following equation (Eq. 2.2.1):

$$E = mgh_1 - mgh_2 \tag{2.2.1}$$

m: mass of the hammer in Figure 2.2.2

h_1: height of the hammer in Figure 2.2.2 before the Charpy impact test.

h_2: height of the hammer in Figure 2.2.2 after the Charpy impact test.

However, during the Charpy impact test, the impact energy can be calculated from the rotated angles, which were read from the angle dial using the following equation (Eq. 2.2):

$$E = m \times g \times l \times \left(cos\alpha - cos\frac{3\pi}{2}\right) \tag{2.2.2}$$

l: distance from rotation axis to the pendulum edge centre.

α: measuring angle on the dial after the Charpy impact test.

Figure 2.2.1 Charpy impact test machine

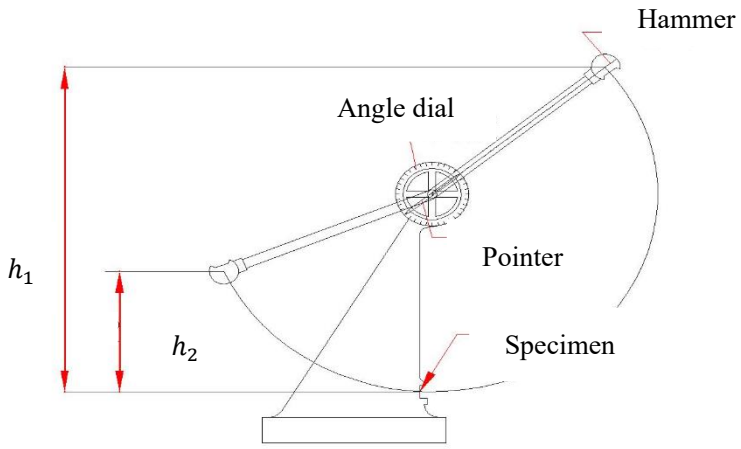

Figure 2.2.2 Calculate mechanical of the Charpy impact test machine

2.3 Charpy impact test of steel welded connections in and after fire

According to the previous research [2.2], steel exhibits a "blue brittleness phenomenon" under the temperature range of 100–300 ºC, and the total elongation under this range is smaller than that under the ambient temperature. Therefore, besides the impact fracture properties of the steel welded connections after fire, the possibility of the brittle fracture must also be investigated for theses member at relatively low fire temperatures, including the blue brittleness temperature during the fire.

2.3.1 Basic configuration of specimens

The steel welded connection specimen is welded by full-penetration weld, the base and welded metal is JIS SN400B and JIS YGW-11 grades steel respectively. The design yield point of the JIS SN400B is 235 MPa and the design tensile strength is 400 MPa in an ambient-temperature environment, and JIS YGW11 is a conventional welding steel wire developed for JIS SN400B. The chemical components based on the mill sheets (quality assurance documents published by the steelmaking industry) are shown in Table 2.3.1.

Table 2.3.1 Chemical components

Chemical (mass %)									
	C	Si	Mn	P	S	Ni	Mo	Cu	Ti+Zr
SN400B	0.12	0.2	0.64	0.011	0.004	0.02	0.01		
YGW-11	0.06	0.77	1.6	0.014	0.011			0.3	0.24

Standard Charpy impact specimens, which were quarried from steel base metal (BM), weld metal (WM) and heat affected zone (HAZ) parts, were prepared, as shown in Fig. 2.3.1. The BM and WM specimens were used to investigate the JIS SN400B steel plate and the weld metal manufactured from the JIS YGW11 steel wire, respectively. HAZ is the base metal adjacent to the weld metal, which subjected to the heat history during the welding process. Fig. 2.3.2 shows the Charpy impact test specimens, and the dimensions of the specimens were 10 × 10 × 55 mm.

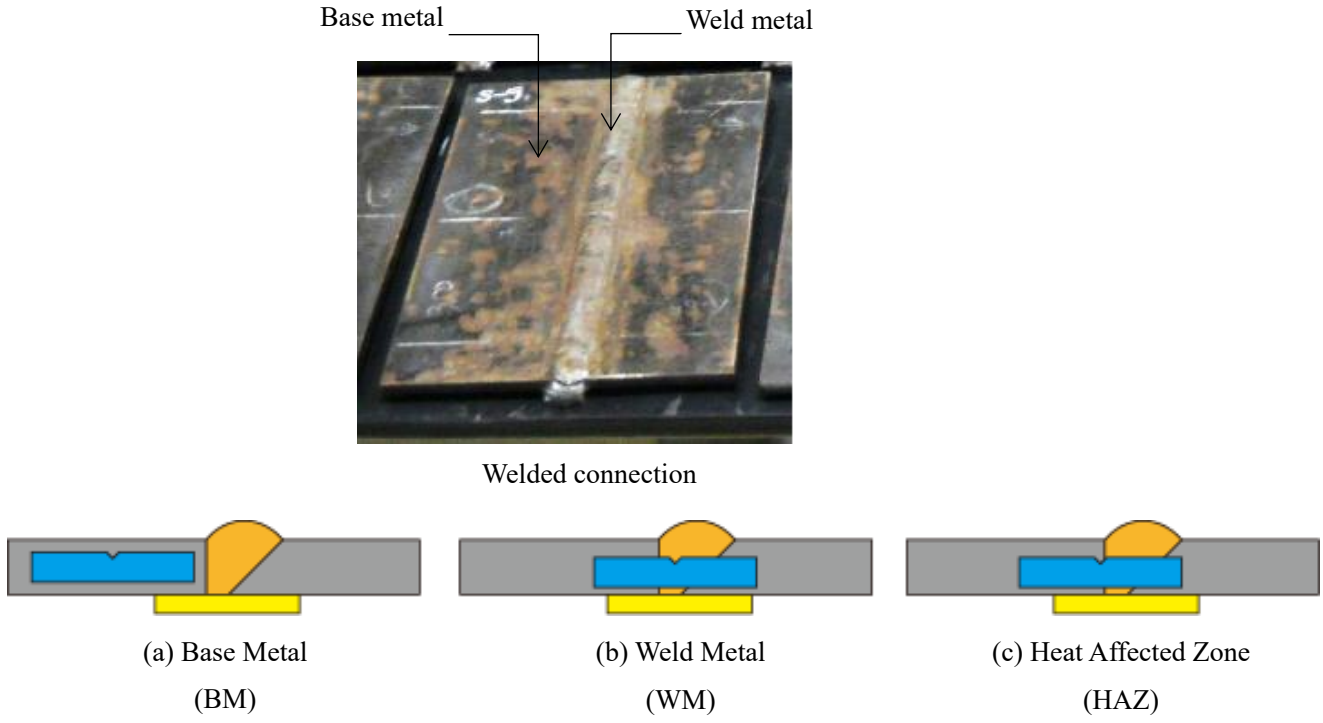

Figure 2.3.1 Steel welded connections specimens

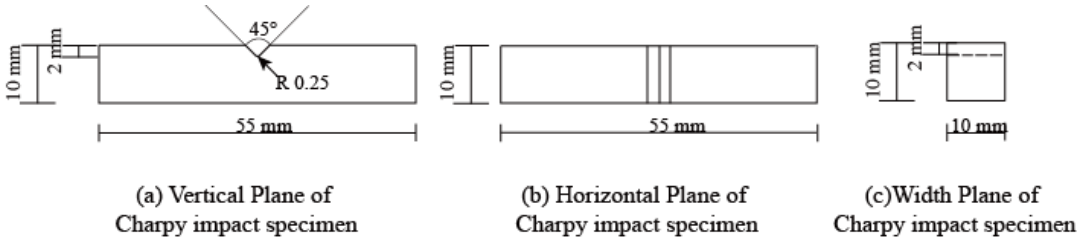

(a) Vertical Plane of Charpy impact specimen

(b) Horizontal Plane of Charpy impact specimen

(c)Width Plane of Charpy impact specimen

Figure 2.3.2 Charpy impact test specimens

2.3.2 Electric furnace and dummy specimens

As shown in 2.3.3, IDK-S cylindrical electric furnace (the inside diameter: 250 mm. the height: 500 mm) were used to heat the specimens. The heating rate of the electric furnace is 10 ºC/min. A dummy specimens attached to a thermocouple were prepared to make sure the accuracy of the temperature for the test specimens as shown in Fig.2.3.4.

Figure 2.3.3 A cylindrical electric furnace

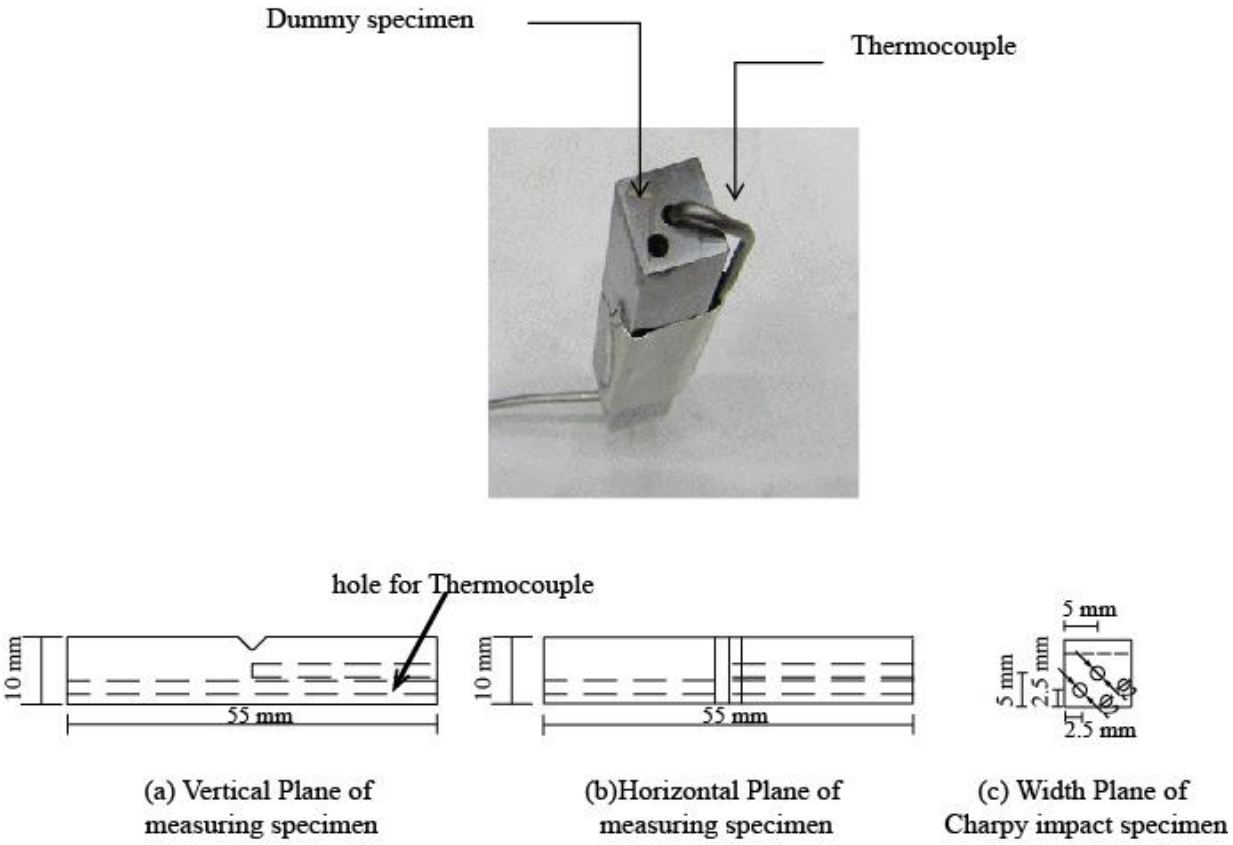

Figure 2.3.4 Dummy test specimens for temperature measurement of the Charpy impact test at elevated temperature.

2.3.3 Charpy impact test at High- and low-temperature

To investigate the Charpy impact energies under the blue brittleness temperatures, the Charpy impact test at elevated temperature test was conducted at 0, 100, 200, 300, 400, 500, and 600 ºC. And low-temperature Charpy impact tests were conducted at −20, −40 and −70 ºC to observe clear brittle fractures. The high temperature tests above 100 ºC were heated by the cylindrical electric furnace in Fig. 2.3.3, test at 0 ºC is cooled by a freezing mixture of water and ice; the Charpy impact test at low-temperature (under -20 ºC) were cooled using the freezing mixture of ethanol and dry ice. For each temperature, three specimens were prepared for the Charpy impact test, both the average value of the Charpy impact energies and the standard deviation of the Charpy impact energies of these specimens were calculated.

Charpy impact test machine was set at a room temperature environment to conduct the Charpy impact tests. For the high-temperature test, specimens were heated by the electric furnace to temperature 20-50 ºC higher than the target temperature, and soaked the specimen in these temperatures for 30 min to ensure the

all the specimens had the uniform temperatures. Then these specimens were removed from the furnace and set to the Charpy impact test machine to be examined their impact fracture energies at the high-temperature. The reason of heating the specimens to the temperatures higher than the target temperatures is because the temperature of these specimen rapidly decreased after the removal from the electric furnace. Fig. 2.3.5 shows the elapsed time and specimen temperature relationships. In Fig 2.3.5, the solid lines labelled "dummy specimen temperature" indicate the relationship between the temperature variation of the dummy specimens and the elapsed time after the dummy specimens were removed from the furnace. For all the specimens above 300 ºC, the elapsed time of the specimens from the removal until the hammer of the machine stroked on these specimens were measured using a stop watch. The vertical broken line was the maximum elapsed time (three specimens were conducted the Charpy impact temperature, the maximum elapsed time is the maximum duration time of the specimen from take out of the furnace to Charpy impact test). It was verified that the Charpy impact tests of these specimens were conducted above the target test temperatures. On the other hand, for 100 and 200 ºC tests, the elapsed times was not measured, because the temperature decreased very slowly.

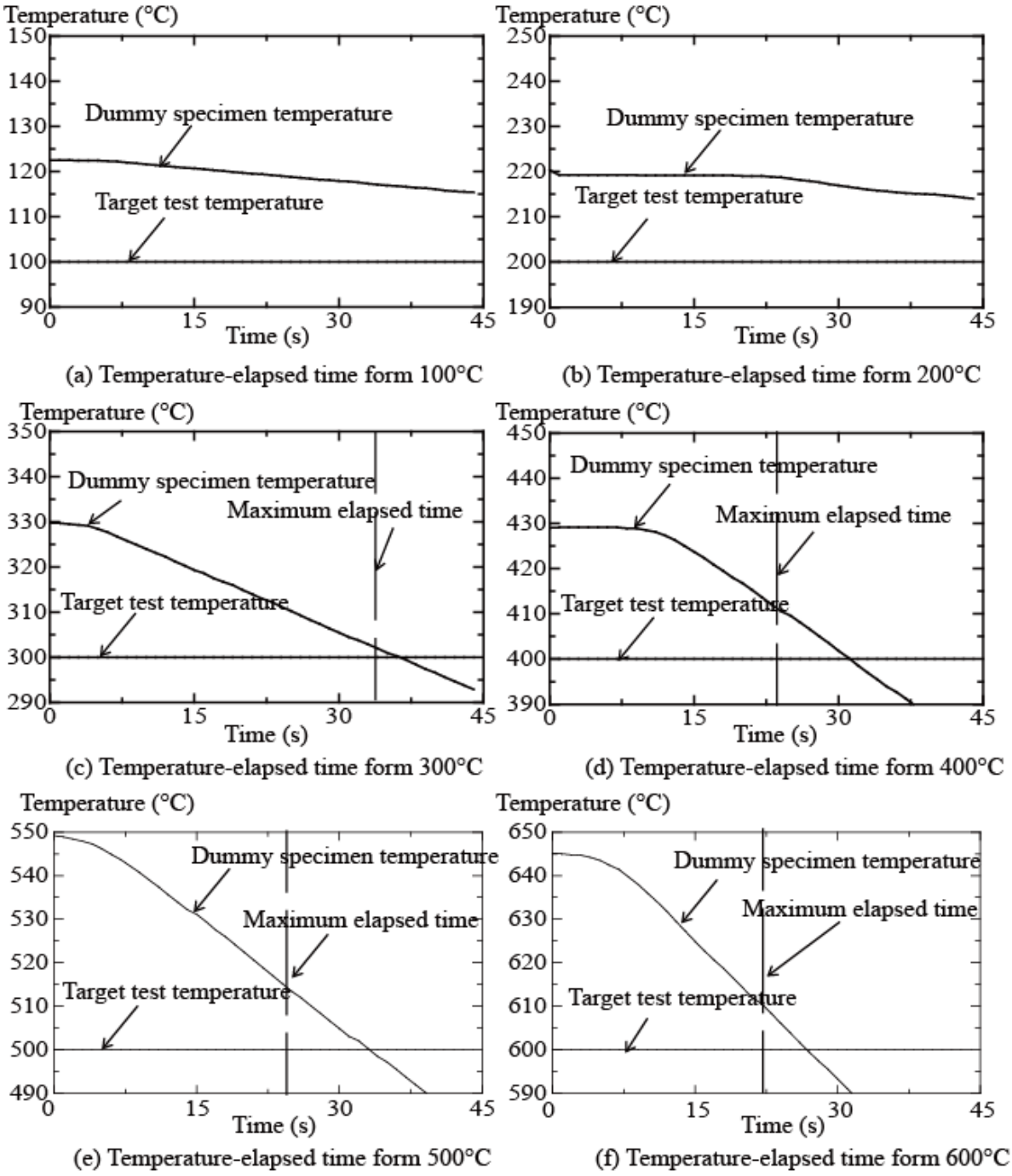

Figure 2.3.5 Elapsed time and specimen temperature relationships

2.3.4 Charpy impact test at ambient-temperature after fire on the specimens

According to some previous studies, it is well known that both the strength and ductile properties of steel materials after fire might change in comparison with the original values. Therefore, considering the reuse of the weld connection member after fire, it is very important to investigate the Charpy impact fracture energies of these specimens after cooling down from fire. When an unprotected steel column was subjected to fire, it is considered that some part in the member might expose under a very high temperature exceed 600 ºC. To evaluate the fracture properties of these member, the specimens were heated to 600, 700, 800, or 900 ºC using the electric furnace simultaneously. When the specimens reached to the target temperature, specimens were soaked for 30 min. After heating, two cases of the temperature changing were considered. They are quenching with water (water cooling) and retaining in the furnace with the temperature gradually decrease after heating (furnace cooling, slower than the air cooling). In water cooling tests the specimens were removed from the furnace and placed in a vessel containing a large quantity of water (the water volume is approximately, 15.4 L); water cooling replicated a critical situation that the specimen temperature significantly reduces owing to the fire-extinguishing. Furnace cooling simulated the situation where the member temperature gradually decreases after the fire. Fig. 2.3.6 shows the specimens temperature at cooling process. From Fig. 2.3.6, the cooling rate of water cooling was calculated at approximately 80 ºC/s. This is a much higher than the real cooling rate generally assumed at the fire-extinguishing situation (for example, in the case of the spray water extinguishing is approximately 1.7 ºC/s in the case of the water spray rate is 20L/min). This situation was used to replicate the critical situation with regard to the fracture-toughness change during the cooling process. In contrast, for the furnace-cooled specimens, the cooling rate was approximately 0.042 ºC/s.

Charpy impact tests of the specimens after heating and cooling treatment were conducted at 0, −20, and −40 ºC. For each testing temperature, three specimens were used. Except for the test under −20 ºC in which two specimens were used, due to a shortage in the number of prepared specimens.

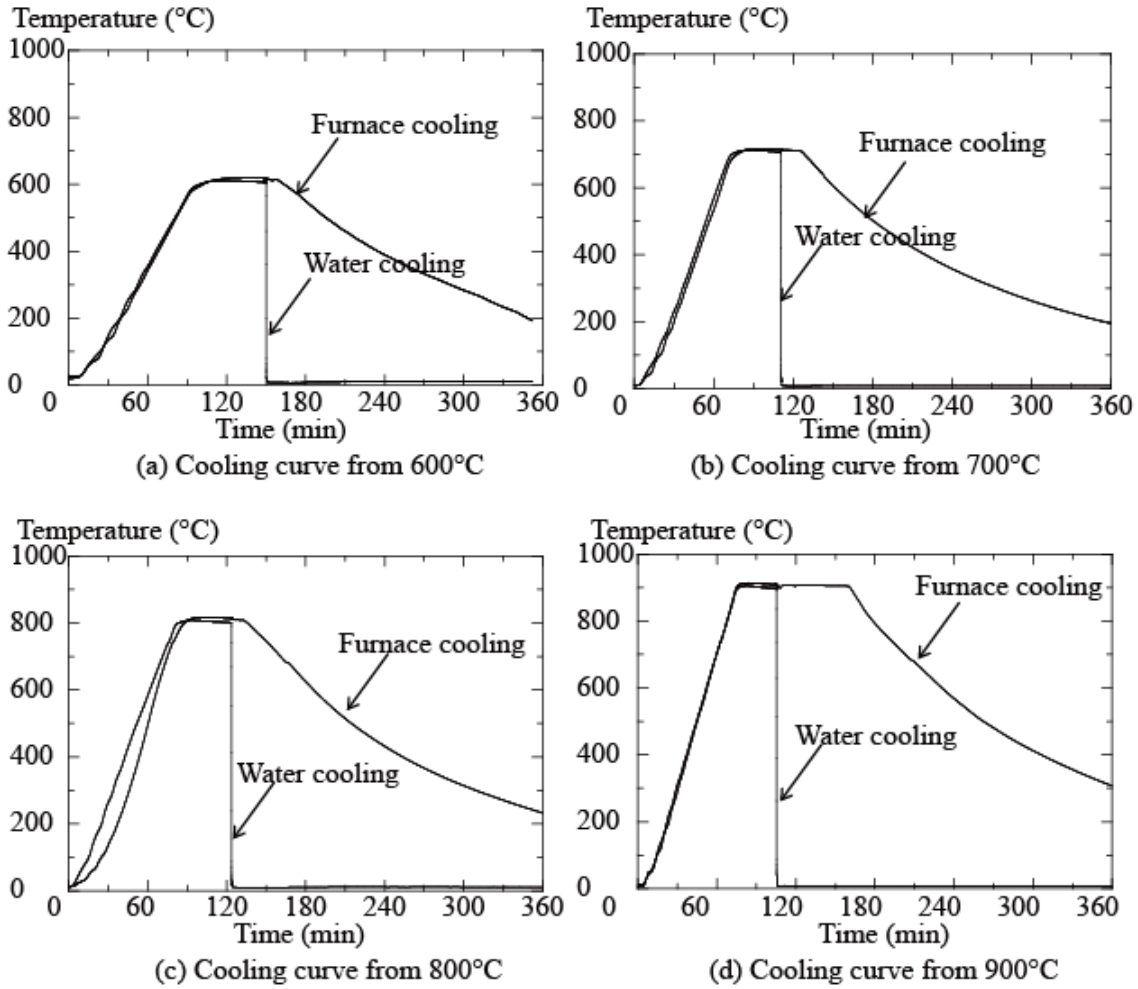

Figure 2.3.6 Specimen temperature at cooling process

2.4 Experimental result of steel welded connection

Before the Charpy impact test results, the coupon tensile test at high-temperature in JIS SN400B steel used in this research is reported. The reason of conduct the coupon tensile test at high-temperature is to confirm the effect of the blue brittleness phenomenon on the specimens at high-temperature. Fig.2.4.1 shows the detail of the coupon test specimens, the dimension of the coupon tensile test specimens is based on the JIS Z2201:1998[2.3]. Then, the test results of the Charpy impact test for the steel welded connection materials at the ambient and high-temperature, the results of the Charpy impact test for the specimens after the heating and cooling treatment are reported. Furthermore, considering the microstructure transition of the steel by the cooling process after the fire, the Vickers Hardness and the Microstructure Observation were also conducted on the specimens after the heating and cooling treatment.

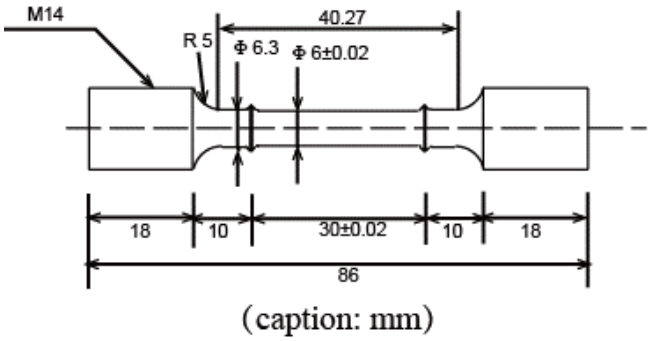

Figure 2.4.1 Coupon test specimen

2.4.1 High-temperature coupon test on JIS SN400B steel

For the high-temperature coupon test on JIS SN400B steel, nine specimens in totals were prepared, and coupon test were conducted at 20, 100, 200, 300, 400, 600, 700, and 800 ºC respectively. For the high-temperature test, the specimens were heated to each target temperature and remained in these temperatures for one hour before loading to make sure the whole specimen possessed the uniform temperature. A constant strain rate of 0.3%/min were used for the loading. Fig.2.4.2 shows the engineering stress and engineering strain relationships of the specimens at ambient and high-temperatures. Fig.2.4.3 shows the relationships between the fracture elongation and the test temperature. Fig.2.4.4 shows the strength reduction of the 0.2% offset yield strength, the stress when the strain is 1.0% and 2.0%, and the tensile strength, at a function of temperature. In general, the strength at the stress ε equal to1.0% is considered in the estimation of the load bearing capacity of steel members in Japanese fire-resistant designs.

As shown in Figs.2.4.3 and 2.4.4, the elongations at break at 100-300 ºC are lower than the elongation at the ambient temperature, and the tensile strength at these temperatures are larger than the ambient temperature, because of the blue brittleness phenomenon. When temperature exceeded 400 ºC, the fracture elongation increased with the temperature. However, the tensile strength decreased with the increasing temperature. It is because, when the steel was heated to high-temperature, the ductile capacity increased and the strength decreased.

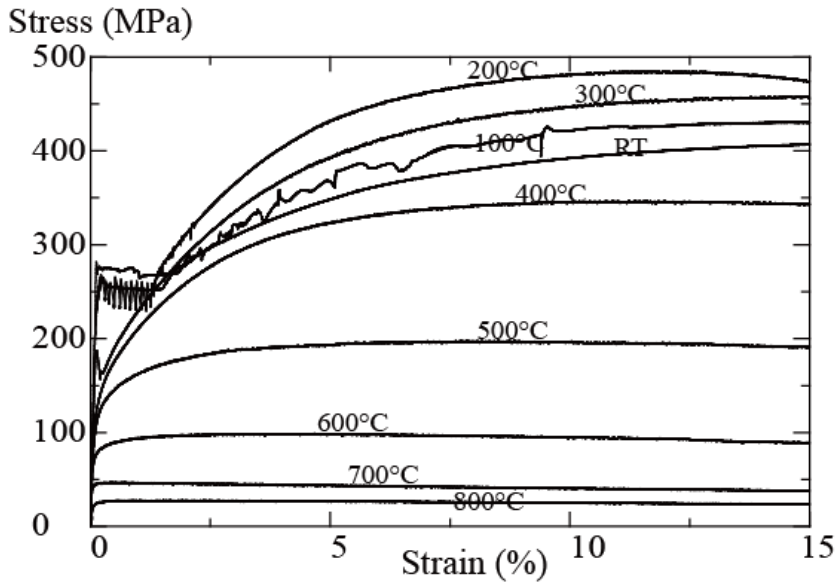

Figure 2.4.2 Stress-strain relationships at ambient and elevated temperature

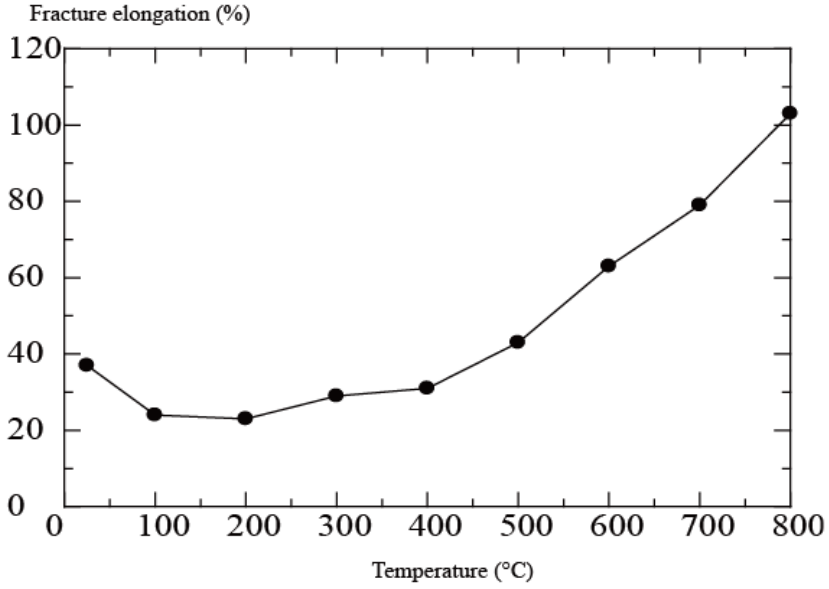

Figure 2.4.3 Fracture elongation at high-temperature

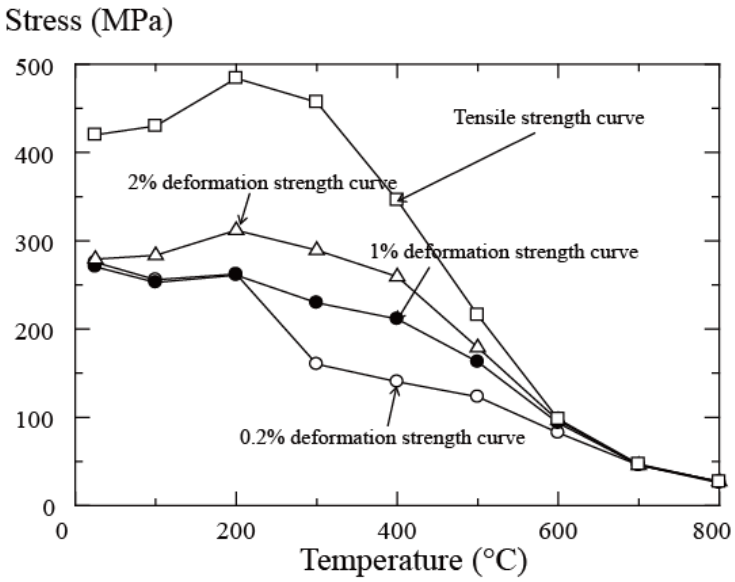

Fig.2.4.4 Strength reduction at high-temperature

2.4.2 Charpy impact test at High- and low-temperature

Table 2.4.1 lists the test result of the Charpy impact energies of the specimens at low- and high-temperatures. The value is the average of three specimens at each test temperature, and the value in parentheses indicates the standard deviation of the test result. Fig.2.4.5 shows the curve of the values in Table 2.4.1. Figs 2.4.6-2.4.8 show the fracture surface of the specimens after the Charpy impact tests.

As shown in Fig. 2.4.5, the Charpy impact energies at -70 ºC were lower than 20J. At -40 and -20 ºC, both the BM and HAZ specimens exhibit a higher value than 100 J, but WM specimens possess the Charpy impact energies lower than 50J. According to Fig 2.4.6, BM, WM, and HAZ specimens at -70 ºC broken into two pieces and exhibit a typical brittle surface with chevron patterns. For the test at -40 and -20 ºC, except for the WM specimens, both BM and HAZ specimens exhibit a ductile-brittle fracture surface (a combination of brittle and ductile surface).

At 0 ºC, both BM and HAZ specimens had a high Charpy impact energy, larger than 200J. According to Fig.2.4.7, both BM and HAZ specimens exhibit a ductile surface with dimple patterns and WM specimen exhibits the ductile-brittle fracture surface. JIS SN400B steel is required a high seismic-resistance performance in steel member; therefore, it has a higher Charpy impact energy than 27J to avoid brittle fractures during severe earthquakes. This test result confirms that the SN400B specimens used in this study satisfy the design requirements. For the WM specimen, generally, the welded connection is more brittle than the base metal, according to the test result, Charpy impact energy of WM specimens is 66J, higher than 27J required in the design.

For the test result of the specimens at blue-brittleness phenomenon temperatures region (100–300 ºC), as shown in Fig.2.4.8, all the specimens exhibit the typical ductile fracture surface. According to Fig.2.4.5,

the Charpy impact energies decreased at 100 ºC, due to the effect of blue-brittleness phenomenon. However, the minimum energy was still higher than 170 J. The maximum Charpy impact energy, which exceeded 250 J was observed at 200 ºC in all the specimens. According to Fig. 2.4.3, the fracture elongations from 100 to 300 ºC were smaller than that at the ambient temperature; however, this did not affect the Charpy impact energies.

In the tests above 300 ºC (high-temperature), the Charpy impact energies of the BM, WM, and HAZ specimens gradually decreased with increase in the temperature. It is because the yield point and tensile strength gradually decreased at elevated temperature. However, as shown in Fig 2.4.8, the specimens at high-temperature exhibited clear ductile fracture surface. Furthermore, as shown in Fig.2.4.3, the fracture elongation significantly increased at high-temperature. Therefore, it can be concluded the brittle fracture could hardly occur at high-temperature.

Table 2.4.1 Charpy impact test result at high-temperature

Temperature (ºC)	Charpy impact energies (J)			
	BM	WM	HAZ	
-70	14.9 (3.6)	11.4 (0.8)	15.8 (4.5)	
-40	136 (76.4)	13.3 (1.0)	163.3 (26.8)	
-20	173.8 (27.2)	18.3 (4.1)	205.9 (38.8)	
0	234.8 (18.7)	66.1 (11.5)	223.2 (6.3)	
100	171.5 (109.2)	208.9 (7.3)	229.1 (6.4)	Ave.
200	267.2 (3.1)	287.3 (14.7)	293.4 (6.2)	(S.D.)
300	247.2 (5.1)	278.8 (2.6)	261.7 (8.4)	
400	167.8 (5.1)	155.4 (8.7)	175.1 (9.9)	
500	116.7 (5.1)	114.3 (4.0)	126.2 (5.1)	
600	152.3 (18.7)	112.2 (3.0)	175.3 (10.4)	

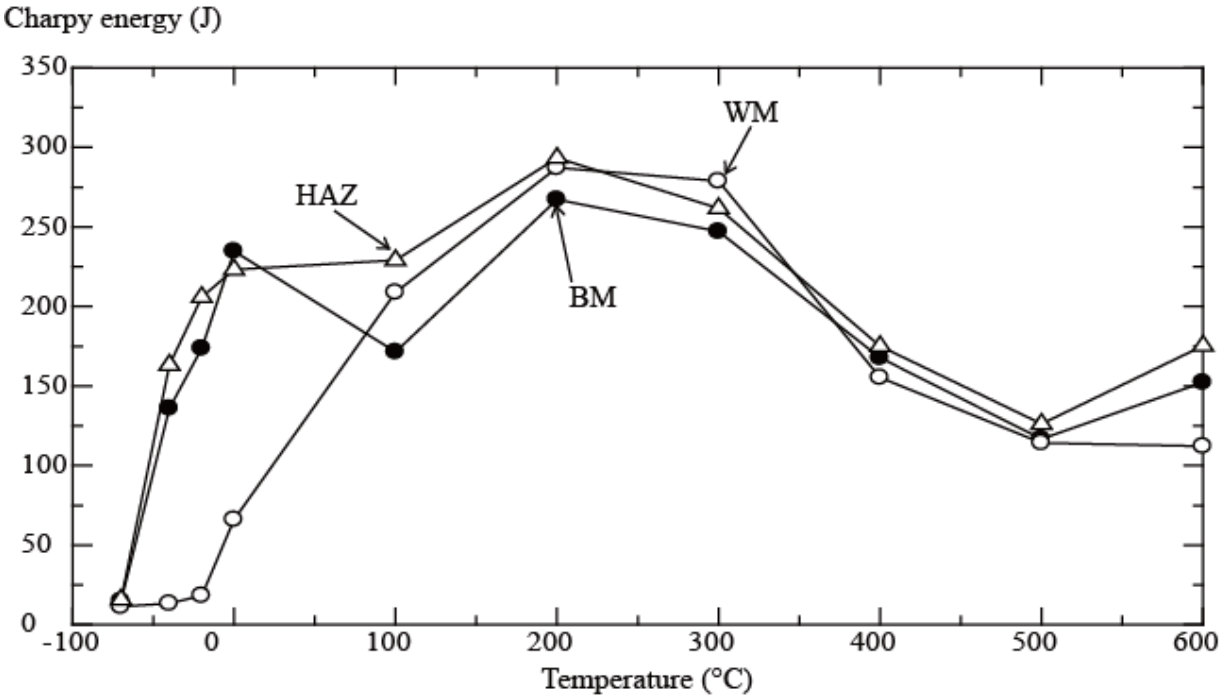

Fig.2.4.5 Experimental results of the Charpy impact test at high temperature

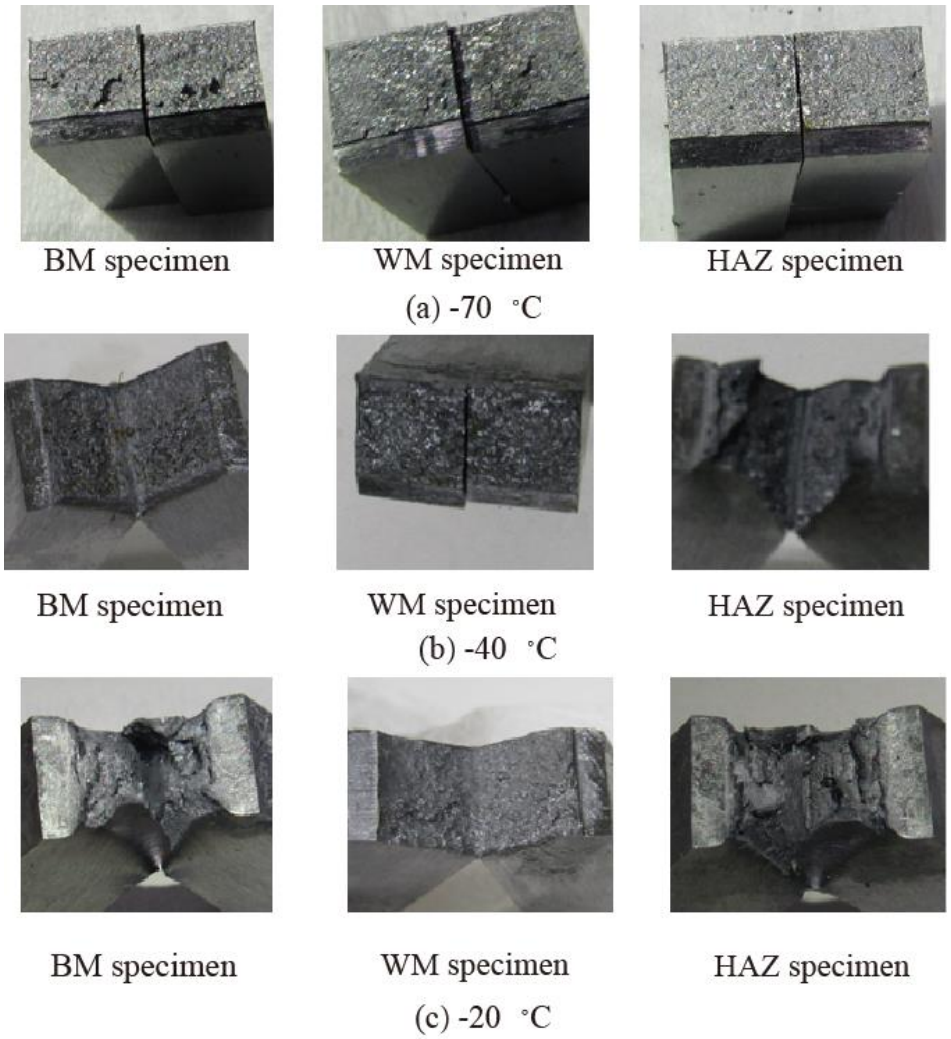

Fig.2.4.6 Fracture surface of specimen at subzero temperature

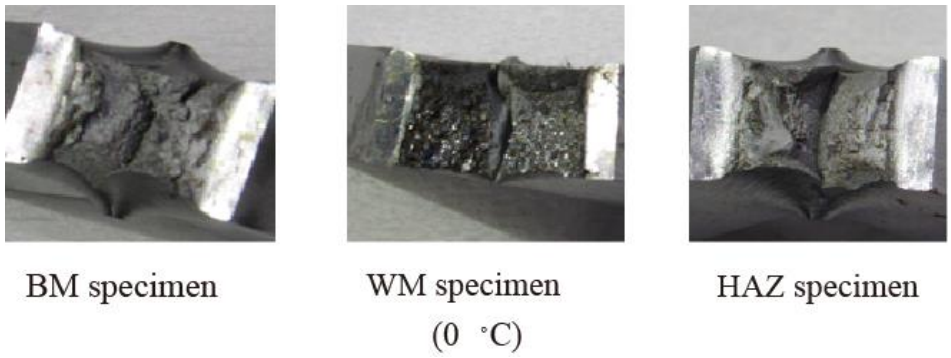

Fig.2.4.7 Fracture surface of Specimen at 0 ºC

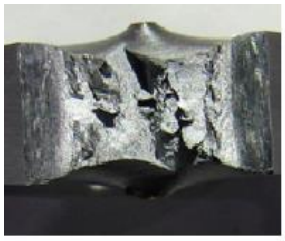

BM specimen

WM specimen

HAZ specimen

(a) 100 °C

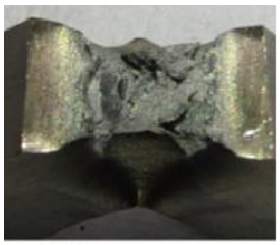

BM specimen

WM specimen

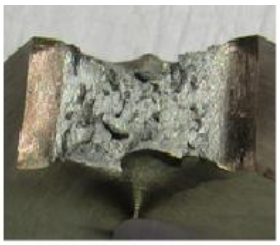

HAZ specimen

(b) 200 °C

BM specimen

WM specimen

HAZ specimen

(c) 300 °C

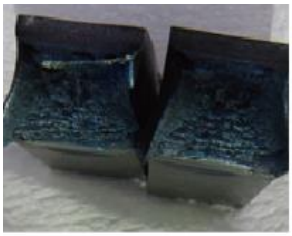

BM specimen

WM specimen

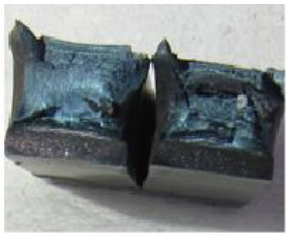

HAZ specimen

(d) 400 °C

BM specimen

WM specimen

HAZ specimen

(e) 500 °C

Fig.2.4.8 Fracture surface of specimen at high-temperature

2.4.3 Charpy impact test results at ambient temperature after heating and cooling processes

Table 2.4.2 lists the average value and standard deviation of the test result of the Charpy impact energies of the specimens after heating and cooling process at 0 ºC. Average values very close to 300 J (the maximum Charpy impact energy of the Charpy impact machine) are the experimental results when the measured energies reached the maximum capacity of the test machine. For these sufficiently large values, the standard deviations were not listed. Fig.2.4.9 shows the relationship between the Charpy impact energies and the heating temperature listed in Table 2.4.2. Figs 2.4.10 and 2.4.11 show the fracture surface of the water- and furnace-cooled specimens after the Charpy impact tests, respectively.

According to Fig.2.4.9, for the specimens that were heated to 600 ºC, both water- and furnace-cooled specimens possess lager Charpy impact energies in comparison with the untreated specimens. Refer to Figs.2.4.10 and 2.4.11, typical ductile surfaces were observed on the BM and HAZ specimen after 600 ºC heating, and ductile-brittle surfaces were observed on the WM specimens after 600 ºC heating.

For the water-cooled specimens that were heated to 700 and 800 ºC, the Charpy impact energies were lower than the untreated specimens. However, except for the water-cooled WM specimens that were heated to 700 ºC, all the values are larger than 27J. As shown in Fig.2.4.10, except for the ductile-brittle fracture surface of the water-cooled HAZ specimen that was heated to 700 ºC, all the specimens exhibit the brittle fracture surface. On the other hand, for the furnace-cooled specimens that were heated to 700 and 800 ºC. both the BM and HAZ specimens exhibit the high energies reality close to 300J, and the WM exhibit larger impact energies than the untreated specimen. In Fig.2.4.11, these specimens exhibit the ductile fracture surface.

Furthermore, for the water-cooled specimens that were heated to 900 ºC, the Charpy impact energies recovered to a higher value than those specimens that were heated to 700-800 ºC, and clear ductile surface were observed. For the furnace-cooled specimen that were heated to 900 ºC, the Charpy impact energies are still larger than 150 J, and those specimens also exhibit the ductile fracture surfaces.

Conclusively, quenching during the water-cooling process significantly reduced the Charpy impact energies of the specimens heated to 700 and 800 ºC, and clear brittle fractures were observed in these specimens; conversely, those heated to 900 ºC recovered and developed ductile-brittle fractures.

Table 2.4.2 Charpy impact test result at 0 ºC

Test Temperature		0 ºC					
Cooling Process		Furnace-Cooling			Water-Cooling		
specimens		BM Ave. (S.D.)	WM Ave. (S.D.)	HAZ Ave. (S.D.)	BM Ave. (S.D.)	WM Ave. (S.D.)	HAZ Ave. (S.D.)
untreated	J	234.8 (18.7)	66.1 (11.5)	223.2 (6.3)	234.8 (18.7)	66.1 (11.5)	223.2 (6.3)
600 ºC treated	J	299.6 (-)	117.7 (41.2)	298.3 (-)	243.4 (4.9)	118.7 (24.2)	233.3 (10.8)
700 ºC treated	J	299.6 (-)	99.7 (45.3)	299.6 (-)	43.8 (24.6)	24.2 (6.3)	158.6 (2.9)
800 ºC treated	J	241.1 (21.1)	173.3 (35.5)	224.9 (9.3)	48.7 (13.4)	32.8 (4.8)	49.1 (15.7)
900 ºC treated	J	218.6 (23.4)	253 (53.5)	172 (9.9)	207.8 (80.7)	101.9 (11.8)	192.6 (8.4)

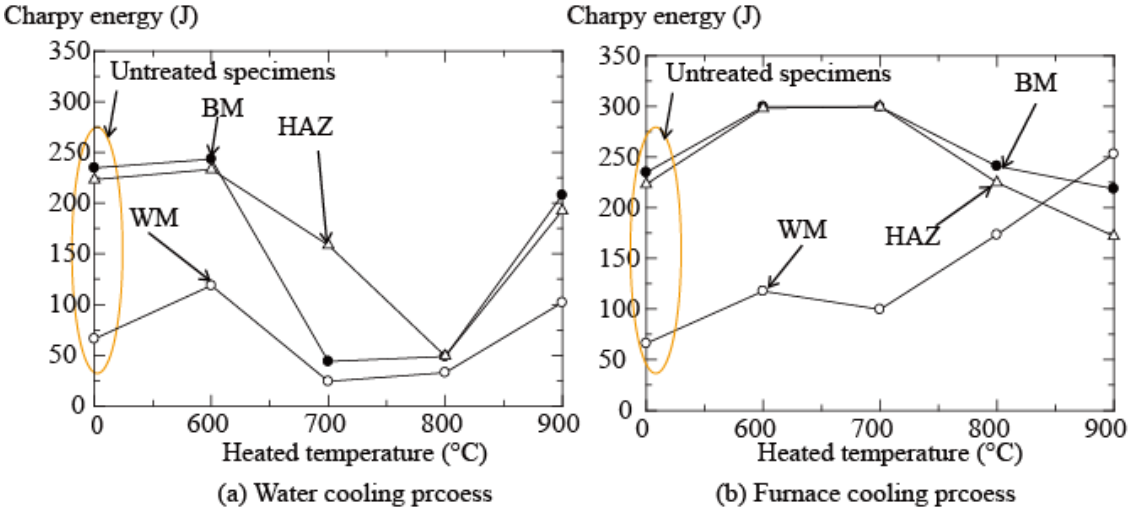

Fig.2.4.9 Experiment results of Charpy impact test at 0 ºC after heating and cooling process

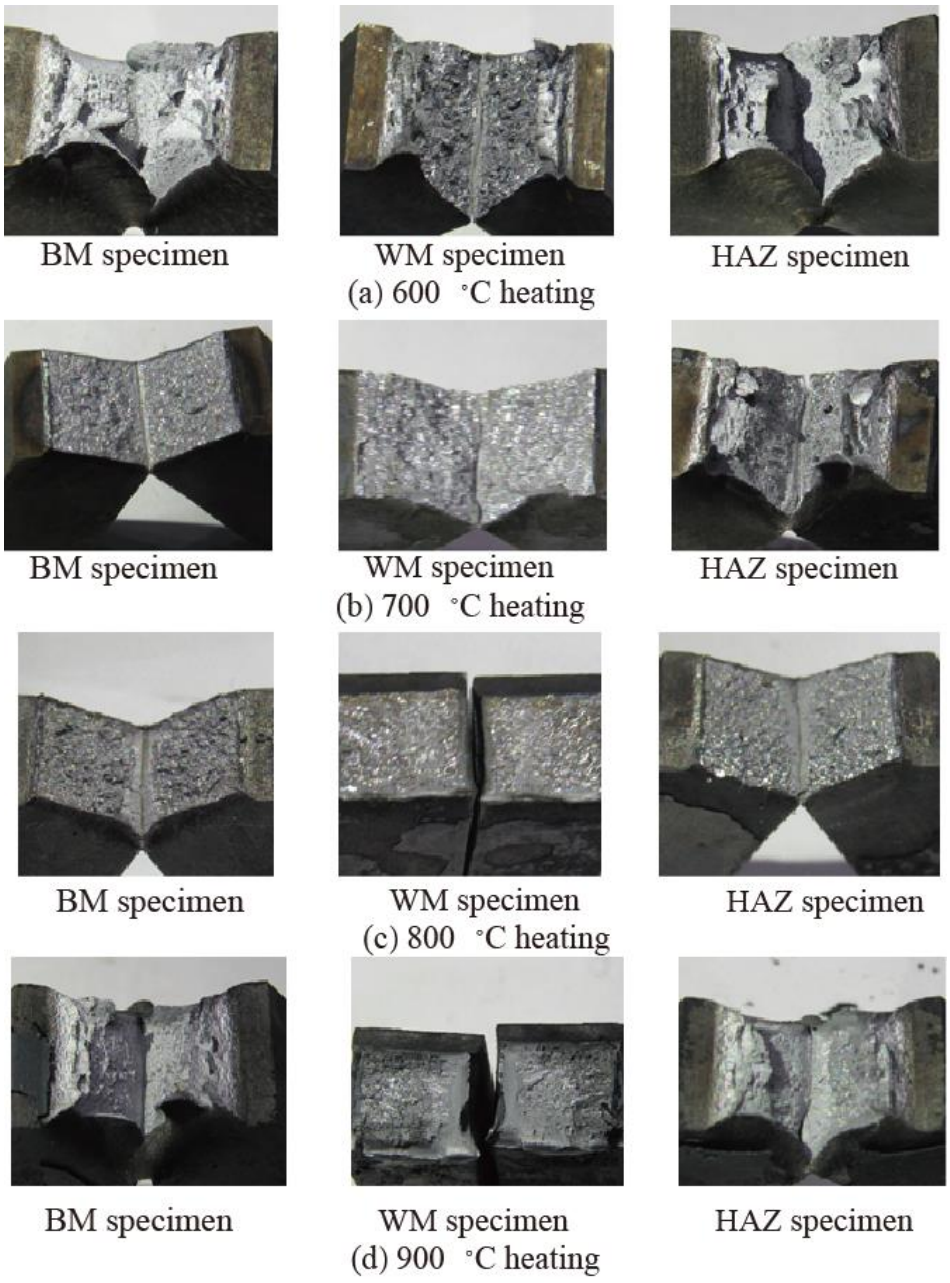

Fig.2.4.10 Fracture surface of water-cooled specimens at 0 ºC

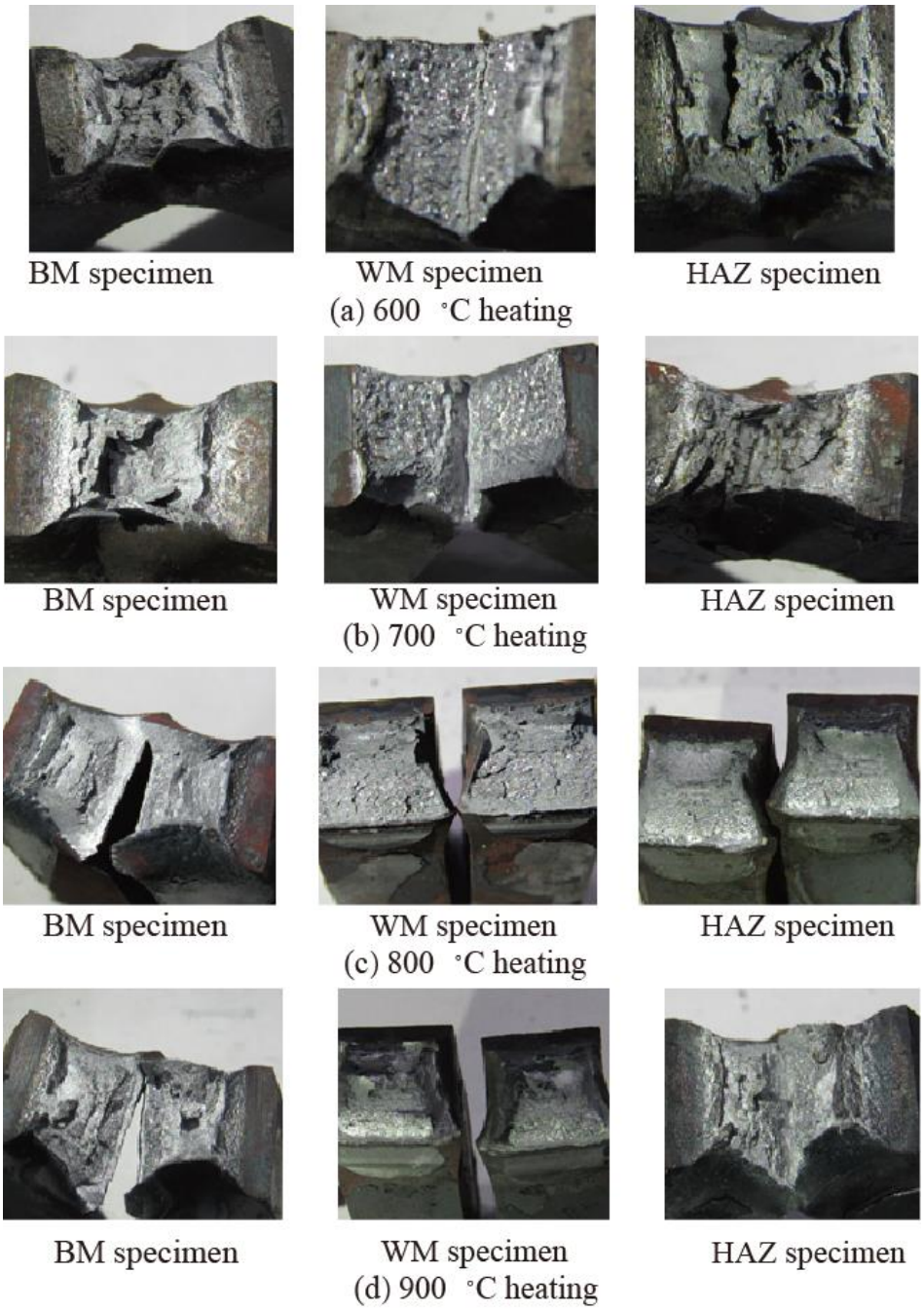

Fig.2.4.11 Fracture surface of furnace-cooled specimens at 0 ºC

2.4.4 Charpy impact test results at −20 and −40 ºC after heating and cooling processes

Charpy impact test for the specimens after heating and cooling process was also conducted at the test temperatures of −20 and −40 ºC. Figs. 2.4.12 and 2.4.13 show the results at −20 and −40 ºC which listed in Tables 2.4.3 and 2.4.4, respectively.

Figs. 2.4.12 and 2.4.13 show a similar to the curves of the test conducted at 0 ºC (Fig. 2.4.9). The

energies of water-cooled specimens that were heated to 700 and 800 ºC decreased significantly. On the other hand, the Charpy impact energy of the water-cooled specimens heated to 900 ºC recovered and developed ductile fractures. Furthermore, in the case of furnace-cooled BM and HAZ specimens, the Charpy impact energies did not decrease, except for the test at −40 ºC (Fig.2.4.13); the furnace-cooled WM specimens exhibited higher impact energies than the untreated specimen.

Table 2.4.3 Charpy impact test result at -20 ºC

Test Temperature		-20 ºC					
Cooling Process		Furnace-Cooling			Water-Cooling		
Spcimens		BM Ave. (S.D.)	WM Ave. (S.D.)	HAZ Ave. (S.D.)	BM Ave. (S.D.)	WM Ave. (S.D.)	HAZ Ave. (S.D.)
Untreated	J	173.8 (27.2)	18.3 (4.1)	205.9 (38.8)	173.8 (11.2)	18.3 (5.1)	205.9 (38.8)
600 ºC treated	J	299.8 (-)	62.6 (70.8)	270.1 (14.2)	190.2 (20.7)	18.7 (5.3)	226.4 (48.9)
700 ºC treated	J	299.7 (-)	19.1 (3.6)	206.4 (132.2)	13.2 (1.8)	13.4 (4.1)	33.4 (24.5)
800 ºC treated	J	208.1 (50.7)	22.7 (10.7)	195.9 (5.3)	20.4 (0.6)	27.3 (9.2)	23.1 (8.2)
900 ºC treated	J	208.4 (24.6)	172.4 (20.2)	148.3 (3.3)	241.8 (16.6)	77.5 (1.5)	180 (4.7)

Table 2.4.4 Charpy impact test result at -40 ºC

Test Temperature		-40 ºC					
Cooling Process		Furnace-Cooling			Water-Cooling		
Spcimens		BM Ave. (S.D.)	WM Ave. (S.D.)	HAZ Ave. (S.D.)	BM Ave. (S.D.)	WM Ave. (S.D.)	HAZ Ave. (S.D.)
Untreated	J	136.1 (76.4)	13.3 (1.0)	163.4 (26.8)	136.1 (76.4)	13.3 (1.0)	163.4 (26.8)
600 ºC treated	J	144.2 (25.2)	9 (0.7)	159.6 (15.7)	143 (20.7)	10 (5.3)	188.1 (48.9)
700 ºC treated	J	21.1 (2.8)	13.1 (1.1)	195 (1.7)	11.6 (1.8)	11.3 (4.1)	13.2 (24.5)
800 ºC treated	J	40.8 (1.0)	48 (3.1)	79.2 (2.1)	14.4 (0.6)	16.4 (9.2)	17.4 (8.2)
900 ºC treated	J	29.9 (24.9)	100.6 (20.2)	16.5 (3.3)	194 (16.6)	48.6 (1.5)	139.2 (4.7)

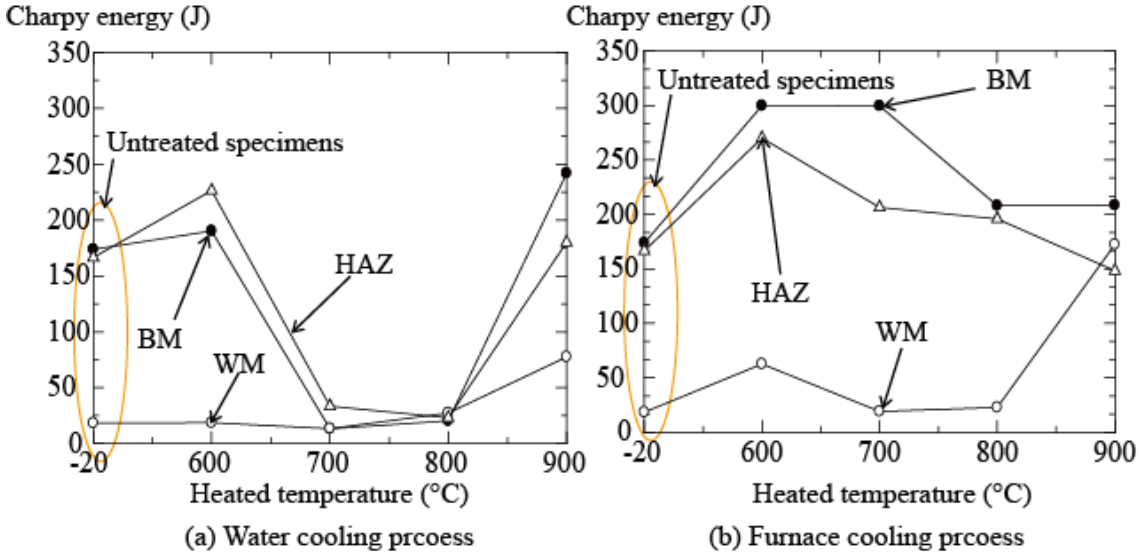

Fig.2.4.12 Experiment results of Charpy impact test at -20 ºC after heating and cooling process

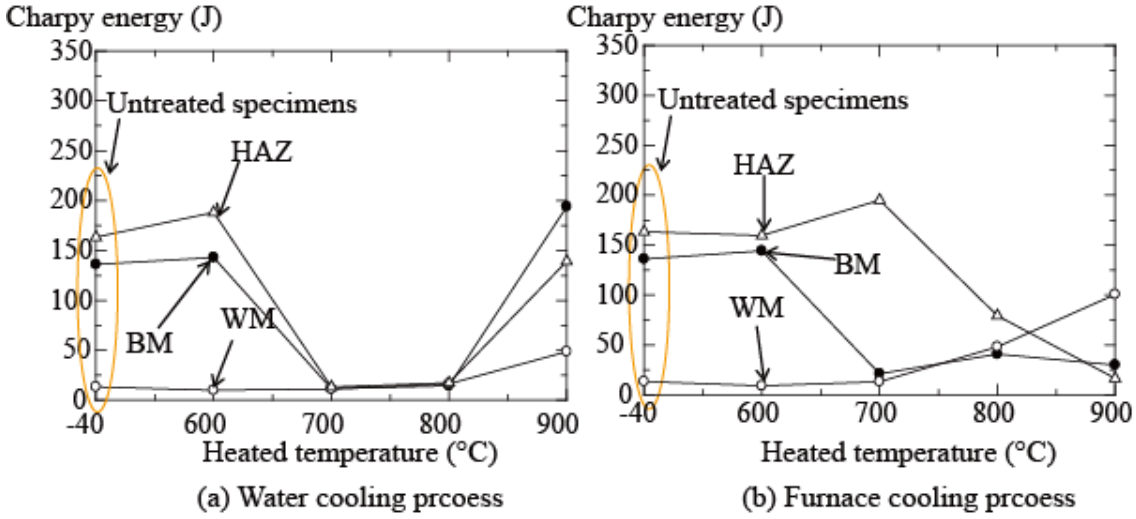

Fig.2.4.13 Experiment results of Charpy impact test at -40 ºC after heating and cooling process

2.4.5 Vickers Hardness test and microstructure observation

To investigate what caused the Charpy impact energy reduction, Vickers Hardness test and microstructure observation for the specimens have been conducted. Vickers hardness is a metal hardness measure test that easily evaluates the strength of the steel. In this test, specimens including the following five cases: the specimens (BM, WM, and HAZ) without heating and cooling process, the water-cooled specimens (BM, WM, and HAZ) after 800 ºC heating, the water-cooled specimens (BM, WM, and HAZ) after 900 ºC heating, the furnace-cooled specimens (BM, WM, and HAZ) after 800 ºC heating, the furnace-cooled specimens (WM) after 900 ºC heating, were measured. The Vickers Hardness at five points immediately under the of the specimens was measured with a 500 g Vickers indenter (HV0.5 [2.4]), and their average values are

shown in Figure 2.4.14. The tensile strength is approximately three times larger than the Vickers hardness values.

As shown in Fig.2.4.14, water-cooled specimens exhibit a larger Vickers Hardness, and furnace-cooled specimens exhibit similar or a little lower value than the untreated specimens. In other words, the tensile strength of the water-cooled specimens increased, and those of furnace-cooled specimens decreased. It is because the mechanical properties change owing to the quenching effect by the water, and it predicted the microstructure change of the specimens after the heating and cooling process.

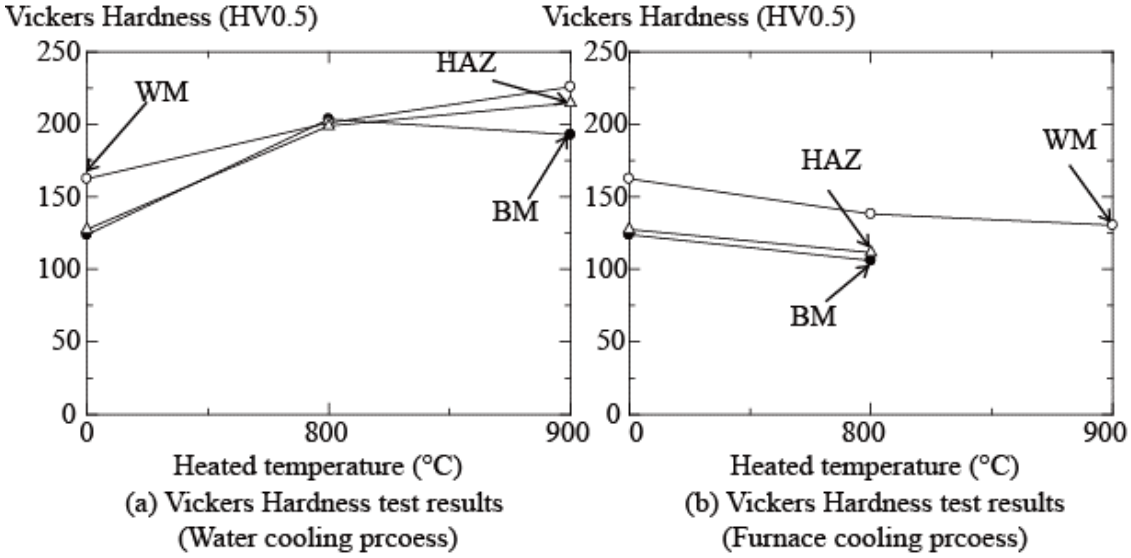

Fig.2.4.14 Vickers Hardness test result

2.4.6 Microstructure observation

To confirm the microstructure transition of the specimens after the heating and cooling process, microstructure observation was also conducted using Light Microscope (LM) and Scanning Electric Microscope (SEM). Figs. 2.4.15-2.4.17 show those results.

a) Microstructure observation of the BM specimens

As shown in Fig.2.4.15, JIS SN400B grade mild steel is produced by controlled rolling and cooling process during manufacture, and the untreated specimens exhibit a microstructure consists of ferrite and pearlite microstructures (F+P microstructures). Refer to the Charpy impact energies shown in Fig.2.4.5, JIS SN400B steel has high fracture toughness. As a result, the untreated BM specimens exhibited ductile fracture surface. Besides, furnace-cooled BM specimens also exhibit the similar F+P microstructures, for this reason, their Charpy impact energies are similar to that of the untreated specimens.

The water-cooled BM specimen heated to 800 and 900 °C exhibited segregated plural microstructures of ferrite, bainite, and martensitic and clear martensitic microstructures, respectively. This difference is occurred because the specimens were imperfectly quenched from the two-phase temperature (800 ºC heating) and perfectly quenched from the austenitic single-phase temperature (900 ºC heating). As a

result, water-cooled specimens that were heated to 800 °C exhibited low Charpy impact energy, while the latter specimens exhibit higher Charpy impact energy than the former one. As shown in Fig.2.4.14, the Vickers Hardness values increased after water cooling from 900 °C because of the martensitic microstructure.

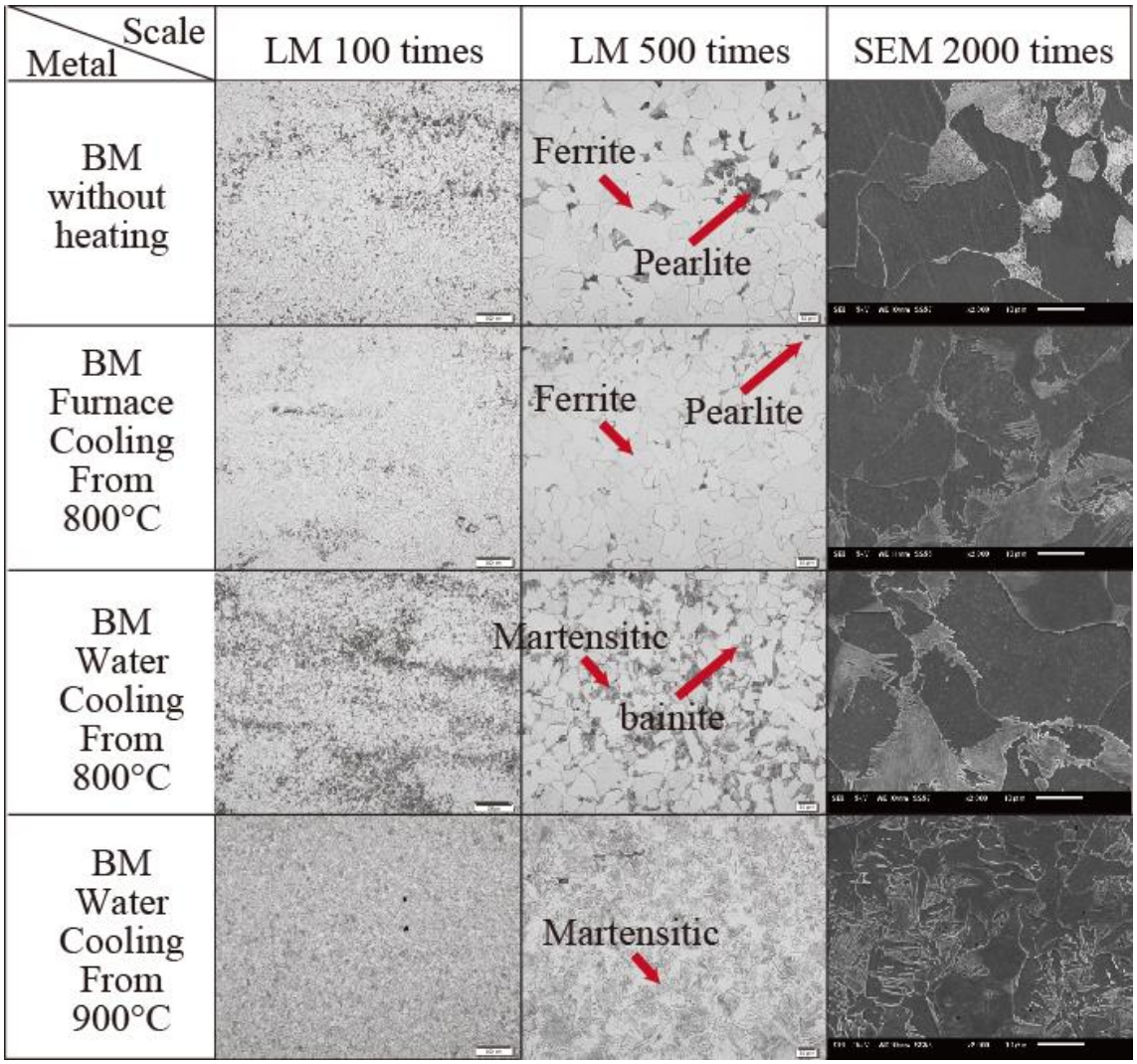

Fig.2.4.15 Steel microstructure of BM specimens

b) Microstructure observation of the WM and HAZ specimens

As shown in Fig.2.4.16 and 2.4.17, the crystal grains of WM specimen without heating were coarser in comparison with that of the BM specimens, owing to the larger heat input and the faster cooling rate during the welding process. Therefore, the untreated WM specimen exhibit lower Charpy impact value in comparison with that of the untreated BM specimen. As for the furnace-cooled WM specimen, the crystal grains are tidy because of the slow cooling rate in the furnace cooling process. As a result, the

Charpy impact energies of these specimens are higher than the untreated WM specimen. As for the microstructure of water-cooled WM specimen, they had coarse plural mixed microstructures at 800 ºC and minute martensitic microstructures at 900 ºC, which is similar to the BM specimens.

Furthermore, according to the microstructure observation of HAZ specimens, a fusion line can be observed between the base and weld metals. HAZ specimens show a similar microstructure to the BM specimen, as the result, HAZ specimens have the similar Charpy impact energies.

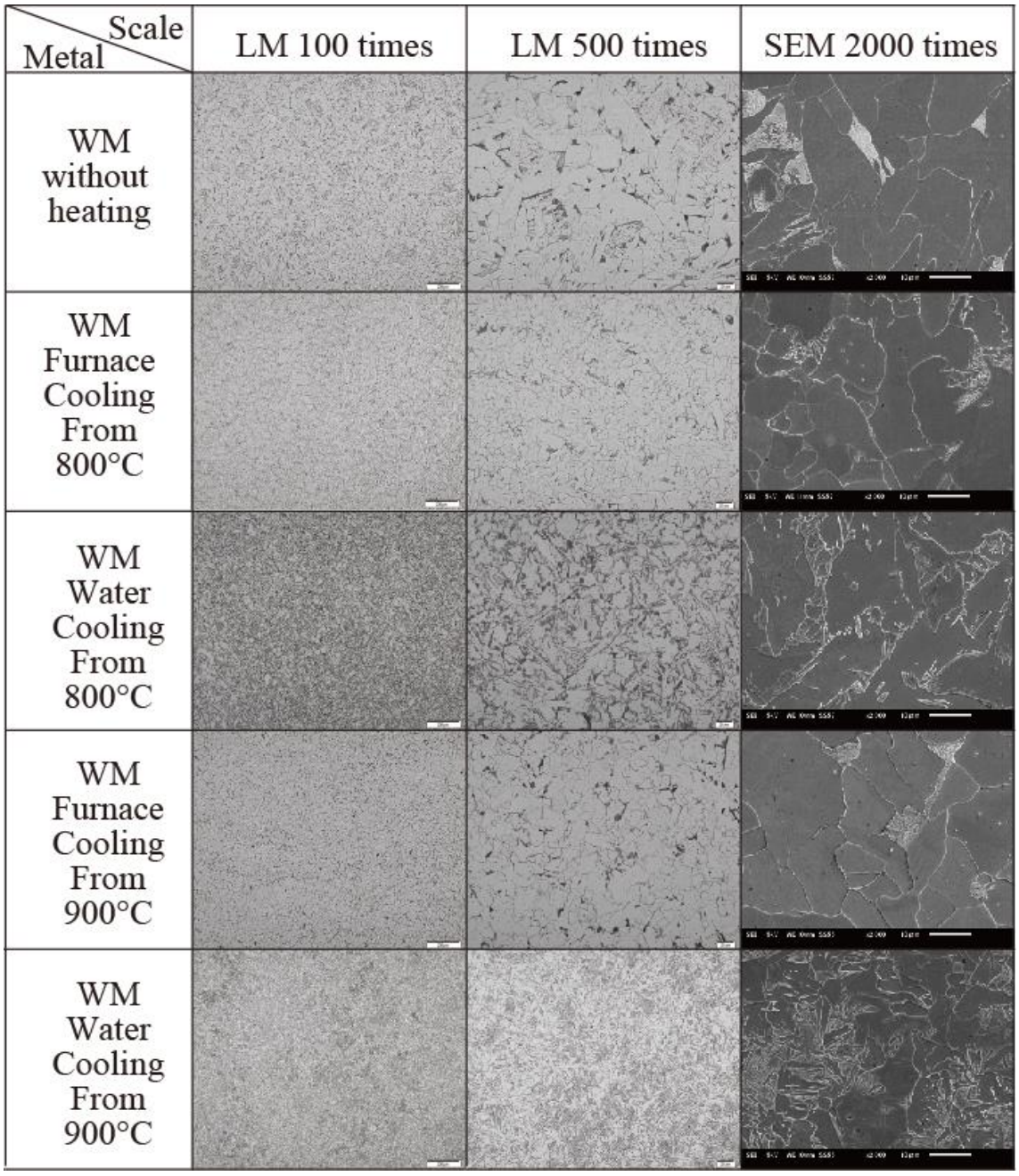

Fig.2.4.16 Steel microstructure of WM specimens

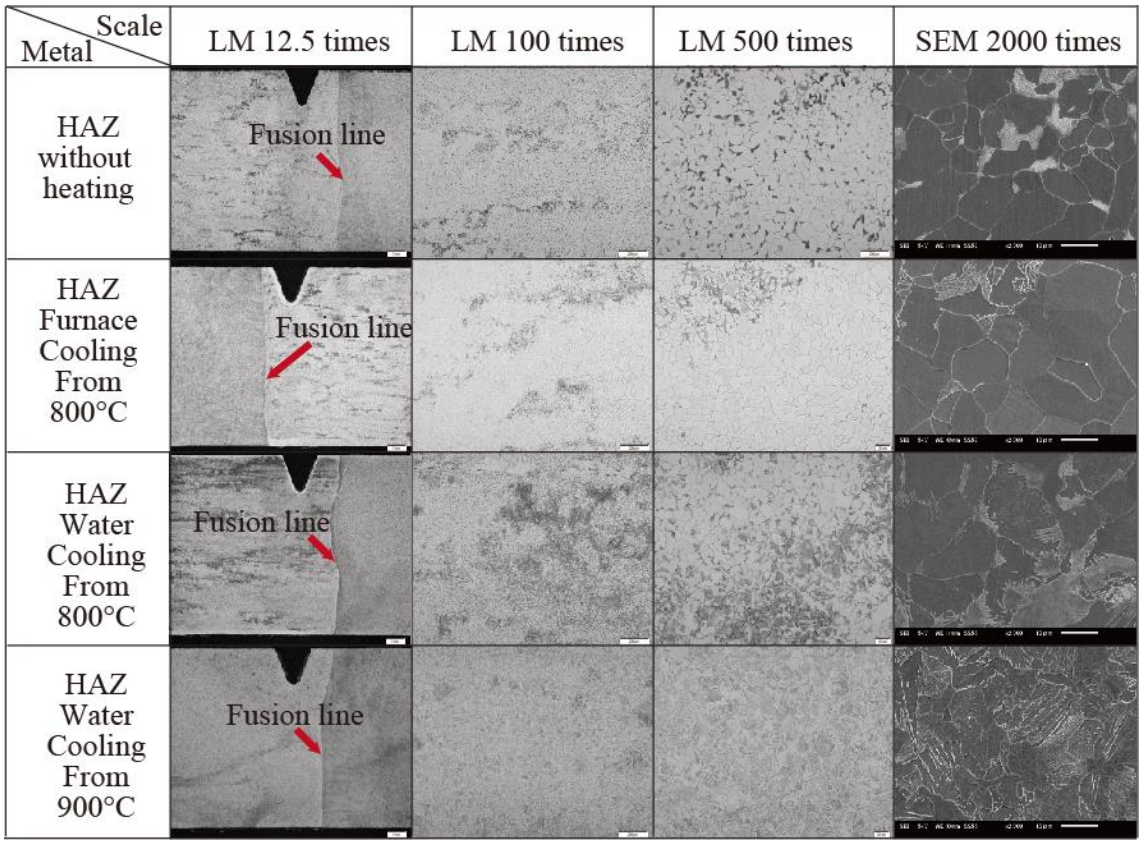

Fig.2.4.17 Steel microstructure of HAZ specimens

2.5 Comparison with previous studies

According to the previous research [2.1], Murakami et al conducted the Charpy impact test on the JIS SN400B steel, JIS SN490B steel, and JIS SA440 steel at the temperature -60, -30, 0, and 60 ºC. They treated the specimens by air-cooled from 500 ºC, air-cooled from 800 ºC, and water-cooled from 800 ºC, respectively. For the heating and cooling process, the specimens were heated by an electric furnace to the target temperature, and remain in the furnace for four hours. After the heating, air-cooled specimens were retained in the furnace with the temperature gradually decreased, therefore, it is considered that the air-cooled specimens in their study were subjected to the same treatment of the furnace-cooled specimens in our study which described in session 2.3.4. Table 2.5.1 cited their test result while the Charpy impact test is conducted at 0 ºC. Fig. 2.5.1 shows the result listed in Table 2.5.1. As shown in Fig. 2.5.1, for the air-cooled specimens, except for the JIS SN490B specimens at 500 ºC, Charpy impact energies exhibit larger values than those of the untreated specimens. For the water-cooled specimens, the Charpy impact energies significantly decreased at 800 ºC.

Fig 2.5.2 compared the test result of BM (JIS SN400B) specimens in our study with those of JIS SN400B steel in the Murakami's study. The produce lot of the JIS400B steel [2.1] is different from that of the BM

specimens. According to this figure, although the production lot is different, the Charpy impact test results of the untreated specimens are similar to each other. According to the results of water-cooled specimens, it is confirmed that the Charpy impact test result of both the BM specimens and the JIS SN400B specimen [2.1] decreased after water-cooled from the two-phase region (700-800 ºC). Therefore, it can be concluded that the Charpy impact energies reduction of the JIS SN400B steel in the case of water-cooled from two-phase temperature is a common phenomenon.

Table 2.5.1 Charpy impact test result of previous research [2.1]

Steel grades	Charpy impact energy (J)	Heating and cooling treatments				standard value (J)
		Untreated	Air-cooled from 500 ºC	Air-cooled from 800 ºC	Water-cooled from 800 ºC	
JIS SN400B		250	284	297	98	
JIS SN490B		185	134	256	17	27
JIS SA440B		256	264	305	40	

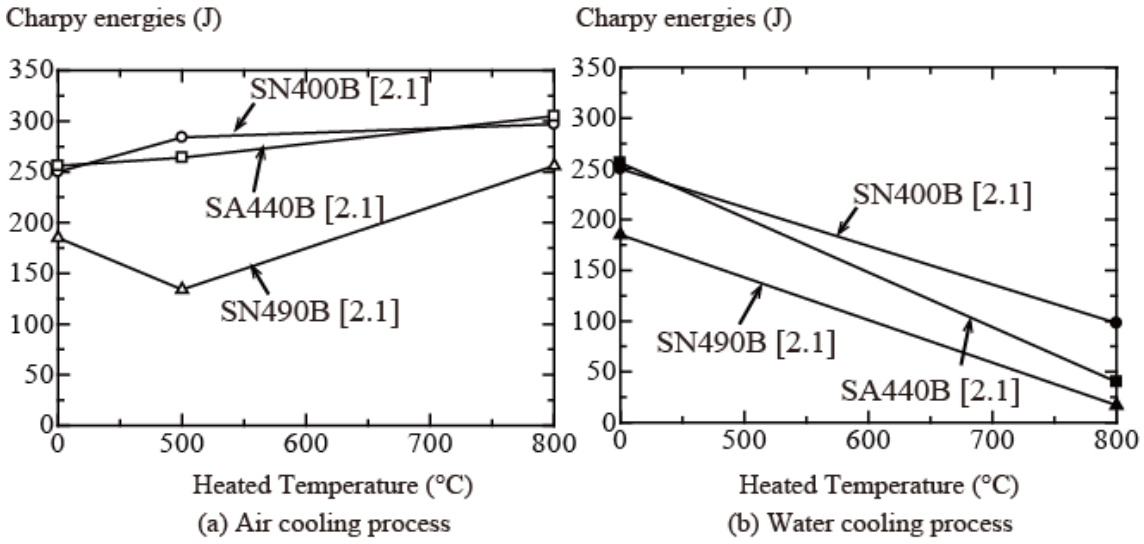

Fig.2.5.1 Experiment results of previous research [2.1]

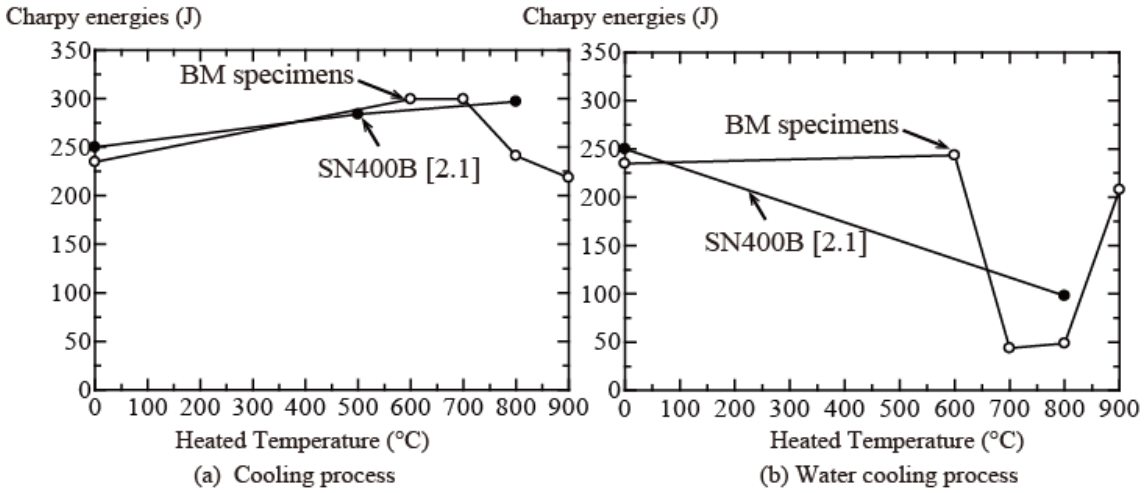

Fig.2.5.2 Experiment results comparison

2.6 Reuseability of the construction steel based on the Charpy impact test results after fire

Fig. 2.6.1 and 2.6.2 summarizes the Charpy impact test results of the JIS SN400B, JIS YGW-11, JIS SA440B and JIS SN490B grades steel after fire. In the figures, the red line is the value of 27 J, which is the lowest requirement for seismic-resistance performance of the steel structural members used in Japan in the Charpy impact value. Fig. 2.6.3 shows the 2% lower limit value of the Charpy impact test result of the welded connection members after fire. The value is calculated by the following equations:

$$E_{2\%} = \bar{E} - 2E_{S.D.} \tag{2.6.1}$$

$E_{2\%}$: the 2% lower limit value of the Charpy impact energies on probability distribution.

$\bar{E}$: the average value of the Charpy impact energies of 3 specimens.

$E_{S.D.}$: the standard deviation of the Charpy impact energies of 3 specimens.

According to the test results, the 2% lower limit value of the specimens cooled from 600 ºC is higher than 27J, it means close to 98% of the specimens that cooled from 600 ºC satisfy the lowest requirement for seismic-resistance performance, but for the specimens cooled from 700 ºC, the 2% lower limit value is lower than 27J, therefore, it is suggested that for the steel members subjected to high-temperature heating of more than 700 ºC, if the steel members are cooled at a relatively high cooling rate such as being water-cooled, the Charpy impact energy may be lower than the required value. If these members are reused after fire, there is a possibility that brittleness fractures will occur to these members under a severe earthquake. However, if the steel members were heated to a temperature of lower than 700 ºC and if they were cooled by fire extinguishing, the members still possess enough fracture properties to avoid brittleness fractures during the earthquakes. Therefore, in the view of the seismic-resistance requirement, it is considered that if

the exterior view of steel members exhibit no obvious damage, and the temperature histories of these members also not exceed 700 ºC in fire, these members could be reused as a seismic-resistance structure after fire.

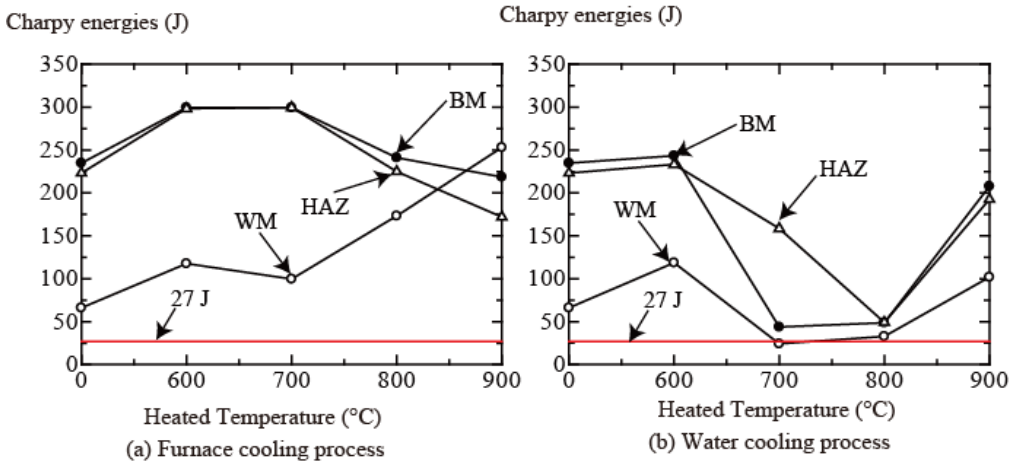

Fig.2.6.1 Charpy impact test result of welded connections after fire

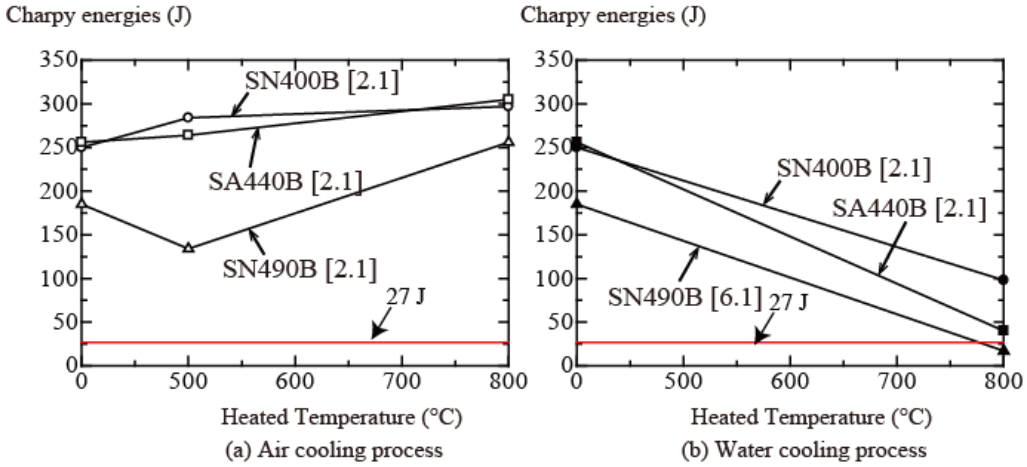

Fig.2.6.2 Charpy impact test result of SN400B, SA440B, and SN490B steel after fire [2.1]

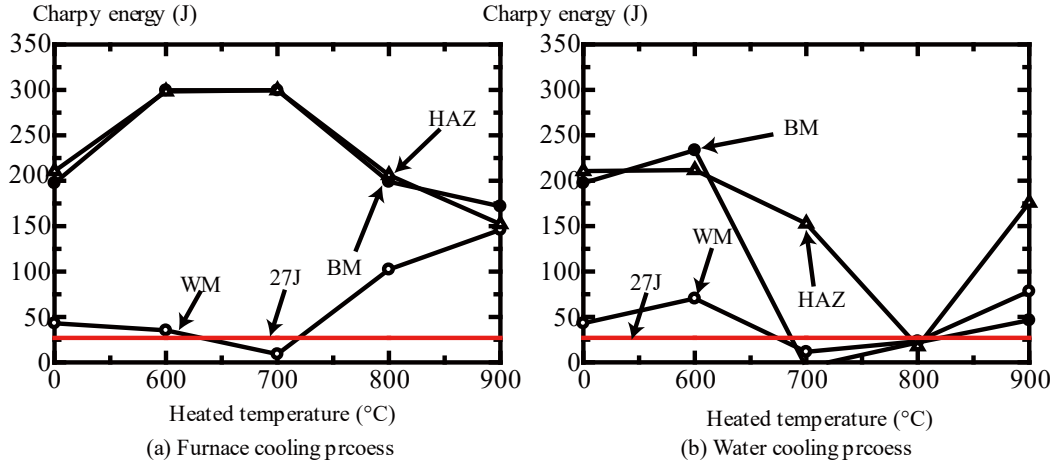

Fig.2.6.3 2% lower limit values of Charpy impact energies of welded connections after fire

2.7 Conclusion

In this Chapter, Charpy impact energies of JIS SN400B base metal, heat affect zone, and YGW-11 welded connection material were investigated at elevated temperatures and at ambient and low temperatures after the heating and cooling processes.

According to the high-temperature test results, it was confirmed that the Charpy impact values hardly decreased in the blue brittleness temperature regions (between 100 and 300 ºC). Therefore, the possibility of brittleness fracture occurring in the welded connections at elevated temperatures is very small. Then, according to the results of the ambient and low-temperature tests on the specimens after the heating and cooling processes, water-cooled specimens subjected to 700-800 ºC heating exhibit the low Charpy impact energies, whereas the Charpy impact energies of water-cooled specimens subjected to 900 ºC recovered to a high Charpy impact energy. Through the microstructure observation of the water-cooled specimens, it is confirmed the Charpy impact energies decreased owing to the incomplete quenching that occurred during the water-cooling process from 700 and 800 ºC. However, the fracture toughness recovered, owing to the occurrence of martensitic transformation in the specimens quenching from 900 ºC. On the other hand, the furnace-cooled specimens exhibit high Charpy impact energies, because, owing to the slowly cooling rate of furnace-cooling, the microstructure of these specimens is similar to the untreated specimen.

Additionally, refer to the test result in the previous study [2.1], it is also confirmed that JIS SN400B grades steel, JIS SN490B steel, and JIS SA440B exhibit the low Charpy impact energies in the case of water-cooled from 800 ºC.

When unprotected steel members are exposed to fire, it is assumed that the steel might be heated to elevated temperatures that exceed the steel transformation temperature before being quenched by fire extinguishers. Therefore, for the reused of the welded connection member, it is very important to evaluate the maximum temperature history and the cooling rate of these members. Although in an actual fire, the cooling rate is slower than the test situation, there is also a great possibility that the microstructure of the members changed, as the result, the toughness capacity of these members may be too low to satisfy the requirement seismic-resistance performance.

Reference

[2.1]. Y. Murakami, M. Katsuo, and F. Ito, A Study on Steel Mechanical Property Considering Heating History Temperature and Cooling Method Part V Effect of Steel Type on Impact properties. Summaries of technical papers of annual meeting Architectural Institute of Japan, tyokoku (Aug 2017), 3079

[2.2]. I. E. Dolzhenkov, "Nature of blue brittleness of steel," Metal Science and Heat Treatment., Vol.13, Issue 3, (March 1971), pp.220-224.

[2.3]. JIS Z2201:1998: Test pieces for tensile test for metallic materials https://kikakurui.com/z2/Z2241-2011-01.html Aug 19, 2021

[2.4]. ISO 6507-1:2018(E): Metallic materials—Vickers hardness test—Par1: Test method https://www.sis.se/api/document/preview/80000572/ Aug 19, 2019

Chapter 3. Impact fracture energy of cold-formed steel square hollow section

3.1 Introduction

In this Chapter, Charpy impact test result of cold-formed steel square hollow sections at low- and ambient-temperature as well as high-temperature, including the blue brittleness temperature range (100-300) ºC, is reported. Then, the Charpy impact test result of the above steel after the heating and cooling treatment (water-cooling, furnace-cooling, and air-cooling) is also investigated at ambient temperature. Furthermore, the Vickers hardness and microstructure observation were conducted to confirmed the microstructural changes in the steel members after the heating and cooling treatment.

3.2 Charpy impact test of cold-formed steel square hollow section

3.2.1 Specimens details

BCR295 steel column is one of the cold-formed steel square hollow section that widely used for steel building structures in Japan. It is formed from the hot-rolled steel plate of SN400B. as descripted in Chapter 2, the design yield point of the JIS SN400B is equal to 235 MPa and the design tensile strength is equal to 400 MPa in an ambient-temperature environment. However, the design yield point and design tensile strength of BCR295 steel at the ambient temperature were 295 and 400 MPa, respectively, owing to the cold-formed manufacturing process. BCR295 steel is charactered as larger yield and tensile strength and yield rate (YR) than the JIS SN400B steel, because, large residual stresses and plastic strains remain in the cross sections. The chemical components based on the mill sheets (quality assurance documents published by the steelmaking industry) are shown in Table 3.2.1.

BCR295 steel with two dimensions of □-250-250-16 mm and □-300-300-12 mm were prepared for the Charpy impact test. Fig.3.2.1 shows the BCR295 steel with the cross section of □-250-250-16 mm, two kind of specimens which is respectively quarried out from the flat part (FP) and corner (CP) part of the □-250-250-16 cross section, because of the different plastic strain in these two parts[3.1]. Additionally, Fig. 3.2.2 shows the BCR295 steel with a cross-section of □-300-300-12 mm, specimens (FPT12) were quarried out from flat part of this cross-section.

The dimensions of these specimens were also 10 × 10 × 55 mm, as shown in Fig.3.2.1. The same IDK-S cylindrical electric furnace and dummy specimens as descripted in section 2.3.2 were used.

Table 3.2.1 Chemical components

Chemical (mass %)									
Metal	C	Si	Mn	P	S	Cu	Ni	Cr	N
BCR295	0.07	0.01	0.55	0.011	0.006	0.14	0.011	0.06	0.23

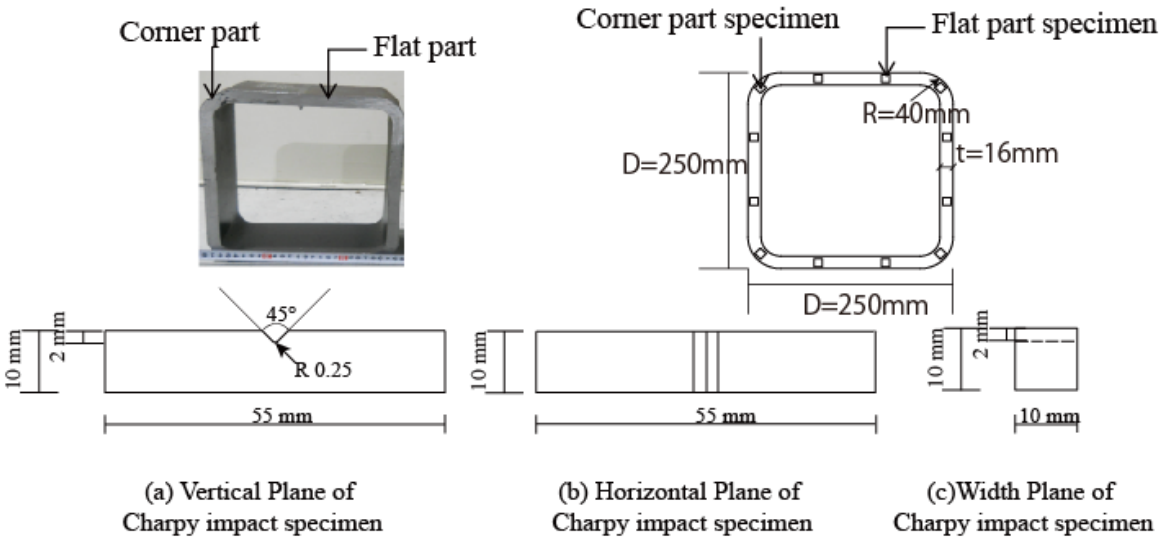

Figure 3.2.1. Test specimens of BCR295 with a cross-section of □-250-250-16 mm

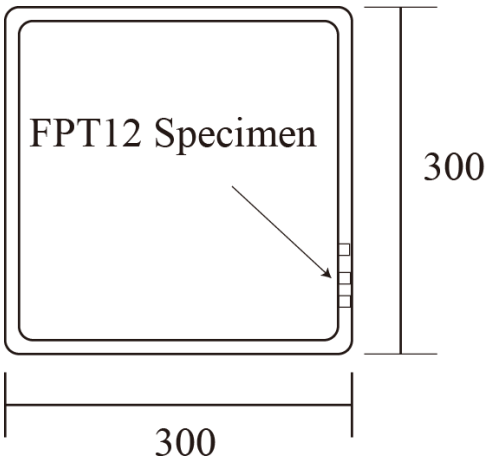

Figure 3.2.2. Test specimens of BCR295 with a cross-section of □-300-300-12 mm

3.2.2 High- and low-temperature test for the FP and CP specimens

To investigate the Charpy impact energies under the blue brittleness temperatures, the elevated temperature test was also conducted at 0, 100, 200, 300, 400, 500, and 600 ºC, and low-temperature Charpy impact tests were conducted at −20, −40 and −70 ºC, which is a similar method to the JIS SN400B described in Chapter 2. Fig. 3.2.3 shows the relationship between elapsed time and specimen temperature. It was verified that the Charpy impact tests of these specimens were conducted above the target test temperatures. On the other hand, for 100 and 200 ºC tests, the elapsed times was not measured, because the temperature changed very slowly.

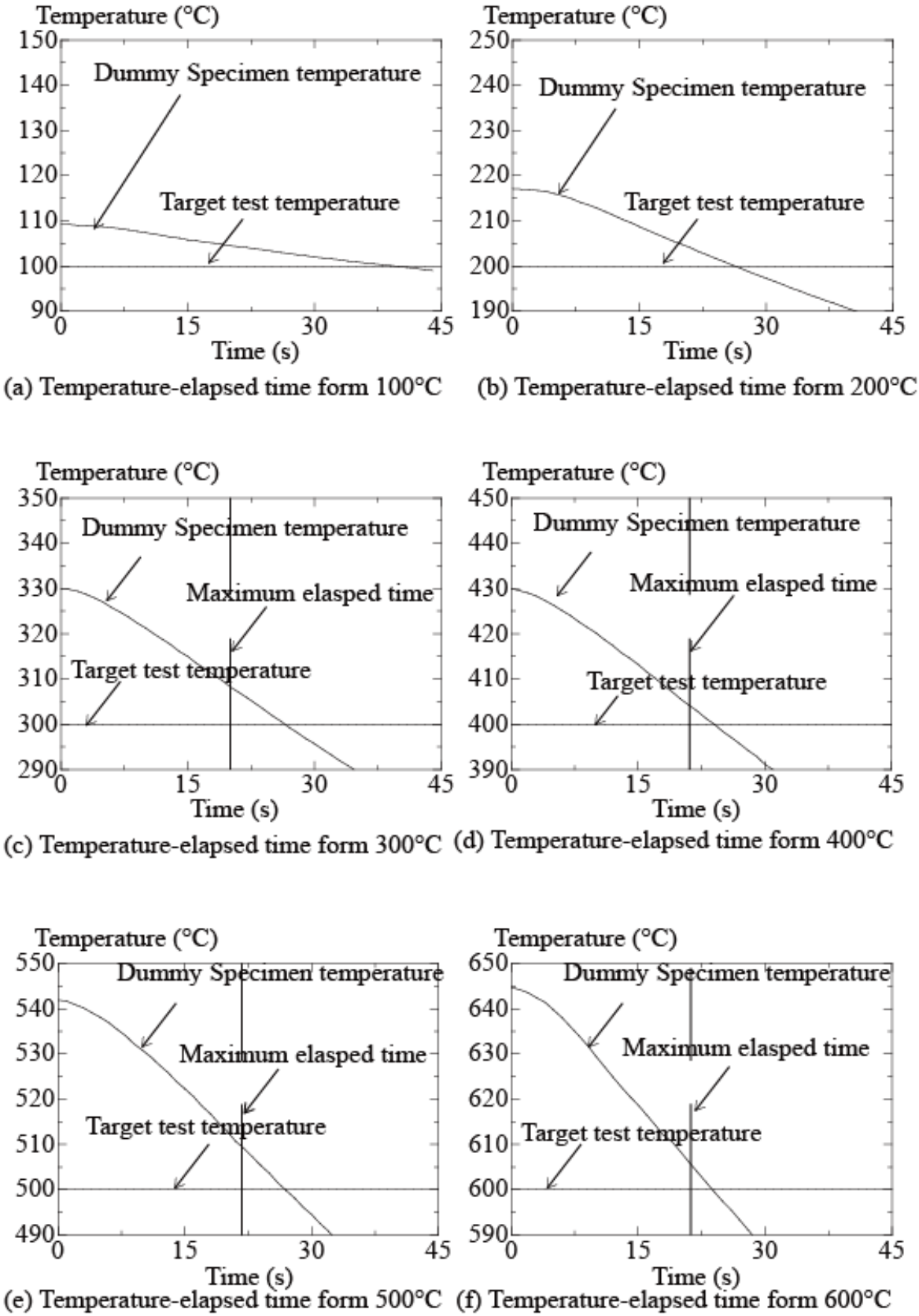

Figure 3.2.3. Elapsed time and specimen temperature relationships

3.2.3 Charpy impact test at ambient-temperature after fire on the specimens

For the test in ambient-temperature after heating and cooling processes on the cold-formed steel square hollow section specimens, water cooling and furnace cooling is considered first. Fig. 3.2.4 shows the specimens (FP and CP) temperature at cooling process. According to the figures, the cooling rate of water cooling was calculated as approximately 80 ºC/s. and the cooling rate of furnace cooling was approximately 0.042 ºC/s. Besides the test in ambient-temperature, the Charpy impact tests of these specimens were also conducted at −20, and −40 ºC. On the other hand, for the FPT12 specimens, the specimens were only heated to 500 and 800 ºC, and cooled by water- and furnace- cooling process. During the heating and cooling process, the FP and CP specimens were treated with the dimension of Charpy impact specimen (10 × 10 × 55 mm), but for the FPT12 specimens, it was treated with a dimension of 45 × 360 × 12 mm as shown in Fig 3.2.5. Fig. 3.2.6 shows the temperature change for FPT12 during the heating and cooling treatment. Both the furnace and water-cooling rate is same to the FP and CP specimens.

Furthermore, to replicate a situation where a steel column covered with fireproofing materials suffered from post-flashover fire or unprotected steel suffers from a localized fire at a distance, some Charpy impact tests were performed on air-cooled specimens that heated to 200, 300, and 400 ºC respectively. Owing to the cold-formed hollow section was subjected to the strong plastic process, it is considered that the strain ageing may accelerate in these medium temperatures (200,300, and 400 ºC), thus, the fracture toughness of these specimens may change after the heating and cooling process. Specimens were soaked at those medium temperatures for 30min, and cooled in the ambient temperature environment (approximately 30 ºC). Fig.3.2.7 shows the specimens temperature at air-cooling process. The cooling rate was approximately 0.33 ºC/s. However, the Charpy impact tests of these specimens were only conducted at 0 ºC, because of the lack of the specimens.

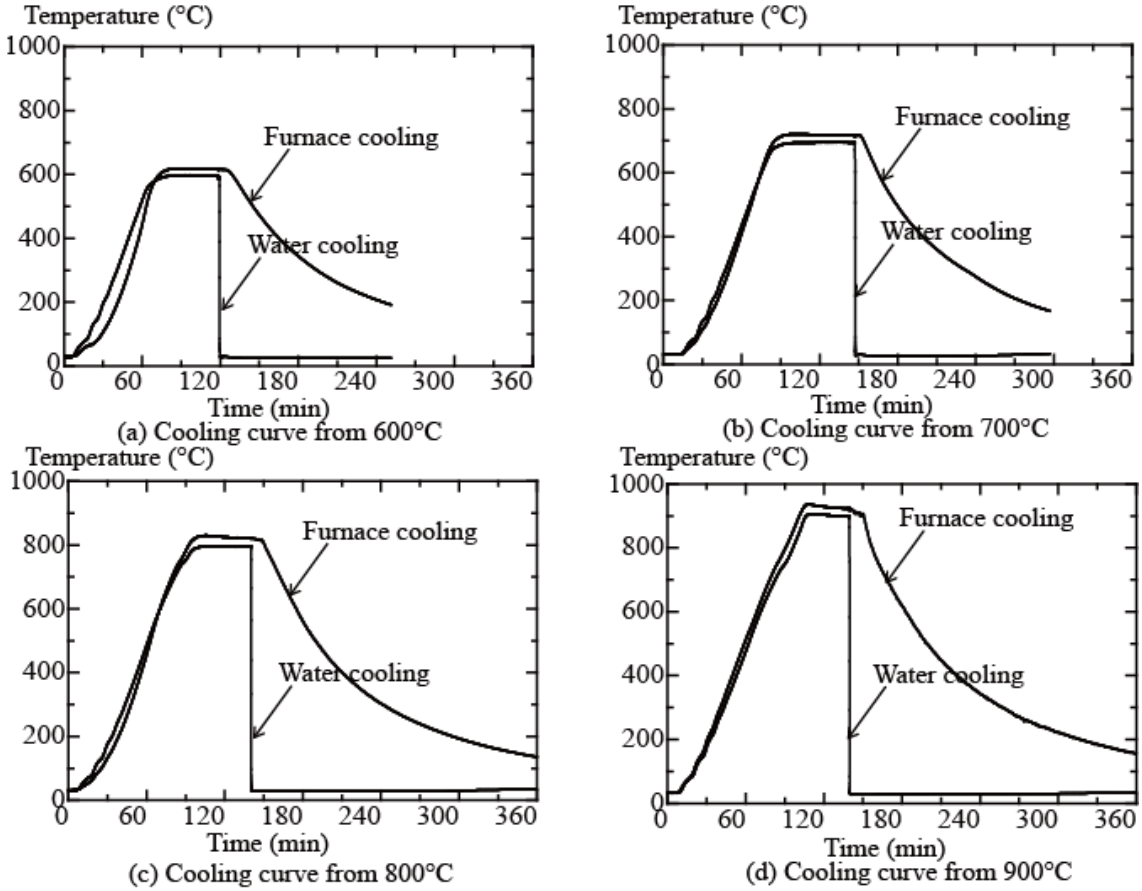

Figure 3.2.4. Specimen temperature at furnace- and water-cooling process for FP and CP specimen

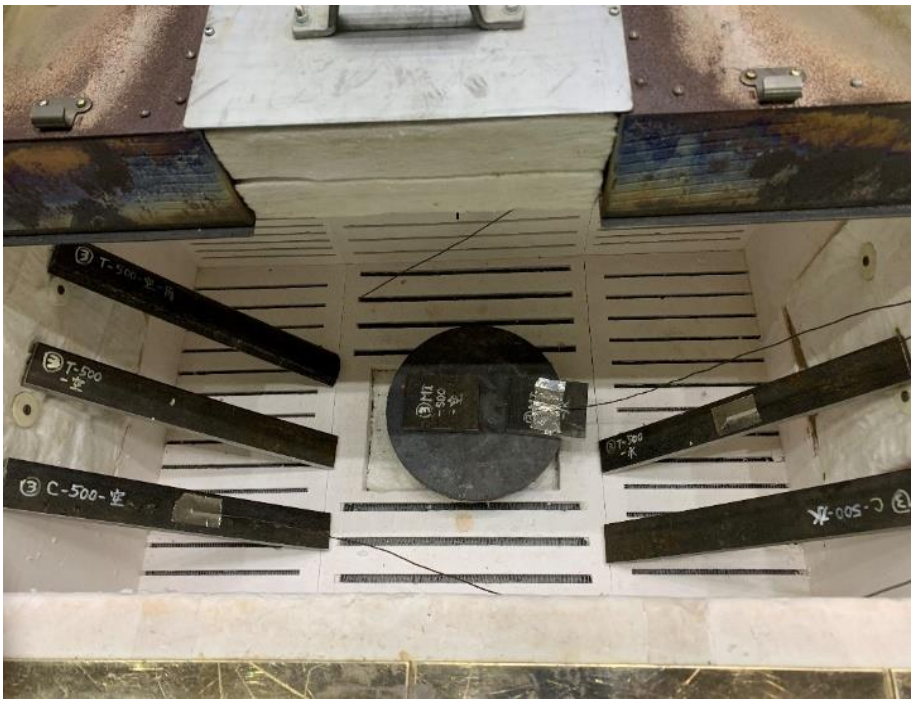

Figure 3.2.5. Heating and cooling treatment of FPT12

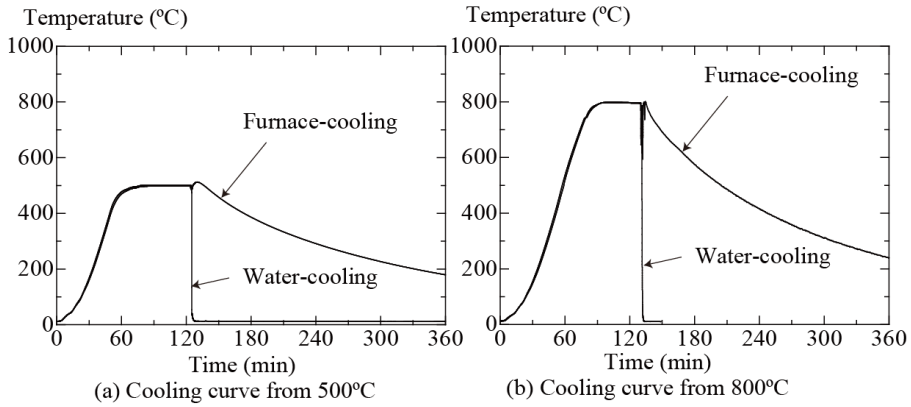

Figure 3.2.6. Specimen temperature at furnace- and water-cooling process for FPT12

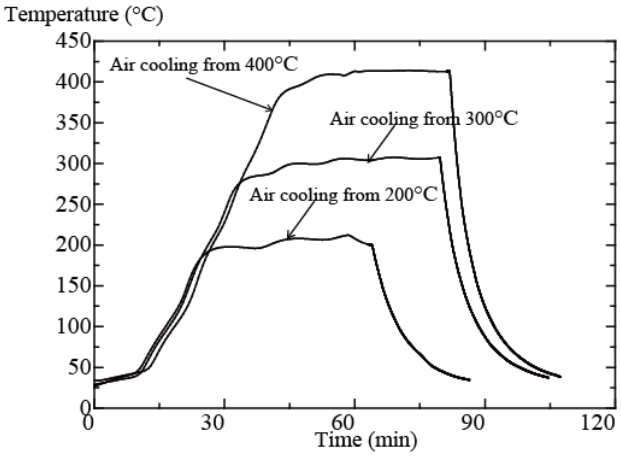

Figure 3.2.7. Specimen temperature at air-cooling process

3.3 Experimental result of cold-formed steel square hollow section

Before the Charpy impact test results, the coupon tensile test at high-temperature in cold-formed steel square hollow section used in this research is reported. The reason of conduct the coupon tensile test at high-temperature is to confirm the effect of the blue brittleness phenomenon on cold-formed steel square hollow section specimens at high-temperature. Fig.3.3.1 shows the detail of the coupon test specimens, the dimension of the coupon tensile test specimens is based on the JIS Z2201:1998[3.2]. Then, the test results of Charpy impact test for cold-formed steel square hollow section at the ambient and high-temperature, the results of the Charpy impact test for the specimens after the heating and cooling treatment are reported. In addition, considering the microstructure transition of the steel by the cooling process after the fire, the Vickers hardness and the Microstructure Observation were also conducted on the specimens after the heating and cooling treatment. Furthermore, the test results were compared with the results of the JIS SN400B steel that conducted in Chapter 2, because the BCR295 is formed from the JIS SN400B steel.

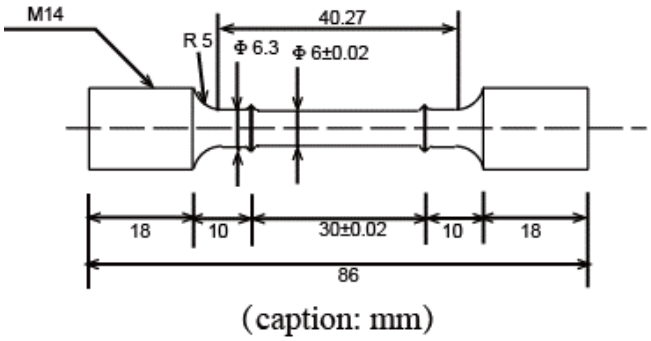

Figure 3.3.1 Coupon test specimen

3.3.1 High-temperature coupon test on cold-formed steel square hollow section

Figs.3.3.2-3.3.4 show the coupon tensile test result for both FP and CP specimens of □-250-250-16 mm cross section. Test temperatures are 20, 100, 200, 300, 400, 600, 700, and 800 ºC. Additionally, a coupon test at 500 ºC was conducted for the FP specimens. Specimens were heated to the target temperature and soaked at those temperatures for 1h before the loading test. A constant strain rate (0.3%/min) was used for the loading test. Fig.3.3.2 shows the engineering stress and engineering strain relationships of the test results. According to this figure, it is easy to know that the yield point and tensile strength of CP specimens are larger than the FP specimen. During the cold-formed manufacture, CP specimens were subjected to more plastic working than the FP specimens. Fig.3.3.3 shows the fracture elongation of the specimens at each temperature. According to the result, the fracture elongation reduces at the temperature within the rage of 100-300 ºC because of the blue brittleness phenomenon. However, the effect of the blue brittleness phenomenon is smaller than JIS SN400B steel, it is, the fracture elongation of the FP specimens increased at 200 ºC. It can be considered that the blue-brittleness phenomenon for the embrittle cold-formed steel was insignificant. Furthermore, Figs 3.3.4 (a)–(d) show the 0.2% offset yield strength ($\sigma_{0.2}$), the stress at strains of 1.0% ($\sigma_{1.0}$) and 2.0% ($\sigma_{2.0}$), and the tensile strength (σ_u) of the FP and CP specimens. Also, the result of JIS SN400B steel are plotted. According to Fig 3.3.4, except for the tensile strength, both the FP and CP specimens of the cold-formed steel square hollow section exhibit larger strength than JIS SN400B at the temperatures below 600 ºC, because of plastic processing at the ambient temperature. However, at the temperature exceed 600 ºC, the strength of cold-formed steel square hollow section is almost equal to the JIS SN400B steel, because the effects of plastic processing were eliminated at high temperatures. Furthermore, among the temperature ranges tested, the CP specimens subjected to strong plastic processing exhibited the highest strength at 20–300 ºC. Coupon tensile test verified the effect of the plastic processing working on the cold-formed steel square hollow section.

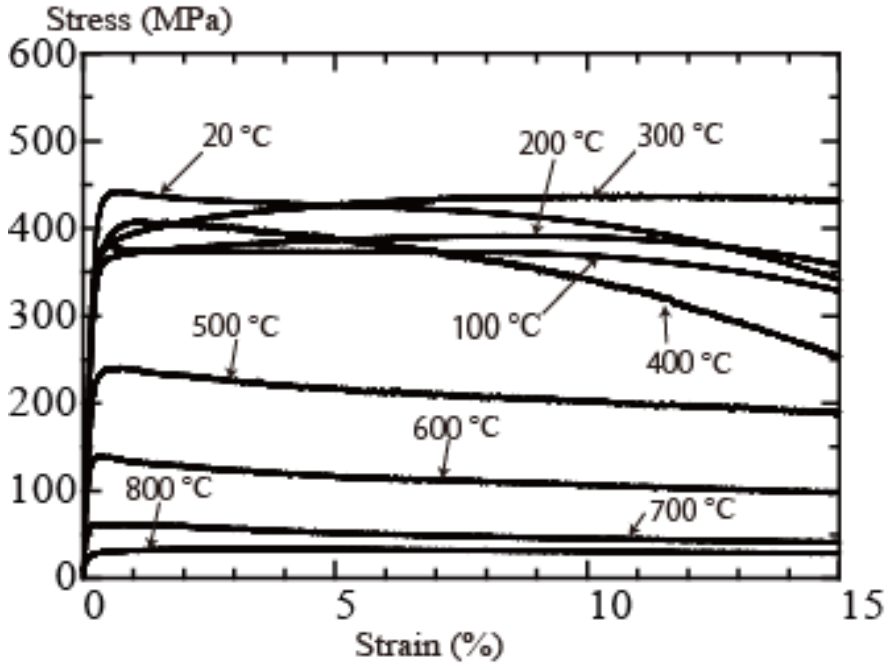

(a) Flat Part (FP)

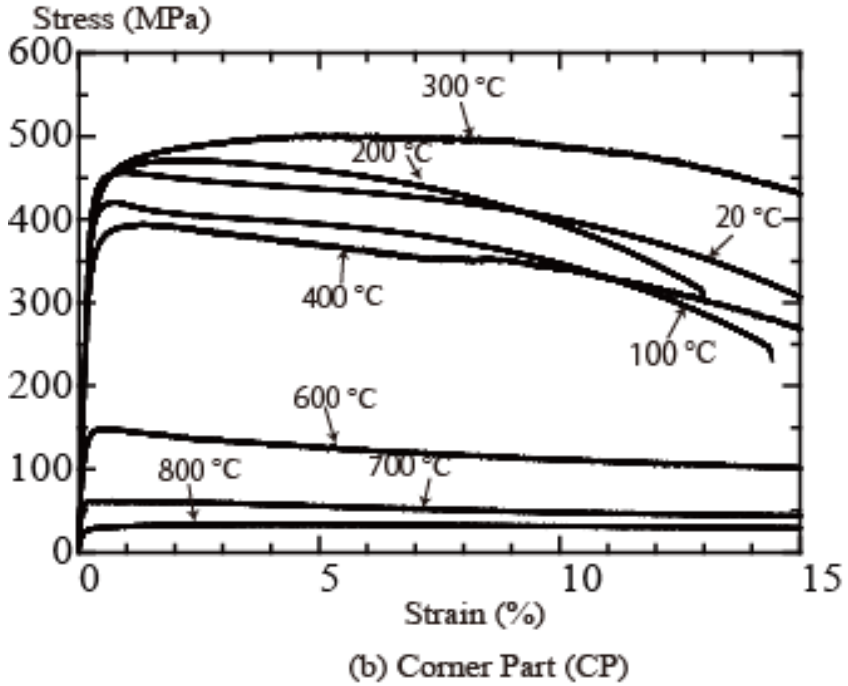

(b) Corner Part (CP)

Figure 3.3.2 Stress-strain relationships at ambient and elevated temperature

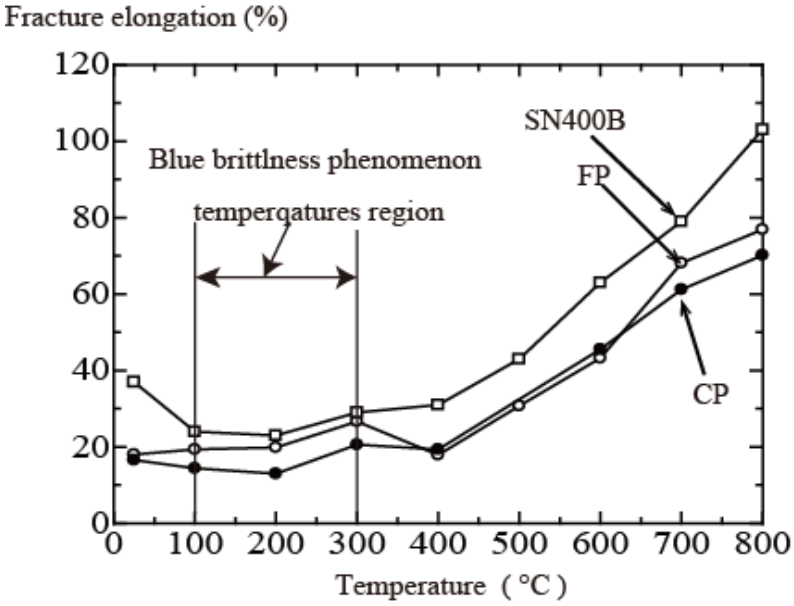

Figure 3.3.3 Breaking elongation at high-temperature

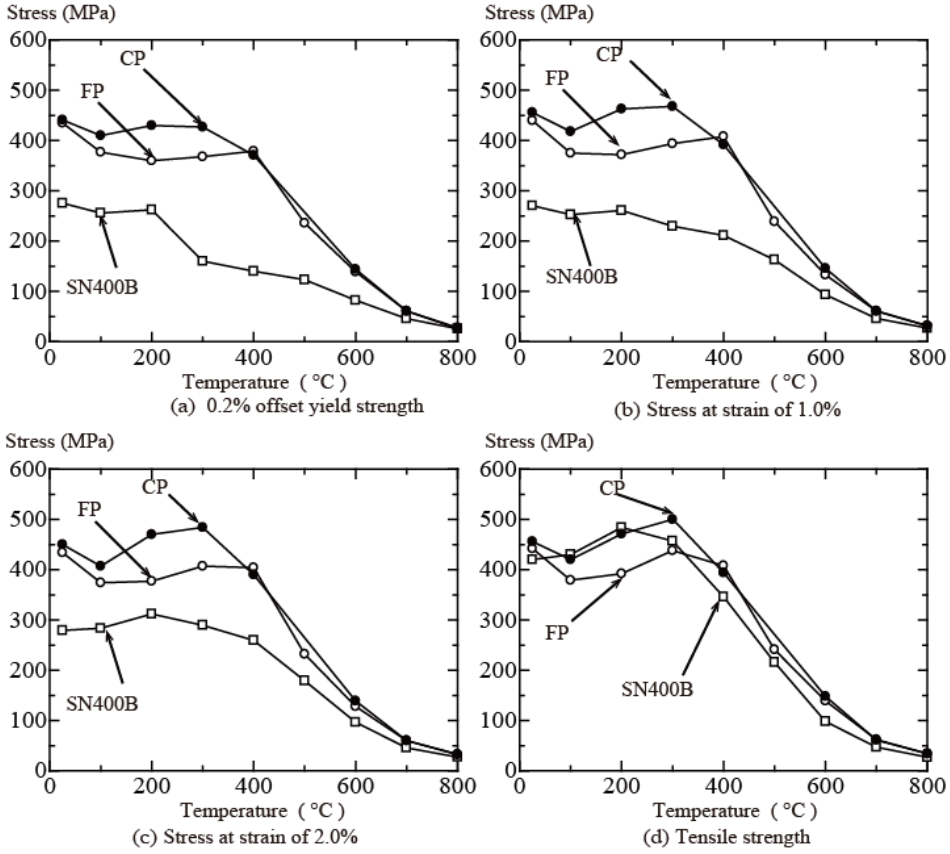

Fig.3.3.4 Strength reduction at high-temperature

3.3.2 High-temperature Charpy impact test for FP and CP specimens

Table 3.3.1 lists the test result of the Charpy impact energies of the cold-formed steel square hollow section specimens and the base metal (BM) of the welded connections at low- and high-temperatures. The average of three specimens at each test temperature, and the value are presented the standard deviation of the test results in parentheses. Fig.3.3.5 shows the results presented in Table 3.3.1. Figs 3.3.6-3.3.8 show the fracture surface of the specimens after the Charpy impact tests.

As shown in Fig. 3.3.5, the Charpy impact energies at subzero temperature were lower than 20J, except for the FP specimens at -20ºC. And both the FP and CP specimens exhibited lower Charpy impact energies than SN400B because of the plastic processing. According to Fig 3.3.6, FP and CP specimens at -70 ºC broken into two pieces and exhibit a typical brittle surface with chevron patterns.

At 0 ºC, both the FP and CP specimens exhibited high Charpy impact energies (>200 J). cold-formed steel square hollow section is requiring a Charpy impact energy that is larger than 27J at 0 ºC to avoid brittle fractures during severe earthquakes. This test result confirms that the both the FP and CP specimens of the cold-formed steel square hollow section cross section used in this study satisfy the design requirements. And as shown in Fig.2.4.6, the specimens exhibited the ductile fracture surface at 0 ºC.

For the test result of the specimens at blue-brittleness phenomenon temperatures range (100–300 ºC), refer to Fig.3.3.8, all the specimens exhibit the typical ductile fracture surface. According to the Fig.3.3.5, the Charpy impact energies decreased at 100 ºC, due to the effect of blue-brittleness phenomenon. However, the minimum energy was still >180 J at this temperature. The maximum Charpy impact energy, which exceeded 250 J, was observed at 200 ºC in all the specimens. Therefore, it is considered that the blue-brittleness phenomenon does not affect the Charpy impact energies.

In the tests above 300 ºC (high-temperature), the Charpy impact energies of the specimens gradually decreased with an increase in the temperature. It is because the yield point and tensile strength gradually decreases at elevated temperature. However, the specimens exhibited ductile fracture surfaces at these temperatures (Fig.3.3.8). Furthermore, as shown in Fig.3.3.3, the breaking elongation significant increase at high-temperature. Therefore, it is considered that the brittle fracture hardly occurs at high-temperature.

Table 3.3.1 Charpy impact test result at high-temperature

Temperature (ºC)	Charpy impact energies (J)		
	FP	CP	
-70	10.2 (1.5)	9.1 (0.3)	Ave. (S.D.)
-40	10.9 (1.9)	14.9 (1.4)	
-20	52.6 (59.4)	19.8 (1.6)	
0	222.1 (11.9)	218.7 (9.1)	
100	212.3 (35.7)	195.4 (43.4)	
200	272.2 (25.1)	279.4 (29.8)	
300	226.2 (9.1)	243.8 (3.6)	
400	165.1 (1.5)	154.3 (15.5)	
500	117.4 (4.3)	97.1 (7.0)	
600	209.4 (42.0)	156.1 (27.4)	

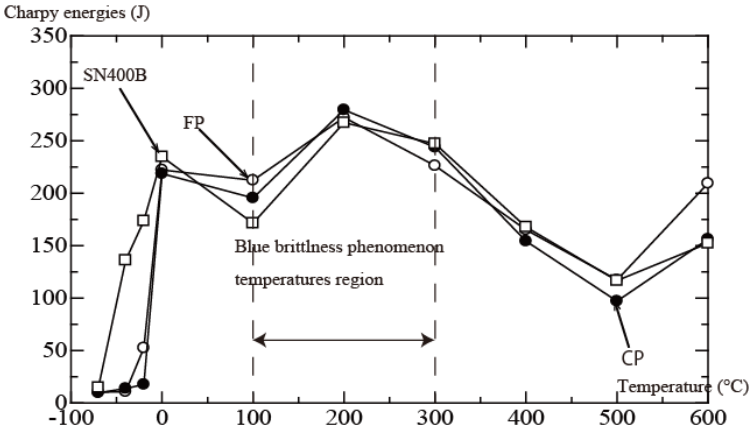

Fig.3.3.5 Experimental results of the Charpy impact test at high temperature

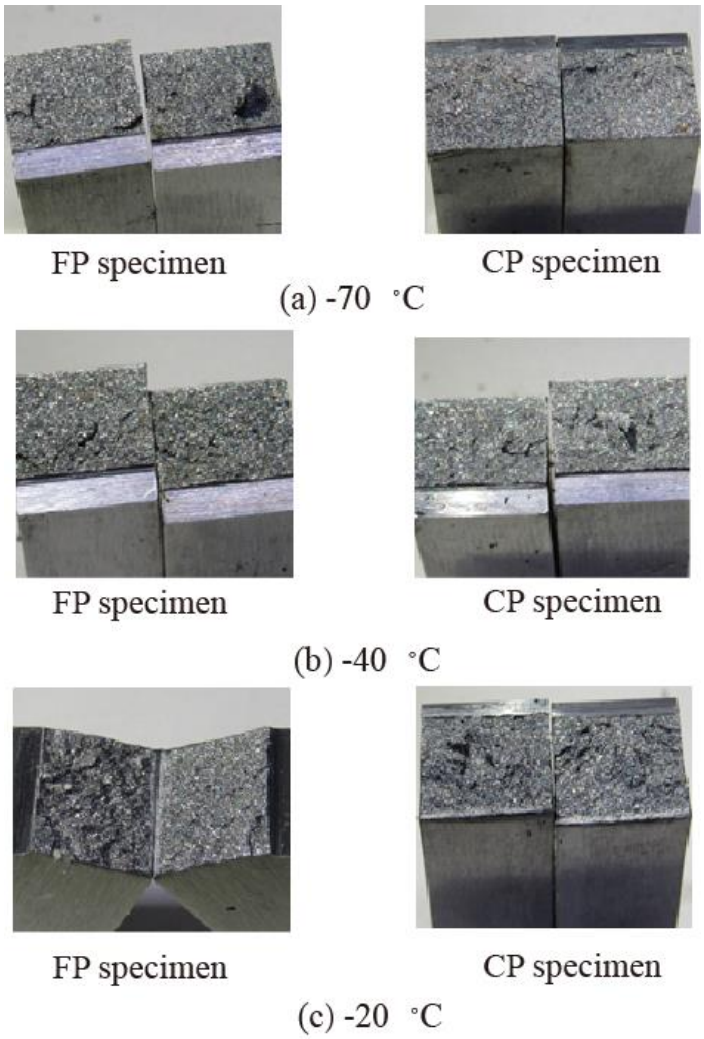

Fig.3.3.6 Fracture surface of specimen at subzero temperature

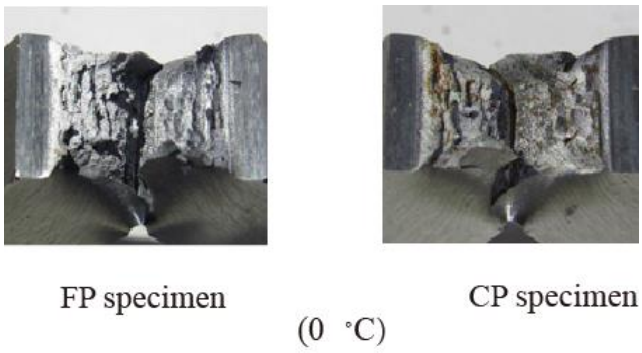

Fig.3.3.7 Fracture surface of Specimen at 0 ºC

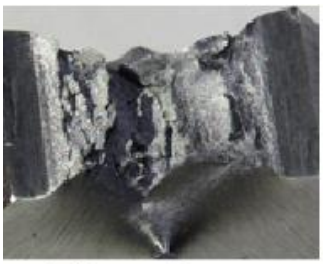

FP specimen

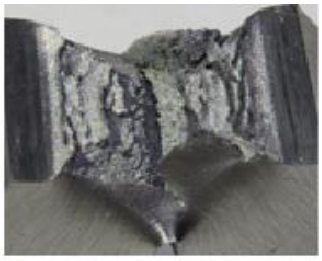

CP specimen

(a) 100 °C

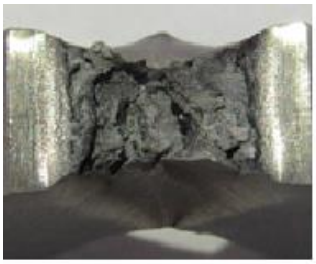

FP specimen

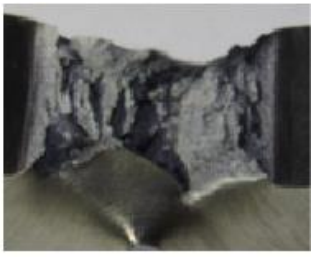

CP specimen

(b) 200 °C

FP specimen

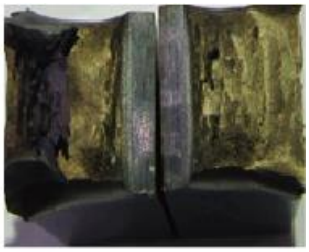

CP specimen

(c) 300 °C

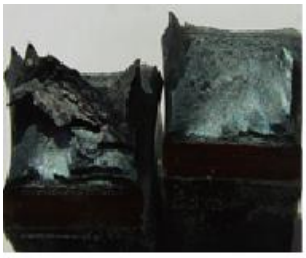

FP specimen

CP specimen

(d) 400 °C

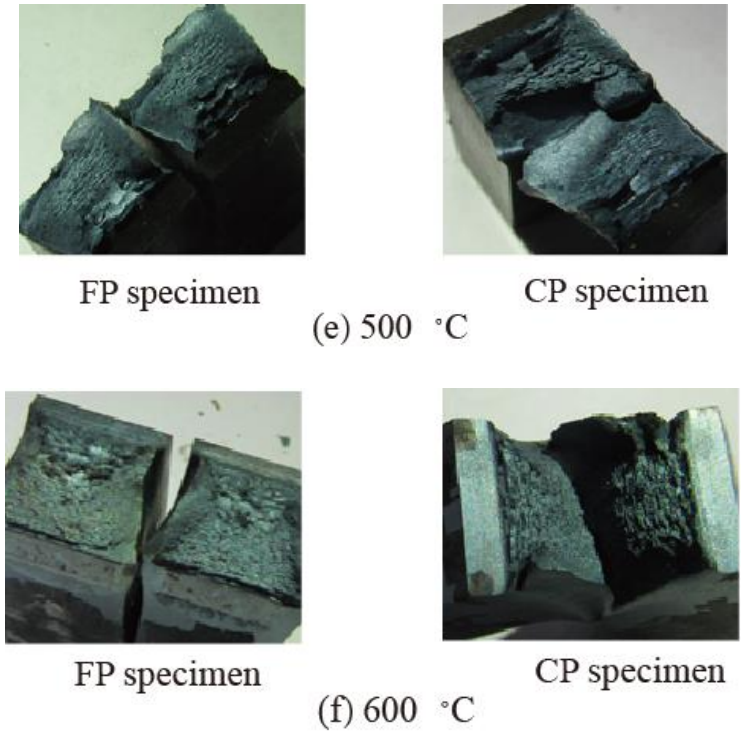

Fig.3.3.8 Fracture surface of specimen at high-temperature

3.3.3 Charpy impact test results at ambient temperature after heating and cooling processes for FP and CP specimens

Table 3.3.2 lists the average value and standard deviation of the test result of the Charpy impact energies of the specimens after heating and cooling process at 0 ºC. Average values very close to 300 J (the maximum Charpy impact energy of the Charpy impact machine) are the experimental results when the measured energies reached the maximum capacity of the test machine, for these sufficiently large values, the standard deviations were not listed. Fig.3.3.9 shows the results presential in Table 2.4.2. Figs 3.3.10 and 3.3.11 show the fracture surface of the water- and furnace-cooled specimens after the Charpy impact tests, respectively. Furthermore, the Charpy impact test results of the base metal of SN400B were also presented in the figures.

According to Fig.3.3.9, for the specimens that were heated to 600 ºC, both water- and furnace-cooled specimens possess higher Charpy impact energies than 150J. FP specimens exhibited a similar Charpy impact energies to the SN400B steel. Refer to Figs.3.3.10 and 3.3.11, typical ductile surfaces were observed on the water-cooled specimen and furnace-cooled CP specimen after 600 ºC heating, and ductile-brittle surfaces were observed on the furnace-cooled FP specimen after 600 ºC heating.

For the water-cooled specimens that were heated to 700 and 800 ºC, the Charpy impact energies is lower than that of the untreated specimens. However, except for the water-cooled FP specimens that were heated to 700 ºC, all the values are higher than 27J. As shown in Fig.3.3.10, all the specimens exhibit the brittle fracture surface. On the other hand, for the furnace-cooled specimens that were heated to 700 and 800 ºC,

the Charpy impact energies is close to 300J. According to Fig.3.3.11, these specimens exhibit the ductile fracture surface.

Furthermore, for the water-cooled specimens that were heated to 900 ºC, the Charpy impact energies recovered to a higher value than those of untreated specimens, and clear ductile surface were observed. For the furnace-cooled specimen that were heated to 900 ºC, the Charpy impact energies are still larger than 250 J, and those specimens also exhibit the ductile fracture surfaces.

Conclusively, quenching during the water-cooling process significantly reduced the Charpy impact energies of the specimens heated to 700 and 800 ºC, and clear brittle fractures were observed in these specimens; conversely, if the specimens were heated to 900 ºC, the Charpy impact energies recovered to a high value and the fracture surfaces developed to ductile-brittle fractures. These trends are similar to those of JIS SN400B specimens.

Table 3.3.2 Charpy impact test result at 0 ºC

Test Temperature		**0 ºC**			
Cooling Process		**Water-Cooling**		**Furnace-Cooling**	
Specimens		**FP**	**CP**	**FP**	**CP**
		Ave. (S.D.)	**Ave. (S.D.)**	**Ave. (S.D.)**	**Ave. (S.D.)**
untreated	**J**	222.1 (11.9)	218.7 (9.1)	222.1 (11.9)	218.7 (9.1)
600 ºC treated	**J**	169.1 (48.3)	232.7 (34.4)	298.1 (-)	298.1 (-)
700 ºC treated	**J**	24.9 (2.3)	55.1 (61.8)	298.2 (-)	298.2 (-)
800 ºC treated	**J**	51.5 (36.0)	90.7 (40.3)	298.2 (-)	298.5 (-)
900 ºC treated	**J**	298.5 (-)	298.5 (-)	273.3 (4.5)	277.7 (1.2)

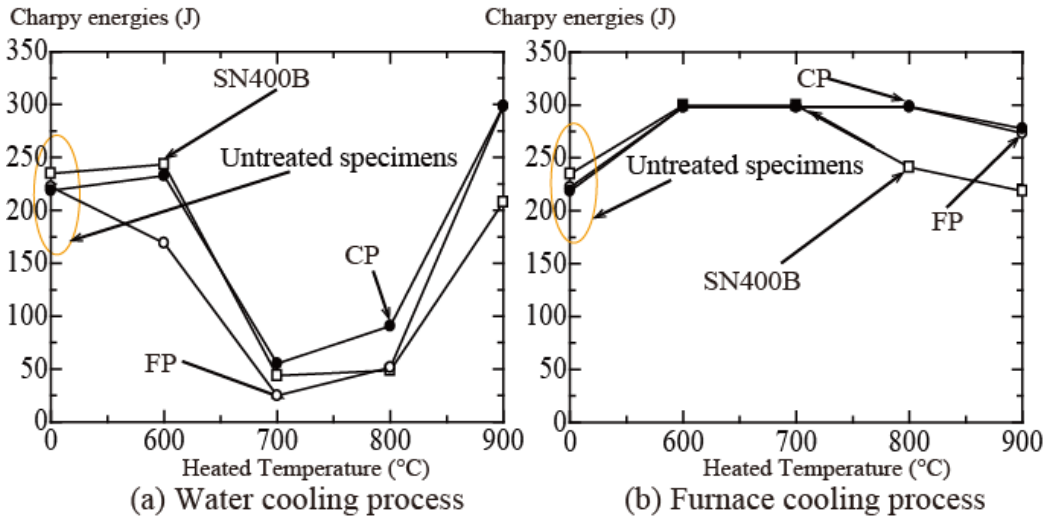

Fig.3.3.9 Experiment results of Charpy impact test at 0 ºC after heating and cooling process

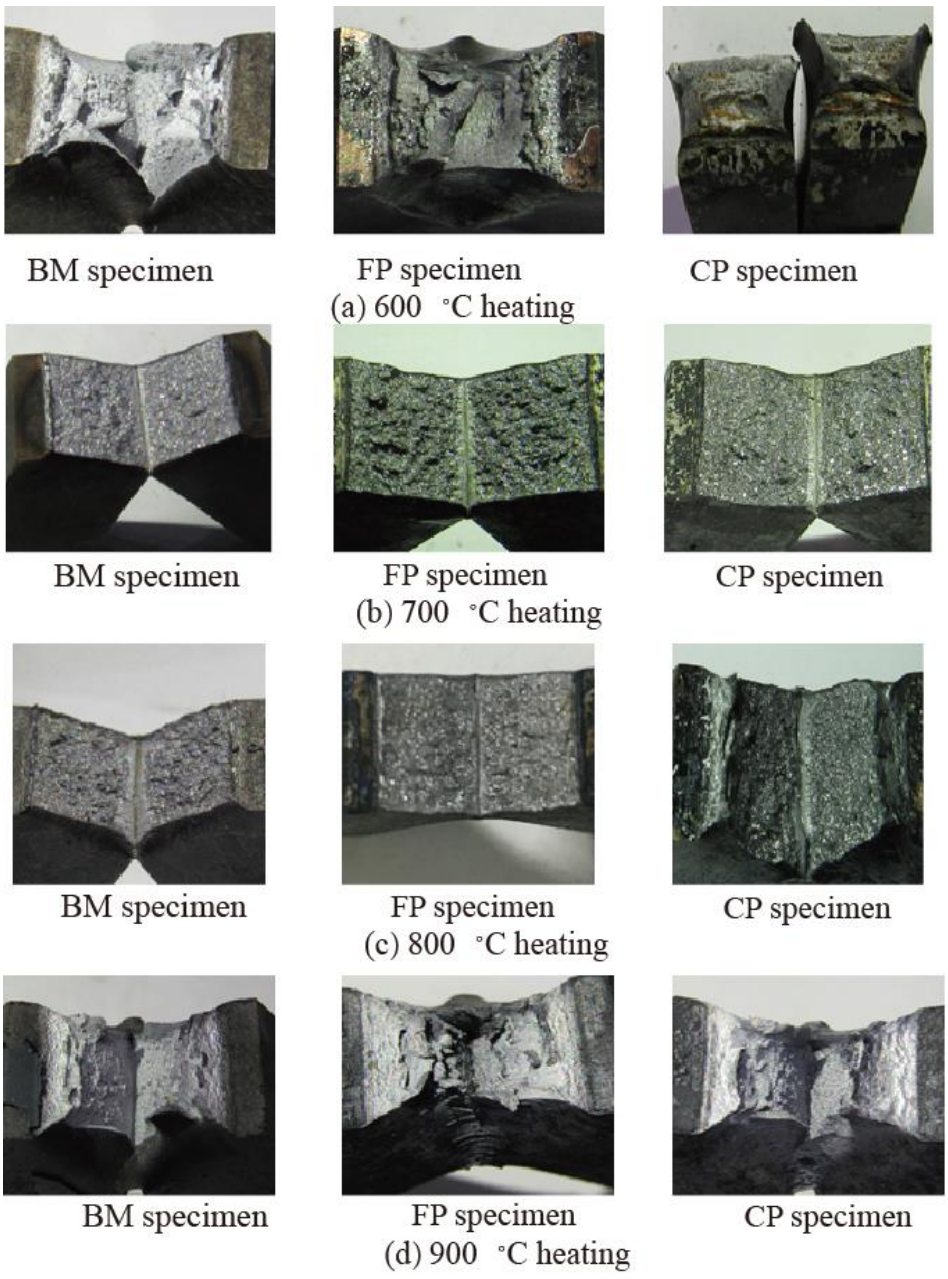

Fig.3.3.10 Fracture surface of water-cooled specimens at 0 ºC

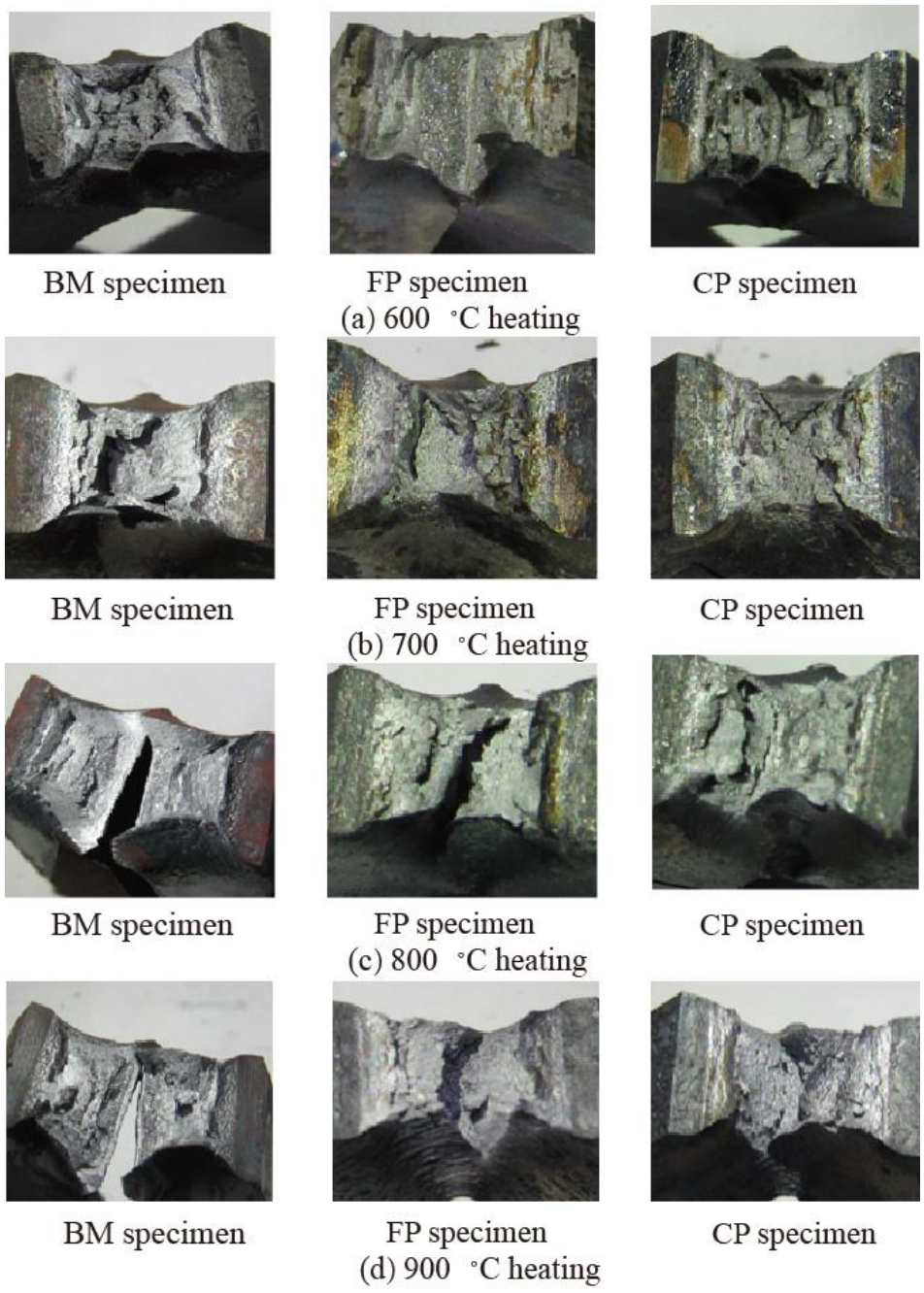

Fig.3.3.11 Fracture surface of furnace-cooled specimens at 0 ºC

3.3.4 Charpy impact test results at −20 and −40 ºC after heating and cooling processes for FP and CP specimens

Charpy impact test for the specimens after heating and cooling process was also conducted at the test temperatures of −20 and −40 ºC. Figs. 3.3.12 and 3.3.13 show the results at −20 and −40 ºC which listed in Tables 3.3.3 and 3.3.4, respectively.

The Charpy impact energies of the specimens tested were lower than those tested in the ambient-

temperature, and the specimens of cold-formed steel (FP and CP specimens) had lower Charpy impact energies than JIS SN400B. The specimens exhibited brittle fracture; however, both the water- and furnace-cooled specimens heated at 900 ºC still exhibited high Charpy impact energies and ductile fracture surfaces in the low-temperature tests.

Table 3.3.3 Charpy impact test result at -20 ºC

Test Temperature		**-20 ºC**			
Cooling Process		**Water-Cooling**		**Furnace-Cooling**	
Specimens		**FP**	**CP**	**FP**	**CP**
		Ave. (S.D.)	**Ave. (S.D.)**	**Ave. (S.D.)**	**Ave. (S.D.)**
untreated	**J**	52.6 (59.4)	19.8 (1.6)	52.6 (59.4)	19.8 (1.6)
600 ºC treated	**J**	38.5 (18.7)	56.5 (63.8)	120.5 (154.3)	192.1 (141.6)
700 ºC treated	**J**	13.5 (1.0)	14.0 (1.7)	23.8 (4.5)	30.0 (13.0)
800 ºC treated	**J**	17.2 (2.4)	18.2 (6.6)	190.0 (62.4)	204.2 (21.1)
900 ºC treated	**J**	298.6 (-)	298.4 (-)	220.1 (39.3)	242.7 (39.8)

Table 3.3.4 Charpy impact test result at -40 ºC

Test Temperature		**-40 ºC**			
Cooling Process		**Water-Cooling**		**Furnace-Cooling**	
Specimens		**FP**	**CP**	**FP**	**CP**
		Ave. (S.D.)	**Ave. (S.D.)**	**Ave. (S.D.)**	**Ave. (S.D.)**
untreated	**J**	10.9 (1.9)	14.9 (1.4)	10.9 (1.9)	14.9 (1.4)
600 ºC treated	**J**	12.1 (2.3)	11.6 (2.3)	12.6 (2.1)	14.9 (3.6)
700 ºC treated	**J**	8.8 (2.4)	8.2 (1.1)	10.6 (1.7)	11.1 (1.8)
800 ºC treated	**J**	11.7 (1.9)	14.8 (4.7)	16.1 (3.7)	17.8 (3.3)
900 ºC treated	**J**	271.3 (25.5)	287.4 (20.1)	128.9 (99.8)	142.3 (83.8)

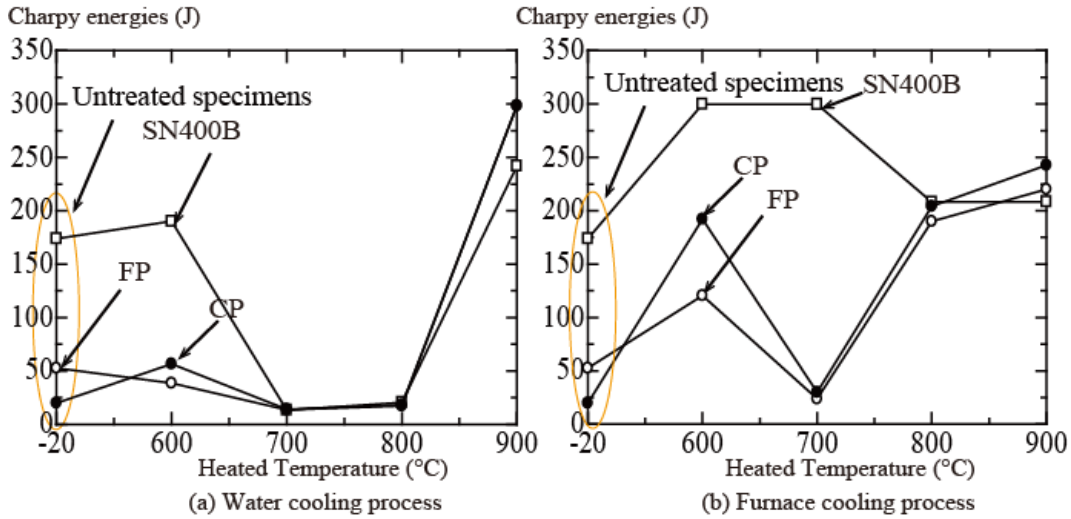

Fig.3.3.12 Experiment results of Charpy impact test at -20 ºC after heating and cooling process

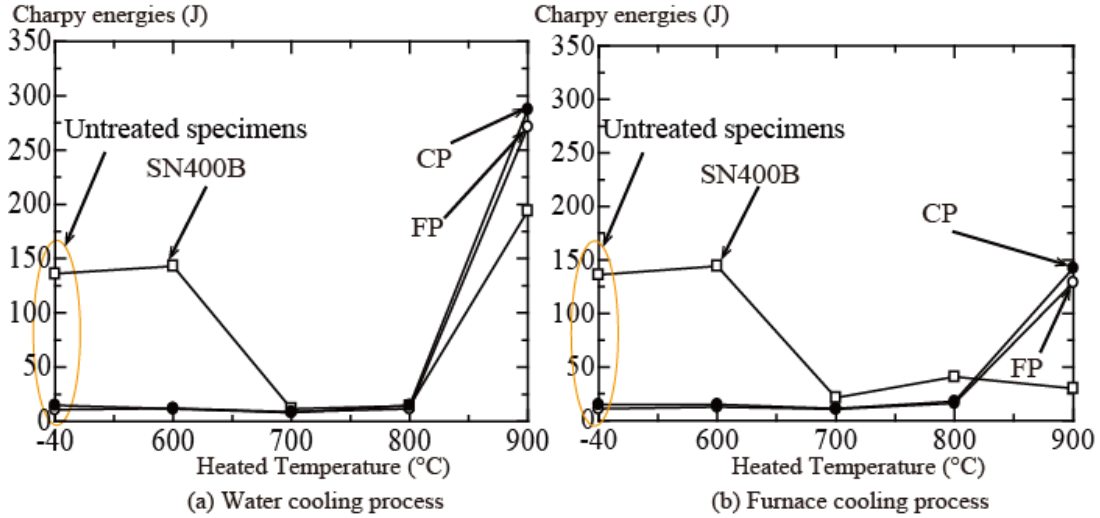

Fig.3.3.13 Experiment results of Charpy impact test at -40 ºC after heating and cooling process

3.3.5 Charpy impact test results at 0 ºC after air-cooling processes for FP and CP specimens

Table 3.3.5 shows the Charpy impact test results of the air-cooled specimens at 0 °C. As described in section 3.2.3, specimens were heated to 200-400 °C. Figs 3.3.14 and 3.3.15 show the test result and the fracture surface of the tests respectively.

As shown in Fig.3.3.14, the CP specimens at 200 °C exhibit lower Charpy impact energies than the FP specimens. And in Fig.3.3.15, CP specimens exhibit a brittle fracture surface, but FP specimens exhibit a ductile-brittle fracture surface. For the test results at 300 and 400 °C, the impact energies of the FP specimens subjected to the air-cooling treatment gradually decreased with the increasing heat temperature. And the CP specimens maintain a lower value than 90 J, and both FP and CP specimens exhibit the brittle fracture surface. The air-cooling process is low-speed cooling. Generally, the microstructure of these steel is not changed by subjected low-speed cooling from the temperature below 400 °C. However, the Charpy

impact energies of the cold-formed steel square hollow section cooled from the medium-temperature range (200–400 ºC) clearly decreased; on the contrary, the specimens slowly cooled from the high-temperature region (600–900 ºC) did not exhibit this tendency. Considering the reuse of the cold-formed steel square hollow section column subjected to a low fire temperature, this column may appear to be intact under visual observations at the damage diagnostics; generally, this member may be reused after fire. However, the CP specimens may occur brittleness fracture if it continues to be used as the resistance-seismic structure after fire. Therefore, careful investigation of the cold-formed steel square hollow section column at the damage diagnostics after fire is required, particularly from the viewpoint of the fracture toughness change due to the relatively low-temperature heating.

Table 3.3.5 Charpy impact test result at 0 ºC (air-cooling processes)

Test Temperature		**0 ºC**	
Cooling Process		**Air-Cooling**	
Specimens		**FP** **Ave. (S.D.)**	**CP** **Ave. (S.D.)**
untreated	**J**	222.1 (11.9)	218.7 (9.1)
200 ºC treated	**J**	233.7 (7.0)	71.7 (99.1)
300 ºC treated	**J**	190.2 (78.8)	87.2 (105.1)
400 ºC treated	**J**	117.8 (75.6)	78.3 (49.3)

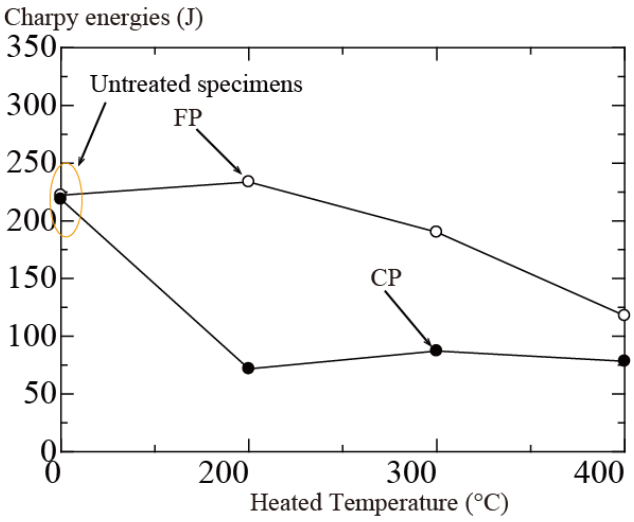

Fig.3.3.14 Experiment results of Charpy impact test at 0 ºC after heating and air-cooling process

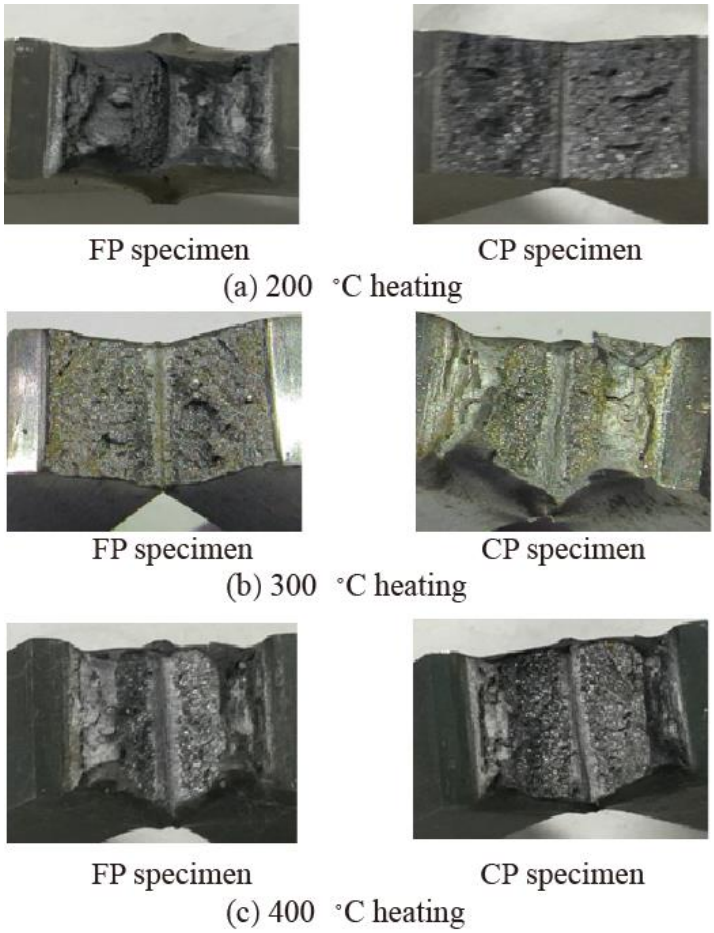

Fig.3.3.15 Experiment results of Charpy impact test at 0 ºC after heating and air-cooling process

3.3.6 Charpy impact test results at 0 ºC after air-cooling processes for FPT12 specimens

Table 3.3.6 shows the Charpy impact test results of the FPT12 (Fig.3.2.2) at 0 °C. Fig.3.3.16 shows the test results of FPT12 after heating and cooling process.

According to the Fig.3.3.17, the Charpy impact test of water-cooled FPT12 that were heated to 500 and 800 °C increased. On the other hand, the Charpy impact energies of the furnace-cooled FPT12 increased when the heating temperature were 500 °C, but decreased after heated to 800 °C and exhibit a brittle fracture behaviours. Fig.3.3.17 compared the test result of FP, CP, and FPT12 after the heating and cooling process. The Charpy impact energies of untreated FPT12 is lower than the untreated FP and CP specimens. Because these two kinds of cross-sections are made by different manufacturing lot. All of the test result of FPT12 exhibit a lower value than the FP and CP specimen, excepted for water-cooled from 800 °C. It is considered if the Charpy impact energies for the untreated cold-formed steel square hollow section is low, and brittle fracture of the member might occur when it was reused after fire.

Table 3.3.6 Charpy impact test result at 0 ºC for FPT12

Test Temeprature		0ºC	
Cooling Process		Water-Cooling	Furnace-Cooling
Untreated	J	46	46
500ºC treated	J	98	120
800ºC treated	J	158	16

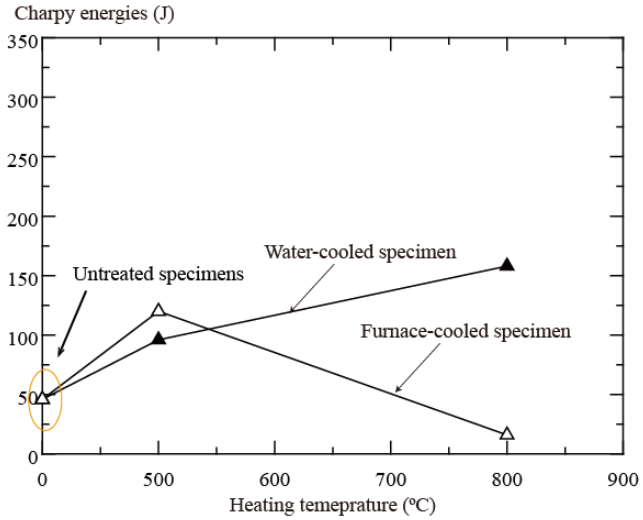

Fig.3.3.16 Experiment results of FPT12 after heating and cooling process

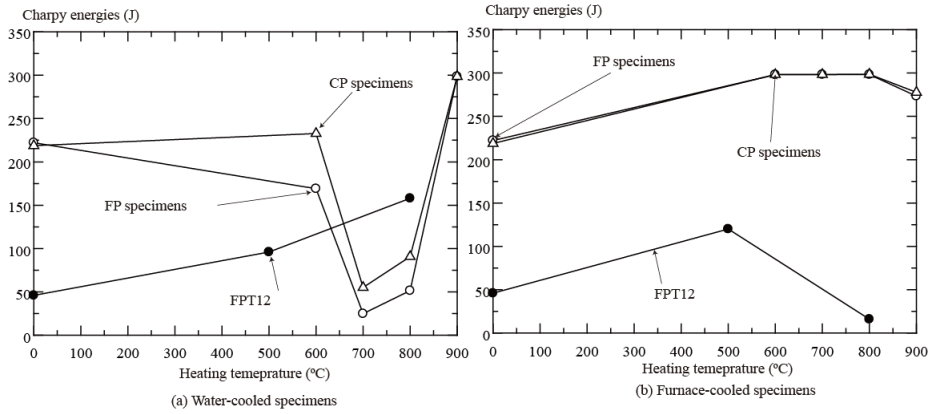

Fig.3.3.17 Results comparison

3.3.7 Vickers Hardness test and microstructure observation

3.3.7.1 FP and CP specimens

The Vickers hardness test and Microstructure Observation were also conducted on the FP and CP specimens after water-, furnace-, and air-cooled specimens to study what cause the change of the Charpy impact energies. Both FP and CP specimens in after the following treatment were conducted the Vickers

hardness test and Microstructure Observation: specimens without heating and cooling process, water- and furnace-cooled specimens after 700 ºC heating, water- and furnace-cooled specimens after 900 ºC heating, air-cooled specimens after 200 ºC heating, and air-cooled specimens after 400 ºC heating. Figs 3.3.18 and 3.3.19 show the Vickers Hardness test result of the specimens, and Figs 3.3.21-3.3.22 show the microstructure observation.

As shown in Fig.3.3.18, water-cooled specimens exhibit a larger Vickers hardness, but furnace-cooled specimens exhibit lower value than the untreated specimens. In other words, the tensile strength of the water-cooled specimens increased, and those of furnace-cooled specimens decreased. This is because of the mechanical properties change owing to the quenching effect by the water. The increasing of tensile strength predicted the microstructure change of the specimens after the heating and cooling process.

On the other hand, as shown in Fig.3.3.19, air-cooled specimens exhibit a little larger Vickers hardness, than the untreated specimens. As the conclusion, air-cooled specimens possess larger tensile strength than untreated specimens.

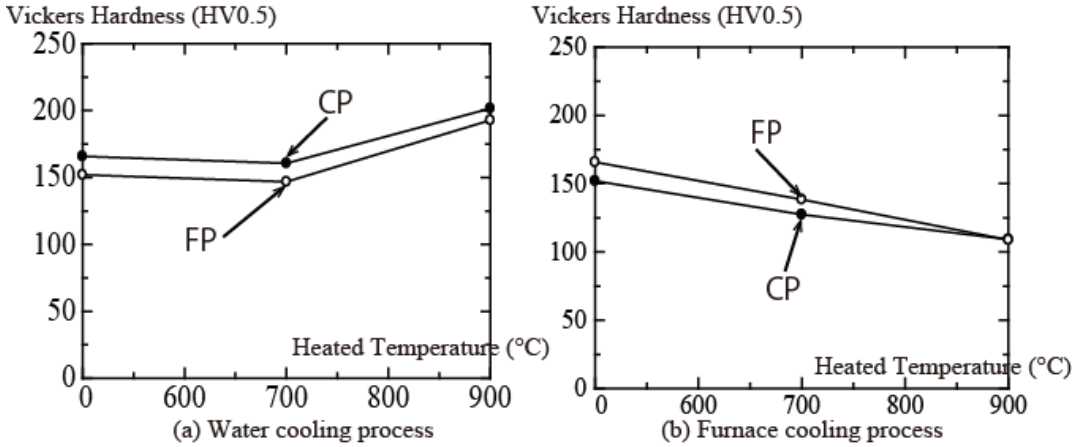

Fig.3.3.19 Vickers Hardness test result on water- and furnace-cooled specimens

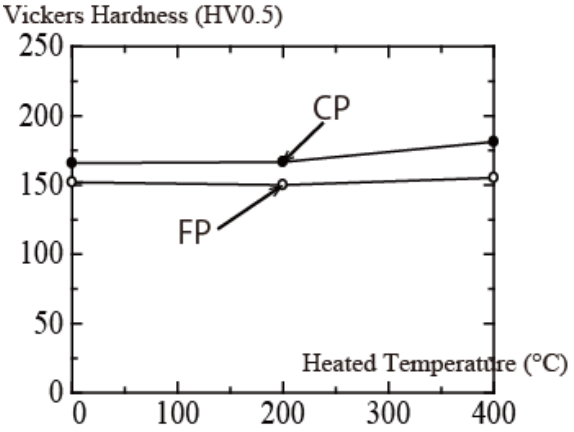

Fig.3.3.20 Vickers Hardness test result on air-cooled specimens

3.3.7.2 FPT12 specimens

Fig.3.3.20 shows the photos of the Vickers Hardness test of the FPT12. The Vickers Hardness is only measured on the water- and furnace-cooled specimens that were subjected to 800 ºC heating. The hardness of furnace-cooled specimens is 107 HV, and for the water-cooled specimen, it is 170 HV. Therefore, the tensile strength of furnace-cooled and water-cooled specimens is calculated as 350 MPa and 539 MPa respectively.

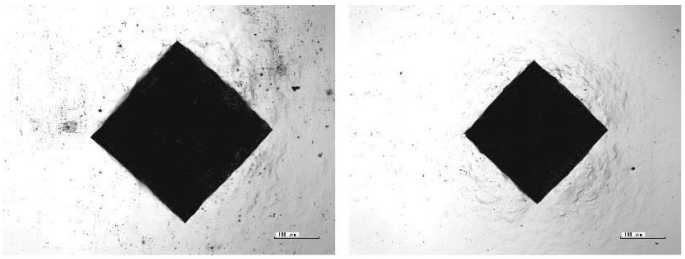

(a) Furnace-cooled specimen (b) Water-cooled specimens

Fig.3.3.20 Vickers Hardness test of FPT12

3.3.8 Microstructure observation

1) Microstructure observations of water- and furnace-cooled specimens (FP and CP specimens)

As shown in Fig.3.3.21 and 3.3.22, FP and CP specimens subjected to the same treatments exhibited similar microstructures, that is, the plastic strain induced by plastic processing did not affect the microstructure. The untreated specimens exhibited ferrite and pearlite microstructures (F+P), which is typical for the low-carbon steel at ambient temperatures. The furnace-cooled specimens exhibited F+P microstructures, similar to those of the untreated specimens. However, for the specimens heated to 900 ºC, local segregation of cementite due to slow cooling (furnace cooling) was observed; therefore, the Charpy impact energies of these specimens were slightly reduced, as shown in Fig.3.3.9. Furthermore, the effect of the plastic processing was eliminated by the heating above the transformation point, and the tensile strength of these specimens decreased (Fig.3.3.18).

In contrast, for the water-cooled specimens, specimens that were heated to 900 ºC exhibited clear martensitic microstructures because of the quenching from a temperature higher than the transformation point. Accordingly, the specimens water-cooled from 900 ºC had a higher Charpy impact energy and Vickers hardness than the untreated specimens. However, the water-cooled specimens heated to 700–800 ºC were imperfectly quenched from the two-phase (ferrite and austenite) temperature; therefore, brittle fracture occurred, and the Charpy impact energies decreased (Fig.3.3.9).

In summarizes, cold-formed steel square hollow section specimens that subjected to water- and furnace-cooled treatment exhibit the similar microstructure to the BM specimens of JIS SN400B steel, which described in Chapter 2.

2) Microstructure observations of air-cooled specimens (FP and CP specimens)

Fig.3.3.23 shows the microstructures of the FP and CP specimens subjected to air cooling from 200 and 400 ºC. All the specimens exhibited typical F+P microstructures, which is similar to the microstructure of untreated specimens; thus, the microstructure was not changed by the air cooling after heating below 400 ºC. However, according to the Fig.3.3.14, the Charpy impact energies of the air-cooled specimens were lower than those untreated specimens; in Fig.3.3.19, the tensile strength of air-cooled specimens was larger than those of the untreated specimens. This can explain as follows: in the significantly deformed parts, e.g. the CP in the square hollow cross section, the strain ageing [3.3] progressed with the temperature rise. In general, with a higher heat history and a higher initial plastic strain, the effect of strain ageing progressed and the steel materials become more brittle, as a result the Charpy impact energies decreased.

The steel temperature increase was not pronounced for the protected steel column under post-flashover fire in a short duration. In many cases, the steel columns after the fire are reused with slight repair, e.g. the replacement of fireproofing materials. However, for the cold-formed steel square hollow section column, careful verification before reuse is needed because of the effect of strain ageing under the low-temperature heating due to fire.

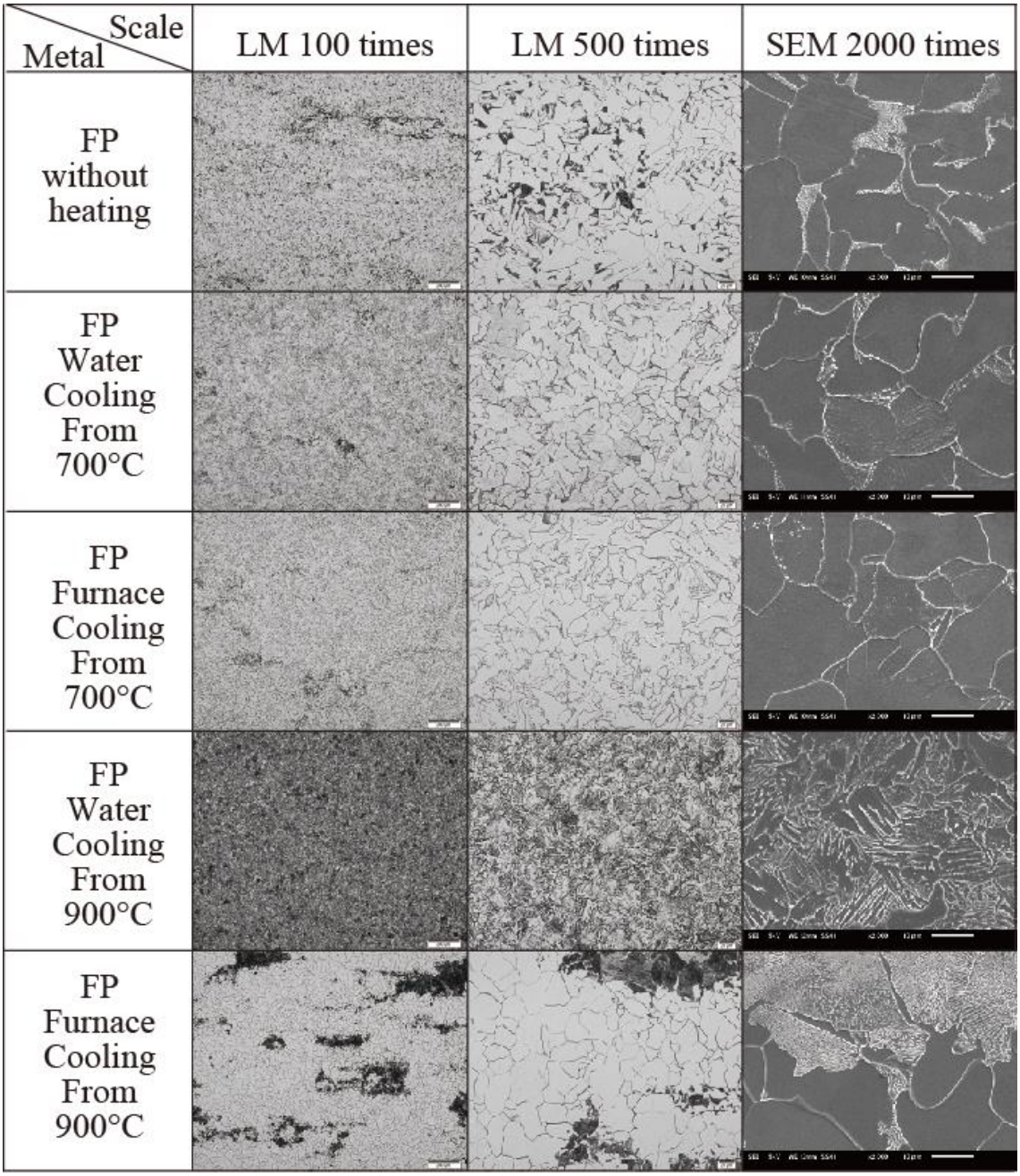

Fig.3.3.21 Steel microstructure of FP specimens (water- and furnace-cooled specimens)

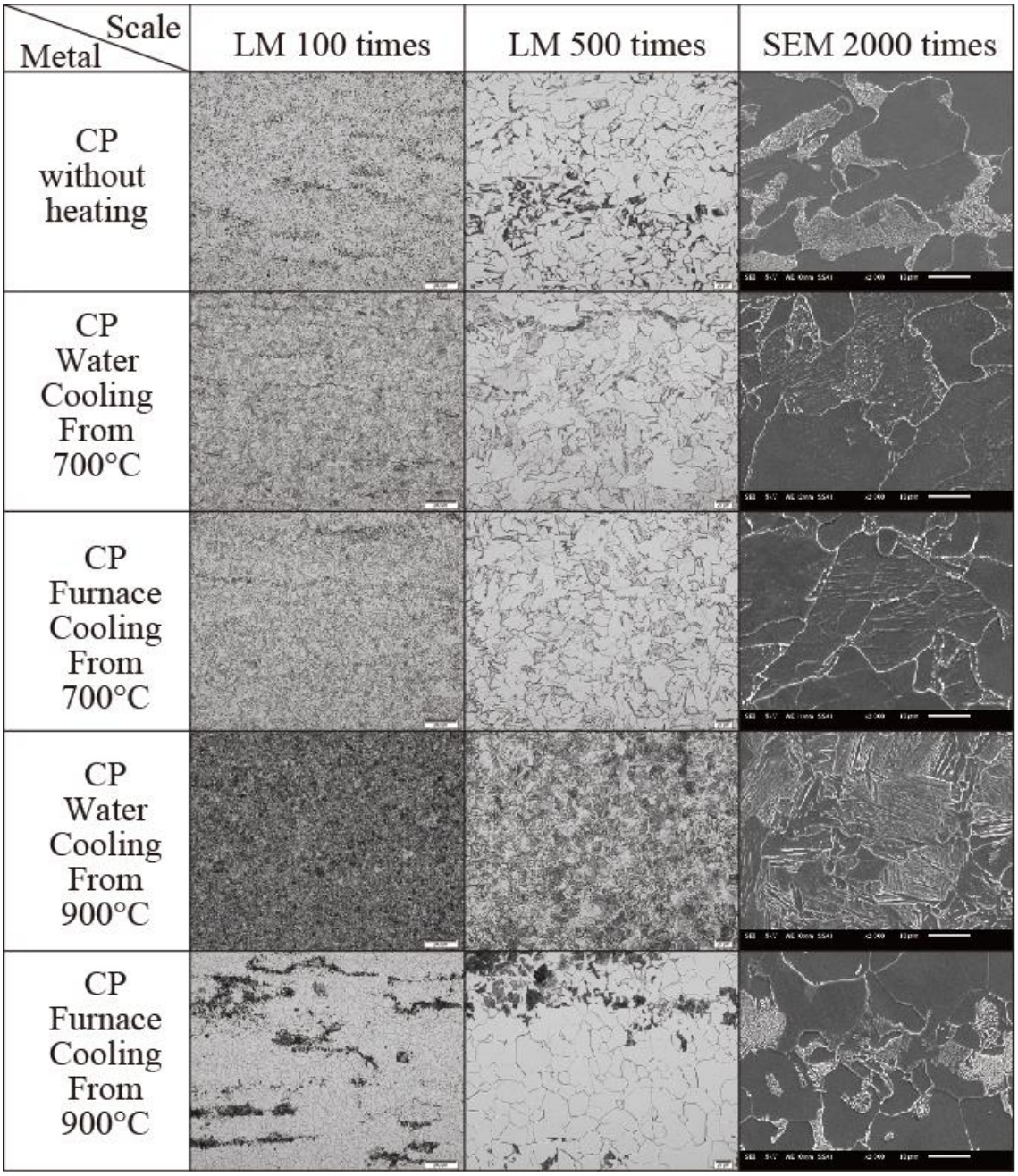

Fig.3.3.22 Steel microstructure of CP specimens (water- and furnace-cooled specimens)

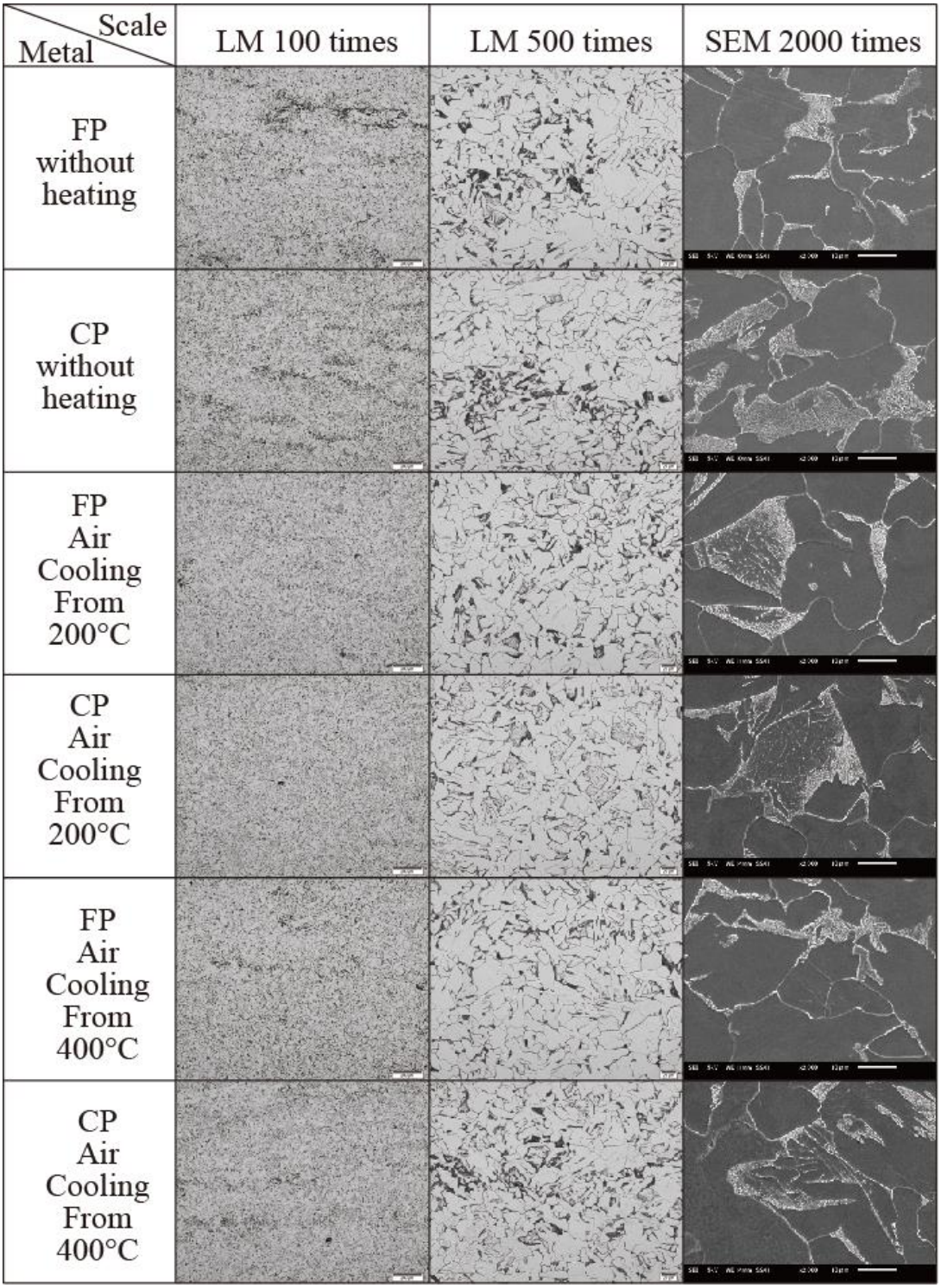

Fig.3.3.23 Steel microstructure of FP and CP specimens (air-cooled specimens)

3) Microstructure observations of water- and furnace-cooled specimens (FPT12)

Fig.3.3.24 shows the steel microstructure of water- and furnace-cooled FPT12 that were heated to 800

ºC. The F+P microstructure were observed in both furnace- and water- cooled specimens. However, as shown in this figure, there is more pearlite microstructure were observed in water-cooled specimen. General, 800 ºC is the two-phase temperature for the steel, and while the temperature is heated this temperature, the microstructure will transition to the austenite microtitrate, and if this microstructure subjected to a fast-cooling rate such as quenching by water, the microstructure will transition to martensite as described former. However, for the FPT12, as shown in Fig.3.3.24 (b), the specimens are still F+P microstructure. The reason is considered as following: as shown in Fig.3.2.5, FPT12 is subjected to the heating and cooling process in the dimension of 45 × 360 × 12 mm, therefore, 30 min heating after the specimen reached the target temperature is not enough for the microstructure transition to a completely austenite microstructure, if this specimen were quenched by water, the microstructure is still exhibit a F+P microstructure, however, compared with the water-cooled specimen that were heated to 500 ºC (Fig.3.3.24 (a)), 800 ºC heated specimens precipitated more pearlite microstructure. As a result, the water-cooled FPT12 after heated to 800 ºC possess large value of Charpy impact energy in comparison with the furnace-cooled FPT12.

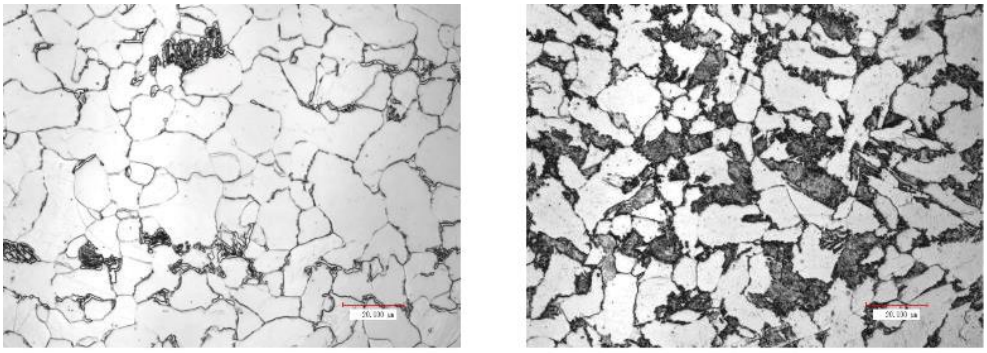

(a) Furnace-cooled specimen (b) Water-cooled specimens

Fig.3.3.24 Steel microstructure of FPT12 (Furnace- and water-cooled specimens)

3.4 Reuseability of the cold-formed steel square hollow section based on the Charpy impact test results after fire

Figure 3.4.1 summarizes the Charpy impact test results of the cold-formed steel square hollow section steel after the fire. In the figure, the red line is the value of 27 J, which is the lowest requirement for seismic-resistance performance of the steel structure members used in Japan in the Charpy impact energy. For the Charpy impact test results of the FP and CP specimens, Fig. 3.4.3 shows the 2% lower limit value of the Charpy impact test result, which is calculated by the Eq.2.6.1.

According to the test results, it is suggested that for the cold-formed steel members subjected to high-temperature heating of more than 700 ºC, if the steel members are cooled at a relatively high cooling rate such as being water-cooled, the Charpy impact test result may be lower than the required value. When these members are reused after fire, there is a possibility that brittleness fractures will occur to these members

while these buildings suffer a severe earthquake. However, if the cold-formed steel members were heated to a temperature of lower than 700 ºC, while cooled by fire extinguishing, the members still possess enough fracture properties to avoid brittleness fractures during the earthquakes. Furthermore, if the cold-formed steel members were air-cooled from the middle-temperature, the Charpy impact energies may decreased owing to the stain ageing. Although the average Charpy impact energy used in this research is enough high, in a view of the probability distribution, less than 98% of the cold-formed steel square hollow section possess enough Charpy impact energies more than 27J at 0 ºC, owing to the strain ageing. Therefore, in the view of the resistance-seismic requirement, it is considered that if the exterior view of steel members exhibit no obvious damage, and the temperature histories of these members also not exceed 700 ºC in fire, these members could be reused as a resistance-seismic structure after fire. However, if these members were cooled from the middle-temperature, it is very important to confirm the fracture properties of these members.

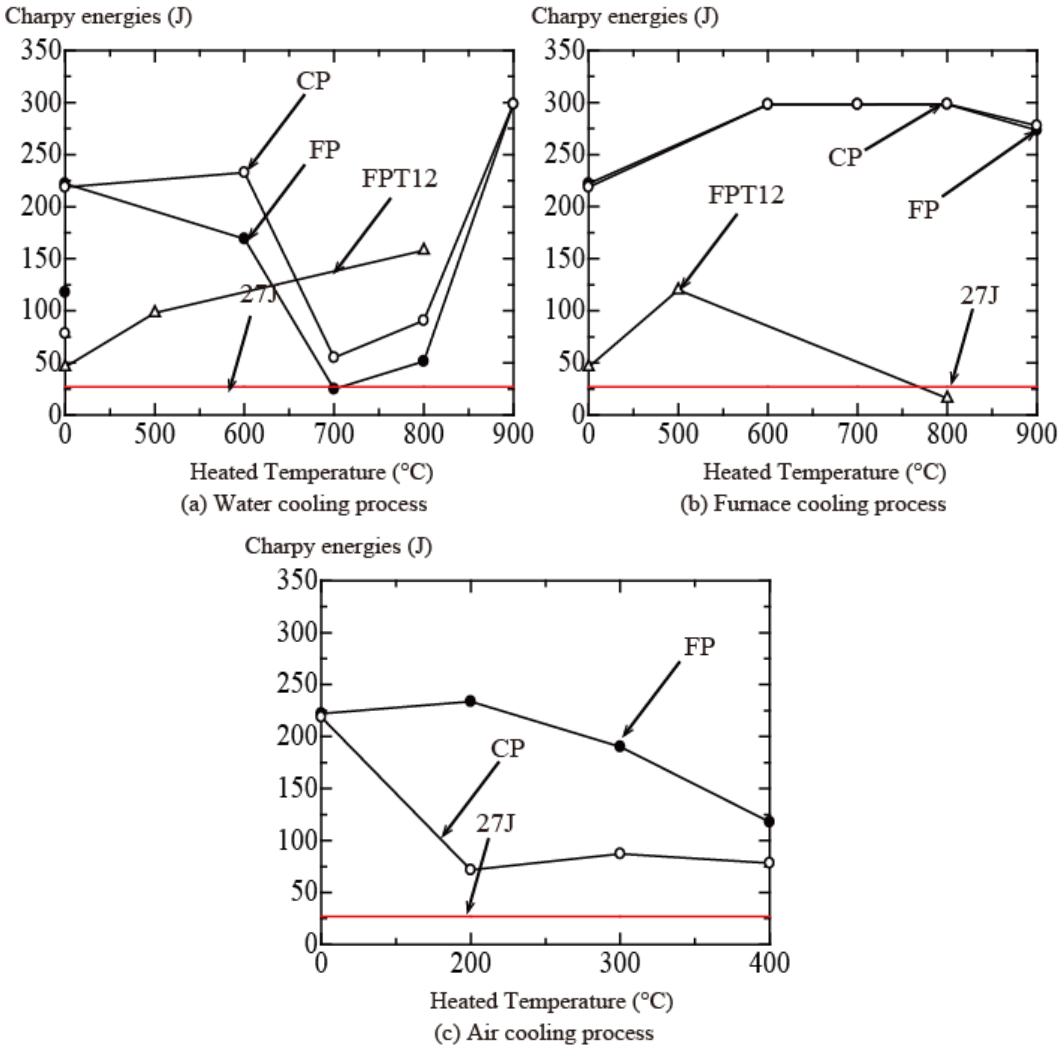

Fig.3.4.1 Charpy impact test result of cold-formed steel square hollow sections after fire

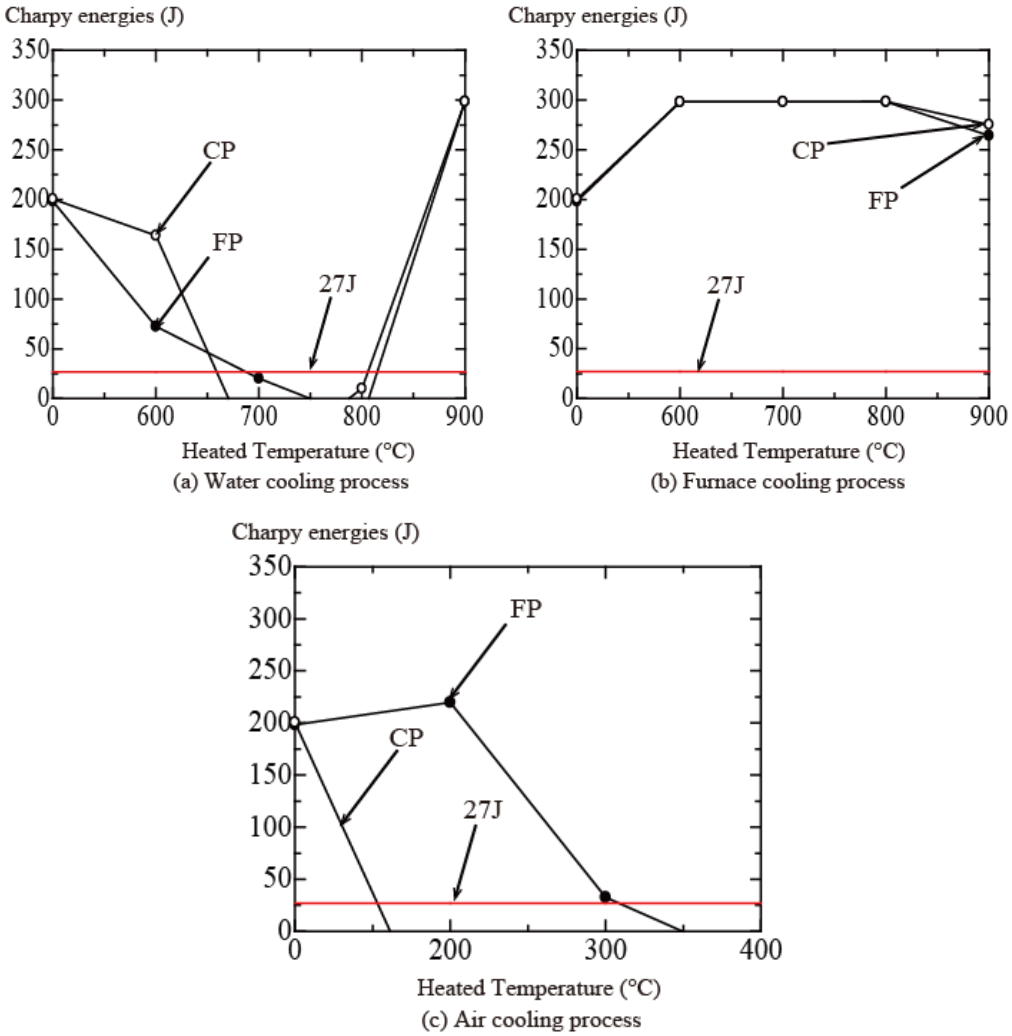

Fig.3.4.2 2% lower limit values of Charpy impact test result of cold-formed steel square hollow sections after fire

3.5 Conclusion

In this Chapter, Charpy impact energies of the flat part and corner part of cold-formed steel square hollow section were investigated at elevated temperatures and at ambient and low temperatures after the heating and cooling processes.

According to the high-temperature test results, it was confirmed that the Charpy impact values hardly decreased in the blue brittleness temperature range (between 100 and 300 ºC). Therefore, the possibility of the occurrence of brittleness fracture at elevated temperatures is very small. Then, according to the results of the ambient- and low-temperature tests on the specimens after the water and furnace cooling processes, water-cooled specimens subjected to 700-800 ºC heating exhibit the low Charpy impact energies, whereas the Charpy impact energies of water-cooled specimens subjected to 900 ºC recovered. Furthermore, according to the results of the ambient-temperature tests on the specimens after the air-cooling process, the

Charpy impact energies of the specimens significantly reduced, and the Vickers hardness increased.

Through the microstructure observation of the water-cooled FP and CP specimen, it is confirmed the Charpy impact energies decreased owing to the incomplete quenching that occurred during the water-cooling process from 700 and 800 ºC. However, the fracture toughness recovered, owing to the occurrence of martensitic transformation in the specimens quenching from 900 ºC. As for the furnace-cooled specimens, they exhibit high Charpy impact energies, because due to the slowly cooling rate of furnace-cooling, the microstructure of these specimens is similar to the untreated specimen. On the other hand, according to the microstructure observation of the air-cooled specimens, the microstructure does not change. However, because of the strain ageing, the fracture toughness of these member decreased after fire. While reusing these members as seismic-resistant members after fire, this local defect might trigger brittle fractures when subjected to sever earthquakes. The careful verification of the damage diagnostics after fire is required.

Furthermore, according to the test result of FPT12, it is confirmed that if the original Charpy impact energies is low, there is also a possibility of brittle fracture while this steel member is reused after fire. On the other hand, according to the microstructure observation of FPT12, it is considered that sometimes the microstructure of the specimens is still possessing the F+P microstructure after the water quenching treatment from the two-phase temperature. The reason is considered the heating time is not enough for the microstructure transition to the austenite microstructure.

Reference

[3.1]. B. Kato, H. AOKI and T. Kurosawa, Plastic strain history and residual stresses locked in cold-formed square steel tube, Architectural Institute of Japan, Vol.385, (March 1988), pp.39-48.

[3.2]. JIS Z2201:1998: Test pieces for tensile test for metallic materials https://kikakurui.com/z2/Z2241-2011-01.html Aug 19, 2021

[3.3]. Mechanical Engineering Dictionary: strain ageing, https://www.jsme.or.jp/jsme-medwiki/08:1010734, Apr. 2nd, 2021, pp.6 (in Japanese)

Chapter 4. Post-fire mechanical properties and buckling strength of cold-formed steel square hollow section columns

4.1. Introduction

Chapters 2 and 3 described the Charpy impact test of the welded connections and cold-formed steel square hollow section steel. In this Chapter, the experimental studies of the mechanical properties of cold-formed steel square hollow section steel columns are reported. Three types of tests were conducted: coupon tensile test, axially loaded compressive test, and stub-column test. Furthermore, the flexural buckling strengths were calculated based on the Eurocode design equations, and the validity was examined on the basis of the test results. For the local buckling strength, the design equations of both Eurocode [4.1, 4.2] and AS/NZS 4600:2005 [4.3] were verified.

4.2. Test methods

4.2.1 Cold-formed steel square hollow section steel

JIS STKR400 steel is used as cold-formed steel square hollow section column in this Chapter, this steel grade is commonly used for steel buildings in Japan. The design yield strength (YS) is equal to 235 MPa and the design tensile strength (TS) is equal to 400 MPa. This grade of steel is manufactured using cold-forming JIS SS400 steel (a structural hot-rolled steel plate; YS equal to 235 MPa; TS equal to 400 MPa). As shown in Fig. 4.2.1, two sectional dimensions of the specimens, namely □-50-50-1.6 mm (Specimen A) and 50-50-3.2 mm (Specimen B), were used in this study. The sectional dimensions were determined on the basis of the dimensions limit of the specimens for an electric furnace and a loading test system used in the heating process and loading tests, respectively. Furthermore, the test parameters of these small sectional columns correspond to the actual values of the effective slenderness and width–thickness ratios of the steel columns commonly used for building structures in Japan. The chemical components based on the mill sheets are listed in Table 4.2.1.

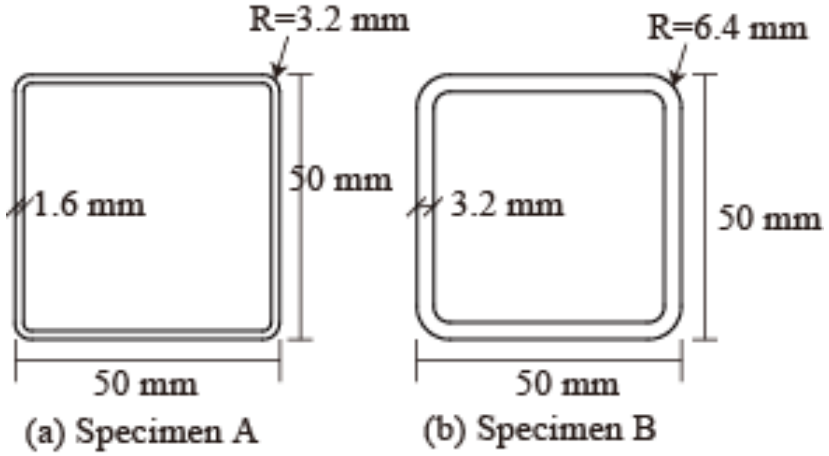

Figure 4.2.1. Sectional shapes and dimensions of specimens A and B

Table 4.2.1. Chemical components

Chemical (mass %)					
Specimen	C	Si	Mn	P	S
Specimen A	0.09	0.01	0.86	0.031	0.004
Specimen B	0.15	0.01	0.49	0.009	0.004

4.2.2 Heating and cooling processes

The specimens were heated in an electric furnace, as shown in Fig. 4.2.2. A thermocouple was attached to the centre of the specimen to measure the temperature history. Specimens were heated up to 200, 300, 400, 500, 600, 700, and 800 °C. The heating rate of the electric furnace used in the test was approximately 10 °C/min. To ensure that all the specimens had uniform temperatures, they were kept at each specified temperature for 30 min. Subsequently, the specimens were cooled using two methods: 1) quenching the specimens that were heated to 600–800 °C with water (water cooling); 2) retaining the specimens that were heated to 200–800 °C with the furnace temperature which gradually decreased (furnace cooling). The same methods of water-cooling and furnace cooling treatment with Chapters 2 and 3 is employed. To evaluate the basic mechanical properties of the specimens after the fire, coupon tensile tests were conducted on both the water- and furnace-cooled specimens (Table 4.2.2). Furthermore, to examine the changes in the compressive load-bearing capacities after the fire, both the axially loaded compressive tests regarding the flexural buckling behaviour, and the stub-column test regarding the local buckling behaviour were conducted for the furnace-cooled specimens (refer to Tables 4.2.3 and 4.2.4).

Fig. 4.2.3 shows the heating and cooling rates of specimens A and B. The water-cooled specimens were removed from the furnace and placed in a vessel containing a large quantity of water (a drum with an inner diameter and height of 450 and 666 mm, respectively). According to the Fig. 4.2.3, the furnace-cooling histories gradually decreased at an approximate rate of 1.1 °C/min. However, the water-cooling histories

show that the specimen temperatures rapidly decreased at an approximately rate of 80 °C/s.

Figure 4.2.2. Specimens placed in an electric furnace

Table 4.2.2. Test parameters (Coupon tests)

Specimen	t	b/t	Heating and cooling processes		
			Untreated	Furnace cooling	Water cooling
Specimen A	1.6 mm	31.3		200℃, 300℃, 400℃, 500℃, 600℃, 700℃,800℃	600℃, 700℃,800℃
Specimen B	3.2 mm	15.6			

Table 4.2.3. Test parameters (Axially loaded compressive tests)

Specimens	t	b/t	λ	Heated temperatures	
Specimen B	3.2 mm	15.6	40	Untreated specimen	200℃, 300℃, 400℃, 500℃, 600℃, 700℃,800℃

Table 4.2.4. Test parameters (Axially loaded compressive tests for stub-column specimens)

Specimen	t	b/t	L	Heated temperatures	
Specimen A	1.6 mm	31.3	150 mm	Untreated	200℃, 300℃, 400℃, 500℃, 600℃, 700℃,800℃

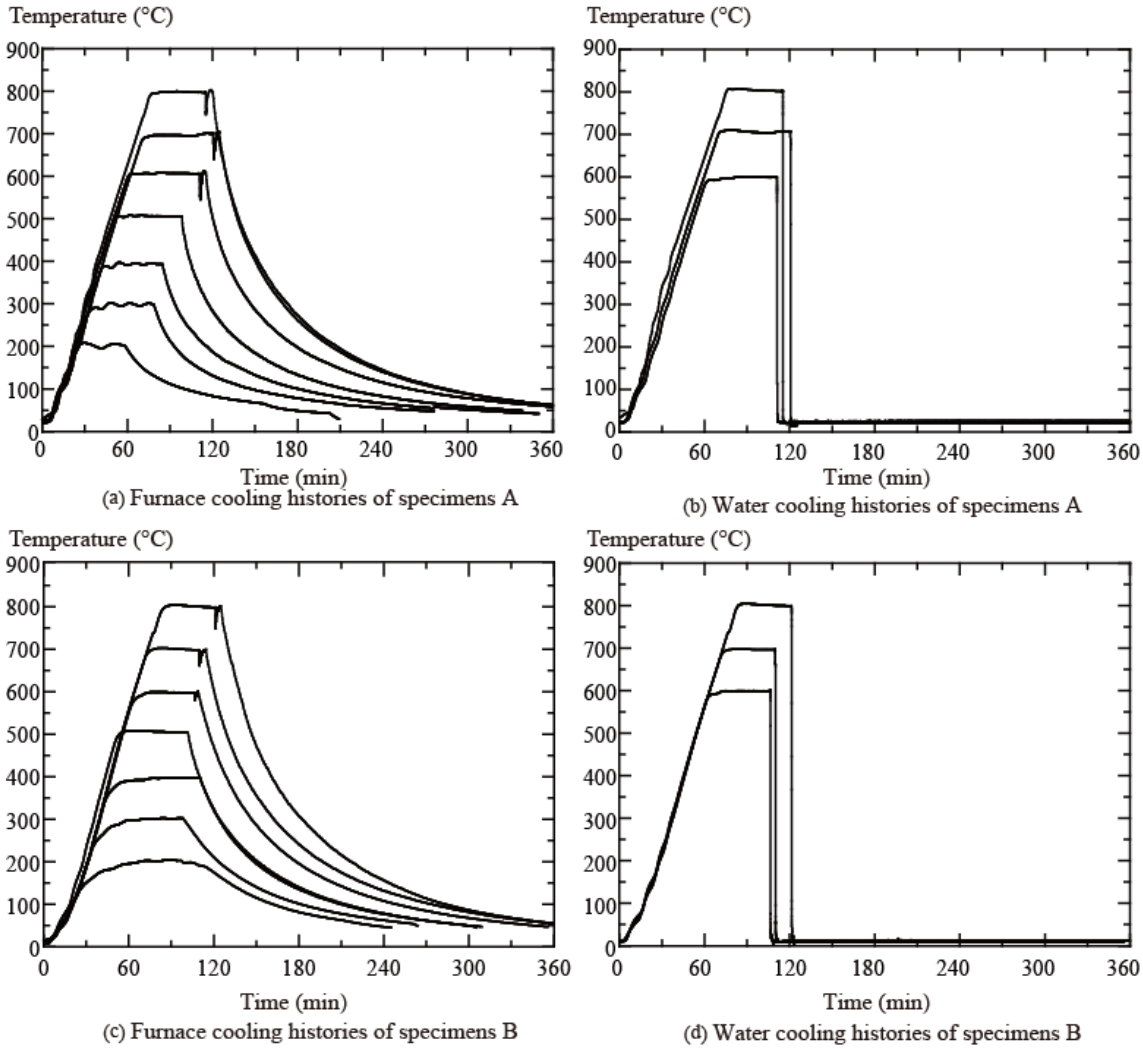

Figure 4.2.3. Time and specimen temperature relationships at heating, furnace-cooling, and water-cooling processes

4.2.3 Test details

Tables 4.2.2-4.2.4 show the test parameter of the coupon test, axially loaded compressive test, and axially loaded compressive tests for the stub-column specimens, respectively. The "t" in the tables is the column thickness, "b/t" is the width-thickness ratio. The stub-column tests were conducted using "thin-sectional shape" specimens A (b/t=31.3), whereas, the axially compressive tests were conducted using "thick-sectional shape" specimens B (b/t=15.6), and the "λ" (effective slenderness ratios) of the axially compressive tests were given by 40 and 50. The slenderness and width-thickness ratios were determined by considering actual steel building structures in Japan. Therefore, the small values of slenderness and width-thickness ratios were used for the steel buildings, to ensure the seismic load-bearing and deformation capacities. In fact, many square hollow section columns employed in Japanese steel structures possess lower

values than the test parameters ((b/t=31.3 and λ=50); for this reason, those specimens were used in the tests. Furthermore, owing to the dimension limit of the electric furnace, the λ values were limited to 50. The axial compressive tests were not conducted for specimens A (b/t=31.3), because these specimens exhibited local buckling behaviors before flexural buckling.

The loading process was conducted using a hydraulic universal testing machine of what maximum loading capacity of 2000 kN, and the maximum load-measurement rages for the coupon, axial-compression, and stub-column tests were 40, 400, and 200 kN, respectively. The loading test was performed based on the displacement controlling method.

1) Coupon tests

Figure 4.2.4 shows the dimensions of the coupon test specimens, which were fabricated based on JIS Z2241 [4.4]. The width and gauge length of the coupon specimen test section are 8 mm (the "d" in Figure 4.2.4) and 50mm (the "Ld" in Figure 4.2.4) , respectively. Two strain gauges were attached to the centre of the coupon tensile test specimen. Fig.4.2.5 shows the coupon test, the specimen was fixed by two steel plate jigs. Furthermore, as shown in Fig.4.2.5, two contact displacement meters touched at the jigs on the test section to measure deformation, and other two contact displacement meters touched at the hydraulic universal testing machine to measure the deformation of the test machine during the coupon tensile test.

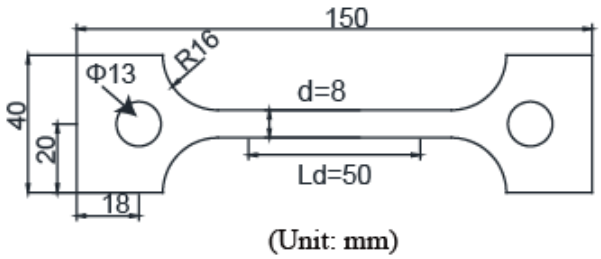

Figure 4.2.4 Dimensions of the coupon test specimens

Figure 4.2.5 Coupon test

2) Axially loaded compressive tests

Table 4.2.3 lists the test parameters of the axially loaded compressive tests, and Fig. 4.2.6 shows the test system. Two pin-ended jigs were installed at both ends of the column specimens. Fig. 4.2.7 shows the details of the pin-ended steel jigs (Fig. 4.2.7 (a)) and the front and side views of the specimens (Fig. 4.2.7 (b)). As shown in Fig. 4.2.7 (a), a groove (length and depth of 51 mm and 15 mm, respectively) was created at the centre of the jigs, and the specimens were inserted into the groove and fixed using steel plates and bolts (Fig. 4.2.7 (b)). The effective buckling length was calculated based on the distance between the arc tops of the two jigs. D1, D2, D3, and D4 in Fig. 4.2.7 (b) indicate the four contact displacement meters used in the test. D1 and D2 touched to the test machine measure the axial deformation, whereas D3 and D4 touched to the centre of the specimens measure the lateral deflections. Furthermore, x, y, and z axis were draw in the Fig.4.2.7 (b).

By the heating and cooling treatment, it is considered that the residual stress in the cross-section changed owing to the heating and cooling effects; however, in this test, the geometric imperfections and residual stress of the specimens were not measured.

Figure 4.2.6. Axially loaded compressive test system

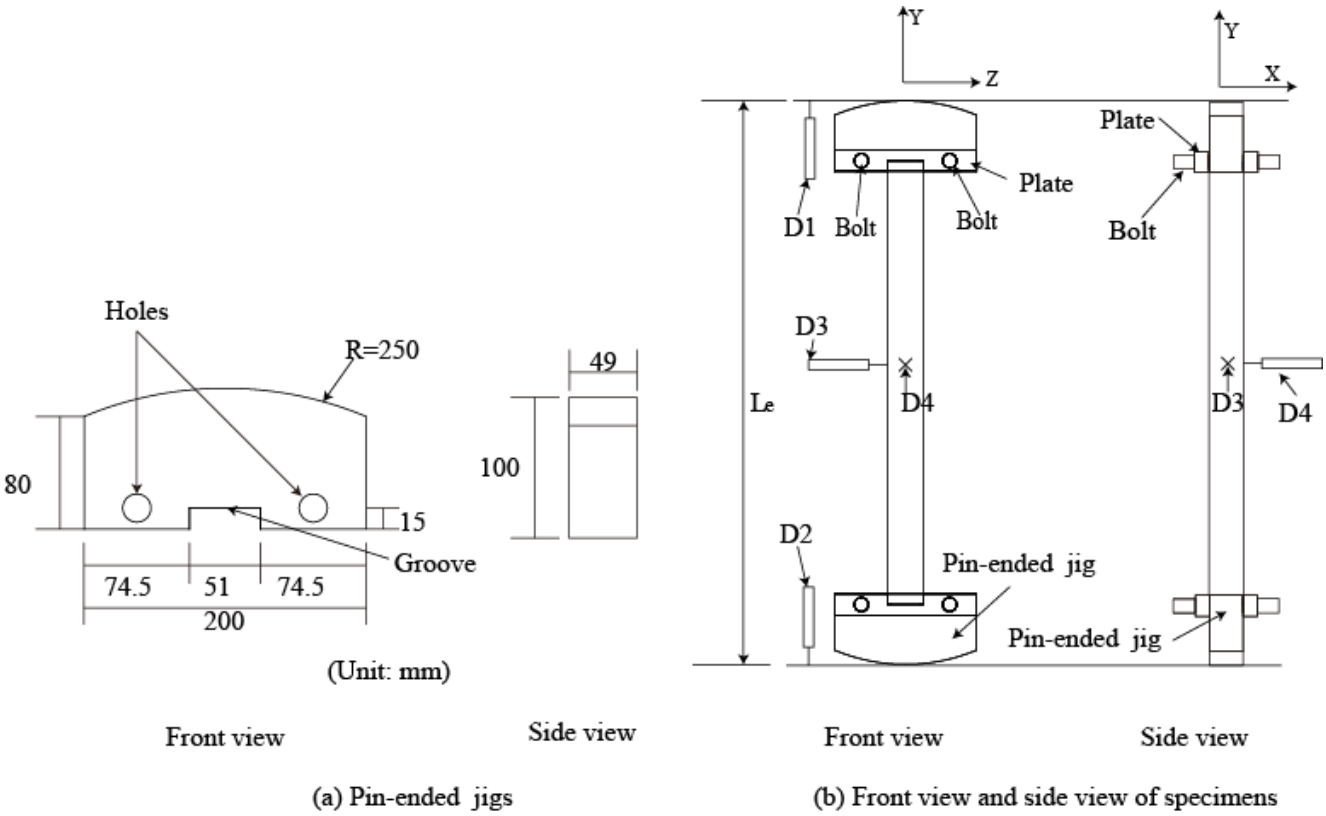

Figure 4.2.7. Details of axially loaded compressive test system

3) Axially loaded compressive tests for stub-column specimens

The length of the stub-column specimens is 150 mm which is three times longer than the width of specimen A (b/t=31.3). As shown in Figure 4.2.8 (a), a round steel plate (10 mm thick) was placed on each end of the stub-column specimens to ensure that those specimens were subjected to a uniform compression force. Four contact displacement meters, namely, D5, D6, D7, and D8 (refer to Fig.4.2.8 (b)) were used. D5 and D6 touched to the two round steel plates measure the axial deformation, whereas D7 and D8 touched to the centre of the specimens to measure the deflections at the centre of the specimens after the occurrence of local buckling.

(a) Axially loaded stub-column test

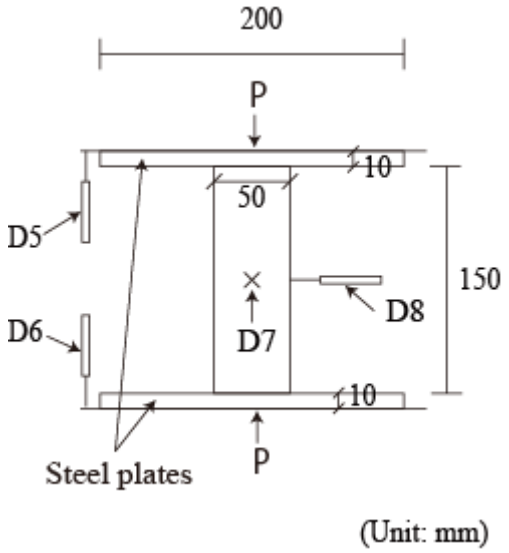

(b) Details of stub-column specimenst

Figure 4.2.8. Axially loaded stub-column test

4.3 Experimental results and discussion

Fig. 4.3.1 shows the photographs of the specimens after the coupon tests, and Table 4.3.1 lists the average loading rate for the coupon, axially loaded compressive, and stub-column tests. According to the previous research [4.5], it was reported that the effect of strain rate on the coupon test results under the ambient temperature environment were very small within the strain rate values (0.01%/s~3%/s) in Table 4.3.1.

Table 4.3.1. Average loading rate of the tests

	Average loading rate (%/min)						
	Coupon test for specimens A		Coupon test for specimens B		Flexural buckling tests		Stub-column tests
Treated methods	Furnace-cooling	Water-cooling	Furnace-cooling	Water-cooling	Furnace-cooling		Furnace-cooling
Heated temperature	t=3.2 mm		t=1.6 mm		λ=40	λ=50	L=150mm
Untreated	1.25	-	1.82	-	0.05	0.02	0.15
200℃ treated	0.7	-	2.04	-	0.06	0.07	0.22
300℃ treated	0.92	-	1.16	-	0.04	0.07	0.17
400℃ treated	1.82	-	1.26	-	0.07	0.08	0.16
500℃ treated	2.49	-	1.56	-	0.09	0.08	0.17
600℃ treated	2.99	1.47	1.89	0.88	0.09	0.05	0.18
700℃ treated	1.55	0.93	1.21	0.94	0.09	0.02	0.19
800℃ treated	2.35	1.08	1.99	0.2	0.08	0.05	0.16

4.3.1 Coupon tensile test results

Fig.4.3.1 shows the coupon tensile test results. FC and WC represent the heating and cooling treatment of the specimen, FC is furnace cooling, and WC is water cooling, respectively. Tables 4.3.2 and 4.3.3 list the yield point (f_y), stress at strain equal to 1.0% ($f_{1.0}$), stress at strain equal to 2.0% ($f_{2.0}$), tensile strength (f_u), uniform elongation, and breaking elongation of the specimens. Owing to the setting fault of the contact displacement meters (Fig 4.2.5), the breaking elongation of the furnace-cooled specimen B that were subjected to heating at 300 °C was not measured. Figs. 4.3.2 and 4.3.3 show the engineering stress and engineering strain relationships of the specimen A and B, respectively. Figs. 4.3.4 and 4.3.5 present the yield point and tensile strength, and Figs. 4.3.6 and 4.3.7 show the uniform and breaking elongation of specimens A and B, respectively. In each graph at Figs 4.3.4-4.3.7, the values at 0 °C represent the test results of the untreated specimens.

According to Figs 4.3.2 and 4.3.3, the stress–strain relationships of untreated specimens A and B is the typical SS curve of the BCR295 steel, which, does not have clear yield shelf because of the plastic

processing working during the cold-formed manufacturing. However, for the specimens that were subjected to heating and cooling process, the yield shelf appeared. It is considered that owing to the effect of heating and cooling process, the plastic working effect of the cold-formed steel square hollow section decreased. Then, specimens quenched with water after heating at 800 °C showed no clear yield shelf and exhibited brittle behaviours. According to the test results presential in Chapters 2 and 3, water-cooled specimens that were heated to 800°C were imperfectly quenched from the two-phase (ferrite and austenite) temperature, and the microstructures of these specimens were transformed to a segregated plural microstructure of ferrite, bainite, and martensitic; thus, the specimens exhibited brittle behaviour.

Comparing the yield and tensile strength of the furnace-cooled specimens to those of the untreated specimens, as shown in Figs 4.3.4 and 4.3.5, furnace cooled specimen that were heated to 200–400 °C exhibited a larger yield point (f_y) and tensile strength (f_u) than the untreated specimens, and both the f_y and f_u of the specimens that were heated to 500–800 °C decreased with increasing heating temperature. Also, the f_y of all specimens were larger than the design standard yield point of 235 MPa for JIS STKR400 grade steel. However, for some specimens such as furnace cooled specimens A (600–800 °C) and B (800 °C), their f_u were lower than the design standard tensile strength of 400 MPa. As described in section 4.2.1, JIS STKR400 is cold-formed from the SS400 steel. The standard design YS and TS of SS400 steel are 235 Pa and 400MPa respectively, these values are the 5% lower limit value for the YS and TS of the SS400. It means for the general JIS SS400 steel, more than 95% of JIS SS400 steel posse a YS and TS more than 235MPa and 400MPa. For the JIS STKR400 steel, it is cold-forming by the JIS SS400 steel. Therefore, most of the JIS STKR400 steel posse much higher YS than 235MPa at ambient temperature. Although the YS of the JIS STKR400 steel decreased with the temperature increasing, it can still be considered that most of the STKR400 steel posse a YS more than 235 MPa after fire.

Furthermore, according to Chapter 3, it is considered that owing to the cold-formed manufacturing process, large plastic strains remain in the cross sections; when these specimens are heated to the medium temperatures (200–400 °C), the strain aging progressed through the heating process, and as a result, the yield and tensile strength increased. For the specimens that were heated to high temperatures (500–800 °C), the plastic work in the section was changed; therefore, the yield and tensile strength decreased. However, the water-cooled specimens presented a higher yield and tensile strength than the furnace-cooled specimens because of the quenching effect. As shown in Figs. 4.3.6 and 4.3.7, test results of uniform and breaking elongation verified that the ductile capacity changed after the heating and cooling processes.

Table 4.3.2. Coupon test results of specimens A

(a) Furnace-cooled specimens

Heated temperature	Yield point (MPa)	$f_{1.0}$ (MPa)	$f_{2.0}$ (MPa)	Tensile strength (MPa)	Uniform elongation (%)	Fracture elongation (%)
Untreated	360	376	386	417	19.3	24.8
200℃ treated	391	394	406	428	9.5	14.8
300℃ treated	408	405	420	438	5.3	10.5
400℃ treated	420	424	441	454	5.4	10.3
500℃ treated	350	368	367	408	10.8	14.3
600℃ treated	340	346	346	396	12.3	17
700℃ treated	323	324	330	384	14.1	19.6
800℃ treated	270	274	276	351	26.8	35.4

(b) Water-cooled specimens

Heated temperature	Yield point (MPa)	$f_{1.0}$ (MPa)	$f_{2.0}$ (MPa)	Tensile strength (MPa)	Uniform elongation (%)	Fracture elongation (%)
600℃ treated	400	402	392	451	9.2	13.3
700℃ treated	410	418	415	452	14.2	18.5
800℃ treated	345	487	559	602	3.2	3.7

Table 4.3.3. Coupon test results of specimens B

(c) Furnace-cooled specimens

Heated temperature	Yield point (MPa)	$f_{1.0}$ (MPa)	$f_{2.0}$ (MPa)	Tensile strength (MPa)	Uniform elongation (%)	Fracture elongation (%)
Untreated	397	410	422	397	12.1	25.3
200℃ treated	448	442	463	448	5.2	12.3
300℃ treated	408	407	420	408	5.6	-
400℃ treated	401	402	418	401	12.3	19.4
500℃ treated	390	389	388	390	14.9	20.9
600℃ treated	345	348	359	345	19.1	27.7
700℃ treated	314	314	323	314	17.9	29.9
800℃ treated	270	281	280	270	24.4	31.9

(d) Water-cooled specimens

Heated temperature	Yield point (MPa)	$f_{1.0}$ (MPa)	$f_{2.0}$ (MPa)	Tensile strength (MPa)	Uniform elongation (%)	Fracture elongation (%)
600℃ treated	409.7	411	417.3	489.4	13.5	21.1
700℃ treated	460.4	461.1	475.9	507.4	6.5	10.6
800℃ treated	307.9	380.4	427.6	512.4	6.9	11.1

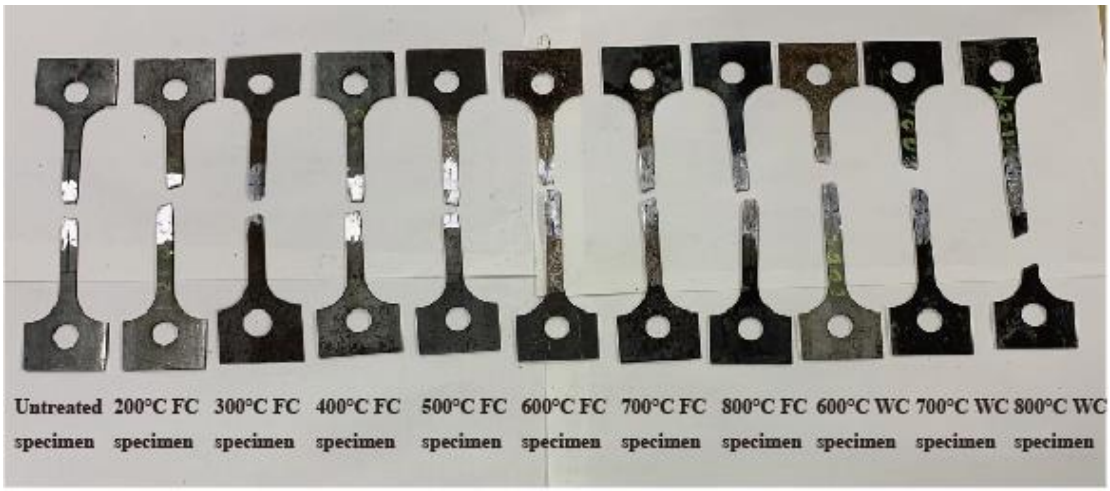

(a) Specimens A

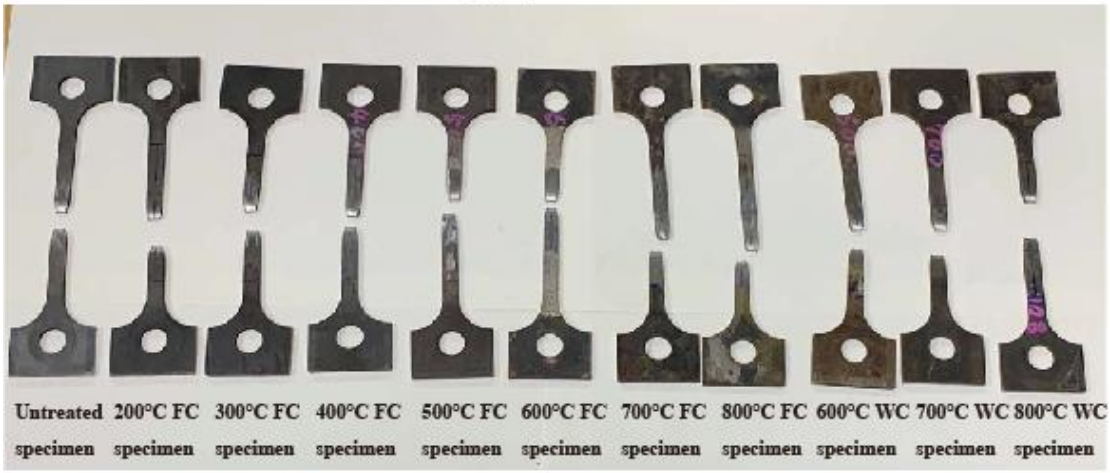

(b) Specimens B

Figure 4.3.1. Coupon test results of the specimens A and B after heating and cooling process

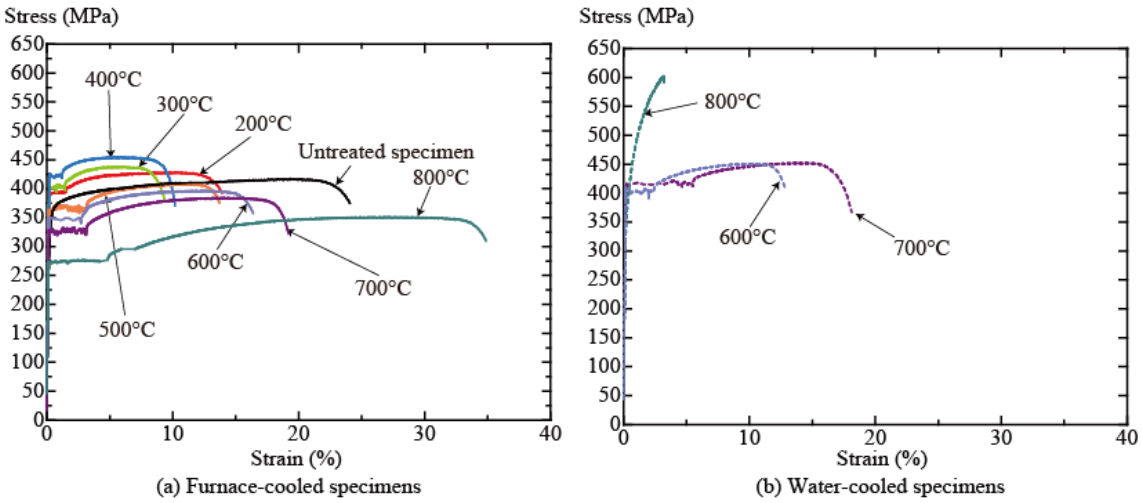

Figure 4.3.2. Engineering stress and engineering strain relationships of specimens A

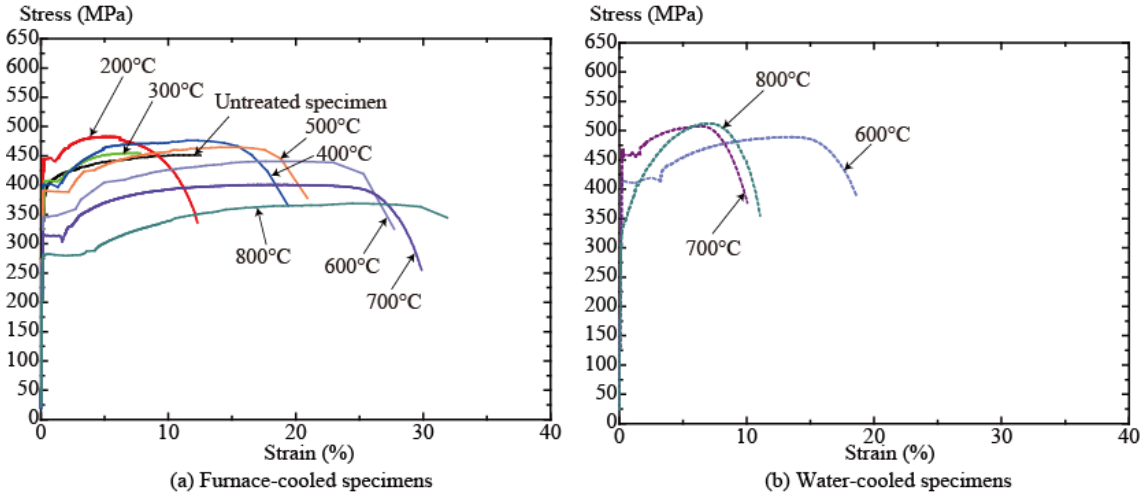

Figure 4.3.3. Engineering stress and engineering strain relationships of specimens B

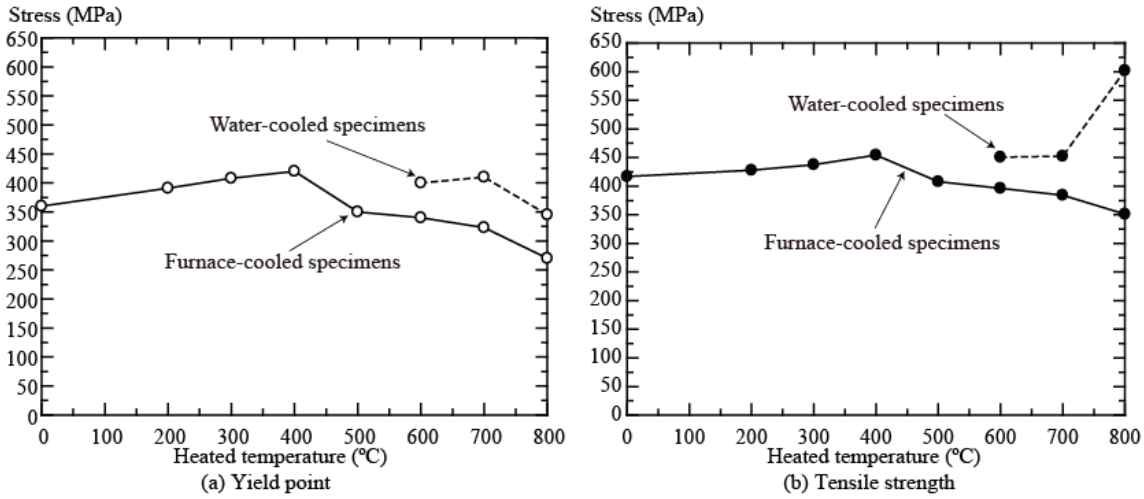

Figure 4.3.4. Yield point and tensile strength of specimens A

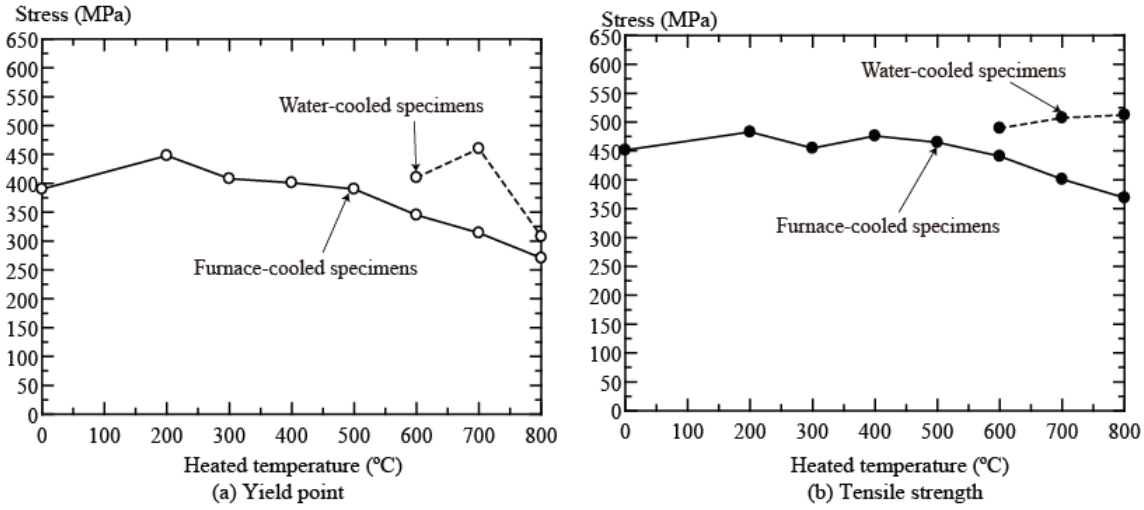

Figure 4.3.5 Yield point and tensile strength of specimens B

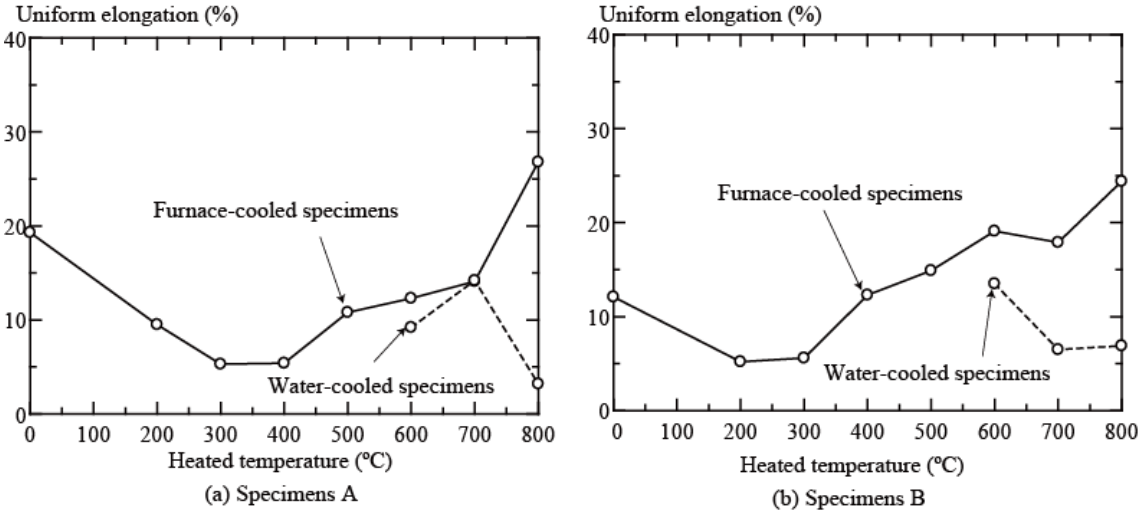

Figure 4.3.6 Uniform elongation

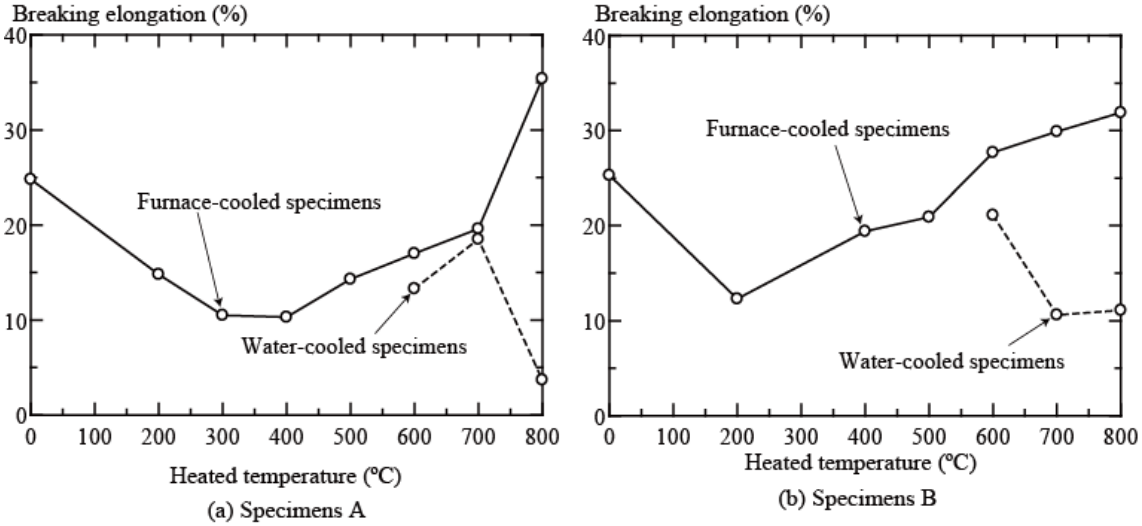

Figure 4.3.7 Breaking elongation

4.3.2 Axially loaded compressive tests results

Table 4.3.4 lists the test results of the flexural buckling test of specimens B. Fig.4.3.8 shows the photos of the specimens with λ=40 and 50 after the test. Figs.4.3.8 (a) and (b) show the specimens after the test in the cases of after 200-800 °C heating. Figs. 4.3.8 (c) and (d) show the front view and side view of the 400 °C heated specimens with λ=40. As shown in Figs. 4.3.8 (a) and (b), all the specimens show a similar exterior to the 400 °C heated specimens with λ=40. According to Fig. 4.3.8, flexural buckling, which exhibited as the bending deformation occurred in the centre of the specimens, were observed on the specimens. For all the axially loaded compressive tests, it was confirmed that flexural buckling occurred before local buckling. Fig. 4.3.9 shows the deflection of the specimen after flexural buckling. As shown in Fig. 4.3.9, the pin-end jigs at both ends of the specimen rotated around the X-axis (draw in Fig.4.2.7), after the occurrence of the flexural buckling, the displacement at the centre of the specimen increased, and finally, the local buckling

occurred in the centre of the specimens (Fig.4.3.8(d)).

Fig.4.3.10 shows the P–δ relationships (where P is the axial load, and δ is the relative deformation of the D1 and D2 displacement meters). The load P and relative deformation δ were divided by the section area A and column length L, respectively. As shown in Fig. 4.3.10 (a), except for the specimen with $\lambda = 40$ that cooled from 200 °C (unloaded at approximate 330MPa), the specimens were unloaded when the axial load decreased to half of the maximum loading. Fig. 4.3.11 shows the P/A–θ relationships, where θ is the drift angle of the pin jigs around the X-axis, which is calculated from the ratio of the lateral deflection δ in the centre of the half specimen length L/2 ($\theta = {}^{\delta}/_{L/2}$). It should be noted that the P/A–θ relationship of the 200 °C specimen with $\lambda = 40$ was not measured because of our work fault. In Fig. 4.3.11, the symbol '○' is marked at the location where the drift angle rapidly increases. This symbol indicates the initial points for the occurrence of flexural buckling. The strength at this point was basically equal to the maximum strength in axially loaded compressive tests. After flexural buckling, local buckling occurred at the centre of the specimens (Fig.4.3.8(d)).

To evaluate the flexural buckling strength f_{cr} after the heating and cooling processes using the existing design code, the test results were compared with the Eurocode design equations [4.1]. The Eurocode design equations regarding the flexural buckling strength are as follows:

$$f_{cr} = \chi f_y \quad \text{(Eq. 4.1)}$$

$$\chi = \frac{1}{\Phi + \sqrt{\Phi^2 - \bar{\lambda}^2}} \quad \text{(Eq. 4.2)}$$

$$\Phi = 0.5 \times \left(1 + \alpha \times \left(\bar{\lambda} - 0.2\right) + \bar{\lambda}^2\right) \quad \text{(Eq. 4.3)}$$

$$\bar{\lambda} = \frac{0.9\lambda_e}{\pi\sqrt{E/f_y}} \quad \text{(Eq. 4.4)}$$

where

λ_e: effective slenderness ratio of the column (λ_e =40 or 50).

α: imperfection factors for buckling curves (in this study, $\alpha = 0.49$).

E: Young's modulus at the ambient temperature (E=205,000 MPa).

χ: reduction factors on the buckling strength.

f_y: yield point obtained from the coupon tensile test of specimen B, or the F value (standard yield strength) of JIS STKR400 steel.

Fig. 4.3.12 shows the flexural buckling test results and calculation results based on the Eurocode equations (Eqs. 4.1-4.4). The solid line with the symbol '○' indicates the axially loaded compressive test results. And the solid line shows the calculation results of the Eurocode equations with the yield strength f_y given by the coupon tensile test result as described in section 4.3.1. The dashed line shows the calculation result of the Eurocode equations with the yield strength f_y given by the F value (the standard design strength of JIS STKR400, F=235 MPa), this calculation result is the general result in the actual design

situation, calculated by the Eurocode equations.

As shown in Fig.4.3.12, the compressive test results exhibit a tendency similar to the coupon test results (Fig. 4.3.5); that is, the flexural buckling strength of the furnace-cooled specimens that were heated at high temperatures decreased as heating temperature rising. Comparing the compressive test results with the Eurocode calculation results, the compressive test results of the specimens (λ=40 and 50) are higher than those results calculated from the yield point after fire. However, comparing the compressive test results with the calculation results based on the F value, all the specimens exhibited larger values than the calculation results, it can be considered that the according to the Eurocode equations (Eqs 4.1-4.4), the flexural buckling could be evaluated based on the F value on the safe side.

It is considered that if the yield strength of the steel member was obtained after the heating and cooling processes, the residual flexural buckling strength after fire can be approximately evaluated using the Eurocode design equations with the yield point from the coupon tests. For an actual fire case, it is very difficult to accurately evaluate the residual flexural buckling strength because the exact evaluation of the temperature history in an actual fire is difficult, and the yield point of the steel member after the fire is unknown in many cases. Therefore, according to the test results obtained from this study, the residual flexural buckling strength, including high-temperature heating conditions such as 800 °C, can be evaluated on the safe side by using the F value (design standard strength) for the yield point. Because, as described in section 4.3.1, most of the JIS STKR400 steel posse much higher YS than F value at ambient temperature or after fire.

Table 4.3.4. Flexural buckling test results of specimens B

Maximum values of P/A (N/mm^2)								
Specimen	Heated temperature							
	Untreated	200℃ treated	300℃ treated	400℃ treated	500℃ treated	600℃ treated	700℃ treated	800℃ treated
λ=40	378.1	427.7	430.3	401.5	356.7	362.1	257	253.7
λ=50	370	360.9	365	383.6	310.8	331.5	234.9	218.6

(a) Specimens of λ=40

(b) Specimens of λ=50

(c) Front view of a specimen after the test

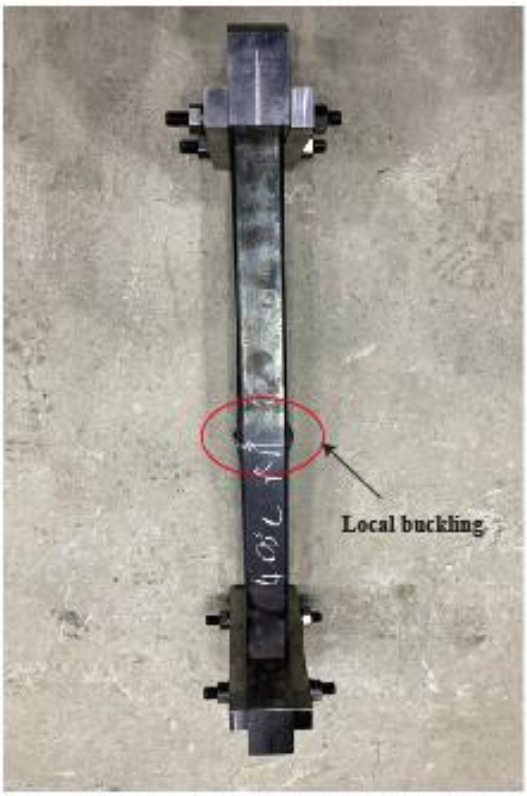

(d) Side view of a specimen after the test

Figure 4.3.8. Axially loaded compressive test results

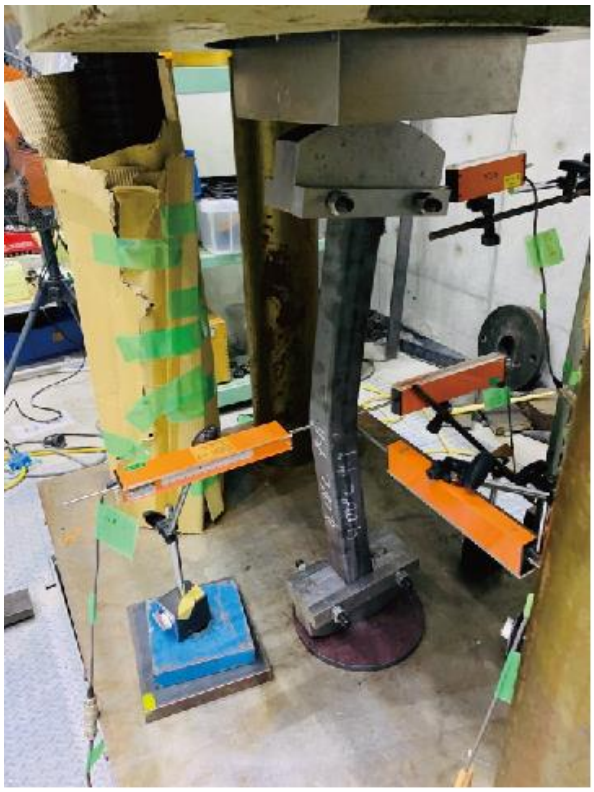

Figure 4.3.9 Deflection of the specimen after flexural buckling

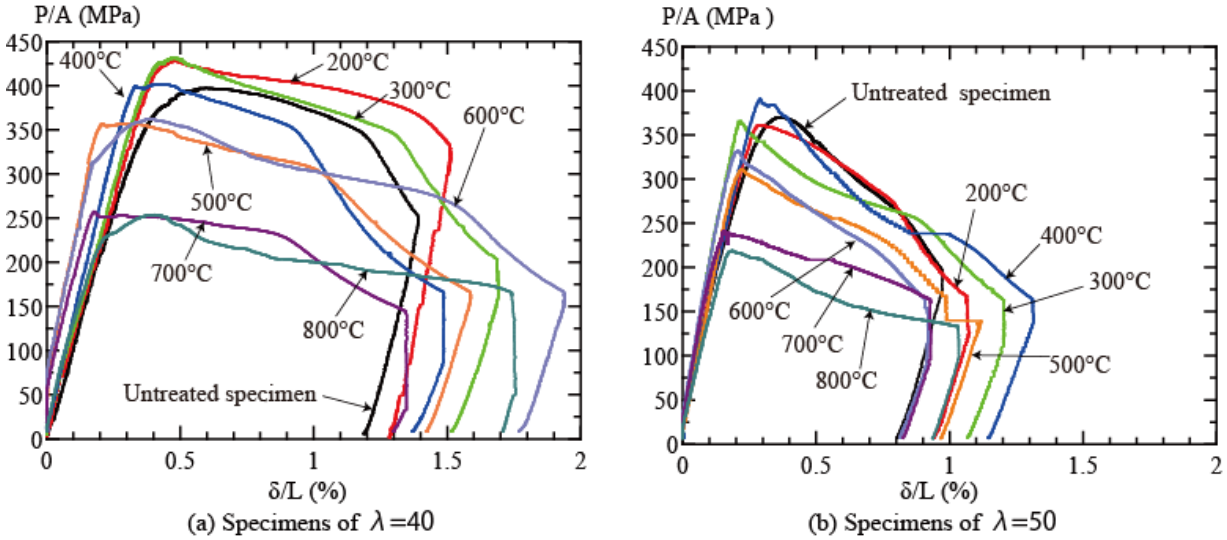

Figure 4.3.10 P/A–δ/L relationships of specimens B

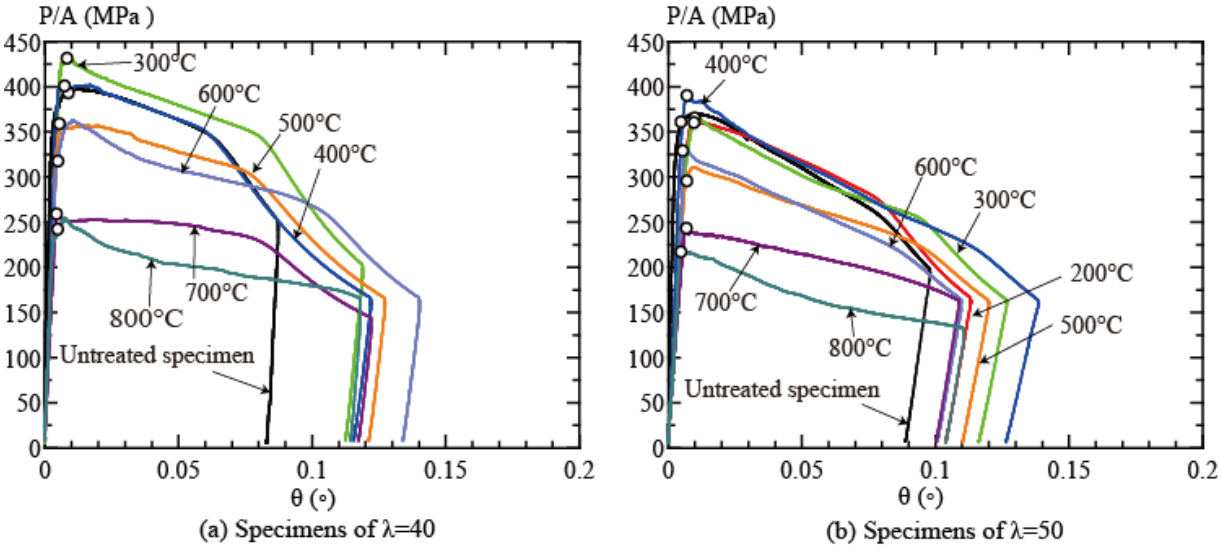

Figure 4.3.11 P/A–θ relationships of specimens B

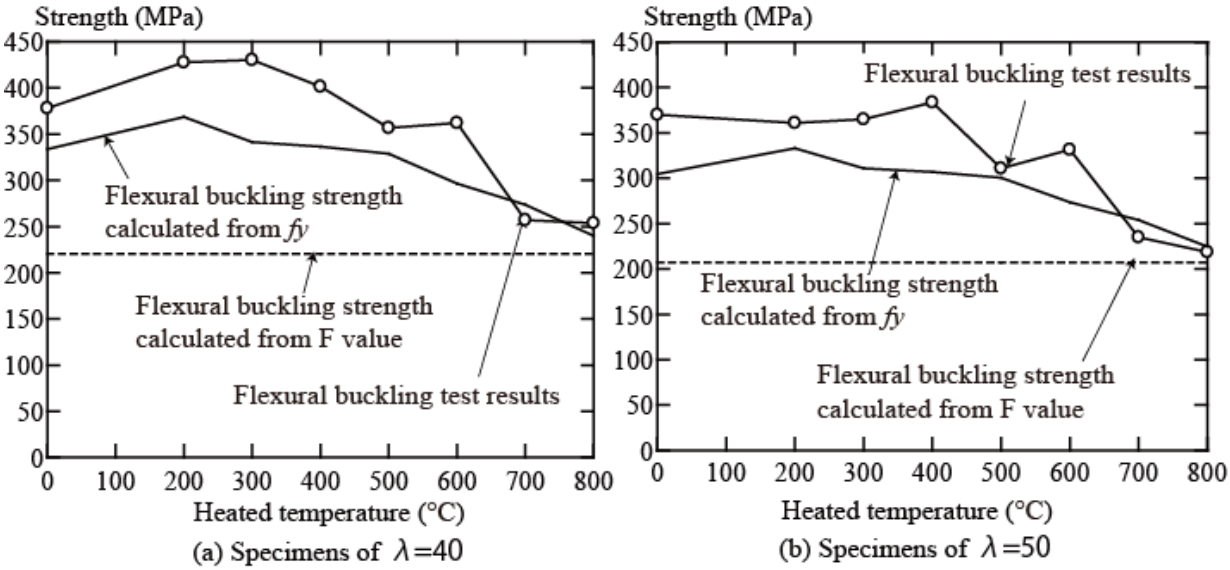

Figure 4.3.12 Flexural buckling test results and calculation results based on Eurocode

4.3.3 Axially loaded compressive tests for stub-column specimens

Table 4.3.5 lists the test results of the compressive tests for stub-column of specimens A. Fig.4.3.13 shows the photos of the specimens A after the test. As shown in Fig.4.3.13, local buckling occurred on the end of the cross section, owing to the open-end test. According to the previous research [4.6] on the local buckling strength for the stub-column test, it is considered that the test results in the case of local buckling at the end cross section can be used for the evaluation of the local buckling strength because the maximum strength for the stub-column test is hardly affected by the buckling location of local buckling. Therefore, the test results of the local buckling in this stub-column is a credible result although the local buckling occurred to

the end cross section of the specimen A. Furthermore, Fig.4.3.14 present the P/A–δ/L relationship of the specimens.

As presented in Table 4.3.5, local buckling strength of the specimen A that were heated to 200-600 °C is larger than the untreated specimen; however, for the specimens that cooled from 700-800 °C, the strength is lower than the untreated specimens, this tendency is similar to the coupon test results of the furnace-cooled specimens A, as shown in Table 4.3.2.

As described in the introduction, the design local buckling strength f_{lcr} was evaluated using two sets of design equations, which are the Eurocode equations (Eqs. (4.5) – (4.7)) [4.2] and AS/NZS 4600:2005 equations (Eqs. (4.8) – (4.11)) [4.3]. It is assumed that the boundary conditions of the steel plates in the cross section are given by a four-side simply supported plate. The equations are expressed as follows:

[Eurocode equations]:

$for\ \bar{\lambda}_p \le 0.5 + \sqrt{0.085 - 0.055\psi}\,,\qquad \rho = 1.0$ (Eq. 4.5)

$for\ \bar{\lambda}_p > 0.5 + \sqrt{0.085 - 0.055\psi}\,,\qquad \rho = \frac{\bar{\lambda}_p - 0.055\times(3+\psi)}{\bar{\lambda}_p{}^2} \le 1.0$ (Eq. 4.6)

$$f_{lcr} = f_y \times \rho \quad \text{(Eq. 4.7)}$$

where,

$$\varepsilon = \sqrt{235/f_y}\ ,\qquad \bar{\lambda}_p = \frac{b/t}{28.4\varepsilon\sqrt{k_\sigma}}$$

f_y: yield point obtained from the coupon tensile test of specimen A, or the F value (standard yield strength) of JIS STKR400 steel.

ρ: reduction factor for local buckling strength.

ψ: stress ratio (in this study, $\psi = 1.0$).

k_σ: buckling factor corresponding to the stress ratio (in this study, $k_\sigma = 4.0$).

[AS/NZS4600:2005 equations]:

$for\ \lambda \le 0.673\,,\qquad \rho = 1.0$ (Eq. 4.8)

$for\ \lambda > 0.673\,,\qquad \rho = \frac{\left(1-\frac{0.22}{\lambda}\right)}{\lambda}$ (Eq. 4.9)

$$\lambda = \frac{1.052}{\sqrt{k_\sigma}}\left(\frac{b_e}{t}\right)\sqrt{\frac{f^*}{E}} \quad \text{(Eq. 4.10)}$$

$$f_{lcr} = \frac{4b_e t f^*}{A} \quad \text{(Eq. 4.11)}$$

b_e: the length of the flat part.

f^*: yield strength range of specimens. (f_y or F values)

Fig. 4.3.15 shows the stub-column test results and calculation results based on the Eurocode and AS/NZS4600:2005 equations. In Fig. 4.3.15(a), the solid line with the symbol '○' indicates the stub-column test results, whereas the solid line represents the calculation results of the Eurocode equations while the yield strength f_y is given by the coupon tensile test result as described in section 4.3.1. The

dashed line shows the calculation result of the Eurocode equations while the yield strength f_y is given by the F value (the standard design strength of JIS STKR400, F=235 MPa). In Fig. 4.3.15 (b), the stub-column test results are compared with the calculation results based on the AS/NZS4600:2005 equations (Eqs. (4.8) – (4.11)) and the yield point of the specimens (dashed line with the symbol '○') obtained from the coupon tensile test.

As shown in Fig. 4.3.15 (a), the strength values in the stub-column test results are lower than the local buckling strength calculated from f_y, and the calculation results from the F values are lower than those of the stub-column test results. On the other hand, compared with the evaluation results calculated based on the AS/NZS4600:2005 equations, as presented in Fig. 4.3.15 (b), the stub-column test results exhibit lower values than the yield point f_y of the steel. Comparing the stub-column test results with the calculation results from f_y, the test results are larger than the latter in many cases. Furthermore, the test results were larger than the results calculated from the F value.

Finally, Fig. 4.3.16 summarizes the reduction factors of the yield point f_y, axially loaded compressive test results, and axially loaded stub-column compressive test results. Each reduction factor is evaluated using R_θ / R_{20}, where R_θ is the test result for the heating process at θ °C, and R_{20} is the test result for the untreated specimen. As shown in this figure, the tendency of the reduction factors for the flexural and local buckling test results is similar to the yield point (dashed line in Fig. 4.3.16). It is indicated that the reduction factors of both the flexural and local buckling strengths strongly depend on the yield point of the steel subjected to the heating and cooling processes.

Table. 4.3.5 Stub-column test results of specimens A

Maximum values of P/A (N/mm^2)								
Specimen	Heated temperature							
	Untreated	200℃ treated	300℃ treated	400℃ treated	500℃ treated	600℃ treated	700℃ treated	800℃ treated
Specimen A	301.1	351.4	364.7	400.8	338.4	315.6	290.8	262.1

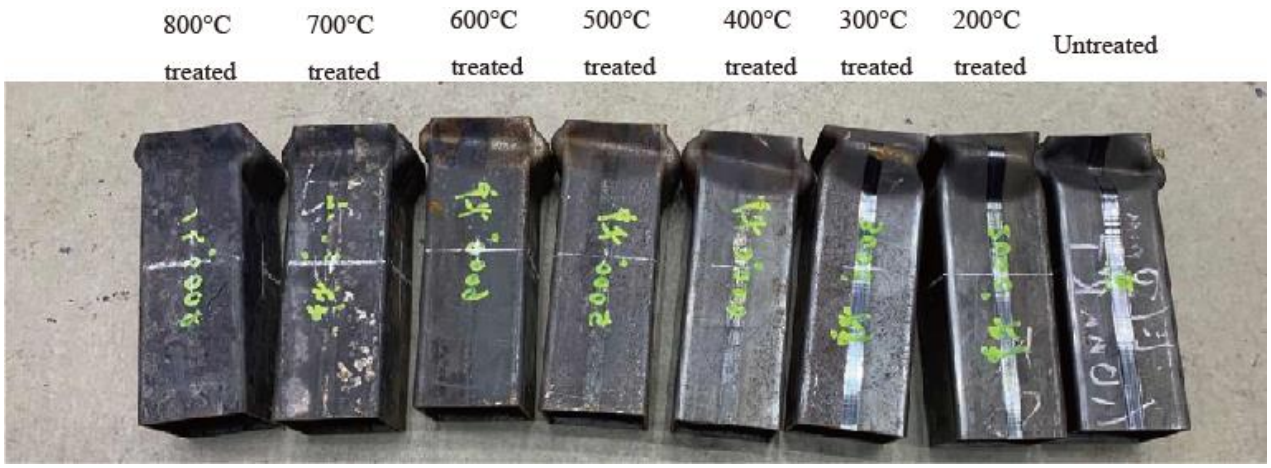

Figure 4.3.13 Stub-column specimens after tests

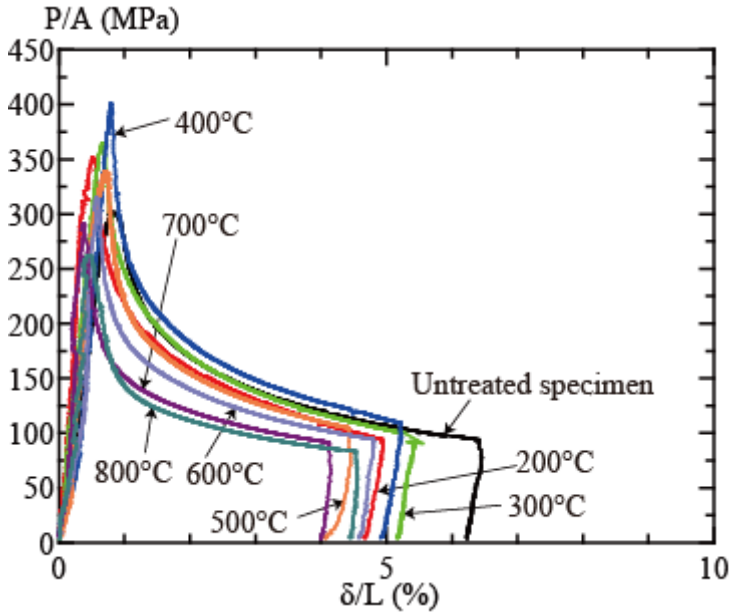

Figure 4.3.14 P/A–δ/L relationships of specimens A

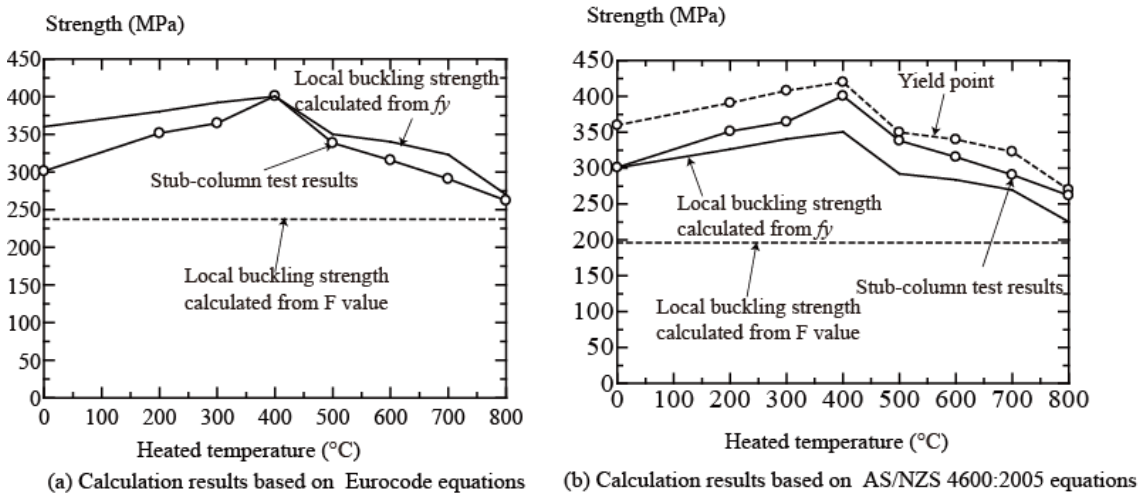

Figure 4.3.15 Stub-column test results and calculation results based on Eurocode and AS/NZS 4600:2005 equations

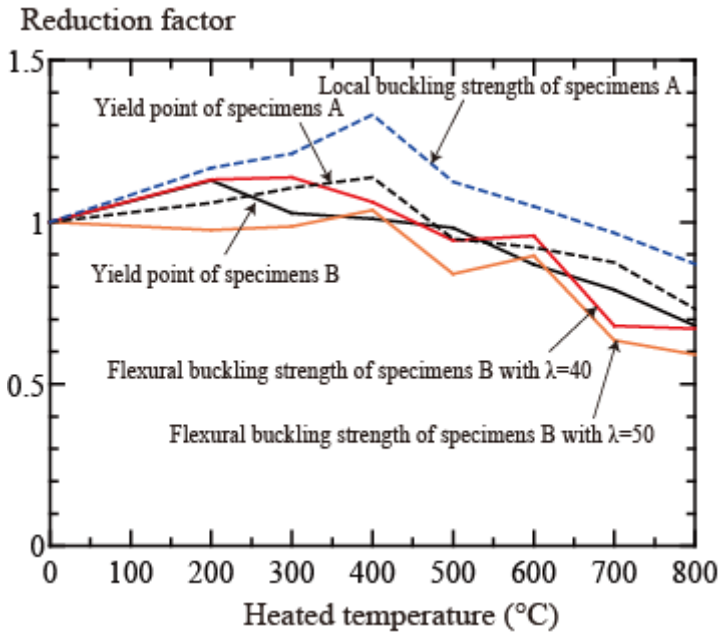

Figure 4.3.16 Reduction factors of tests results

4.4 Conclusion

In this Chapter, the test result of the yield, tensile, flexural buckling, and local buckling strength of the cold-formed steel square hollow section after the heating and cooling process were reported, these mechanical properties are very important to evaluate if the cold-formed steel section can be reused after fire. The conclusions are summarized as follows:

1) According to the coupon tensile test results, it was confirmed that the yield point and tensile strength of the cold-formed steel square hollow section steel that were subjected to a slow cooling rate

after the low and medium temperature (200-400 °C) increased in comparison with the untreated specimens. However, when the specimens were subjected to heating at high-temperature (500–800 °C), the yield strength and tensile strength started to decrease in comparison with the specimens that were heated to 400 °C, but it is larger than the design yield point of the steel (235 MPa). It is important to consider the strength change caused by fire heating when these steel columns are repaired or reused after a fire.

2) According to the test result of the axially loaded compressive test and stub-column tests, it was confirmed that both the residual flexural and local buckling strengths changed after the heating and cooling process. It is mostly because of the change from both yield strength and tensile strength. And the flexural buckling strength can be evaluated using the Eurocode equations based on the residual yield strength, local buckling strength can be evaluated using both the Eurocode equations and AS/NZS design equations based on the residual yield strength. However, in the actual fire, it is very difficult to accurately evaluate the temperature history of the steel column after a fire, since the yield strength of steel after fire is unknown. Therefore, it is recommended that the residual flexural and local buckling should be evaluated using the design standard strength (F-value) at ambient temperature to achieve a safe-side evaluation.

3) The standard design yield point and tensile strength of STKR400 steel are 235 and 400MPa respectively, these values are the 5% lower limit value for the yield point and tensile strength of the JIS SS400 steel. For the JIS SS400 steel, these standard design yield point and tensile strength is 5% lower limit value on the probability distribution for this steel. JIS STKR400 steel is cold-formed by the JIS SS400 steel. Therefore, theoretically, the 5% lower limit value of the yield point on the JIS STKR400 steel is much higher than 235 MPa. However, in the actual structural design, 235 MPa is still considered as the standard design yield point of the JIS STKR400 steel. As a result, the yield point of the STKR400 steel after fire is still higher than 235MPa. This is advantageous as it can improve reusability without replacement.

Reference

[4.1]. EN 1993-1-1, Eurocode 3 - Design of steel structures – Part 1-1: General rules and rules for buildings, May. 2005.

[4.2]. EN 1993-1-5, Eurocode 3 - Design of steel structures – Part 1-5: Plated structural elements, Oct. 2006.

[4.3]. AS/NZS 4600, cold-formed steel structures, AS/NZS 4600:2005

[4.4]. JIS G 3466, https://kikakurui.com/z2/Z2241-2011-01.html, Oct 28, 20 (in Japanese)

[4.5] W. Luecke, S. W. Banovic and J. D. McColskey (2011), High-temperature tensile constitutive data and models for structural steels in fire, National Institute of Standards and Technology Technical Note 1714, Natl. Inst. Stand. Technol. Technical Note 1714.

[4.6]. T. ONO, K. ISHIDA, F. YOSHIDA, An experimental study on local buckling zone of box-section stub-column subjected to axial compression. J. Struct. Constr. Eng. AIJ, Mar 1997, No. 493, pp.107-114. (In Japanese)

Chapter 5. Prediction equations of the residual displacement of the cold-formed steel square hollow section column after fire

5.1. Introduction

In this Chapter, a prediction equation of the post-fire residual displacement (the plastic displacement by the fire heating) for the column in a 1-storey steel frame is proposed, and the calculation result of the prediction equation is compared with the FEM analysis result of a 1-storey steel frame model, so as to evaluate the accuracy of the prediction equation. In general, the residual displacement of a column after fire could be calculated using the FEM analysis. FEM analysis is a very complicated way to calculate the residual displacement of the column. Therefore, a simple prediction equation based on the structural mechanics is proposed. Fig. 5.2.1 shows the basic model used in this Chapter. As shown in Fig. 5.2.1, both the column AB and beam BC are heated by the fire. In an actual fire, when a frame is subjected to heating, the strength of the steel members in both column and beam reduces with increasing temperature. Therefore, it needs to consider the effect of the strength reducing of the steel members in both column and beam when calculating the residual displacement of the column. Actually, it is very difficult to consider the residual displacement of the column under the effect of strength reduction in both column and beam; and the research focus in the Chapter is to predict the residual displacement of the column according to the strength change of the column after the heating and cooling process. If considering the strength reduction of beam, the residual displacement will be greatly affected by the deflection of the beam at high temperature. And the calculation mechanical will become more complex. Therefore, in the prediction equation, only the strength reduction of the steel member in column AB at high-temperature is considered; while for the beam BC, only the stress-strain curve at ambient temperature and the linear temperature expansion coefficient of steel member ($12 \times 10^{-6}\ ℃^{-1}$) are considered. In further work, the effect of beam will be considered base on these equations.

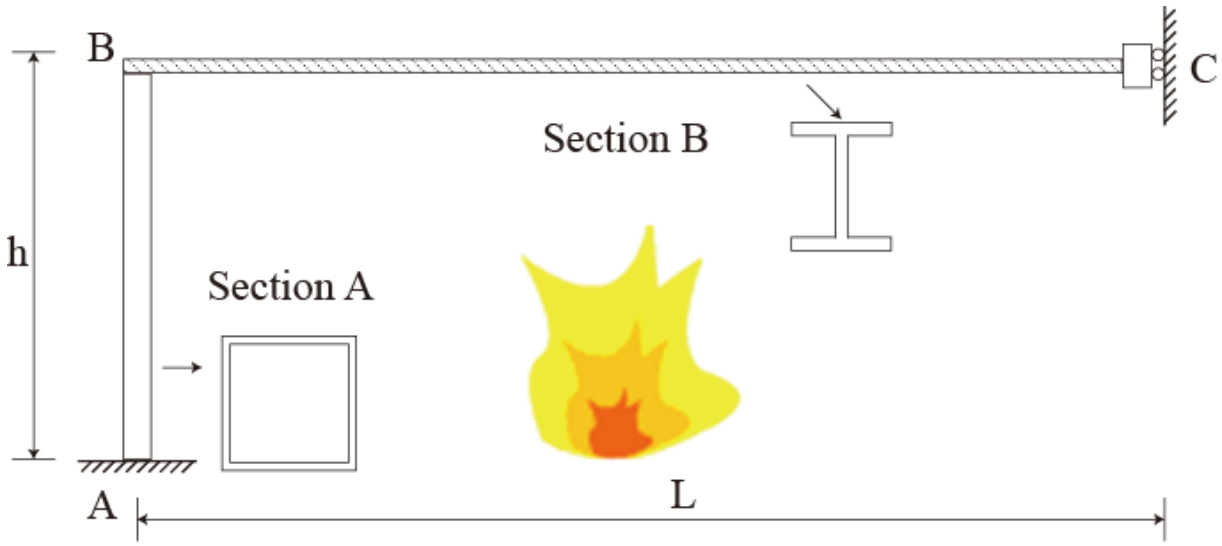

Figure 5.2.1. Basic model

5.2. Basic FEM analysis model and formulated stress-strain relationship

5.2.1. Basic model

As shown in Fig. 5.2.1, column AB is considered as a fixed support at the base of the column, and Beam BC is the sliding support at Point C. Section A is the cross-section of Column AB, the grade of the steel is BCR295 steel, which is one of the cold-formed steel square hollow section that widely used for steel building structures in Japan. Section B is the cross-section of Beam BC, it is an H-shaped cross-section steel that is given by JIS SS400B steel. Both Column AB and the Beam BC were heated with fire. Parameters of the basic FEM analysis model are listed in Table 5.2.1. The height of Column AB is given by H = 4000 mm, and the length of Beam BC is given by L = 10000 ~ 40000 mm (L/H is taken as 2.5, 5, 7.5, and 10 respectively). Section A is given by □-400-400-28 mm, and Section B is given by H-500-200-12-22, based on previous research [5.1]. In that research [5.1], the accuracy of the FEM analysis is compared with the test result, and it confirmed that FEM analysis based on the parameter in Table 5.2.1 could evaluate the test results. According to the parameter, $M_{Pc}/M_{Pb} = 2.3 > 1.5$ (where, M_{Pc} is the full plastic moment of the Column AB, M_{Pb} is the full plastic moment of Beam BC). Furthermore, the FEM analysis in this Chapter simulated for a whole process in a 1-storey steel frame in case that subjected to heating and the cooling process in the fire and fire extinguishing proceed.

Table 5.2.1. Parameters of the basic FEM analysis model

Section (mm)				h (mm)	L (mm)	L/h
Section A	□-400-400-28	Section B	H-500-200-12-22	4000	10000, 20000, 30000, 40000	2.5, 5, 7.5, 10

5.2.2. Formulated stress-strain relationship in the FEM analysis

In the FEM analysis, the stress-strain curve of the BCR295 column is a formulation equation based on the coupon test results as described in Chapter 3.2.1. Fig.5.2.2 shows the coupon test result of both FP and CP specimens. However, the formulated equation of the BCR295 steel in the FEM analysis only evaluate the SS-curves of FP specimens.

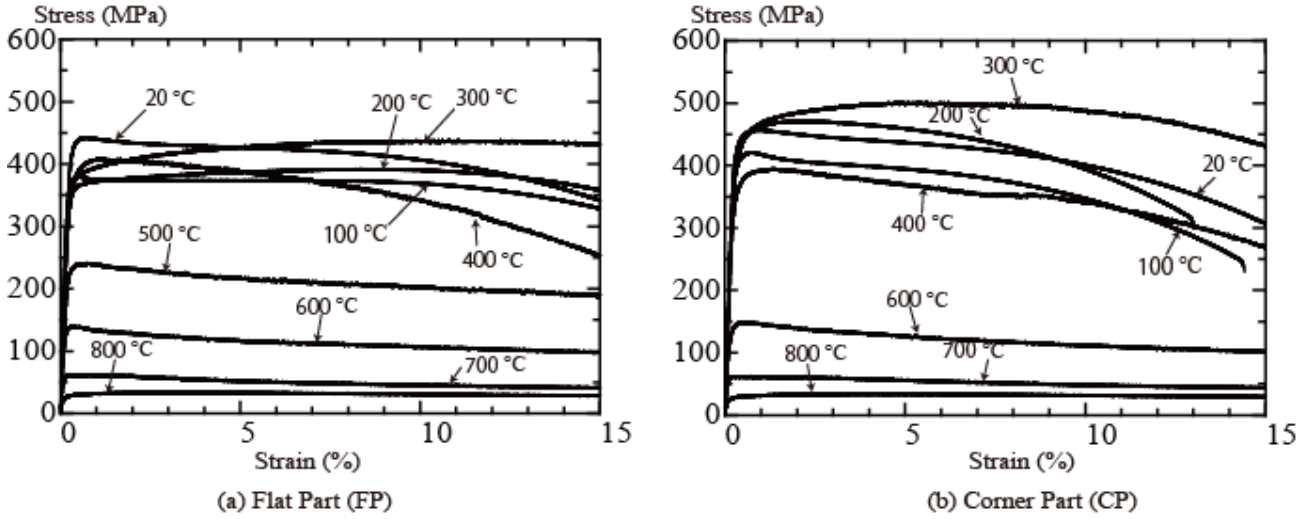

Figure 5.2.2 Stress-strain relationships at ambient and elevated temperature

The following formulas of stress-strain relationship of the BCR295 steel at 0-800 ºC are proposed by Umemura et al. [5.2] are employed as follow:

$$\varepsilon < \varepsilon_y \qquad \sigma_0 = E\varepsilon \qquad (Eq.5.1)$$

$$\varepsilon_y < \varepsilon \leq \varepsilon_{st} \qquad \sigma_0 = \sigma_y \qquad (Eq.5.2)$$

$$\varepsilon_{st} < \varepsilon \leq \varepsilon_u \qquad \sigma_0 = \sigma_u - (\sigma_u - \sigma_y)\left(\frac{{\varepsilon_u}^k - \varepsilon^k}{\varepsilon_u - \varepsilon_{st}^k}\right)^n \qquad (Eq.5.3)$$

$$\varepsilon_u \leq \varepsilon \qquad \sigma_0 = \sigma_u - (\sigma_u - \sigma_{20})\left(\frac{\varepsilon_u - \varepsilon}{\varepsilon_u - \varepsilon_{20}}\right)^n \qquad (Eq.5.4)$$

Where,

E: Yong's modulus of BCR295 steel at 0~800 ºC.

σ_y: yield point of the BCR295 steel at 0~800 ºC.

σ_u: tensile strength of the BCR295 steel at 0~800 ºC.

ε_y: the strain at yield point (σ_y/E).

ε_{st}: the strain at the yield shelf.

ε_u: the strain at the tensile strength.

σ_{20}: the strength while the strain is 0.2.

ε_{20}: the strain of 0.2.

k and n: parameters of stress hardening.

Tables 5.2.2 and 5.2.3 show the parameters of JIS SS400 and BCR295 steel used in the equations. Figs 5.2.3 and 5.2.4 show the stress-strain curve relationships of JIS SS400 and BCR295 steel respectively. In the Figures, the blue dashed line indicates the formulation result used in the FEM analysis, and the orange solid line refers to the result obtained from the coupon test. As is described above, only the linear coefficient of the thermal expansion of JIS SS400 steel is considered, therefore, the stress-strain curve of JIS SS400 steel at ambient temperature as shown in Fig.5.2.3 is used. For BCR295 steel used in the column, the stress-strain curve of it at elevated temperature as shown in Fig 5.2.4 is respectively considered. These stress-strain curves are used in the FEM analysis at both heating and cooling stage. For the heating stage, the actual experimental result can be used for the high-temperature stress-strain curve, but in the cooling stage, there is no data showing how the stress-strain is changed in this stage, although the material properties are changed after fire. Therefore, the stress-strain curve of BCR295 steel at elevated temperature is also used temporarily for the cooling stage in this research. According to Figs 5.2.3 and 5.2.4, it is confirmed that the coupon test result is accurately evaluated by the formulation equations. Therefore, in the subsequent FEM analysis, these formulation equations are used.

Table 5.2.2. Parameters of JIS SS400 steel

Temperature (ºC)	σ_y (MPa)	σ_u (MPa)	ε_{st}	ε_u	k	n	E
RT	240	440	0.14	440	0.15	8	2.05

Table 5.2.3. Parameters of BCR295 steel

Temperature (°C)	σ_y (MPa)	σ_u (MPa)	ε_{st}	ε_u	k	n	E
RT	290	442	0.007	442	1.2	5	2.05
100	280	379	0.05	379	0.1	11	1.8
200	250	385	0.094	385	0.1	8	1.7
300	350	426	0.1	426	0.45	5	1.7
400	220	407	0.012	407	0.8	5.5	1.7
500	150	240	0.008	240	0.6	5.5	1.2
600	85	139	0.003	139	1	3.5	1.2
700	43	62	0.003	62	0.3	3	0.7
800	14	33	0.0035	33	0.15	3	0.5

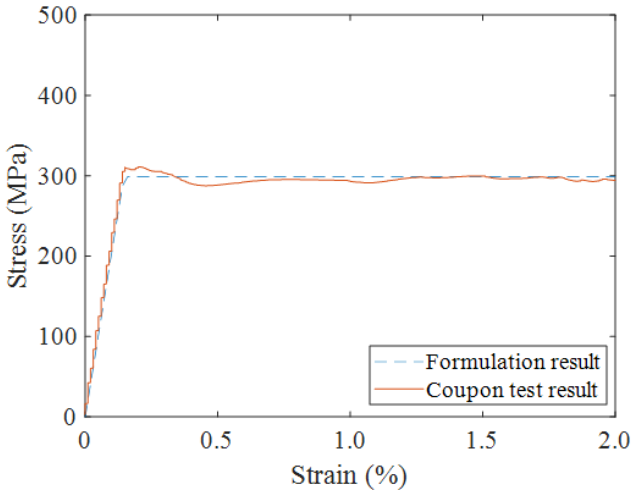

Figure 5.2.3. Stress-strain relationships of JIS SS400 steel

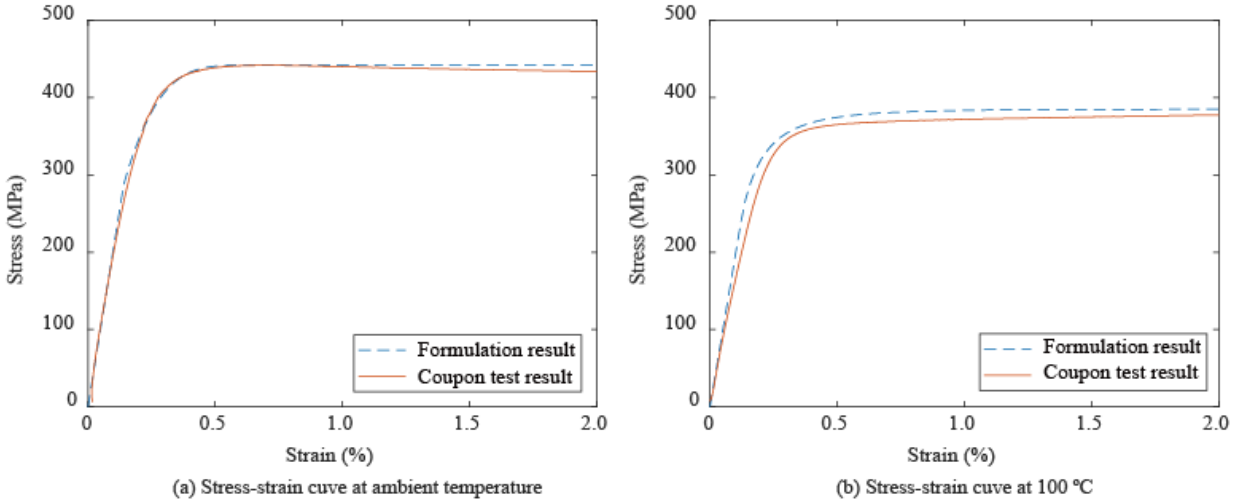

(a) Stress-strain cuve at ambient temperature

(b) Stress-strain cuve at 100 ℃

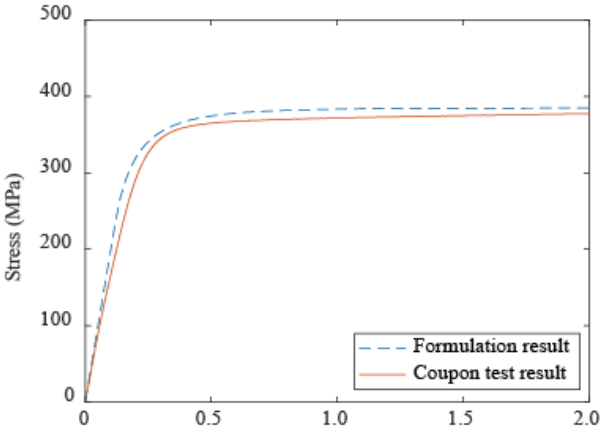

(c) Stress-strain cuve at 200 ℃

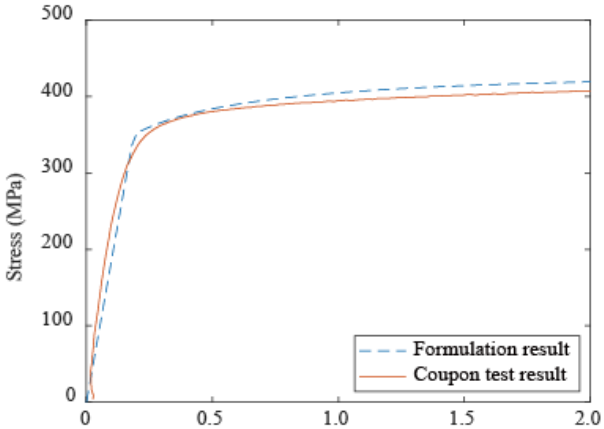

(d) Stress-strain cuve at 300 ℃

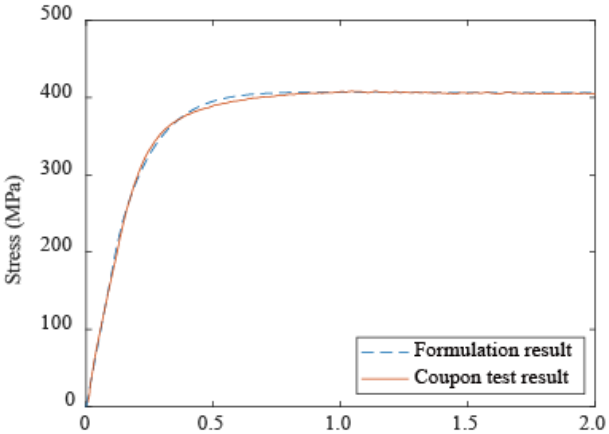

(e) Stress-strain cuve at 400 ℃

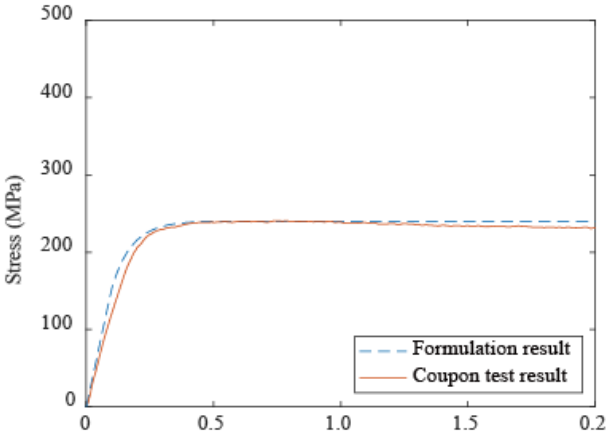

(f) Stress-strain cuve at 500 ℃

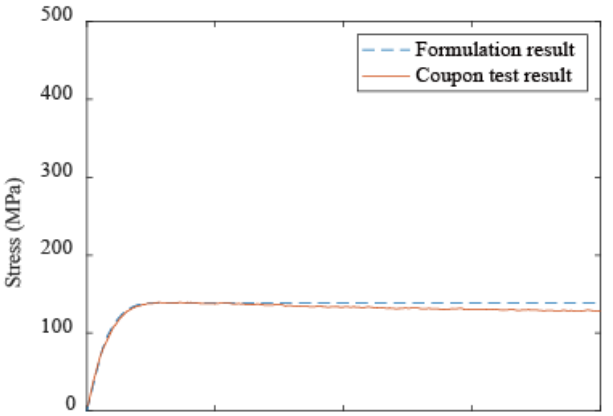

(g) Stress-strain cuve at 600 ℃

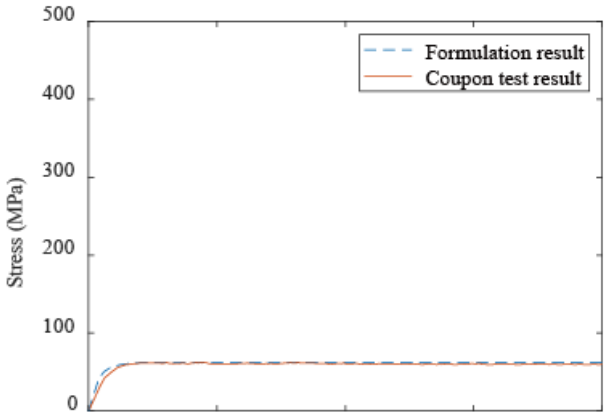

(h) Stress-strain cuve at 700 ℃

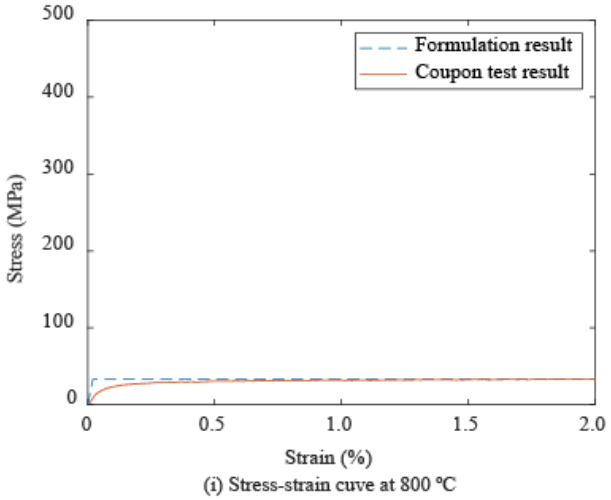

Figure 5.2.4. Stress-strain relationships of BCR295 steel

5.3. Prediction equations of residual displacement

The prediction equation of residual displacement is developed considering three steps to construct, they are model without axial load (the 1st step of the model, in this model, the axial load on the column is not considered.), model considering the axial load (the 2nd step of the model, in this model, the axial load on the column is considered but does not consider the local buckling of the column) and prediction equations of residual displacement considering the local buckling (the 3rd step of the model, both the axial load and local buckling on the column is considered).

5.3.1 Prediction equations of the model without axial load

Firstly, the basic model as shown in Fig.5.2.1 is considered, in which there is no axial load, and the temperature of both Beam BC and Column AB is suffers a fire. After it, both the beam and the column are cooled to ambient temperature. In the FEM analysis, the temperature of the model is increased to 200, 300, 400, 500, 600, 700, and 800 ºC from 0 ºC; after reaching the target temperature, it is decreased to 0 ºC, with both the increase and decrease rate given by 10 ºC/min. Fig.5.3.1 shows the heating and cooling temperature history used in FEM analysis. In Chapters 2-4, it is described that the material properties of the steel are affected by the cooling rate, in the FEM analysis, the material properties of BCR295 steel regarding the stress-strain curve at high-temperature are formulated based on the coupon tensile test results. In the heating stage, both the yield and tensile strength decreased with increasing temperature, and for the cooling stage, both the yield and tensile strength recovered.

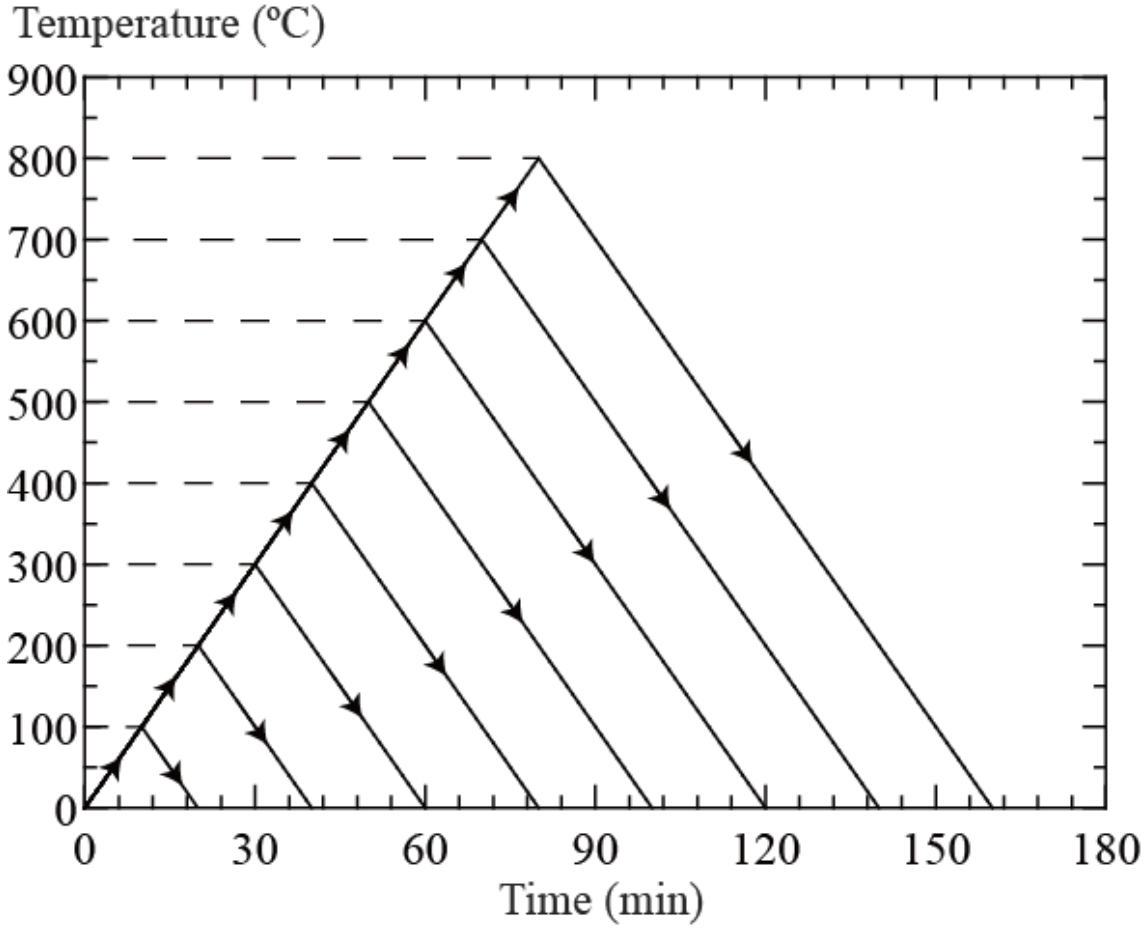

Figure 5.3.1. Heating and cooling temperature history used in FEM analysis

During the heating stage, it is considered that Column AB is subjected to the lateral force on the top of the column because of the temperature expansion of the beam. It is explained by that when the temperature of Beam BC increased, a linear expansion occurred; as a result, a counterforce occurs in the column to prevent the linear temperature expansion of Beam BC. In the cooling stage, shrinkage occurs to the beam owing to the decreasing temperature, therefore, a pulling force (opposite to the direction of the displacement on the column at elevated temperature) acts on the column, as shown in Fig. 5.3.2. The linear expansion of the beam is considered, because compared with the length of the beam, the height of the column is very short, as is listed in Table 5.2.1. In Fig. 5.3.2, it is considered that when increasing to the target temperature T_{max}, the displacement of column at elevated temperature increases to $\delta_{T_{max}}$. If $\delta_{T_{max}}$ of the column larger than the displacement of the column in elastic stage, when cooled down to the ambient temperature, residual displacement δ_r is remained in the column. If we focus on the structural behaviours of the column during the whole heating and cooling process, the column is subjected to the loading, unloading and reverse loading processes. Therefore, $F \sim \delta$ relationship could be given as shown in Fig 5.3.3, where F is the lateral force acted on the top of the column, and δ is the displacement at the top of the column.

As shown in Fig.5.3.3, it is assumed that the temperature of the beam and the column rises from "T_0", where "T_0" means the ambient temperature, during the temperature rising, "T_1" and "T_2" is given in the figure. "T_1" is the temperature when the displacement of the column equal to "δ_{T_1}"(the elastic displacement of the column) and "T_2" is the maximum temperature, in this temperature, the displacement of the column is equal to "δ_{T_2}". After the temperature reaches the maximum "T_2", it starts reducing. "T_3" is the temperature when the force in the beam is equal to 0, and "δ_{T_3}" is the displacement of the column while it is subjected to no lateral force at temperature "T_3". Finally, the temperature continues reducing after Point "T_3", and during this stage, the column is subjected to reverse loading. Furthermore, according to Fig.5.3.3, the stage between "$T_0 - T_1$" and "$T_3 - T_4$" means the elastic stage of the column, and that between "$T_1 - T_2$" and "$T_4 - T_5$" means that the column enters the plastic stage.

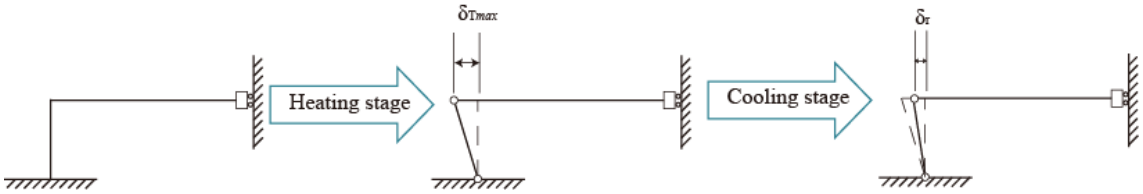

Figure 5.3.2. Displacement changes of the column during the heating and cooling stage.

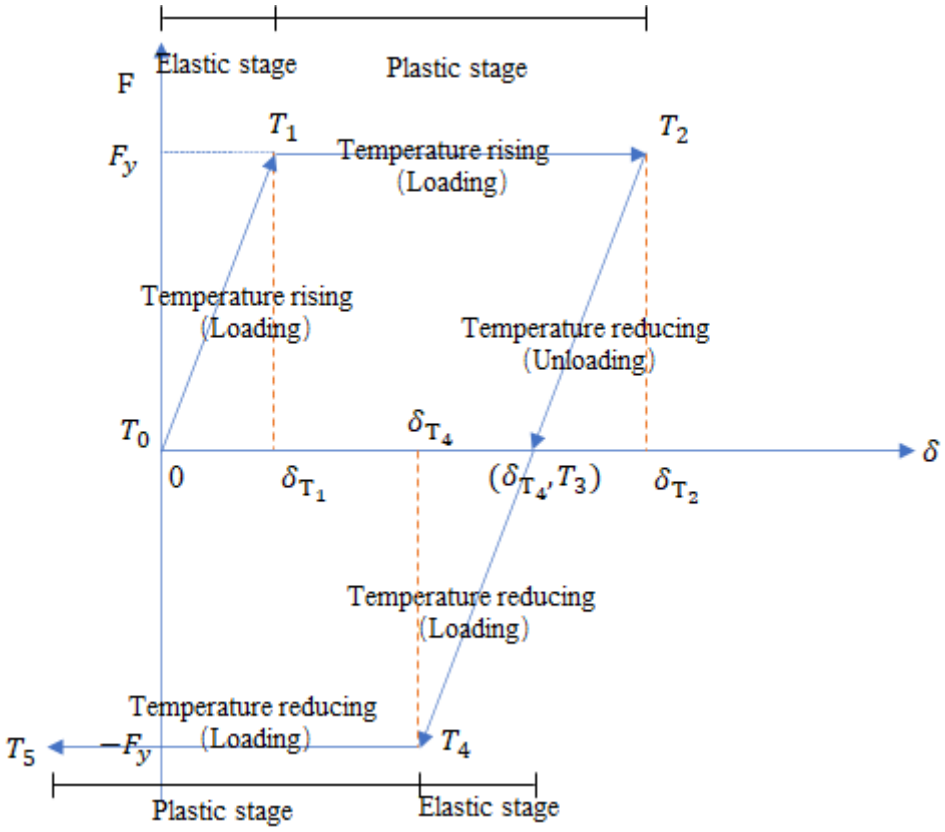

Figure 5.3.3 $F \sim \delta$ relationship during the heating and cooling process

Fig. 5.3.4 shows the model of the column and the beam, while the displacement δ_c and δ_b occurs to them (δ_c is the displacement of the column, δ_b is the displacement of the beam). Furthermore, it is easy

to know that $\delta_c = \delta_b$. When the temperature of the beam rises, the same displacement occurs to both the beam and the column, which are subjected to the same force F. Therefore, the equations are given as follow.

$$\delta_c = \frac{F}{k_c} = \frac{Fh^3}{12E_cI_c} \qquad (Eq.5.5)$$

$$\delta_b = \alpha TL - \frac{F(\alpha T + 1)L}{E_bA_b} \qquad (Eq.5.6)$$

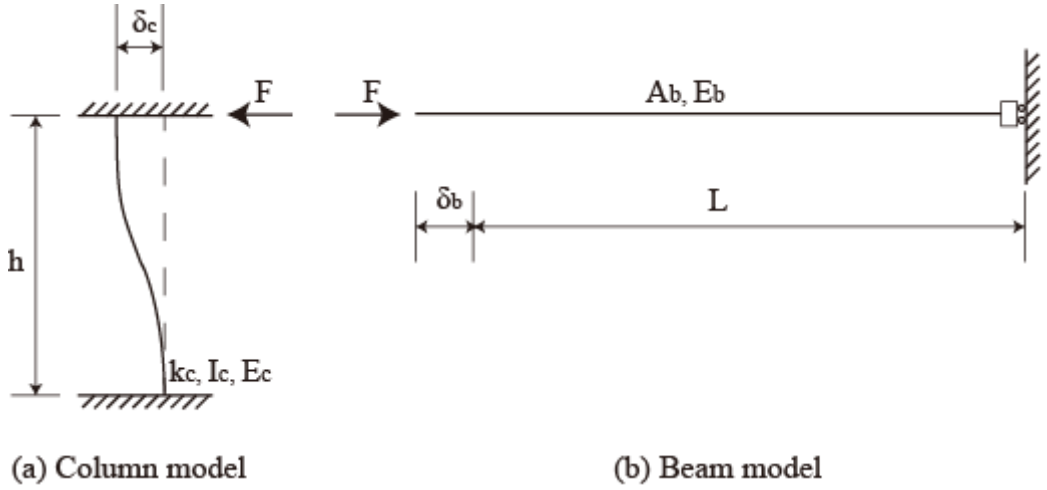

Figure 5.3.4 Displacement of column and beam

where,

h: the height of the column.

k_c: the rigidity of the column while the lateral displacement occurs at the end (two-side fixed-end column).

E_c: Yong's modulus of BCR295 steel.

I_c: moment of inertia for the area of the cross-section of the column.

α: the linear temperature expansion coefficient of the beam ($12 \times 10^{-6}\ m\ /\ (m\ ℃)$).

T: the value of rising temperature.

L: the length of the beam.

E_b: Yong's modulus of JIS SS400 steel.

A_b: cross-section area of the beam.

F_{cy} can be calculated based on the column collapse model, as shown in Fig.5.3.2, and the following equation is given:

$$F_{cy} = \frac{2M_p}{h} \qquad (Eq.5.7)$$

where,

M_p: the full plastic moment of the column

According to Fig 5.3.4, Eq 5.5 equal to Eq 5.6, therefore, temperature T_1 could be predicted by the following equations:

$$T_1 = \frac{2M_p(T_1)L + \delta_{T_1}E_bA_bh}{\alpha LE_bA_bh - 2\alpha M_p(T_1)L} \quad (Eq.5.8)$$

$$\delta_{T_1} = \frac{M_p(T_1)h^2}{6E_c(T_1)I_c} \quad (Eq.5.9)$$

where,

$M_p(T_1)$: the full plastic moment of the column at Temperature T_1.

$E_c(T_1)$: Yong's modulus of BCR295 steel at Temperature T_1.

According to Fig. 5.3.3, when the maximum temperature is between T_0 and T_1, the column is in the elastic stage, and the residual displacement δ_r of the column is 0. Then, the maximum displacement of the column when the temperature reaches the maximum value can also be predicted by the equations given as follow:

$$if\ T_0 \le T_{max} \le T_1, \qquad \delta_{T_{max}} = \frac{\alpha T_{max}Lh^3E_bA_b}{12(\alpha T_{max}+1)E_c(T_{max})I_c + E_bA_bh^3} \quad (Eq.5.10)$$

$$\delta_r = 0 \quad (Eq.5.11)$$

where,

$$E_c(T) = (1 - 10^6T^2) \times 205000 \quad (Eq.5.12)[5.3]$$

T_{max}: the maximum temperature of the steel members during the heating stage.

$E_c(T_{max})$: Yong's modulus of BCR295 steel at Temperature T_{max}

On the other hand, if the heating temperature T_{max} is higher than T_1, it is assumed that the plastic hinge occurs to the column, and then, the beam starts a free thermal expansion. Therefore, the displacement at elevated temperature $\delta_{T_{max}}$ is given as follow:

$$if\ T_1 < T_{max}, \qquad \delta_{T_{max}} = \alpha T_{max}L - \frac{2M_p(T_{max})(\alpha T_{max}+1)L}{E_bA_bh} \quad (Eq.5.13)$$

where,

$M_p(T_{max})$: the full plastic moment of the column at the maximum heating temperature

To calculate the residual displacement δ_r after the cooling process in case that the heating temperature T_{max} exceeds T_1, the unloading process needs to be considered. In other words, temperature T_3 in Fig.5.3.3 must be calculated. The calculation equations of T_3 and the displacement of Column δ_{T_3} at this temeprature are given as follow:

$$\delta_{T_3} = \alpha L\, T_3 = \delta_{T_{max}} - \frac{M_p(T_3)h^2}{6E_c(T_3)I_c} \quad (Eq.5.14)$$

where,

$M_p(T_3)$: the full plastic moment of the column at Temperature T_3

$E_c(T_3)$: Yong's modulus of BCR295 steel at Temperature T_3

After unloading, the temperature continues decreasing to 0 ºC, and at this time, the column is subjected

to the negative direction loading. Similar to the heating stage, it also needs to consider if the column enters the plastic stage during the unloading process at Temperature T_4. Therefore, Temperature T_4 is given as the following equation, which means the time when the column enters the plastic stage:

$$T_4 = \frac{\left(\delta_{T_3} - \frac{M_p(T_4)h^2}{6E_c(T_4)I_c}\right)E_bA_bh - 2M_p(T_4)L}{2\alpha M_p(T_4)L + \alpha E_bA_bhL} \qquad (Eq.5.15)$$

where,

$M_p(T_4)$: the full plastic moment of the column at Temperature T_3

$E_c(T_4)$: Yong's modulus of the BCR295 steel at Temperature T_4

If $T_4 \geq 0$, it means that the column does not enter the plastic stage during the cooling process, but if $T_4 < 0$, the column enters the plastic stage. In conclusion, the residual displacement can be calculated as follow:

$$\begin{cases} \delta_r = 0 & (T_{max} < T_1) \\ \delta_r = \dfrac{12E_c(T_{RT})I_cL\delta_{T_3}}{12E_c(T_{RT})I_cL + E_bA_bh^3} & (T_{max} > T_1 \ and \ T_4 < 0) \\ \delta_r = \dfrac{2M_p(T_{RT})L}{E_bA_bh} & (T_{max} > T_1 \ and \ T_4 > 0) \end{cases} \qquad (Eq.5.16)$$

$M_p(T_{RT})$: the full plastic moment of the column at the ambient temperature

$E_c(T_{RT})$: Yong's modulus of the BCR295 steel at ambient temperature

Figs. 5.3.5-5.3.8 show the comparison between results of the FEM analysis and the calculation of the prediction equations. The solid line means the calculation results and the solid line with the symbol '○' indicates the results of the FEM analysis. In the FEM analysis, the analysis model is a basic model, as shown in Fig 5.2.1 and Table 5.2.1. Both the beam and the column are heated to 100-800 ºC in the heating stage, which are then cooled to 0 ºC. The height of the column is 4000 mm, and the length of the beam is 10000, 20000, 30000, as well as 40000 mm, respectively. The "L/h" in the graphs means the value of length of the beam divided by the height of the column. Fig. 5.3.5 shows displacement ($\delta_{T_{max}}$) of the column at a high-temperature, which is calculated by Eqs 5.10 and 5.11. In Fig. 5.3.6, the vertical axis means the temperature (T_3, calculated from Eq 5.14) while the column is subjected to no lateral force in the cooling stage, and the horizontal axis means the maximum temperature of the model in the heating stage. Figs. 5.3.7 shows the relationship between the displacement (δ_{T_3}, calculated through Eq. 5.14) of the column at Temperature T_3 and the heating temperature. Figs. 5.3.8 shows the relationship between the residual displacement (δ_{T_3}, calculated through Eq. 5.16) of the column at the cooling and the heating temperature.

According to Fig.5.3.5, it is confirmed that the high-temperature displacement of the column could be predicted by Eqs. 5.10 and 5.11. Regarding Temperature T_3 and Displacement δ_{T_3}, the calculation results based on Eq. 5.14 are mostly equal to the FEM analysis results. Furthermore, according

to Fig.5.3.8, it is verified that during the elastic stage, Eq.5.16 could be used to evaluate the residual displacement of the column at a safe side, however, if the column enters the plastic stage during cooling stage, the residual displacement calculated based on the Eq. 5.16 is a little bit lower than the FEM analysis result, it is because in the FEM analysis, when the column enters the plastic stage, the full plastic moment of it increased owing to the strain hardening of the steel; however in the prediction equation, the strain hardening when the column enters to the plastic stage is not considered.

These results indicate that equations 5.7~5.16 could be used to predict the displacement of the column during the whole heating and cooling process without considering the effect of the beam. Also, more data of the cold-formed steel square hollow section with other dimensions is needed to verify the accuracy of these equations.

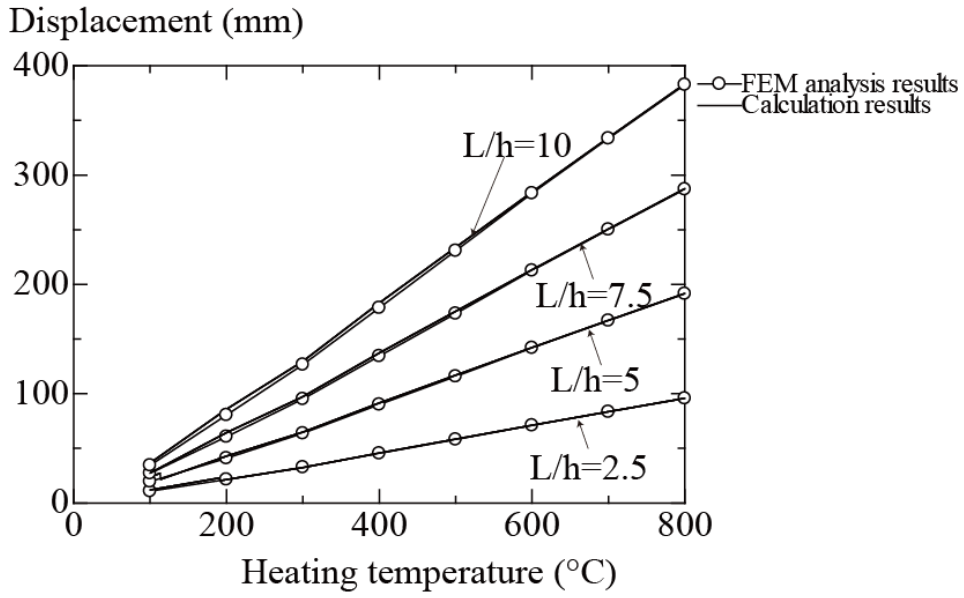

Figure 5.3.5 Displacement of the column at high-temperature

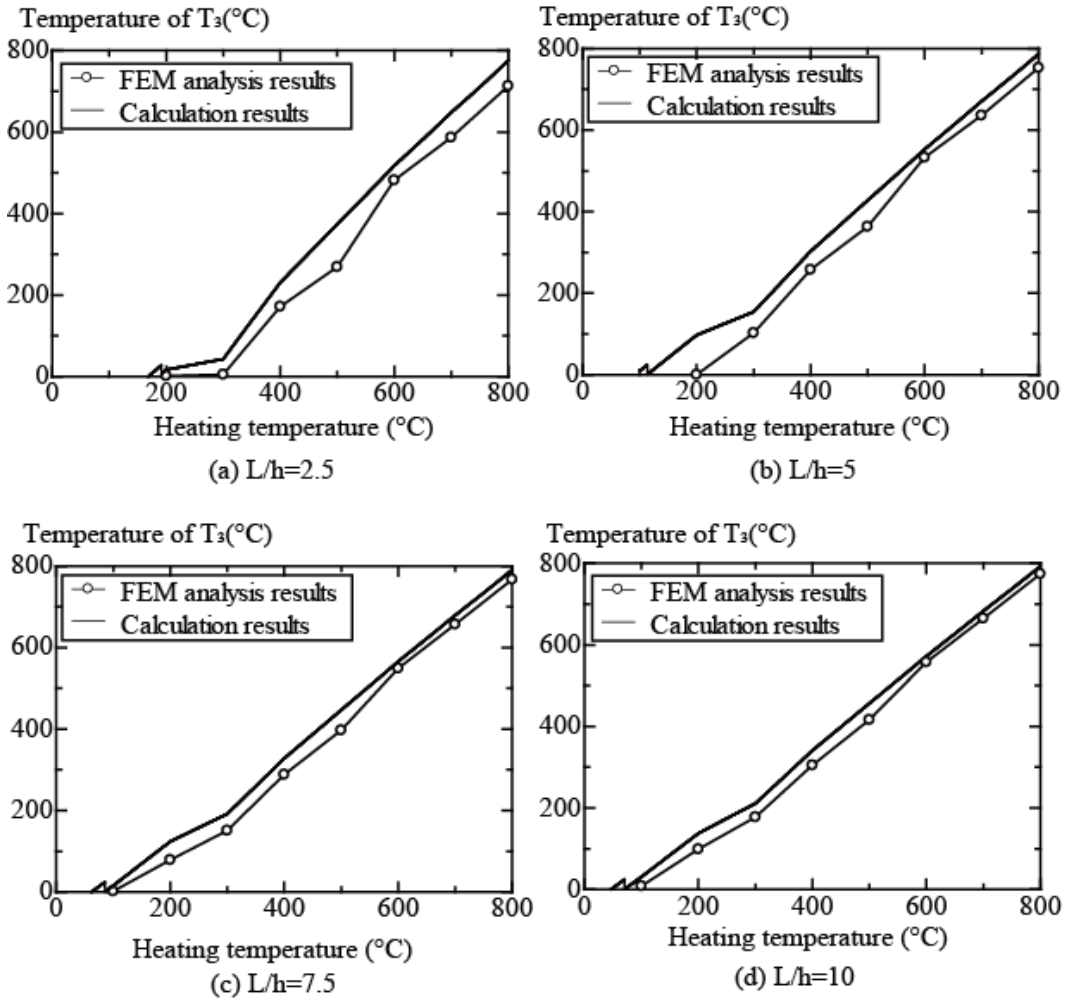

Figure 5.3.6 Temperature T_3 of the column while the force = 0

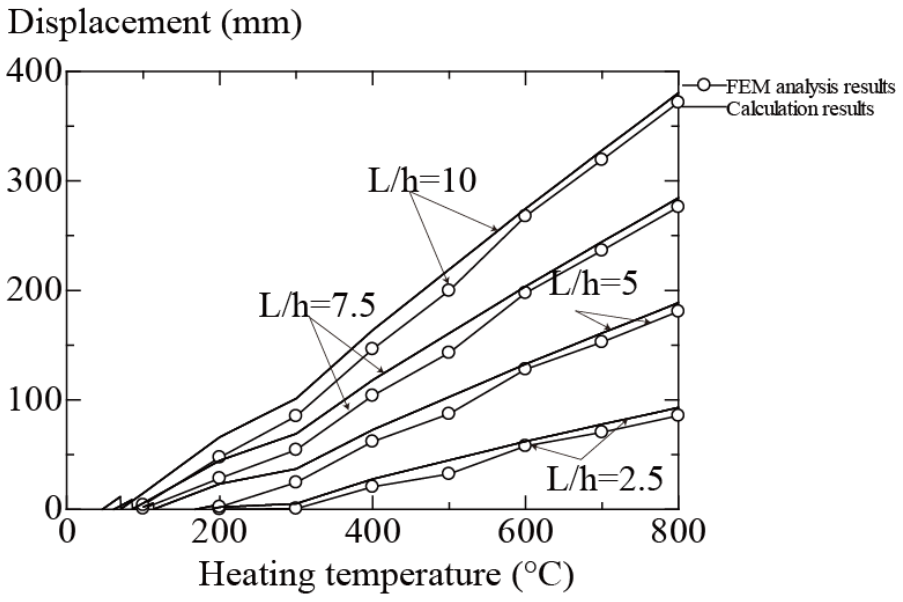

Figure 5.3.7 Displacement of the column at Temperature T_3

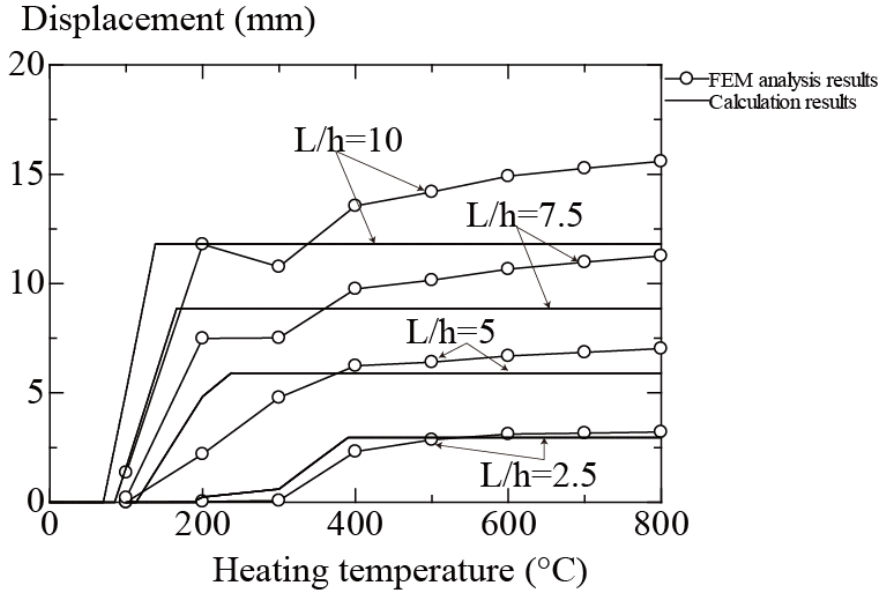

Figure 5.3.8 Residual displacement of the column after heating

5.3.2 Prediction equations of the model subjected to the axial load

Secondly, the model subjected to the axial load as shown in Fig.5.3.9 is considered, in which Column AB is subjected to an axial load P at the Point B, which is replicated to the general column of a steel structure building. Except that the uniform load on the beam is not considered, because the effect of the beam is not considered. Table 5.3.1 shows the parameters of the model in Fig. 5.3.9, most of which are the same as the basic model, however, the axil load P is considered. “p” in the table means the axial force ratio (the value of P divided by F_c, which the N_{cr} is the yield strength of the column), and “p” is given by 0.2 and 0.4.

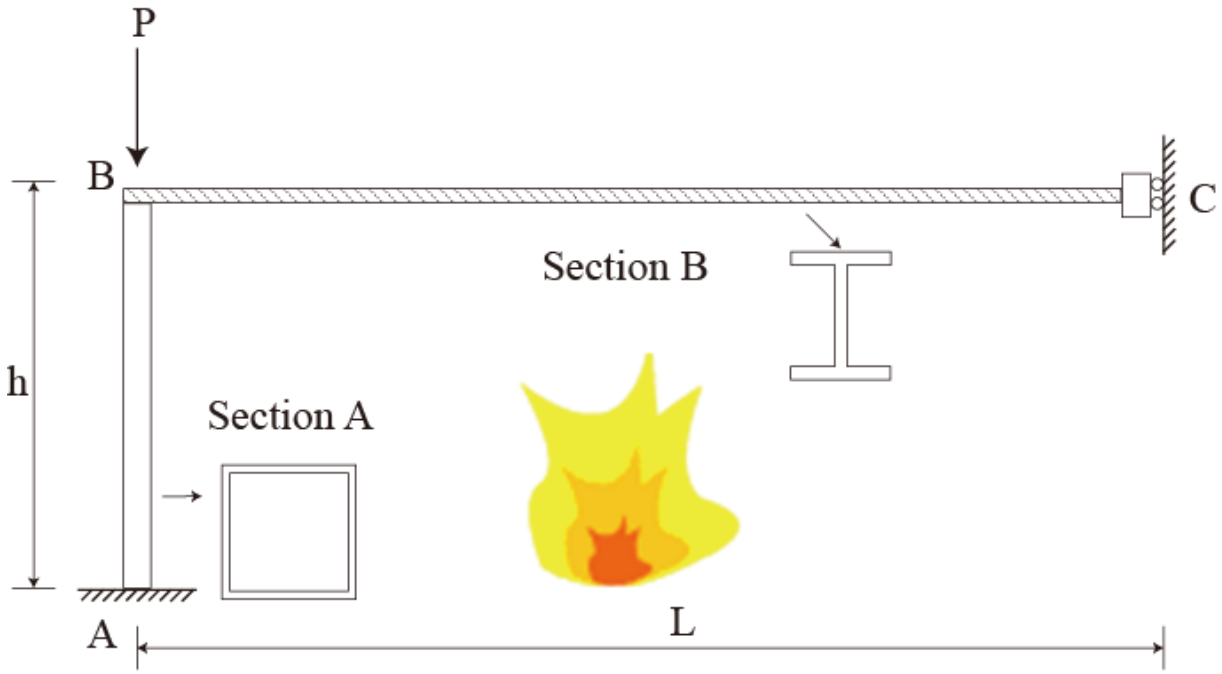

Figure 5.3.9. FEM analysis model subjected to the axial load

Table 5.3.1. Parameters of the FEM analysis model subjected to the axial load

Section (mm)				h (mm)	L (mm)	L/h	p (P/F_c)
Section A	□-400-400-28	Section B	H-500-200-12-22	4000	10000, 20000, 30000, 40000	2.5, 5, 7.5, 10	0.2,0.4

Regarding the predication equations of the residual displacement, most of the equations used in Eqs. 5.5 ~ 5.16 could be employed. However, according to the AIJ Recommendations for Fire Resistant design of Steel Structures [5.3], the full plastic moment reduction affected by the axial load should be considered. Therefore, the full plastic moment correlation equation related to the axial load of the steel square hollow section is given as the following:

$$\tau(p) = \frac{M_{pnew}}{M_p} = \begin{cases} 1 - \frac{4}{3}p^2 : 0 \le p \le \frac{1}{2} \\ \frac{4}{3}(1-p) : \frac{1}{2} \le p \le 1 \end{cases} \qquad (Eq.\,5.17)$$

where.

$\tau(p)$: the reduction factor of the moment related to the axial load.

M_{pnew}: the full plastic moment of the column under the axial load effect.

In the prediction equations, the axial force ratio at elevated temperature should be considered, and the

following equations are given:

$$p(T) = \frac{pF_c}{F_c(T)} \qquad (Eq.5.18)$$

$$\tau\big(p(T)\big) = \frac{M_{pnew}}{M_p} = \begin{cases} 1 - \frac{4}{3}p^2 : 0 \le p \le \frac{1}{2} \\ \frac{4}{3}(1-p) : \frac{1}{2} \le p \le 1 \end{cases} \qquad (Eq.5.19)$$

where,

$F_c(T)$: the yield strength of the column at elevated temperature.

$p(T)$: the axial force ratio at elevated temperature.

$\tau\big(p(T)\big)$: the reduction factor of the moment related to the axial load at elevated temperature.

Therefore, according to the Eqs.5.18-5.19, the following equations are obtained:

$$T_1 = \frac{2\tau\big(p(T_1)\big)M_p(T_1)L + \delta_{T_1}E_bA_bh}{\alpha LE_bA_bh - 2\alpha\tau\big(p(T_1)\big)M_p(T_1)L} \qquad (Eq.5.20)$$

$$\delta_{T_1} = \frac{\tau\big(p(T_1)\big)M_p(T_1)h^2}{6E_c(T_1)I_c} \qquad (Eq.5.21)$$

$$if\ T_0 \le T_{max} \le T_1, \qquad \delta_{T_{max}} = \frac{\alpha T_{max}Lh^3E_bA_b}{12(\alpha T_{max}+1)E_c(T_{max})I_c + E_bA_bh^3} \qquad (Eq.5.22)$$

$$if\ T_1 < T_{max}, \qquad \delta_{T_{max}} = \alpha T_{max}L - \frac{2\tau\big(p(T_{max})\big)M_p(T_{max})(\alpha T_{max}+1)L}{E_bA_bh} \qquad (Eq.5.23)$$

$$\delta_{T_3} = \alpha L\ T_3 = \delta_{T_{max}} - \frac{\tau\big(p(T_3)\big)M_p(T_3)h^2}{6E_c(T_3)I_c} \qquad (Eq.5.24)$$

$$T_4 = \frac{\left(\delta_{T_3} - \frac{\tau\big(p(T_4)\big)M_p(T_4)h^2}{6E_c(T_4)I_c}\right)E_bA_bh - 2\tau\big(p(T_4)\big)M_p(T_4)L}{2\alpha\tau\big(p(T_4)\big)M_p(T_4)L + \alpha E_bA_bhL} \qquad (Eq.5.25)$$

$$\begin{cases} \delta_r = 0 & (T_{max} < T_1) \\ \delta_r = \dfrac{12E_c(T_{RT})I_cL\delta_{T_3}}{12E_c(T_{RT})I_cL + E_bA_bh^3} & (T_{max} > T_1\ and\ T_4 < 0) \\ \delta_r = \dfrac{2\tau\big(p(T_{RT})\big)M_p(T_{RT})L}{E_bA_bh} & (T_{max} > T_1\ and\ T_4 > 0) \end{cases} \qquad (Eq.5.26)$$

Figs. 5.3.10 and 5.3.11 show the comparison of the FEM analysis and calculation results while the axial load ratio is 0.2 and 0.4 respectively. In the figures, the vertical axis is the residual drift angle of the column after fire. The value of the residual drift angle is that of the residual displacement δ_r divided by the height of the Column AB. The horizontal axis represents the maximum heating temperature in the heating stage. The solid line shows the calculation results and the solid line with the symbol '○' indicates the results of the FEM analysis. The heating temperature (0℃~ 800℃) is

employed to calculate residual displacement δ_r based on Eqs. 5.20~5.26. However, in the FEM analysis, the maximum heating temperature of each case is given as the temperature 1 step before the collapse temperature of the model, which, for example, is 693 ºC in the case that L/h =2.5 and p=0.2, therefore, the heating temperature of this model in the FEM analysis is given by 100, 200, 300, 400, 500, 600, and 692 ºC, as shown in Fig. 5.3.10. On the other hand, according to the Recommendation for diagnosis and repair methods of fire-damaged building [5.4], three lines of δ_r/h are drawn in the figures, namely 1/200 (A rank in the temporary risk evaluation), 1/700 (the limit tolerance of steel column) and 1/1000 (the controlled tolerance of steel column). According to the comparison results, it is considered that the results of prediction equations are similar to the FEM analysis results in the case that L/h =2.5 and 5; however, when L/h=10 and 7.5, the calculation results are lower than the FEM results, which means that if the beam became longer, the accuracy of the prediction equations will decrease. Furthermore, all the FEM analysis and calculation results are lower than the line of 1/200, which means that these columns could be reused after repairing. However, this conclusion is based on the model used in this research.

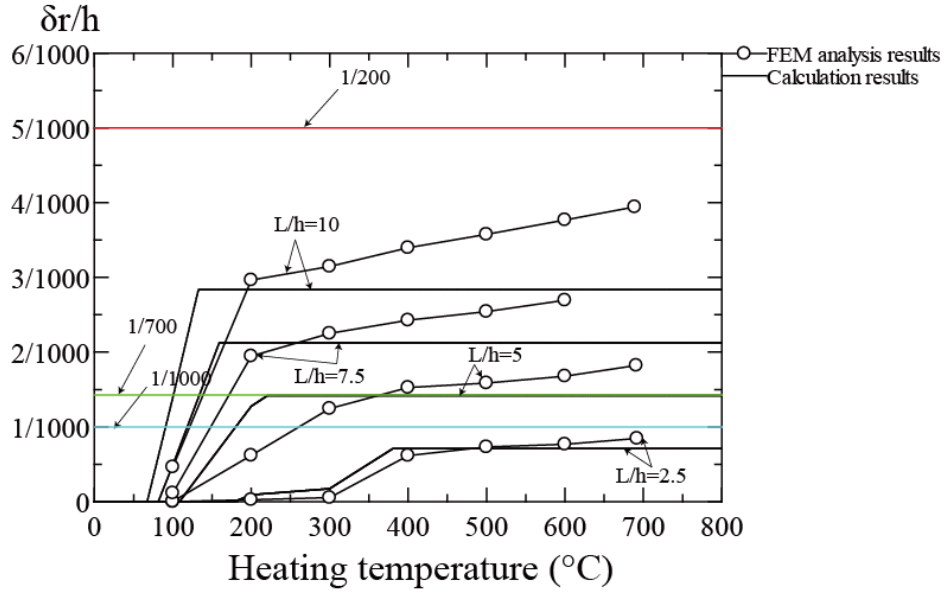

Figure 5.3.10 Result comparison while the axial load ratio p=0.2

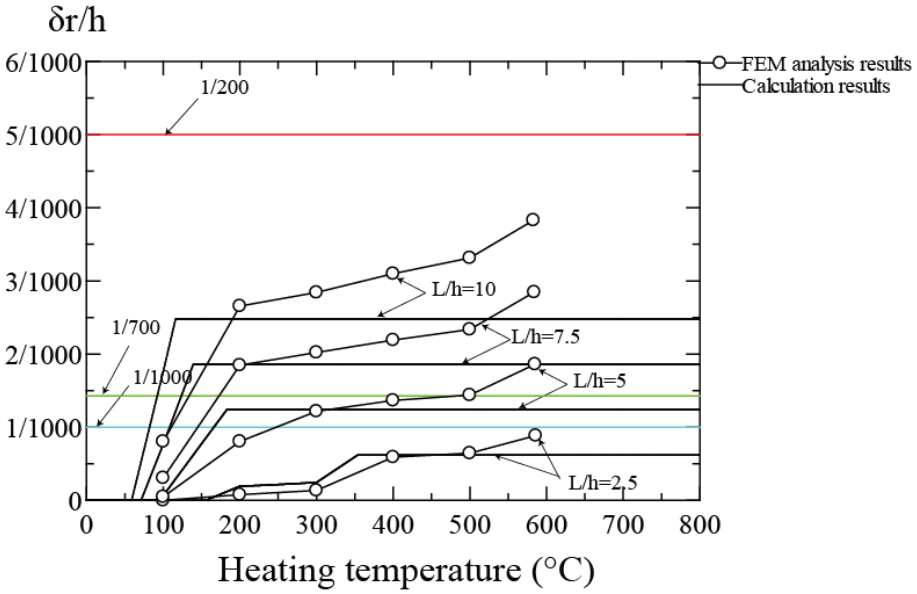

Figure 5.3.11 Result comparison while the axial load ratio p=0.4

Additionally, to evaluate the residual displacement at a more safer side, according to the AIJ Recommendations for Design of Connections in steel structure [5.5], it is considered that if the steel enters the plastic stage, the full plastic moment Mp of the column should be multiplied by 1.2 times because of strain hardening of the steel during the yield point to the tensile strength; therefore, all the Mp should be given as 1.2Mp, as a result, the following equations are given:

$$T_1 = \frac{2.4\tau\big(p(T_1)\big)M_p(T_1)L + \delta_{T_1}E_bA_bh}{\alpha LE_bA_bh - 2.4\alpha\tau\big(p(T_1)\big)M_p(T_1)L} \qquad (Eq.5.27)$$

$$\delta_{T_1} = \frac{1.2\tau\big(p(T_1)\big)M_p(T_1)h^2}{6E_c(T_1)I_c} \qquad (Eq.5.28)$$

$$if\ T_0 \le T_{max} \le T_1, \qquad \delta_{T_{max}} = \frac{\alpha T_{max}Lh^3E_bA_b}{12(\alpha T_{max}+1)E_c(T_{max})I_c + E_bA_bh^3} \qquad (Eq.5.29)$$

$$if\ T_1 < T_{max}, \qquad \delta_{T_{max}} = \alpha T_{max}L - \frac{2.4\tau\big(p(T_{max})\big)M_p(T_{max})(\alpha T_{max}+1)L}{E_bA_bh} \qquad (Eq.5.30)$$

$$\delta_{T_3} = \alpha L\ T_3 = \delta_{T_{max}} - \frac{1.2\tau\big(p(T_3)\big)M_p(T_3)h^2}{6E_c(T_3)I_c} \qquad (Eq.5.31)$$

$$T_4 = \frac{\left(\delta_{T_3} - \frac{1.2\tau\big(p(T_4)\big)M_p(T_4)h^2}{6E_c(T_4)I_c}\right)E_bA_bh - 2.4\tau\big(p(T_4)\big)M_p(T_4)L}{2.4\alpha\tau\big(p(T_4)\big)M_p(T_4)L + \alpha E_bA_bhL} \qquad (Eq.5.32)$$

$$\begin{cases} \delta_r = 0 & (T_{max} < T_1) \\ \delta_r = \dfrac{12E_c(T_{RT})I_cL\delta_{T_3}}{12E_c(T_{RT})I_cL + E_bA_bh^3} & (T_{max} > T_1 \ and \ T_4 < 0) \\ \delta_r = \dfrac{2.4\tau\big(p(T_{RT})\big)M_p(T_{RT})L}{E_bA_bh} & (T_{max} > T_1 \ and \ T_4 > 0) \end{cases} \quad (Eq.5.33)$$

Figs. 5.3.12 and 5.3.13 show the comparison of the FEM analysis and calculation results when the Mp is given by 1.2Mp. According to these figures, it is confirmed that if the full plastic moment of the column is multiplied by 1.2 times in the calculation, the prediction equations could be used to calculate the residual displacement of the column after fire more accurately.

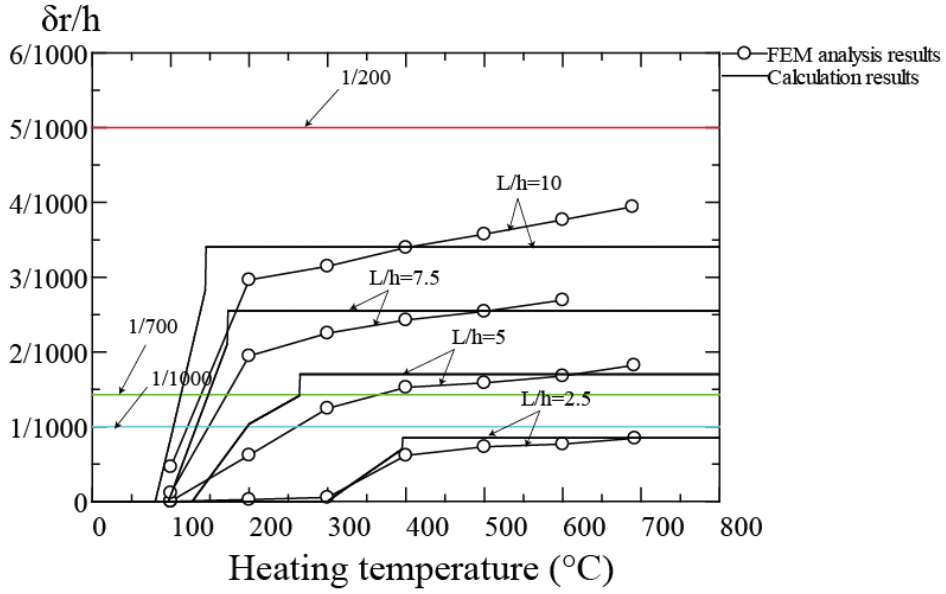

Figure 5.3.12 Result comparison while the axial load ratio p=0.2 (1.2Mp)

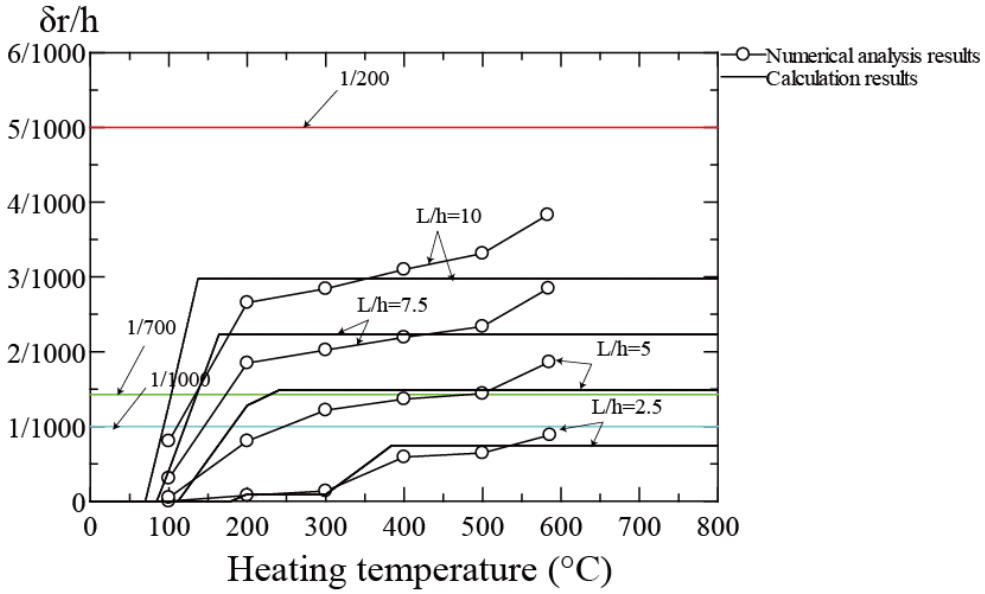

Figure 5.3.13 Result comparison while the axial load ratio p=0.4 (1.2Mp)

5.3.3 Prediction equations of the model subjected to the axial load considering the local buckling

The prediction equations of the model subjected to the axial load are explained in Section 5.3.2; however, the local buckling is not considered in the equations. In this session, both the axial load and local buckling of the column are considered in the prediction equations. The cross-section of the column (□-400-400-28) is considered in the former equations, the width-thickness of this steel cross-section is b/t = 14.3, and the effective slenderness ratio (λ) of the column in the model is calculated as 26.3. In this section, a new cross-section of □-400-400-12 (b/t = 33.3) of the column is used, because the local buckling easily occurs to the column with a large b/t ratio. Table 5.3.2 shows the new parameters of the FEM analysis model.

Table 5.3.2. Parameters of the FEM analysis model subjected to the axial load considering local buckling

Section (mm)				h (mm)	L (mm)	L/h	p (P/F_c)	b/t
Section A	□-400-400-28	Section B	H-500-200-12-22	4000	10000, 20000, 30000, 40000	2.5, 5, 7.5, 10	0.2,0.4	33.3

According to the AIJ Recommendations for Fire Resistant design of Steel Structures [5.3], local

buckling strength of the steel is calculated as follow:

$$p_{max} = \frac{P_{max}}{F_c} = \begin{cases} 20.7\dfrac{t}{b} & : \dfrac{b}{t} > 28 \\ 0.552 + 3.88\dfrac{t}{b} + \left(\dfrac{5.56}{b/t - 3}\right)^2 & : \dfrac{b}{t} \leq 28 \end{cases} \qquad (Eq.5.34)$$

where.

F_c: the yield strength of the column without considering the local buckling.

p_{max}: the ratios of the local buckling strength divided by the yield strength of the column.

P_{max}: the local buckling strength

The collapse temperature "T_{local}" could be calculated through the following equation in the case of column collapse model:

$$p = p_{max}k(T_{local}) \qquad (Eq.5.35)$$

where.

$k(T_{local})$: the reduction factor of the cold-formed steel square hollow section at elevated temperature.

As a result, the prediction equations of the model subjected to the axial load considering local buckling is given as follow:

$if\ T_{max} \leq T_{local}$:

$$Eqs.5.27 \sim 5.33\ is\ available$$

$if\ T_{max} > T_{local}$:

$$M_{plocal}(T) = M_p(T)p_{max}$$

$$T_1 = \frac{2.4\tau\big(p(T_1)\big)M_{plocal}(T_1)L + \delta_{T_1}E_bA_bh}{\alpha LE_bA_bh - 2.4\alpha\tau\big(p(T_1)\big)M_{plocal}(T_1)L} \qquad (Eq.5.36)$$

$$\delta_{T_1} = \frac{1.2\tau\big(p(T_1)\big)M_p(T_1)h^2}{6E_c(T_1)I_c} \qquad (Eq.5.37)$$

$$if\ T_0 \leq T_{max} \leq T_1, \qquad \delta_{T_{max}} = \frac{\alpha T_{max}Lh^3E_bA_b}{12(\alpha T_{max}+1)E_c(T_{max})I_c + E_bA_bh^3} \qquad (Eq.5.38)$$

$$if\ T_1 < T_{max}, \qquad \delta_{T_{max}} = \alpha T_{max}L - \frac{2.4\tau\big(p(T_{max})\big)M_{plocal}(T_{max})(\alpha T_{max}+1)L}{E_bA_bh} \qquad (Eq.5.39)$$

$$\delta_{T_3} = \alpha L\ T_3 = \delta_{T_{max}} - \frac{1.2\tau\big(p(T_3)\big)M_{plocal}(T_3)h^2}{6E_c(T_3)I_c} \qquad (Eq.5.40)$$

$$T_4 = \frac{\left(\delta_{T_3} - \dfrac{1.2\tau\big(p(T_4)\big)M_{plocal}(T_4)h^2}{6E_c(T_4)I_c}\right)E_bA_bh - 2.4\tau\big(p(T_4)\big)M_{plocal}(T_4)L}{2.4\alpha\tau\big(p(T_4)\big)M_{plocal}(T_4)L + \alpha E_bA_bhL} \qquad (Eq.5.41)$$

$$\begin{cases} \delta_r = 0 & (T_{max} < T_1) \\ \delta_r = \dfrac{12E_c(T_{RT})I_cL\delta_{T_3}}{12E_c(T_{RT})I_cL + E_bA_bh^3} & (T_{max} > T_1\ and\ T_4 < 0) \\ \delta_r = \dfrac{2.4\tau\big(p(T_{RT})\big)M_{plocal}(T_{RT})L}{E_bA_bh} & (T_{max} > T_1\ and\ T_4 > 0) \end{cases}$$

$(Eq. 5.42)$

Figs. 5.3.14 and 5.3.15 show the comparison of FEM analysis and calculation results of the column in the case of local buckling. The horizontal axis refers to the maximum heating temperature in the heating stage, the solid line refers to the calculation results and the solid line with the symbol '○' indicates the results of the FEM analysis. Similar to Figs 5.3.10 and 5.3.11, the heating temperature (0 ~ 800℃) is employed to calculate residual displacement. In the FEM analysis, the maximum heating temperature of each case is given by the temperature 1-step before the collapse temperature of the model. The vertical line is named local buckling collapse temperature. According to Eq.5.35, the local buckling collapse temperature of the model is 605 ℃ in the case that p=0.2, and for the model in the case that p=0.4, the temperature is 459 ℃. As shown in the figures, the FEM analysis results are lower than the 1/700 standard line. Thus, it is confirmed that considering the local buckling of the column, the residual displacement of the column increases firstly, and then decreases after a temperature, which is because when local buckling occurs, the reaction force F on the beam (Fig 5.3.4 (b)) decreases in comparison with the model without considering local buckling. As a result, the residual displacement decreases. However, the initial local buckling temperature in the FEM analysis is different from the local buckling collapse temperature calculated by Eq. 5.35. It is considered that the actual local buckling collapse temperature in the FEM analysis is different from the AIJ Recommendations for Fire Resistant design of Steel Structures. The collapse temperature is calculated based on the temperature reduction curves of the BCR steel in the AIJ Recommendations for Fire Resistant design of Steel Structures, on the contrary, in the FEM analysis, the ss-curve of the BCR295 steel is formulated based on the actual coupon test result in Chapter 3. Furthermore, by comparing the calculation results with the FEM analysis results, it is confirmed that the prediction equations could be used to evaluate the residual displacement of the column after fire. Because, the FEM analysis results is lower than the calculation results, which means the prediction equation can evaluate the residual displacement on the safe side.

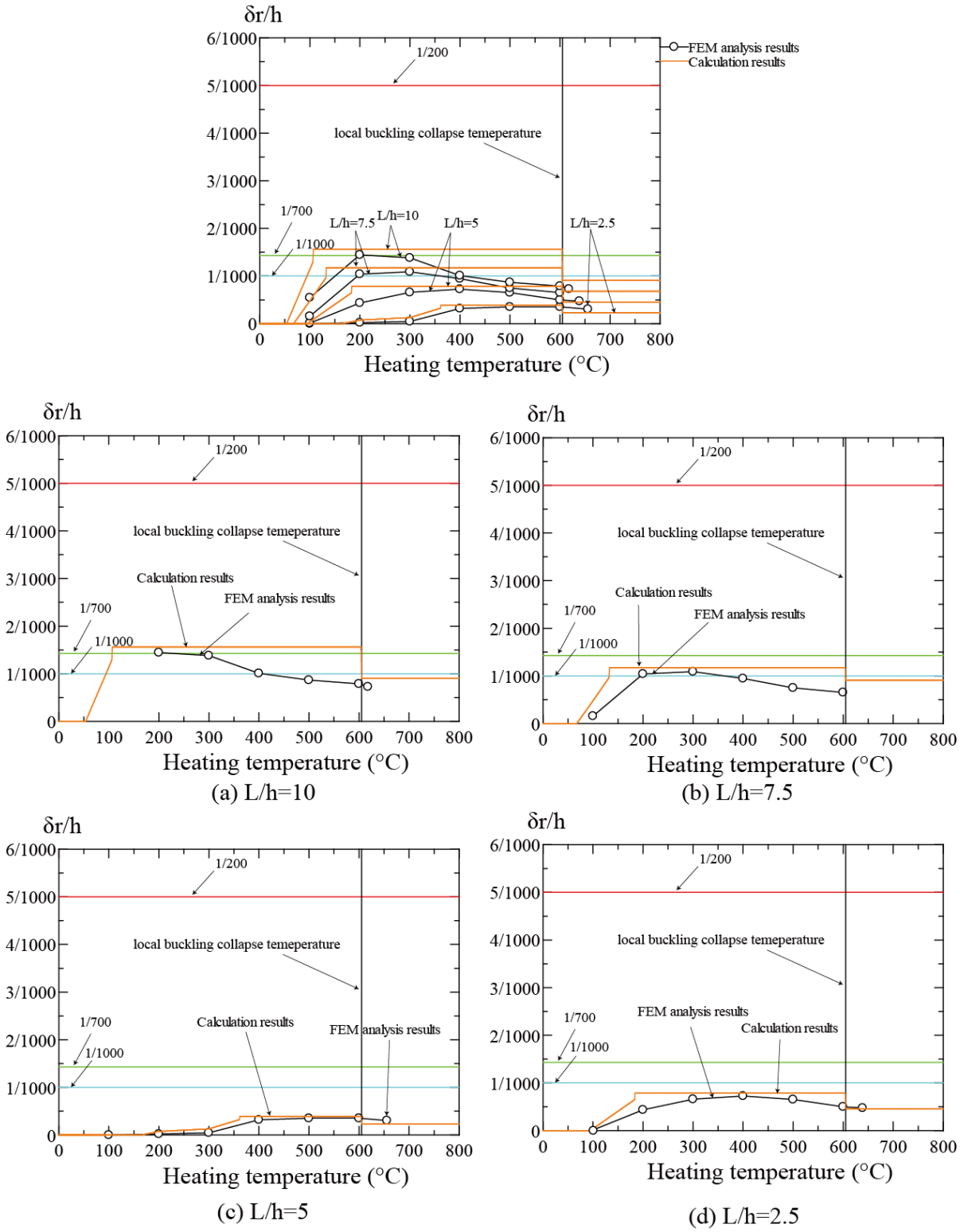

Figure 5.3.14 Result comparison between prediction equation and FEM analysis while p=0.2 (considering T_{local})

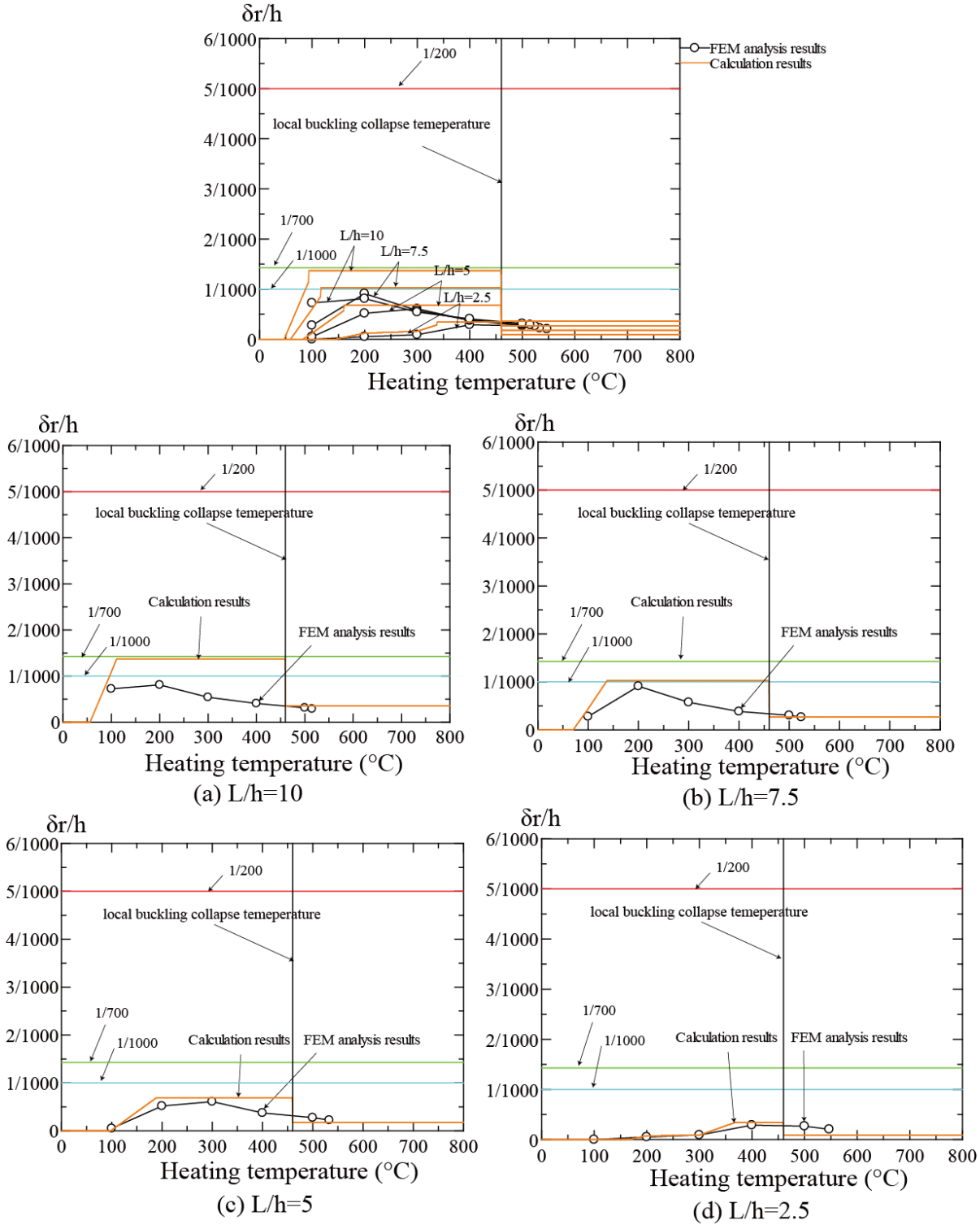

Figure 5.3.15 Result comparison between prediction equation and FEM analysis while p=0.4 (considering T_{local})

Figs 5.3.16 and 5.3.17 show the comparison of Eqs. 5.27~5.33 with the FEM analysis results considering local buckling. As described before, the FEM analysis results of the models considering both the axial load and local buckling on the column decrease after the local buckling temperature. As shown in Figs 5.3.16 and 5.3.17, the residual displacement of the column could be evaluated on the safe side through Eqs. 5.27~5.33. Therefore, to simplify the calculation steps, it is considered that Eqs. 5.27~5.33 could be used to evaluate the residual displacement of the column correctly, no matter the local buckling occurs or not.

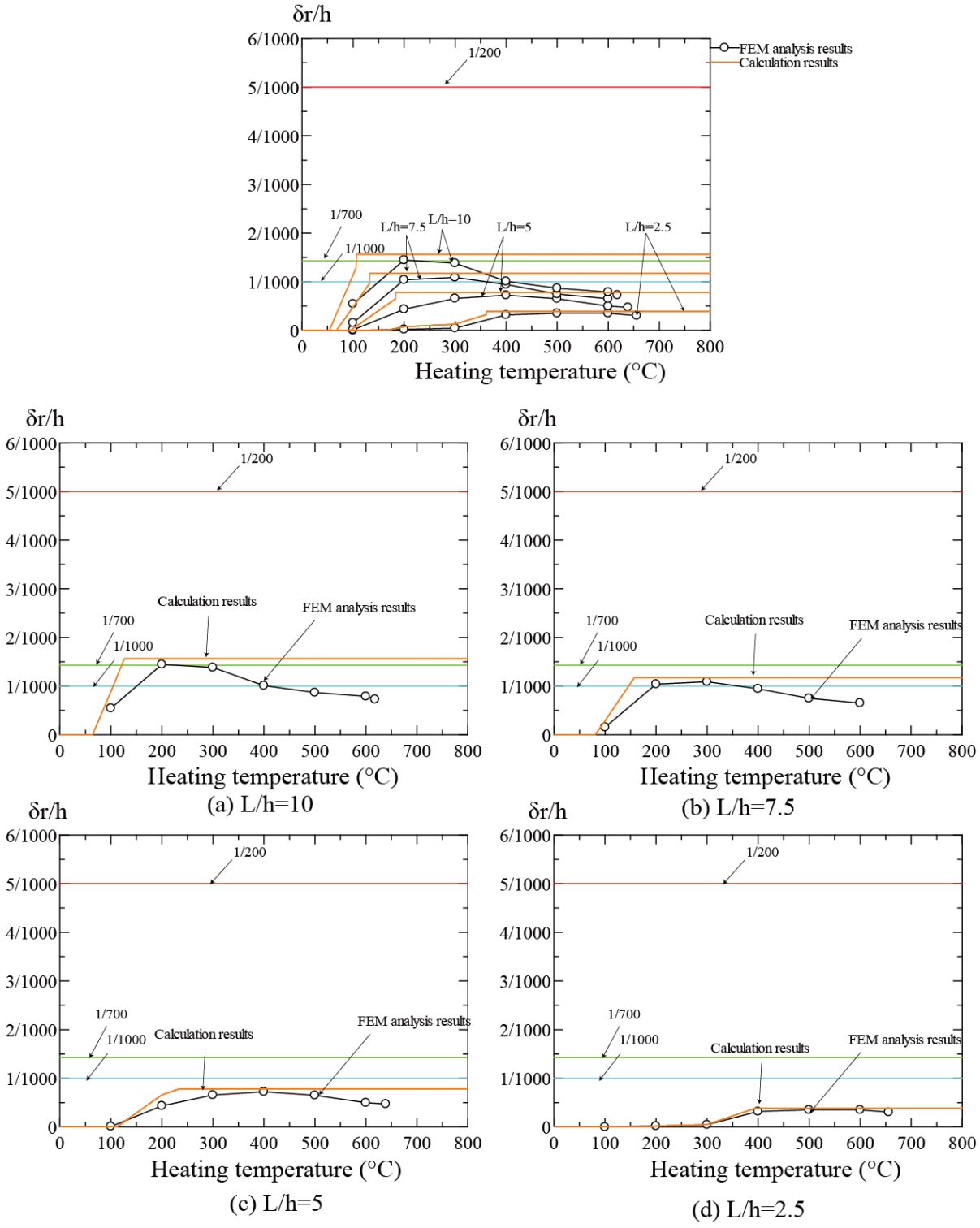

Figure 5.3.16 Result comparison between prediction equation and FEM analysis while p=0.2

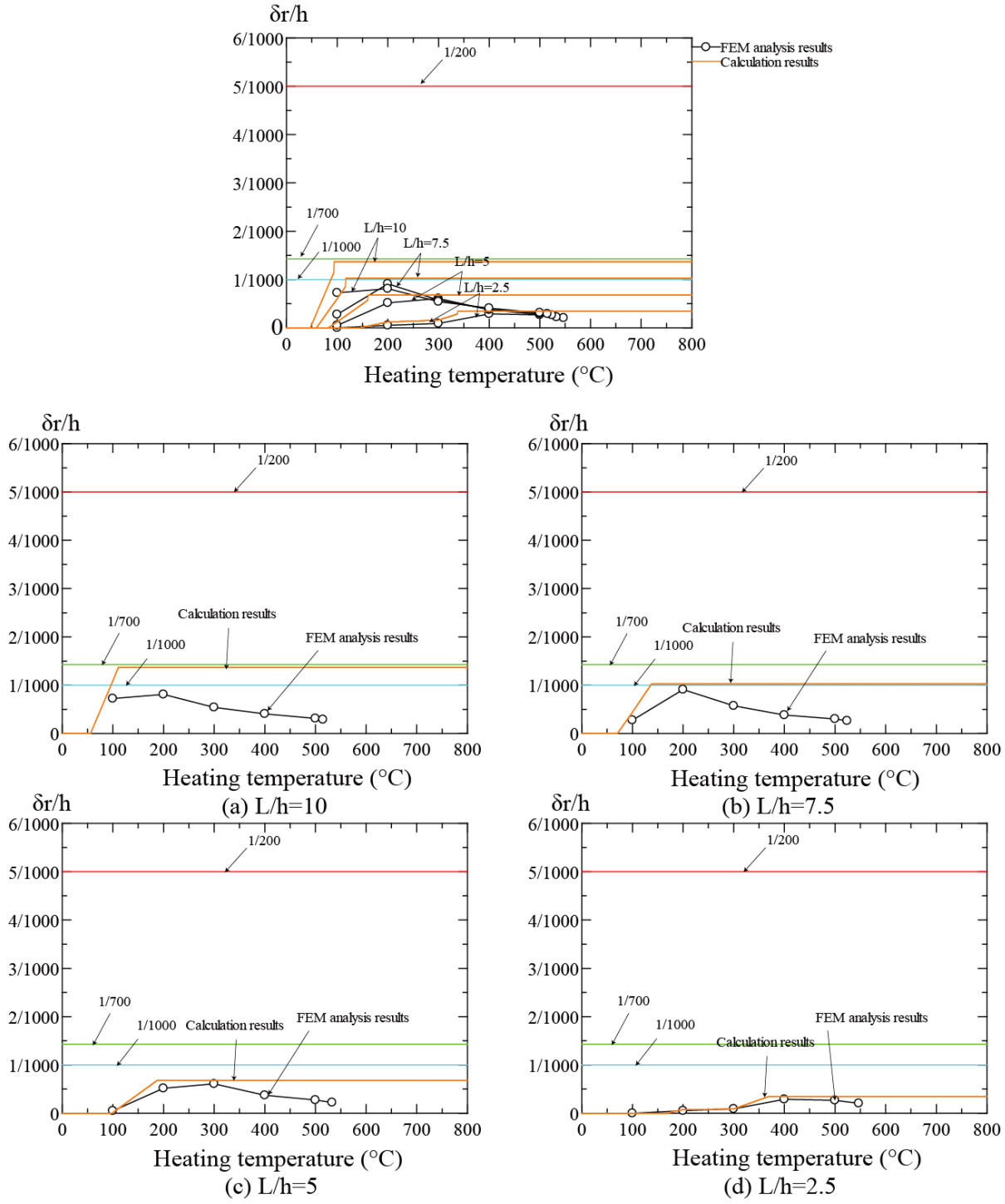

Figure 5.3.16 Result comparison between prediction equation and FEM analysis while p=0.4

5.4. Conclusion

In this Chapter, a prediction equation for the residual displacement of the cold-formed steel square hollow section column after fire were assumed. The calculation result based on these equations was compared with the FEM analysis results. According to the comparison, the following conclusions were summarized.

(1) According to the comparison results, it is considered that the prediction equations (Eqs, 5.7~5.16) of the displacement of the column at high temperature and the residual displacement after fire could be used to evaluate the displacement of the column during the whole heating and cooling process without considering the effect of the beam. Then, in the case that the column is subjected to the axial load, the residual displacement of the column could be evaluated by the prediction equations (Eqs. 5.27 ~5.33), because strain hardening progresses with the formation of the plastic hinge. Furthermore, considering the local buckling of the column, it is confirmed that Eqs. 5.27 ~5.33 could be used to predict the residual displacement on the safe side of the column after fire. It is because if local buckling occurs in the column during the fire, the residual displacement of the column will reduce.

(2) The prediction equations could be used to ensure the safety of the fire diagnosis and the repair work for a steel structure after fire. Because if the heating temperature of the building in fire is known, the residual drift angle of the building after fire can be predicted through the prediction equations. It is considered that if the residual drift angle after fire is lower than the value of 1/200, the building could be reused after the repair work; while if the residual drift angle is larger than this value, it is very dangerous to repair the building. However, the effect of the beam is not considered in the prediction equations. According to the Recommendation for diagnosis and repair methods of fire-damaged building, it is also suggested that the deflection of the beam not exceed 1/250 if the building is reused after fire.

(3) The accuracy of the prediction equations proposed in this Chapter has only been verified by the selected dimension and the actual stress-strain curves of the cold-formed steel square hollow section in this research. Therefore, more verification of the prediction equations is needed considering the dispersion of the actual cold-formed steel square hollow section.

Reference

[5.1]. Y. Iwai and F. Ozaki, Collapse temperature of steel plane frames considering fire spreads, Japanese society of steel structure: Steel Construction Engineering, Vol 28(109), (March 2021), pp.79-88. (In Japanese).

[5.2]. T. UMEMURA, F. OZAKI. Effects that strain rate of steels causes to fire resistance of steel member. Journal of Structural Engineering 2020, 66B.

[5.3]. AIJ Recommendations for Fire Resistant design of Steel Structures, 2017, pp.16 (in Japanese)

[5.4]. Recommendation for diagnosis and repair methods of fire-damaged building, 2015, pp.159 (in Japanese)

[5.5]. AIJ Recommendations for Design of Connections in steel structure, 2012, pp.128 (in Japanese)

Chapter 6. Conclusions

6.1 Summaries and conclusions

6.1.1 Conclusions of Chapter 2

(1) According to the high-temperature test results of the welded connection member, it was confirmed that the Charpy impact values hardly decreased in the blue brittleness temperature regions (between 100 and 300 ºC). Therefore, the possibility of brittleness fracture occurring in the welded connections at elevated temperatures is very small. Then, according to the results of the ambient and low-temperature tests on the specimens after the heating and cooling processes, water-cooled specimens subjected to 700-800 ºC heating exhibit the low Charpy impact energies, whereas the Charpy impact energies of water-cooled specimens subjected to 900 ºC recovered to a high Charpy impact energy. Through the microstructure observation of the water-cooled specimens, it is confirmed the Charpy impact energies decreased owing to the incomplete quenching that occurred during the water-cooling process from 700 and 800 ºC. However, the Charpy impact energies recovered, owing to the occurrence of martensitic transformation in the specimens quenching from 900 ºC. On the other hand, the furnace-cooled specimens exhibit high Charpy impact energies, because, owing to the slowly cooling rate of furnace-cooling, the microstructure of these specimens is similar to the untreated specimen. Furthermore, it is also confirmed that JIS SN400B grades steel, JIS SN490B steel, and JIS SA440B exhibit the low Charpy impact energies in the case of water-cooled from 800 ºC.

(2) For the reusabilities of these steel members, it is suggested that for the steel members subjected to high-temperature heating of more than 700 ºC, if the steel members are cooled at a relatively high cooling rate such as being water-cooled, the Charpy impact test result may be lower than the required value 27 J, and when these members are reused after fire, there is a possibility that brittleness fractures will occur to these members while these buildings suffer a severe earthquake. However, if the steel members were heated to a temperature of lower than 700 ºC, while cooled by fire extinguishing, the members still possess enough fracture properties to avoid brittleness fractures during the earthquakes. Therefore, in the view of the resistance-seismic requirement, it is considered that if the exterior view of steel members exhibit no obvious damage, and the temperature histories of these members also not exceed 700 ºC in fire, these members could be reused as a resistance-seismic structure after fire.

6.1.2 Conclusions of Chapter 3

(1) According to the high-temperature test results of cold-formed steel square hollow section steel, it was confirmed that the Charpy impact values hardly decreased in the blue brittleness temperature range (between 100 and 300 ºC). Therefore, the possibility of the occurrence of brittleness fracture at elevated temperatures is very small. Then, according to the results of the ambient- and low-temperature tests on the specimens after the water and furnace cooling processes, water-cooled

specimens subjected to 700-800 ºC heating exhibit the low Charpy impact energies, whereas the Charpy impact energies of water-cooled specimens subjected to 900 ºC recovered. Furthermore, according to the results of the ambient-temperature tests on the specimens after the air-cooling process, the Charpy impact energies of the specimens significantly reduced, and the Vickers hardness increased. Through the microstructure observation of the water-cooled FP and CP specimen, it is confirmed the Charpy impact energies decreased owing to the incomplete quenching that occurred during the water-cooling process from 700 and 800 ºC. However, the Charpy impact energies recovered, owing to the occurrence of martensitic transformation in the specimens quenching from 900 ºC. As for the furnace-cooled specimens, they exhibit high Charpy impact energies, because due to the slowly cooling rate of furnace-cooling, the microstructure of these specimens is similar to the untreated specimen. On the other hand, according to the microstructure observation of the air-cooled specimens, the microstructure does not change. However, because of the strain ageing, the Charpy impact energies of these member decreased after fire. While reusing these members as seismic-resistant members after fire, this local defect might trigger brittle fractures when subjected to sever earthquakes. The careful verification of the damage diagnostics after fire is required.

(2) Considering the reusabilities of the cold-formed steel square hollow section steel, it is suggested that for the cold-formed steel members subjected to high-temperature heating of more than 700 ºC, if the steel members are cooled at a relatively high cooling rate such as being water-cooled, the Charpy impact test result may be lower than the required value of 27 J, and when these members are reused after fire, there is a possibility that brittleness fractures will occur to these members while these buildings suffer a severe earthquake. However, if the cold-formed steel members were heated to a temperature of lower than 700 ºC, while cooled by fire extinguishing, the members still possess enough fracture properties to avoid brittleness fractures during the earthquakes. Furthermore, if the cold-formed steel members were air-cooled from the middle-temperature, the Charpy impact energies may decreased owing to the stain aging, although the average Charpy impact energy used in this research is enough high, in a view of the probability distribution, less than 98% of the cold-formed steel square hollow section possess enough Charpy impact energies more than 27J at 0 ºC, owing to the strain aging. Therefore, in the view of the resistance-seismic requirement, it is considered that if the exterior view of steel members exhibit no obvious damage, and the temperature histories of these members also not exceed 700 ºC in fire, these members could be reused as a resistance-seismic structure after fire. However, if these members were cooled from the middle-temperature, it is very important to confirm the fracture properties of these members.

6.1.3 Conclusions of Chapter 4

(1) According to the coupon tensile test results, it was confirmed that the yield point and tensile strength of the cold-formed steel square hollow section steel that were subjected to a slowly cooling

rate after the low and medium temperature (200-400 °C) increased in comparison with the untreated specimens. However, when the specimens were subjected to heating at high-temperature (500–800 °C), the yield strength and tensile strength started decrease in comparison with the specimens that were heated to 400 °C, but it is larger than the design yield point of the steel (235 MPa). It is important to consider the strength change caused by fire heating when these steel columns are repaired or reused after a fire.

(2) According to the results of the axially loaded compressive test and stub-column tests, it was confirmed that both the residual flexural and local buckling strengths changed after the heating and cooling process. It is mostly because of the change from both yield strength and tensile strength. And the flexural buckling strength can be evaluated using the Eurocode equations based on the residual yield strength, local buckling strength can be evaluate using both the Eurocode equations and AS/NZS design equations based on the residual yield strength. However, in the actual fire, it is very difficult to accurately evaluate the temperature history of the steel column after a fire, since the yield strength of steel after fire is unknown. Therefore, it is recommended that the residual flexural and local buckling should be evaluated using the design standard strength (F-value) at ambient temperature to achieve a safe-side evaluation.

(3) The standard design yield point and tensile strength of STKR400 steel are 235 Pa and 400MPa respectively, these values are the 5% lower limit value for the yield point and tensile strength of the JIS SS400 steel. For the JIS SS400 steel, these standard design yield point and tensile strength is 5% lower limit value on the probability distribution for this steel. JIS STKR400 steel is cold-formed by the JIS SS400 steel. Therefore, theoretically, the 5% lower limit value of the yield point on the JIS STKR400 steel is much higher than 235 MPa. However, in the actual structural design, 235 MPa is still considered as the standard design yield point of the JIS STKR400 steel. As a result, the yield point of the STKR400 steel after fire is still higher than 235MPa. This is advantageous as it can improve reusability without replacement.

6.1.4 Conclusions of Chapter 5

(1) According to the comparison results, it is considered that the prediction equations (Eqs, 5.7~5.16) of the displacement of the column at high temperature and the residual displacement after fire could be used to evaluate the displacement of the column during the whole heating and cooling process without considering the effect of the beam. Then, in the case that the column is subjected to the axial load, the residual displacement of the column could be evaluated by the prediction equations (Eqs. 5.27 ~5.33), because strain hardening progresses with the formation of the plastic hinge. Furthermore, considering the local buckling of the column, it is confirmed that Eqs. 5.27 ~5.33 could be used to predict the residual displacement on the safe side of the column after fire. It is because if local buckling occurs in the column during the fire, the residual displacement of the column will reduce.

(2) The prediction equations could be used to ensure the safety of the fire diagnosis and the repair work for a steel structure after fire. Because if the heating temperature of the building in fire is known, the residual drift angle of the building after fire can be predicted through the prediction equations. It is considered that if the residual drift angle after fire is lower than the value of 1/200, the building could be reused after the repair work; while if the residual drift angle is larger than this value, it is very dangerous to repair the building. However, the effect of the beam is not considered in the prediction equations. According to the Recommendation for diagnosis and repair methods of fire-damaged building, it is also suggested that the deflection of the beam not exceed 1/250 if the building is reused after fire.

(3) The accuracy of the prediction equations proposed in this Chapter has only been verified by the selected dimension and the actual stress-strain curves of the cold-formed steel square hollow section in this research. Therefore, more verification of the prediction equations is needed considering the dispersion of the actual cold-formed steel square hollow section.

6.1.5 Reuse of the steel buildings after fire

In this paper, it is suggested that more attention is need the steel members subjected to high-temperature heating of more than 700 ºC. Therefore, it needs to evaluate how many temperatures does the steel members subjected in the fire diagnosis. Actually, the methods of temperature estimation have been suggested by the Recommendations for the Diagnosis and Repair Methods of Fire-damaged Buildings [6.1]. In recent year, considering the environment protection, lead and chromium free anti-corrosive pigments is wildly used to protect the steel column. Therefore, as listed in Table 6.1.1, the methods of temperature estimation, and the reuse methods of cold-formed steel square hollow section is also listed in Table 6.1.2 on the basis of this paper, if the deformation on the cold-formed steel square hollow section members is not observed on these members.

Table 6.1.1. Temperature estimation from the anti-corrosive pigment [6.1]

Estimated Temperature	Cyanamide lead Anti-Corrosive Pigments Color on the surface: red rust	General Anti-Corrosive Pigments Color on the surface: red rust	Lead and chromium free anti-corrosive pigments Color on the surface: red rust
800℃	Significant peeling	Significant peeling	Significant peeling
700℃		Gradual fading of the brown	Gradual fading of the brown
600℃			
500℃	Discolor to light gray	Cracking	Cracking
400℃	Gradual fading of the black	Partly discolor to black (300-400℃)	Discolor to black
300℃	Discolor to black (300-400℃)		

Table 6.1.2. Reuse methods of the cold-formed steel square hollow section columns

Estimated Temperature	800℃	700℃	600℃	500℃	400℃	300℃	200℃
Reuse methods	Replace with a new member		Repaire the Anti-Corrosive Pigments		Repaire the Anti-Corrosive Pigments & Pay more attention on the fracture ductile capacity		

6.2 Future works

The reuse ability of cold-formed steel square hollow section columns is investigated and the residual displacement of the 1-storey frame is calculated through the prediction equation. However, further experimental and analytical work is necessary to enrich this research.

In Chapter 3, it is assumed that the strain ageing progresses, making the steel materials be more brittle. Therefore, it needs more experimental investigations to confirm this view.

On the other hand, in Chapter 4, the experimental studies of the mechanical properties as well as flexural and local buckling strength of JIS STKR400 steel columns after fire are conducted. Moreover, experimental evaluations such as cyclic loading tests focused on seismic performance, must be conducted in future work, so as to accelerate the reuse and repair of steel members after fire accidents in earthquake areas.

Furthermore, in Chapter 5, a prediction equation for the residual displacement of columns in the 1-storey and 1-span model is considered. However, in an actual building, prediction equations of plural-storeys and plural-spans models should be considered. However, the accuracy of the prediction equations proposed in this Chapter has only been verified by the selected dimension and the actual stress-strain curves of the cold-formed steel square hollow section in this research. More verification of the prediction equations is needed considering the dispersion of the actual cold-formed steel square hollow section. Furthermore, the effect of the beams on the residual displacement of the columns after fire is also needs to be considered. The above work is required in future research.

Reference

[6.1]. Recommendation for diagnosis and repair Methods of fire-damaged Buildings, 2015 (in Japanese)

Appendix A: Charpy impact results

1. Welded connection materials

Table. A-1 Charpy impact test at -70℃

Temperature（℃）	-70				
Specimen	No.		Temperature	Charpy impact angle	A_V(J)
BM	B-70-1	B36	-74	138.5	11.60
	B-70-2	B37	-74	137.1	14.31
	B-70-3	B38	-74	134.9	18.72
WM	W-70-1	W34	-73	138.2	12.17
	W-70-2	W35	-73	139	10.65
	W-70-3	W36	-73	138.6	11.41
HAZ	H-70-1	H35	-72	136.5	15.49
	H-70-2	H37	-72	138.6	11.41
	H-70-3	H38	-72	134.1	20.36

Table. A-2 Charpy impact test at -40℃

Temperature（℃）	-40				
Specimen	No.		Temperature	Charpy impact angle	A_V(J)
BM	B-40-1	B01	-38.9	122	47.79
	B-40-2	B02	-39	74.4	179.77
	B-40-3	B03	-39.2	132.5	23.72
	B-40-4	B04	-39	74.1	180.60
WM	W-40-1	W01	-40.6	138	12.56
	W-40-2	W02	-39.2	137.8	12.94
	W-40-3	W04	-39.9	137	14.51
HAZ	H-40-1	H01	-40.1	74.5	179.49
	H-40-2	H02	-40.5	91	132.45
	H-40-3	H03	-40.1	75	178.10

Table. A-3 Charpy impact test at -20℃

Temperature（℃）	-20				
Specimen	No.		Temperature	Charpy impact angle	A_V(J)
BM	B-20-1	B05	-20.6	74	180.88
	B-20-2	B06	-20.6	68.2	196.69
	B-20-3	B07	-20.6	35.1	270.51
	B-20-4	B08	-20.6	87.1	143.69
WM	W-20-1	W03	-20.9	137.5	13.53
	W-20-2	W05	-20.9	133.9	20.78
	W-20-3	W06	-20.9	134	20.57
HAZ	H-20-1	H04	-20.7	74.9	178.38
	H-20-2	H05	-20.7	45	252.16
	H-20-3	H06	-20.7	45.9	250.31
	H-20-4	H07	-20.7	71	189.13

Table. A-4 Charpy impact test at 0℃

Temperature（℃）	0				
Specimen	No.		Temperature	Charpy impact angle	A_V(J)
BM	B0-1	B09	1.7	48.2	245.46
	B0-2	B10	1.7	48.1	245.67
	B0-3	B11	1.7	61.9	213.15
WM	W0-1	W07	1.7	119.9	52.98
	W0-2	W08	1.7	112.9	71.05
	W0-3	W09	1.7	111.7	74.25
HAZ	H0-1	H08	0.8	59.8	218.44
	H0-2	H09	0.8	58.8	220.92
	H0-3	H10	0.8	54.9	230.34

Table. A-5 Charpy impact test at 100℃

Temperature（℃）	100				
Specimen	No.		Temperature	Charpy impact angle	A_V(J)
BM	B100-1	B12			
	B100-2	B13	105	54.1	232.21
	B100-3	B14	105	483	45.35
	B100-4	B15	105	52.1	236.83
WM	W100-1	W10	105	66.5	201.22
	W100-2	W11	105	63.2	209.83
	W100-3	W12	105	60.9	215.69
	W100-4	W13			
HAZ	H100-1	H11	105	52.8	235.23
	H100-2	H12	105	58.2	222.40
	H100-3	H13	105	55.2	229.63
	H100-4	H14			

Table. A-6 Charpy impact test at 200℃

Temperature（℃）	200				
Specimen	No.		Temperature	Charpy impact angle	A_V(J)
BM	B200-1	B32	200	11.2	297.40
	B200-2	B33	200	38.2	265.17
	B200-3	B34	200	37.9	265.70
	B200-4	B35	200	34.9	270.84
WM	W200-1	W30	200	46.5	249.06
	W200-2	W31	200	35.1	270.51
	W200-3	W32	200	17	293.33
	W200-4	W33	200	10.2	297.94
HAZ	H200-1				
	H200-2	H32	200	24	286.27
	H200-3	H33	200	11.8	297.06
	H200-4	H34	200	12.1	296.88

Table. A-7 Charpy impact test at 300℃

Temperature（℃）	300				
Specimen	No.		Temperature	Charpy impact angle	A_V(J)
BM	B300-1	B19	330	47.1	247.80
	B300-2	B20	330	49.9	241.76
	B300-3	B21	330	45.1	251.96
WM	W300-1	W17	330	30.3	277.98
	W300-2	W18	330	31.1	276.80
	W300-3	W19	330	27.6	281.75
HAZ	H300-1	H18	330	44	254.18
	H300-2	H19	330	40.9	260.21
	H300-3	H20	330	34.9	270.84

Table. A-8 Charpy impact test at 400℃

Temperature（℃）	400				
Specimen	No.		Temperature	Charpy impact angle	A_V(J)
BM	B400-1	B22	425	79	166.86
	B400-2	B23			
	B400-3	B24	425	76.7	173.34
	B400-4	B25	425	80.3	163.17
WM	W400-1	W20	425	86.4	145.71
	W400-2	W21	425	82.2	157.76
	W400-3	W22	425	80.5	162.60
	W400-4	W23			
HAZ	H400-1	H21	425	74.5	179.49
	H400-2	H22	425	73.6	181.98
	H400-3	H23	425	80.1	163.74
	H400-4	H24			

Table. A-9 Charpy impact test at 500℃

Temperature（℃）	500				
Specimen	No.		Temperature	Charpy impact angle	A_V(J)
BM	B500-1	B23	540	97.9	112.63
	B500-2	B26	540	94.5	122.37
	B500-3	B28	540	97	115.20
WM	W500-1	W23	540	97.7	113.20
	W500-2	W24	540	95.8	118.64
	W500-3	W25	540	98.5	110.92
HAZ	H500-1	H24	540	95	120.94
	H500-2	H25	540	93	126.69
	H500-3	H26	540	91.5	131.01

Table. A-10 Charpy impact test at 200℃

Temperature（℃）	600				
Specimen	No.		Temperature	Charpy impact angle	A_V(J)
BM	B600-1	B27	640	87.7	141.97
	B600-2	B29	640		
	B600-3	B30	640	88	141.10
	B600-4	B31	640	76.5	173.90
WM	W600-1	W26	640	98.4	111.20
	W600-2	W27	640	86.7	144.85
	W600-3	W28	640	96.9	115.49
	W600-4	W29	640	98.9	109.78
HAZ	H600-1	H27	640	74.8	178.65
	H600-2	H28	640	80.1	163.74
	H600-3	H29	640	73	183.64
	H600-4	H30	640	89	138.22

Table. A-11 Charpy impact test of furnace-cooled specimens (0℃)

Furnace-cooled specimens at 0 ℃															
600 ℃				700 ℃				800 ℃				900 ℃			
No.	Temperature (℃)	Charpy impact angle	A_V(J)	No.	Temperature (℃)	Charpy impact angle	A_V(J)	No.	Temperature (℃)	Charpy impact angle	A_V(J)	No.	Temperature (℃)	Charpy impact angle	A_V(J)
B01	0.7	6.2	299.59	B19	0.4	6.1	299.62	B37	0.7	47.2	247.59	B55	0.2	69.5	193.20
B02	0.7	6	299.65	B20	0.4	6.1	299.62	B38	0.7	60.2	217.44	B56	0.2	51	239.31
B03	0.7	6	299.65	B21	0.4	6.3	299.55	B39	0.7	42	258.12	B57	0.2	57.8	223.38
W01	0.7	91	132.45	W19	0.4	84.4	151.46	W37	0.7	72.3	185.57	W55	0.2	70	191.84
W02	0.7	112.9	71.05	W20	0.4	114.3	67.35	W38	0.7	90.7	133.32	W56	0.2	31.9	275.60
W03	0.7	85.1	149.45	W21	0.4	109.5	80.19	W39	0.7	66.6	200.95	W57	0.2	19.1	291.46
H01	0.7	6	299.65	H19	0.4	6.1	299.62	H37	0.7	53.3	234.07	H55	0.2	79.2	166.29
H02	0.7	12.5	296.64	H20	0.4	6.1	299.62	H38	0.7	61	215.43	H56	0.2	73.1	183.36
H03	0.7	9	298.52	H21	0.4	6.1	299.62	H39	0.7	57.1	225.08	H57	0.2	79.2	166.29

Table. A-12 Charpy impact test of water-cooled specimens (0℃)

Water-cooled specimens at 0 ℃															
600 ℃				700 ℃				800 ℃				900 ℃			
No.	Temperature (℃)	Charpy impact angle	A_V(J)	No.	Temperature (℃)	Charpy impact angle	A_V(J)	No.	Temperature (℃)	Charpy impact angle	A_V(J)	No.	Temperature (℃)	Charpy impact angle	A_V(J)
B10	0.2	47.7	246.53	B28	0.4	112.7	71.58	B46	0.4	128.1	33.39	B39	0.3	97.2	114.63
B11	0.2	51.7	237.73	B29	0.4	131.9	25.00	B47	0.4	117.9	58.03	B65	0.3	43.5	255.18
B12	0.2	48	245.89	B30	0.4	127.5	34.76	B48	0.4	119.2	54.73	B66	0.3	44.3	253.58
W10	0.2	94.5	122.37	W28	0.4	129.1	31.14	W46	0.4	130	29.14	W64	0.3	97	115.20
W11	0.2	88.1	140.81	W29	0.4	134.8	18.92	W47	0.4	126	38.23	W65	0.3	105	92.58
W12	0.2	104.9	92.85	W30	0.4	133.1	22.45	W48	0.4	129.2	30.92	W66	0.3	103.1	97.89
H10	0.2	50.5	240.43	H28	0.4	80.9	161.47	H46	0.4	116.1	62.65	H64	0.3	71.2	188.58
H11	0.2	58.8	220.92	H29	0.4	81.9	158.62	H47	0.4	128.8	31.81	H65	0.3	71.8	186.94
H12	0.2	51.3	238.64	H30	0.4	82.9	155.76	H48	0.4	120	52.73	H66	0.3	66.1	202.27

Table. A-13 Charpy impact test of furnace-cooled specimens (-20℃)

Furnace-cooled specimens at -20 ℃															
600 ℃				700 ℃				800 ℃				900 ℃			
No.	Temperature (℃)	Charpy impact angle	A_V(J)	No.	Temperature (℃)	Charpy impact angle	A_V(J)	No.	Temperature (℃)	Charpy impact angle	A_V(J)	No.	Temperature (℃)	Charpy impact angle	A_V(J)
B07	-19.6	5	299.92	B25	-21.7	6	299.65	B43	-20	48.9	243.94	B61	-20	56.8	225.80
B08	-19.3	5.8	299.71	B26	-21.7	6	299.65	B44	-22.1	77.1	172.22	B62	-20	70.3	191.03
B09				B27				B45				B63			
W07	-20.5	97.9	112.63	W25	-21.2	136	16.49	W43	-19.3	129.5	30.25	W61	-20.1	71.9	186.66
W08	-20.3	138	12.56	W26	-20.8	133.5	21.61	W44	-19.6	136.7	15.10	W62	-20	82.1	158.04
W09				W27				W45				W63			
H07	-21.5	28.8	280.12	H25	-19.9	5.2	299.87	H43	-19.2	67.1	199.63	H61	-19.9	87.1	143.69
H08	-21.3	41	260.03	H26	-19.1	97.8	112.91	H44	-19.3	69.9	192.11	H62	-19.7	85.5	148.30
H09				H27				H45				H63			

Table. A-14 Charpy impact test of water-cooled specimens (-20℃)

Water-cooled specimens at -20 ℃															
600 ℃				700 ℃				800 ℃				900 ℃			
No.	Temperature (℃)	Charpy impact angle	A_V(J)	No.	Temperature (℃)	Charpy impact angle	A_V(J)	No.	Temperature (℃)	Charpy impact angle	A_V(J)	No.	Temperature (℃)	Charpy impact angle	A_V(J)
B16	-20.3	65.1	204.90	B34	-20	138.3	11.98	B52	-20.9	133.9	20.78	B70	-21.2	44.3	253.58
B17	-20	75.9	175.59	B35	-20.4	137	14.51	B53	-19.7	134.3	19.95	B71	-21.1	55	230.10
B18				B36				B54				B72			
W16	-20.8	133.1	22.45	W34	-21.5	139.1	10.46	W52	-19.5	133.9	20.78	W70	-20.8	110.9	76.40
W17	-19.9	136.8	14.90	W35	-21.6	136.1	16.29	W53	-19.5	127.9	33.85	W71	-20.6	110.1	78.56
W18				W36				W54				W72			
H16	-20.4	40.5	260.97	H34	-136.2	136.2	16.09	H52	-20.7	135.6	17.29	H70	-20.5	73.1	183.36
H17	-21.8	70	191.84	H35	-120.8	120.8	50.74	H53	-20.6	130.1	28.92	H71	-20.2	75.5	176.70
H18				H36				H54				H72			

Table. A-15 Charpy impact test of furnace-cooled specimens (-40℃)

Furnace-cooled specimens at -40 ℃															
600 ℃				700 ℃				800 ℃				900 ℃			
No.	Temperature (℃)	Charpy impact angle	A_V(J)	No.	Temperature (℃)	Charpy impact angle	A_V(J)	No.	Temperature (℃)	Charpy impact angle	A_V(J)	No.	Temperature (℃)	Charpy impact angle	A_V(J)
B04	-39.2	77.8	170.25	B22	-40.7	135.6	17.29	B40	-40.7	123.2	44.87	B58	-39.3	131.1	26.73
B05	-38	87.9	141.39	B23	-39.8	130.6	27.82	B41	-41	126.7	36.60	B59	-40.1	136.8	14.90
B06	-39.5	95	120.94	B24	-39.9	135.2	18.10	B42	-41.1	124.9	40.81	B60	-39.6	121.9	48.03
W04	-39.9	139.8	9.15	W22	-41.1	138	12.56	W40	-39.8	136.6	15.30	W58	-40.6	81	161.18
W05	-40.1	139.8	9.15	W23	-42	138.5	11.60	W41	-39.8	137.6	13.33	W59	-41	96.2	117.49
W06	-39.8	140	8.77	W24	-41.7	136.7	15.10	W42	-39.3	96.9	115.49	W60	-41.2	132.8	23.08
H04	-40	63.5	209.05	H22	-42	118.2	57.26	H40	-40.6	84.1	152.32	H58	-41.1	×	×
H05	-40	78.5	168.27	H23	-39.2	55.8	228.20	H41	-40.7	116	62.91	H59	-41	136.5	15.49
H06	-39.9	101.8	101.55	H24	-41.2	6.1	299.62	H42	-40.1	133.1	22.45	H60	-41.2	135.5	17.50

Table. A-16 Charpy impact test of water-cooled specimens (-40℃)

Water-cooled specimens at -40 ℃															
600 ℃				700 ℃				800 ℃				900 ℃			
No.	Temperature	Charpy impact angle	A_V(J)	No.	Temperature	Charpy impact angle	A_V(J)	No.	Temperature	Charpy impact angle	A_V(J)	No.	Temperature	Charpy impact angle	A_V(J)
B13	-40.1	80.1	163.74	B31	-39.5	139.1	10.46	B49	-39.6	137.1	14.31	B67	-40.2	73.2	183.09
B14	-40.2	84.8	150.31	B32	-41.5	139.6	9.52	B50	-40.2	136.5	15.49	B68	-40.2	70.1	191.57
B15	-41.1	97.1	114.92	B33	-41.1	136.9	14.70	B51	-40.4	137.5	13.53	B69	-40.9	64.2	207.24
W13	-41.8	139.1	10.46	W31	-41.8	138.5	11.60	W49	-40.7	137.1	14.31	W67	-40	122.1	47.54
W14	-39.5	139.2	10.27	W32	-39.2	139.3	10.08	W50	-40	136.8	14.90	W68	-40	117.9	58.03
W15	-42.5	139.8	9.15	W33	-39.6	138.2	12.17	W51	-39.2	134.3	19.95	W69	-39.5	125.1	40.34
H13	-39.1	68.1	196.96	H31	-39.9	138.3	11.98	H49	-40.9	134.9	18.72	H67	-39.9	78.9	167.14
H14	-38.3	67.9	197.49	H32	-40.5	136.7	15.10	H50	-40.1	135	18.51	H68	-41.7	87	143.98
H15	-38.8	77.9	169.97	H33	-39.8	138	12.56	H51	-40.2	136.8	14.90	H69	-40.9	100.1	106.36

2. Cold-formed steel square hollow section

Table. A-17 Charpy impact test at -70℃

Temperature（℃）	-70				
Specimen	No.	Time (s)	Temperature	Charpy impact angle	A_V(J)
FP	B104	×	-70.7	138.6	11.41
	B108	×	-71.3	140.1	8.59
	B109	×	-71.3	138.9	10.84
CP	C107	×	-70.6	138.7	11.22
	C108	×	-71.7	139.7	9.33
	C109	×	-71.6	139.9	8.96

Table. A-18 Charpy impact test at -40℃

Temperature（℃）	-40				
Specimen	No.	Time (s)	Temperature	Charpy impact angle	A_V(J)
FP	B105	×	-41.1	138.5	11.60
	B106	×	-39.4	140	8.77
	B107	×	-39.4	138.1	12.36
CP	C104	×	-41.1	138.3	11.98
	C105	×	-40.1	136.3	15.89
	C106	×	-41.2	137.3	13.92

Table. A-19 Charpy impact test at -20℃

Temperature（℃）	-20				
Specimen	No.	Seconds	Temperature	Charpy impact angle	A_V(J)
FP	B101	×	-21.5	134.3	19.95
	B102	×	-21.4	135.9	16.69
	B103	×	-21.6	94.9	121.22
CP	C101	×	-21.6	137.5	13.53
	C102	×	-21.2	134.9	18.72
	C103	×	-21.1	133.8	20.98

Table. A-21 Charpy impact test at 0℃

Temperature（℃）	0				
Specimen	No.	Time (s)	Temperature	Charpy impact angle	A_V(J)
FP	B97	×	1.5	62.9	210.60
	B98	×	1.5	58.5	221.66
	B100	×	1.5	53.2	234.30
CP	C97	×	1.5	63.2	209.83
	C99	×	1.5	55.9	227.96
	C100	×	1.5	59.9	218.19

Table. A-22 Charpy impact test at 100℃

Temperature（℃）	100				
Specimen	No.	Time (s)	Temperature	Charpy impact angle	A_V(J)
FP	B84	6	100+	50	241.53
	B92	5	100+	58	222.89
	B93	5	100+	77	172.50
CP	C89	8	100+	69	194.54
	C91	8	100+	84	152.61
	C92	6	100+	51	239.31

Table. A-23 Charpy impact test at 200℃

Temperature（℃）	200				
Specimen	No.	Time (s)	Temperature	Charpy impact angle	A_V(J)
FP	B91	7	200+	10	298.04
	B94	6	200+	35	270.67
	B95	6	200+	47	248.01
CP	C94	6	200+	32	275.45
	C95	6	200+	34	272.31
	C96	6	200+	20	290.59

Table. A-24 Charpy impact test at 300℃

Temperature（℃）	300				
Specimen	No.	Time (s)	Temperature	Charpy impact angle	A_V(J)
FP	B110	12.98	330	49.1	227.24
	B111	19.46	330	47.2	216.69
	B116	16.67	330	50.5	234.77
CP	C90	14.98	330	56.2	247.59
	C112	12.77	330	60.5	243.51
	C115	15.7	330	53	240.43

Table. A-25 Charpy impact test at 400℃

Temperature（℃）	400				
Specimen	No.	Time (s)	Temperature	Charpy impact angle	A_V(J)
FP	B117	15.32	430	79.9	164.31
	B123	14.69	430	79	166.86
	B125	17.75	430	79.9	164.31
CP	C118	16.69	430	86.9	144.27
	C119	14.76	430	86.1	146.57
	C120	20.88	430	77.1	172.22

Table. A-26 Charpy impact test at 500℃

Temperature（℃）	500				
Specimen	No.	Time (s)	Temperature	Charpy impact angle	A_V(J)
FP	B113	15.6	540	97.1	114.92
	B122	16.11	540	97.1	114.92
	B126	21.52	540	94.5	122.37
CP	C121	14.75	540	101.2	103.25
	C122	16.66	540	102.8	98.73
	C123	11.58	540	106.1	89.52

Table. A-27 Charpy impact test at 600℃

Temperature（℃）	600				
Specimen	No.	Time (s)	Temperature	Charpy impact angle	A_V(J)
FP	B118	15.88	648	76.5	173.90
	B119	13.9	648	67.5	198.56
	B121	13.03	648	43.2	255.77
CP	C116	21.44	648	89	138.22
	C117	14.19	648	71.5	187.76
	C124	16.4	648	87.5	142.54

Table. A-28 Charpy impact test of furnace-cooled specimens (0℃)

Furnace-cooled specimens at 0 ℃															
600 ℃				700 ℃				800 ℃				900 ℃			
No.	Temperature (℃)	Charpy impact angle	A_V(J)	No.	Temperature (℃)	Charpy impact angle	A_V(J)	No.	Temperature (℃)	Charpy impact angle	A_V(J)	No.	Temperature (℃)	Charpy impact angle	A_V(J)
B1	0	9.9	298.09	B23	0	9.8	298.14	B46	0	10	298.04	B68	0	36.5	268.15
B2	0	9.9	298.09	B24	0	9.9	298.09	B47	0	9	298.52	B69	0	31.3	276.51
B3	0	10	298.04	B25	0	9.5	298.29	B48	0	10	298.04	B70	0	32.1	275.29
C1	0	9.9	298.09	C24	0	9.8	298.14	C45	0	9	298.52	C67	0	29.5	279.13
C2	0	9.9	298.09	C25	0	10	298.04	C46	0	9.1	298.47	C68	0	31	276.95
C3	0	10.1	297.99	C33	0	9.4	298.33	C47	0	9	298.52	C69	0	30.9	277.10

Table. A-29 Charpy impact test of water-cooled specimens (0℃)

Water-cooled specimens at 0 ℃															
600 ℃				700 ℃				800 ℃				900 ℃			
No.	Temperature (℃)	Charpy impact angle	A_V(J)	No.	Temperature (℃)	Charpy impact angle	A_V(J)	No.	Temperature (℃)	Charpy impact angle	A_V(J)	No.	Temperature (℃)	Charpy impact angle	A_V(J)
B13	0	95.1	120.65	B41	0	131	26.95	B57	0	125.1	40.34	B79	0	9	298.52
B14	0	78.1	169.40	B42	0	133.1	22.45	B58	0	133.1	22.45	B80	0	9	298.52
B15	0	60.26	217.29	B43	0	131.7	25.43	B59	0	105.3	91.74	B81	0	9	298.52
C12	0	56.1	227.48	C40	0	134	20.57	C56	0	123.5	44.15	C79	0	9	298.52
C13	0	66.5	201.22	C41	0	93.1	126.40	C57	0	97	115.20	C78	0	9	298.52
C14	0	35.7	269.50	C42	0	135.1	18.31	C58	0	97.9	112.63	C80	0	9	298.52

Table. A-30 Charpy impact test of furnace-cooled specimens (-20℃)

Furnace-cooled specimens at -20 ℃															
600 ℃				700 ℃				800 ℃				900 ℃			
No.	Temperature (℃)	Charpy impact angle	A_V(J)	No.	Temperature (℃)	Charpy impact angle	A_V(J)	No.	Temperature (℃)	Charpy impact angle	A_V(J)	No.	Temperature (℃)	Charpy impact angle	A_V(J)
B4	-20	9	298.52	B26	-20	130.1	28.92	B54	-20	92	129.57	B76	-20	61.2	214.93
B5	-20	131.9	25.00	B27	-20	134.2	20.15	B55	-20	72	186.39	B77	-20	40.1	261.71
B6	-20	126.1	37.99	B28	-20	133.1	22.45	B56	-20	44	254.18	B78	-20	73	183.64
C8	-20	47.7	246.53	C30	-20	123.5	44.15	C48	-20	73.5	182.26	C70	-20	63.5	209.05
C9	-20	9.1	298.47	C31	-20	135	18.51	C49	-20	57.38	224.40	C72	-20	54	232.45
C11	-20	129	31.36	C32	-20	130.8	27.38	C50	-20	64.7	205.94	C75	-20	23.7	286.62

Table. A-31 Charpy impact test of water-cooled specimens (-20℃)

Water-cooled specimens at -20 ℃															
600 ℃				700 ℃				800 ℃				900 ℃			
No.	Temperature (℃)	Charpy impact angle	A_V(J)	No.	Temperature (℃)	Charpy impact angle	A_V(J)	No.	Temperature (℃)	Charpy impact angle	A_V(J)	No.	Temperature (℃)	Charpy impact angle	A_V(J)
B16	-20	131.2	26.51	B36	-20	137.2	14.11	B60	-20	134.3	19.95	B86	-20	8.1	298.90
B18	-20	130.1	28.92	B37	-20	137.3	13.92	B61	-20	136.5	15.49	B87	-20	9.2	298.43
B22	-20	117.1	60.07	B38	-20	138.1	12.36	B62	-20	136.1	16.29	B88	-20	9	298.52
C15	-20	134.1	20.36	C37	-20	136.5	15.49	C59	-20	137.1	14.31	C81	-20	8.2	298.86
C16	-20	134.8	18.92	C38	-20	138.2	12.17	C60	-20	137	14.51	C82	-20	8.1	298.90
C20	-20	91.8	130.15	C39	-20	137.1	14.31	C61	-20	131.5	25.86	C88	-20	10.9	297.57

Table. A-32 Charpy impact test of furnace-cooled specimens (-40℃)

Furnace-cooled specimens at -40 ℃															
600 ℃				700 ℃				800 ℃				900 ℃			
No.	Temperature (℃)	Charpy impact angle	A_V(J)	No.	Temperature (℃)	Charpy impact angle	A_V(J)	No.	Temperature (℃)	Charpy impact angle	A_V(J)	No.	Temperature (℃)	Charpy impact angle	A_V(J)
B9	-40	137.9	12.75	B29	-40	140	8.77	B51	-40	134.1	20.36	B73	-40	82.8	156.04
B10	-40	139.1	10.46	B30	-40	138.9	10.84	B52	-40	137.1	14.31	B74	-40	135.1	18.31
B11	-40	136.9	14.70	B31	-40	138.2	12.17	B53	-40	137.5	13.53	B75	-40	62.2	212.39
C5	-40	134.9	18.72	C26	-40	139.1	10.46	C53	-40	135.1	18.31	C76	-40	122.9	45.60
C6	-40	138.5	11.60	C27	-40	137.7	13.14	C54	-40	137.1	14.31	C77	-40	68.9	194.81
C7	-40	137	14.51	C28	-40	139.5	9.71	C55	-40	133.9	20.78	C78	-40	72	186.39

Table. A-33 Charpy impact test of water-cooled specimens (-40℃)

Water-cooled specimens at -40 ℃															
600 ℃				700 ℃				800 ℃				900 ℃			
No.	Temperature (℃)	Charpy impact angle	A_V(J)	No.	Temperature (℃)	Charpy impact angle	A_V(J)	No.	Temperature (℃)	Charpy impact angle	A_V(J)	No.	Temperature (℃)	Charpy impact angle	A_V(J)
B17	-40	138.2	12.17	B39	-40	140.8	7.30	B63	-40	139.5	9.71	B83	-40	8.8	298.61
B19	-40	139.5	9.71	B40	-40	140.7	7.49	B64	-40	137.6	13.33	B89	-40	37.1	267.11
B20	-40	137.1	14.31	B44	-40	138.5	11.60	B67	-40	138.2	12.17	B90	-40	46.9	248.22
C19	-40	139.9	8.96	C34	-40	141	6.94	C62	-40	134.2	20.15	C83	-40	8	298.94
C21	-40	137.5	13.53	C35	-40	139.9	8.96	C65	-40	138.1	12.36	C84	-40	7.6	299.10
C22	-40	138.2	12.17	C36	-40	140.1	8.59	C66	-40	138.4	11.79	C87	-40	38.7	264.28

Table. A-34 Charpy impact test of air-cooled specimen from 200℃

Air-cooled from 200 °C				
No.	cooling process	temperaure	Charpy impact angle	AV(J)
B127	water-cooling	0.0	54.1	232.2
B128	water-cooling	0.0	56.1	227.5
B129	water-cooling	0.0	50.1	241.3
C127	water-cooling	0.0	72.1	186.1
C128	water-cooling	0.0	136.9	14.7
C129	water-cooling	0.0	137.1	14.3

Table. A-35 Charpy impact test of air-cooled specimen from 300℃

Air-cooled from 300 °C				
No.	cooling process	temperaure	Charpy impact angle	AV(J)
B96	water-cooling	0.0	79.5	165.4
B112	water-cooling	0.0	93.0	126.7
B114	water-cooling	0.0	30.0	278.4
C110	water-cooling	0.0	133.2	22.2
C113	water-cooling	0.0	63.7	208.5
C114	water-cooling	0.0	129.2	30.9

Table. A-36 Charpy impact test of air-cooled specimen from 400℃

Air-cooled from 400 °C				
No.	cooling process	temperaure	Charpy impact angle	AV(J)
B130	water-cooling	0.0	129.1	31.1
B131	water-cooling	0.0	77.8	170.3
B132	water-cooling	0.0	84.2	152.0
C130	water-cooling	0.0	104.5	94.0
C131	water-cooling	0.0	132.8	23.1
C132	water-cooling	0.0	96.1	117.8

Appendix B: Material records for welded connection.

ミルシート例2

MF A　　79 J 04

検査証明書
INSPECTION CERTIFICATE

住友金属工業株式会社　鹿島製鉄所
〒314−0014 茨城県鹿嶋市大字光3番地
SUMITOMO METAL INDUSTRIES,LTD.
KASHIMA STEEL WORKS
3 Hikari Kashima Ibaraki 314-0014 Japan

証明書番号 Certificate No. : 45458-002　日付 Date: 2010- 3-24
船番 Ship No.:
需要家管理番号 Order No.:
注文者 Shipper : 057FHEKY スミトモ ショウジ トウキョウ
需要家 Customer :
規格 Standard : JIS G3136 SN490B　SN490B　SN490B
PROJECT NAME :
品名 Commodity : アツイタ

需要家照合子番号 Order Item No.	板番号 Plate No.	数量 Quantity Mass KG	製鋼番号 Cast No.	区分 ＊1	方向	引張試験 Tensile Test 試験片熱処理区分 ＊5	降伏点 Y.P. N/MM2	引張強さ T.S.	R.A. Y.R.	伸び EL. %	標点距離 ＊4	位置 ＊2	衝撃試験 IMPACT TEST 区分 ＊1	方向	試験温度 Test Temp. °C	J 1.	2.	3.	AV.	熱処理記号 ＊7	C ×100	Si	Mn ×1000	P	S ×1000	Cu	Ni	Cr	Mo ×100	V	Ti	Nb	Sol Al ×1000	N ×10000	B	Ceq.	PCM ×100	寸法・外観・形状 ＊9	表面仕上り ＊11
製作番号 Our Ref. No. G92Z		寸法 Size (MM)		試番 Test Piece No.	位置 ＊3																																		
	225471663	1	0212219																																			
6245	32.00X1200X3900	1176	BZ6046T		C	2	378	530	71	35	T	L	2	O	265	274	257	265	L17	38	131	11	4		1	2	1	0							41		G
			0212219																																			
			B06046T		C	2	393	539	73	32	T	L	2	O	272	248	250	257	L17	38	131	11	4		1	2	1	0							41			
		SPEC.	MIN.				325	490		21						19	19	19	27	-	-	-	-	-		-	-	-	-							-			
			MAX.				445	610	80	-						-	-	-	-	L18	55	160	30	15		-	-	-	-							44			

備考 Remarks: TOTAL 7　15344KG

CEQ=C+MN/6+SI/24+NI/40+CR/5+MO/4+V/14

NOTES:The Material Tests are same results in case of the same Test Piece Number.The Chemical Compositions are same results in case of the same Cast Number.
＊1 試験片熱処理区分 Heat Treatment for Test Piece… 条件は備考欄へ表示、Conditions to be Stipulated in Remarks.　＊2 位置 Position…T:Top, B:Bottom.　＊3 方向 Direction…L:Lengthwise, C:Crosswise, Z:Through Thickness.
＊4 標点距離 Gauge Length 平型試験片 Rectangular Tensile Test Specimen…2:200mm(8"), 5:50mm(2"), 6:5.65√A　丸棒試験片 Round Tensile Test Specimen…A:50mm(2"), D:5D(5.65√A).
＊5 降伏点又は耐力 Y.P. orY.S.…Y.P. :Upper yield point, L.P. :Lower yield point, .2YS:0.2%offset, .5YS:0.5% extension-under-load.　＊6 曲げ試験 Bend Test…G:Good.
＊7 分析区分 Analysis…L:Ladle, P:Product.　＊8 探傷波試験 Ultrasonic Test…G:Good　＊9 寸法、外観、形状検査 Dimension, Visual, Shape Inspection…G:Good　＊12 硬度試験位置 Hardness Test Position…SUR. :Surface, 1/2T: 1/2 t, 1/4T: 1/4 t.
＊10 衝撃試験片形状 Impact Test Specimen <2MM V> 2:10MMFULL　＊11 仕上り状態 Conditions of Supply

上記注文品は、御指定の規格または仕様に従って製造され、その要求事項を満足していることを証明します。

F. Furukawa
品質保証室
Manager of Quality Assurance

名古屋大学　試験体他

材料検査証明書

平成 29 年　6 月

㈱瀧上工作所

名古屋大学　試験体他

材料検査証明書

頁	メーカー	規　格	板　厚	巾	長 さ	員 数	板　番	適　　用
1	JFEスチール㈱	SN400B	12	2100	12500	1	KK72901	衝撃試験・引っ張り試験用
2	新関西製鐵㈱	SN490B	9	25	6000	1	U70655	突合溶接の裏当て材用
3	JFEスチール㈱	SS400	25	2100	6096	1	TN67208	衝撃試験機台座製作用
4	日本ファスナー工業㈱	SCM435	16.2φ				6M33509	台座取り付けBN　M16
5	日鐵住金溶接工業㈱	YGW11	1.2φ				SF68980	突合せ溶接用
6	㈱中山製鋼所	SS400	1.6	1219	2438	2	KK440318	開断面試験体用

検査証明書
INSPECTION CERTIFICATE

JFE スチール 株式会社 東日本製鉄所(京浜地区)
JFE Steel Corporation East Japan Works(Keihin)

需要家 Customer :MARUSADA SANGYO
需要家管理番号 Customer's Control No. :
注文者 Shipper :MM&KENZAI CORPORATION
注文者照合番号 Reference No. :8ZE -6B70040
品名 Commodity & :HOT ROLLED STEEL PLATE
規格 Specification :JIS G3136 SN400B

証明書番号 Certificate No. :161121-ASH -8980
日付 Date :2016-11-21
船番 Ship No. :
工事番号 Construction No. :
注文番号 Order No. :6GR5062

#1 製品番号 Roll No. / 鋼番 Heat No.	行番 Item No.	需要家管理番号 Customer's Control No. / 寸法 Size (MM) T X W X L	員数 Quantity	質量 Mass (CAL)	化学成分 Chemical Composition (%) #3 C (X100)	Si (X100)	Mn (X1000)	P (X100)	S (X100)	NIMO (X100)	V (X1000)	CR (X10)	CEQ2 (X100)	#4	引張試験 Tensile Test 降伏点/耐力 Y.P./Y.S. N/MM2	引張強さ T.S. N/MM2	伸び El #5 %	降伏比 YR %	曲げ UBT
SPECIFIED VALUE (STANDARD)		LADLE :		MIN.											235	400	18	-	
				MAX.											355	510	-	80	
				MIN.	-	-	60	-	-				-						
				MAX.	20	35	150	30	15				36						
定 KK72901 09798	001	12 X 2100 X 12500	1	2547	12	20	64	11	4	2	1	0	5	25	TC	284	421	32 A	67
		TOTAL	1	2547	KG														
		VISUAL & DIMENSIONS : GOOD																	

(注) (Notes)
#1 厚板製品番号の表示方法 Indication of Plate Roll Number
:上5桁:圧延番号, 2 letters&the 1st 3 figures:mother Plate Numbers
:下2桁:分割番号, the last 2 figures:divided Plate Numbers
#2 DG:脱ガス, Degassed
#4 位置, Position T:頭部, Top M:中部, Middle B:底部, Bottom
方向, Direction L:縦, Longitudinal C:横, Transverse Z:厚, Through-thickness
衝撃試験片寸法, Size of Impact Test Specimen 1:10X10mm 2:7.5X10mm 3:2/3X10mm 4:5X10mm 5:1/3X10mm 6:2.5X10mm 7:ThicknessX10mm
衝撃試験値特性単位, Unit of Impact Test Property
吸収エネルギー, Absorbed Energy:K:kgf.m, C:kgf.m/cm², J:Joule, U:J/cm², F:ft.lbf, L:ft.lbf/cm²
破面率, Fracture: S:延性, Shear B:脆性, Brittle
横膨出量, Lateral Expansion: M:mm I:mil
#5 標点距離, Gauge Length A:200mm(■) D:50mm(■) E:50mm(●) H:8″(■) J:2″(●) K:5D(●) M:5.65√A(●) P:5.65√A(■) R:4D(●) S:80mm(■) U:100mm(■) Y:2″(■) T:70mm(●)
#6 BT :曲げ試験, Bend Test UST:超音波探傷, Ultrasonic Examination G :合格, Good

定 印のみ有効
#3 CEQ2=C+MN/6+SI/24+NI/40+CR/5+MO/4+V/14

丸定産業株式会社
発行責任者 谷川善計 印

上記商品は検査の結果指定の規格に合格していることを証明いたします。
WE HEREBY CERTIFY THAT THE MATERIAL DESCRIBED HEREIN HAS BEEN TESTED AND INSPECTED WITH SATISFACTORY RESULTS IN ACCORDANCE WITH THE REQUIREMENTS OF THE ABOVE SPECIFICATION.

(ABX045001IAA)
SC20 1 A39

東日本製鉄所(京浜地区):〒210-0868神奈川県川崎市川崎区扇島1番地1 East Japan Works(Keihin):1-1, OHGISHIMA, KAWASAKI 210-0868 JAPAN

T. Yamazaki
東日本製鉄所(京浜地区)品質保証室
Quality Assurance Section
East Japan Works(Keihin)

This Inspection Certificate is printed with special forgery proof technology.
―このミルシートは特殊偽造防止技術を使用しております―

鋼材検査証明書
INSPECTION CERTIFICATE

証明書番号
Certificate No.: H17- 5041(01)

品名
Commodity : FLAT BAR

需要家
Customer : FURUSATO KOGYO K.K.

商社
Supplier : MM&KENZAI CORPORATION

JIS表示認証番号
JIS CERTIFICATION NO. QA0507045

日付
Date : 23 MAY 2017

契約番号
Contract No.: 307486

規格
Specification : JIS G 3136 SN490B

	Charge No.	Mfg. No.	Dimension	Length	Pieces	Mass (kg)	Control No.
1	U70655		9 X 25	6000	458	4,855	
2							
3							
4							
5							
6							
7							
8							
			-TOTAL-		458	4,855	

Application

※1 : Bend Test G : Good
※2 : Ultrasonic Test A : Acceptable

	Chemical Composition (%)														Ceq (%)	Pcm (%)	Tensile Test						Bend Test	Impact Test 0℃	Hard-ness	Ultrasonic Test	Remarks
	C	Si	Mn	P	S	Cu	Ni	Cr	Mo	V	Sn	B					G.L.	Y.P.	T.S.	Y.R.	EL.	R.A.					
	×100			×1000		×100					×1000				×100		mm	N/mm²		%	%	%					
Min																		325	490		17			27			
Max	18	55	165	30	15										44	29			610				※1			※2	
1	12	23	119	15	13	7	5	8	2	2	6	TR			35	20		365	509		28			---			
2																											
3																											
4																											
5																											
6																											
7																											
8																											

上記鋼材は、検査の結果、ご指定の規格または仕様に合格している事を証明致します。 We Hereby certify that the material described herein has been tested and inspected satisfactorily in accordance with the requirements of the above specification.

新関西製鐵株式会社
SHINKANSAI STEEL CORPORATION

星田工場
HOSHIDA WORKS
交野市星田北４丁目26番１号 〒576-0017
4-26-1 Hoshidakita, Katano, Osaka Japan
Tel.072-891-0624 Fax.072-893-1319

Masahiko Yamamoto
MASAHIKO YAMAMOTO
Manager of Quality Control Group

JFE スチール 株式会社 東日本製鉄所(京浜地区)
JFE Steel Corporation East Japan Works(Keihin)

検査証明書
INSPECTION CERTIFICATE

需要家 Customer	:KITO KOZAI CO., LTD.
需要家管理番号 Customer's Control No.	:
注文者 Shipper	:JFE SHOJI TRADE CORPORATION
注文者照合番号 Reference No.	:CG6 -1
品名 Commodity & 規格 Specification	HOT ROLLED STEEL PLATE JIS G3101 SS400

証明書番号 Certificate No.	:160427- ASH -2172-001 CONTINUED
日付 Date	:2016-04-27
船番 Ship No.	:
工事番号 Construction No.	:
注文番号 Order No.	:6AJ7424

#1 製品番号 Roll No. / 鋼番 Heat No.	行番 Item No.	需要家管理番号 Customer's Control No. / 寸法 Size (MM) T X W X L	員数 Quantity	質量 Mass (CAL)	化学成分 Chemical Composition (%) C X100	Si	Mn X1000	P	S X100	X1000	X10	X100	引張試験 Tensile Test #4 降伏点/耐力 Y.P./Y.S. N/MM2	引張強さ T.S. N/MM2	伸び El #5 %	降伏比 YR %	曲げ BT	UST
SPECIFIED VALUE (STANDARD) LADLE :				MIN.									235	400	21			
				MAX.									-	510	-			
				MIN.														
				MAX.			50	50										
TK50309 01788	003	25 X 1524 X 6096	1	1878	17	1	68	19	4				TC 280	429	31 A			
TN67203 02040	004	25 X 2100 X 6096	1	2586	16	1	68	29	4				TC 291	433	30 A			
TN67206 02040	004	25 X 2100 X 6096	1	2586														
TN67207 02040	004	25 X 2100 X 6096	1	2586														
定 TN67208 02040	004	25 X 2100 X 6096	1	2586														
TN68001 02042	003	25 X 1524 X 6096	1	1878	16	1	67	24	4				TC 285	422	32 A			
TN68002 02042	003	25 X 1524 X 6096	1	1878														
TN68003 02042	003	25 X 1524 X 6096	1	1878														

(注) (Notes)
#1 原板製品番号の表示方法, Indication of Plate Roll Number
:上5桁:圧延番号, 2 letters&the 1st 3 figures:mother Plate Numbers
:下2桁:分割番号, the last 2 figures:divided Plate Numbers
#2 DG:脱ガス, Degassed

#4 位置, Position
T:頭部, Top M:中部, Middle
B:底部, Bottom
方向, Direction
L:縦, Longitudinal
C:横, Transverse
Z:厚, Through-thickness

衝撃試験片寸法, Size of Impact Test Specimen
1:10X10mm 2:7.5X10mm 3:2/3X10mm 4:5X10mm
5:1/3X10mm 6:2.5X10mm 7:ThicknessX10mm
衝撃試験値特性単位, Unit of Impact Test Property
吸収エネルギー, Absorbed Energy:K:kgf.m C:kgf.m/cm², J:Joule,
U:J/cm², F:ft.lbf, L:ft.lbf/cm²
破面率, Fracture: S:延性, Shear B:脆性, Brittle
横膨出量, Lateral Expansion: M:mm I:mil

#5 標点距離, Gauge Length
A:200mm (■) D:50mm (■)
E:50mm (●) H:8″ (■)
J:2″ (●) K:5D (●)
M:5.65√A (●) P:5.65√A (■)
R:4D (●) S:80mm (■)
U:100mm (■) Y:2″ (■)
T:70mm (●)

#6 BT :曲げ試験, Bend Test
UST:超音波探傷, Ultrasonic Examination
G :合格, Good

〒476-0001 愛知県東海市荒尾町二の割170-5
鬼頭鋼材株式会社
TEL (052) 604 - 5111

定印のみ有効
丸定産業株式会社
発行責任者 谷川善計 印

○印のみ有効

上記商品は検査の結果指定の規格に合格していることを証明いたします。

WE HEREBY CERTIFY THAT THE MATERIAL DESCRIBED HEREIN HAS BEEN TESTED AND INSPECTED WITH SATISFACTORY RESULTS IN ACCORDANCE WITH THE REQUIREMENTS OF THE ABOVE SPECIFICATION.

(2B39420011CA)
S803 1 A33

東日本製鉄所(京浜地区):〒210-0868神奈川県川崎市川崎区扇島1番地1 East Japan Works(Keihin):1-1, OHGISHIMA, KAWASAKI 210-0868 JAPAN

T. Yanazaki
東日本製鉄所(京浜地区)品質保証室
Quality Assurance Section
East Japan Works(Keihin)

名古屋大学　試験体他

材料検査証明書

平成 29 年　6 月

㈱瀧上工作所

名古屋大学　試験体他

材料検査証明書

頁	メーカー	規　格	板　厚	巾	長 さ	員 数	板　番	適　　用
1	JFEスチール㈱	SN400B	12	2100	12500	1	KK72901	衝撃試験・引っ張り試験用
2	新関西製鐵㈱	SN490B	9	25	6000	1	U70655	突合溶接の裏当て材用
3	JFEスチール㈱	SS400	25	2100	6096	1	TN67208	衝撃試験機台座製作用
4	日本ファスナー工業㈱	SCM435	16.2φ				6M33509	台座取り付けBN　M16
5	日鐵住金溶接工業㈱	YGW11	1.2φ				SF68980	突合せ溶接用
6	㈱中山製鋼所	SS400	1.6	1219	2438	2	KK440318	開断面試験体用

検査証明書
INSPECTION CERTIFICATE

JFE スチール 株式会社 東日本製鉄所(京浜地区)
JFE Steel Corporation East Japan Works(Keihin)

需要家 Customer :MARUSADA SANGYO
需要家管理番号 Customer's Control No. :
注文者 Shipper :MM&KENZAI CORPORATION
注文者照合番号 Reference No. :8ZE -6B70040
品名 Commodity & 規格 Specification : HOT ROLLED STEEL PLATE JIS G3136 SN400B

証明書番号 Certificate No. :161121-ASH -8980
日付 Date :2016-11-21
船番 Ship No. :
工事番号 Construction No. :
注文番号 Order No. :6GR5062

製品番号 #1 Roll No. 鋼番 Heat No.	行番 Item No.	需要家管理番号 Customer's Control No. 寸法 Size T X W X L (MM)	員数 Quantity	質量 Mass (CAL)	化学成分 Chemical Composition (%) #3 C X100	Si	Mn X1000	P	S	NI	MO X100	V	CR X1000	X10	CEQ2 X100	引張試験 Tensile Test 降伏点/耐力 Y.P./Y.S. #4 N/MM2	引張強さ T.S.	伸び El #5 %	降伏比 YR %	曲げ BT	UST
SPECIFIED VALUE (STANDARD) LADLE :				MIN.	-	-	60	-	-							235	400	18	-		
				MAX.	20	35	150	30	15						36	355	510	-	80		
KK72901 09798	001	12 X 2100 X 12500	1	2547	12	20	64	11	4	2	1	0	5		25	TC	284	421	32 A	67	
		TOTAL	1	2547 KG																	
VISUAL & DIMENSIONS : GOOD																					

(注) (Notes)
#1 厚板製品番号の表示方法, Indication of Plate Roll Number
:上5桁:圧延番号, 2 letters&the 1st 3 figures:mother Plate Numbers
:下2桁:分割番号, the last 2 figures:divided Plate Numbers
#2 DG:脱ガス, Degassed
#3 CEQ2=C+MN/6+SI/24+NI/40+CR/5+MO/4+V/14
#4 位置, Position T:頭部, Top M:中部, Middle B:底部, Bottom
方向, Direction L:縦, Longitudinal C:横, Transverse Z:厚, Through-thickness
衝撃試験片寸法, Size of Impact Test Specimen 1:10X10mm 2:7.5X10mm 3:2/3X10mm 4:5X10mm 5:1/3X10mm 6:2.5X10mm 7:ThicknessX10mm
衝撃試験値材性単位, Unit of Impact Test Property
吸収エネルギー, Absorbed Energy:K:kgf.m C:kgf.m/cm² J:Joule, U:J/cm², F:ft.lbf, L:ft.lbf/cm²
破面率, Fracture: S:延性, Shear B:脆性, Brittle
横膨出量, Lateral Expansion: M:mm I:mil
#5 標点距離, Gauge Length A:200mm(■) D:50mm(■) E:50mm(●) H:8″(■) J:2″(●) K:5D(●) P:5.65√A(■) R:4D(●) S:80mm(■) U:100mm(■) Y:2″(■) T:70mm(●)
#6 BT :曲げ試験, Bend Test UST:超音波探傷, Ultrasonic Examination G :合格, Good

定 印のみ有効

丸定産業株式会社

発行責任者 谷川善計 印

上記商品は検査の結果指定の規格に合格していることを証明いたします。

WE HEREBY CERTIFY THAT THE MATERIAL DESCRIBED HEREIN HAS BEEN TESTED AND INSPECTED WITH SATISFACTORY RESULTS IN ACCORDANCE WITH THE REQUIREMENTS OF THE ABOVE SPECIFICATION.

(ABX0450011AA)
SC20 1 A39

東日本製鉄所(京浜地区):〒210-0868神奈川県川崎市川崎区扇島1番地1 East Japan Works(Keihin):1-1, OHGISHIMA, KAWASAKI 210-0868 JAPAN

T. Yanagiki
東日本製鉄所(京浜地区)品質保証室
Quality Assurance Section
East Japan Works(Keihin)

This Inspection Certificate is printed with special forgery proof technology.
―このミルシートは特殊偽造防止技術を使用しております―

証明書番号
Certificate No.: H17- 5041(01)

鋼材検査証明書
INSPECTION CERTIFICATE

日付
Date :23 MAY 2017

品名
Commodity :FLAT BAR

需要家
Customer :FURUSATO KOGYO K.K.

商社 105-6ZE
Supplier :MM&KENZAI CORPORATION

契約番号
Contract No.:307486

規格
Specification :JIS G 3136 SN490B

JIS表示認証番号
JIS CERTIFICATION NO. QA0507045

	Charge No.	Mfg. No.	Dimension	Length	Pieces	Mass (kg)	Control No.
1	U70655		9 X 25	6000	458	4,855	
2							
3							
4							
5							
6							
7							
8							
			-TOTAL-		458	4,855	

Application

※1 : Bend Test G : Good
※2 : Ultrasonic Test A : Acceptable

	Chemical Composition (%)														Ceq (%)	Pcm (%)	Tensile Test						Bend Test	Impact Test 0℃	Hard-ness	Ultrasonic Test	Remarks
	C	Si	Mn	P	S	Cu	Ni	Cr	Mo	V	Sn	B					G.L.	Y.P.	T.S.	Y.R.	EL.	R.A.					
	×100			×1000		×100					×1000				×100		mm	N/mm²		%	%	%					
Min																		325	490		17			27			
Max	18	55	165	30	15										44	29			610				※1			※2	
1	12	23	119	15	13	7	5	8	2	2	6	TR			35	20		365	509		28			---			
2																											
3																											
4																											
5																											
6																											
7																											
8																											

上記鋼材は、検査の結果、ご指定の規格または仕様に合格している事を証明致します。 We Hereby certify that the material described herein has been tested and inspected satisfactorily in accordance with the requirements of the above specification.

新関西製鐵株式会社
SHINKANSAI STEEL CORPORATION

星田工場
HOSHIDA WORKS
交野市星田北４丁目26番１号 〒576-0017
4-26-1 Hoshidakita, Katano, Osaka Japan
Tel.072-891-0624 Fax.072-893-1319

Masahiko Yamamoto
MASAHIKO YAMAMOTO
Manager of Quality Control Group

鋼材検査証明書
INSPECTION CERTIFICATE

商　社 (SUPPLIER) : 中山通商 株式会社(大阪)
需要家 (CUSTOMER) : 日本ファスナー工業株式会社(鶴見区)
発行年月日 (DATE) : AUG . 02 . 2016
証明書番号 (CERTIFICATE No) : 803-00140　頁: PAGE 1
契約番号 (CONTRACT No) : 252511D35－001
註文者照合番号 (ORDER No) :
需要家管理番号 (CUSTOMER No) :
工　事　名 (CONSTRUCTION NAME) :

品　名 (DESCRIPTION) : WIRE RODS
規　格 (SPECIFICATION) : JIS G 4053 SCM435
規格コード (SPEC CODE) : SCM435

〒538-0041
大阪市鶴見区今津北4－7－18
日本ファスナー工業株式会社(鶴見区)

技管 16.8.-8 東浦

寸法 DIMENSIONS (mm)	溶鋼番号 CHARGE No	製品番号 PLATE No & LOT No & COIL No	数量 QUANTITY	質量 MASS Kg ACTUAL	引張試験 TENSILE TEST 降伏点 YP N/mm2	引張強さ TS N/mm2	伸び EL %	標点距離 GL	絞り RA %	降伏比 YR %	厚さ方向特性 RAZ	C X100	Si X100	Mn X100	P X1000	S X1000	Cu X100	Ni X100	Cr X100	Ni+Cr X100	Cu+Ni+Cr X100	Mo X100	Nb X1000	Ti X1000	Al X1000	Ceq(W) X100	Pcm X100
												33	15	60	MAX	MAX	MAX	MAX	90			15					
												36	35	90	25	10	30	25	120			30					
16.2	6M33509		5	10064								34	21	72	15	6	2	2	103			16					
GRAND TOTAL			5	10064																							

Signed by:
M16
SURVEYOR TO

上記の鋼材は、検査の結果、御指定の規格または仕様に合格していることを証明します。
WE HEREBY CERTIFY THAT THE STEEL DESCRIBED HEREIN HAS BEEN SATISFACTORILY TESTED AND INSPECTED IN ACCORDANCE WITH THE REQUIREMENTS OF THE ABOVE SPECIFICATION.

株式会社中山製鋼所 船町工場
NAKAYAMA STEEL WORKS, L T D.
大阪市大正区船町一丁目1番66号
1-1-66, Funamachi, Taisho-Ku, Osaka, Japan

Signed by: H. Haraguchi 原口秀見
HIDEAKI HARAGUCHI
生産技術部 品質総括室長
GROUP MANAGER OF QUALITY ADMINISTRATION SEC.
PRODUCTION & TECHNICAL CONTROL DEPT.

(注) NOTES GL: 標点距離 Gauge Length‥‥1=50mm, 2=200mm, 3=4D, 4=8D, 5=5.65√A , 6=2", 7=70mm
HBW:ブリネル硬さ Brinell hardness HRB/HRC:ロックウェル硬さ Rockwell hardness CH:シャルピー衝撃試験 Charpy Impact Test
ZN,C:亜鉛付着量 Zn Coating‥‥両面三点平均付着量, (*) 一点最小付着量 CB:曲げ剥離 Coating Bend Test
RA(Z):厚さ方向特性 Specification for through thickness characteristics UT:超音波探傷試験 Ultrasonic Test
YR:降伏比 Yield Ratio Ceq(W) :炭素当量(%) =C+Mn/6+Si/24+Ni/40+Cr/5+Mo/4+V/14
RA:絞り Reduction of Area PCM:溶接割れ感受性組成(%)=C+Si/30+Mn/20+Cu/20+Ni/60+Cr/20+Mo/15+V/10+5B

INSPECTION CERTIFICATE
検 査 証 明 書

Customer
(需要家) 株式会社 瀧上工作所 殿

Certificate No.
(証明書番号) 1706954V
Date (発行日) 平成29年6月5日

Trade Designation (銘柄)	Size mm (寸法)	Manuf.No. (製造番号)	Heat No. (製鋼番号)	Weight kg (数量)	Remark (備考)
NSSW YM-26	1.2	7W55230098	SF68980	-	JIS Z 3312 YGW11

Chemical Composition of Wire (ワイヤの化学成分%)

C	Si	Mn	P	S	Cu	Ti+Zr						
0.06	0.77	1.60	0.014	0.011	0.30	0.24						

We hereby certify that above welding materials satisfy the requirements of the applicable specification.

上記溶接材料は、適用規格の要求事項を満足していることを証明します。

Group manager,Quality Control Dept.
Nippon Steel & Sumikin Welding Co., Ltd.
Hikari Plant
日鐵住金溶接工業株式会社
光工場 品質管理グループ長
4-2-1,ASAE,HIKARI-SHI,YAMAGUCHI-KEN,JAPAN
山口県光市浅江4丁目2番1号 TEL 0833(71)3390 FAX 0833(71)3394

鋼材検査証明書
INSPECTION CERTIFICATE

商　社 (SUPPLIER) : 三井物産スチール 株式会社(中部支社)
需要家 (CUSTOMER) : 明鋼材株式会社 弥富センター
発行年月日 (DATE) : APR . 28 . 2017
証明書番号 (CERTIFICATE No) : 429-00279　　頁: PAGE 1
契約番号 (CONTRACT No) : 26170308P－001
註文者照合番号 (ORDER No) :
需要家管理番号 (CUSTOMER No) :
工　事　名 (CONSTRUCTION NAME) :

品　名 (DESCRIPTION) : HOT ROLLED STEEL SHEETS
規　格 (SPECIFICATION) : JIS G 3101 SS400
規格コード (SPEC CODE) : SS400

〒450-0003
名古屋市中村区名駅南1丁目16番21号(名古屋三井物産ビル)
三井物産スチール 株式会社(中部支社)
営業第三部

本証明書は◯本中、2本のみ有効です。

明鋼材株式会社

寸法 DIMENSIONS (mm)	溶鋼番号 CHARGE No	製品番号 PLATE No & LOT No & COIL No	数量 QUANTITY	質量 MASS Kg CAL	引張試験 TENSILE TEST 降伏点 YP N/mm2	引張強さ TS N/mm2	伸び EL %	標点距離 GL	絞り RA %	降伏比 YR %	厚さ方向特性 RAZ	化学成分 CHEMICAL COMPOSITION % C X100	Si X100	Mn X100	P X1000	S X1000	Cu X100	Ni X1000	Cr X1000	Ni+Cr X1000	Cu+Ni+Cr X1000	Mo X1000	Nb X1000	Ti X1000	Al X1000	Ceq (W) X100	Pcm X100
1.6X1219X2438	6WLB457	C42014 KK440318	53	1977	326	417	37	1				9	2	48	18	3											
GRAND TOTAL			53	1977																							

◎印 2 枚のみ有効

〒456-0013 名古屋市熱田区外土居町7番37号
三重鋼材株式会社
電話〈052〉681－8131番

Signed by:

SURVEYOR TO

上記の鋼材は、検査の結果、御指定の規格または仕様に合格していることを証明します。
WE HEREBY CERTIFY THAT THE STEEL DESCRIBED HEREIN HAS BEEN SATISFACTORILY TESTED AND INSPECTED IN ACCORDANCE WITH THE REQUIREMENTS OF THE ABOVE SPECIFICATION.

株式会社 中山製鋼所 船町工場
NAKAYAMA STEEL WORKS, LTD. Funamachi Works
大阪市大正区船町一丁目1番66号
1-66, Funamachi 1-chome, Taisho-ku, Osaka-shi, Osaka, Japan

Signed by: H. Haraguchi 原口秀晃 HIDEAKI HARAGUCHI
生産技術部 品質総括室長
GROUP MANAGER OF QUALITY ADMINISTRATION SEC.
PRODUCTION & TECHNICAL CONTROL DEPT.

(注) NOTES
GL: 標点距離 Gauge Length・・・・1=50mm, 2=200mm, 3=4D, 4=8D, 5=5.65√A, 6=2", 7=70mm, 8=80mm
HBW:ブリネル硬さ Brinell hardness HRB/HRC:ロックウェル硬さ Rockwell hardness CH:シャルピー衝撃試験 Charpy Impact Test
ZN,C:亜鉛付着量 Zn Coating・・・・両面三点平均付着量, (e)一点最小付着量 CB:曲げ剥離 Coating Bend Test
RAZ:厚さ方向特性 Specification for through thickness characteristics UT:超音波探傷試験 Ultrasonic Test
YR:降伏比 Yield Ratio Ceq(W):炭素当量(%)=C+Mn/6+Si/24+Ni/40+Cr/5+Mo/4+V/14
RA:絞り Reduction of Area PCM:溶接割れ感受性組成(%)=C+Si/30+Mn/20+Cu/20+Ni/60+Cr/20+Mo/15+V/10+5B

名古屋大学　試験体

材料検査証明書

平成 29 年 10 月

㈱瀧上工作所

名古屋大学　試験体他

材料検査証明書

頁	メーカー	規　格	板　厚	巾	長 さ	員 数	板　番	適　　用
1	JFEスチール㈱	SN400B	12	2100	12500	1	KK72901	衝撃試験・引っ張り試験用
2	新関西製鐵㈱	SN490B	9	25	6000	1	U70655	突合溶接の裏当て材用
3	日鐵住金溶接工業㈱	YGW11	1.2φ				SF68980	突合せ溶接用

検査証明書
INSPECTION CERTIFICATE

JFE スチール 株式会社 東日本製鉄所(京浜地区)
JFE Steel Corporation East Japan Works(Keihin)

JFE

証明書番号 Certificate No.	:161121-ASH -8980
日付 Date	:2016-11-21
船番 Ship No.	:
工事番号 Construction No.	:
注文番号 Order No.	:6GR5062

需要家 Customer :MARUSADA SANGYO
需要家管理番号 Customer's Control No. :
注文者 Shipper :MM&KENZAI CORPORATION
注文者照合番号 Reference No. :8ZE -6B70040
品名 Commodity & 規格 Specification : HOT ROLLED STEEL PLATE / JIS G3136 SN400B

#1 製品番号 Roll No. / 鋼番 Heat No.	行番 Item No.	需要家管理番号 Customer's Control No. / 寸法 Size T X W X L (MM)	員数 Quantity	質量 Mass (CAL)	化学成分 Chemical Composition (%) C x100	Si	Mn x1000	P	S	Ni x100	Mo	V	Cr x1000	x10	#3 CEQ2 x100	引張試験 Tensile Test #4 降伏点/耐力 Y.P./Y.S. N/MM2	引張強さ T.S.	伸び El % #5	降伏比 YR %	曲げ UBT
SPECIFIED VALUE (STANDARD) LADLE :				MIN.												235	400	18	-	
				MAX.												355	510	-	80	
				MIN.	-	-	60	-	-						-					
				MAX.	20	35	150	30	15						36					
KK72901 09798	001	12 X 2100 X 12500	1	2547	12	20	64	11	4	2	1	0	5		25	TC	284	421	32	67	A
		TOTAL	1	2547 KG																
VISUAL & DIMENSIONS : GOOD																				

(注) (Notes)
#1 原板製品番号の表示方法, Indication of Plate Roll Number
:上5桁:圧延番号, 2 letters&the 1st 3 figures:mother Plate Numbers
:下2桁:分割番号, the last 2 figures:divided Plate Numbers
#2 DG:脱ガス, Degassed

#4 位置, Position
T:頭部, Top M:中部, Middle
B:底部, Bottom
方向, Direction
L:縦, Longitudinal
C:横, Transverse
Z:厚, Through-thickness

衝撃試験片寸法, Size of Impact Test Specimen
1:10X10mm 2:7.5X10mm 3:2/3X10mm 4:5X10mm
5:1/3X10mm 6:2.5X10mm 7:ThicknessX10mm
衝撃試験値特性単位, Unit of Impact Test Property
吸収エネルギー, Absorbed Energy:K:kgf.m C:kgf.m/cm² J:Joule, U:J/cm² F:ft.lbf, L:ft.lbf/cm²
破面率, Fracture: S:延性, Shear B:脆性, Brittle
横膨出量, Lateral Expansion; M:mm I:mil

#5 標点距離, Gauge Length
A:200mm (■) D:50mm (■)
E:50mm (●) H:8" (■)
J:2" (●) K:5D (●)
M:5.65√A (●) P:5.65√A (■)
R:4D (●) S:80mm (■)
U:100mm (■) Y:2" (■)
T:70mm (●)

#6 BT :曲げ割れ, Bend Test
UST:超音波探傷, Ultrasonic Examination
G :合格, Good

(定)印のみ有効
#3 CEQ2=C+MN/6+SI/24+NI/40+CR/5+MO/4+V/14

丸定産業株式会社
発行責任者 谷川善計 印

上記商品は検査の結果指定の規格に合格していることを証明いたします。
WE HEREBY CERTIFY THAT THE MATERIAL DESCRIBED HEREIN HAS BEEN TESTED AND INSPECTED WITH SATISFACTORY RESULTS IN ACCORDANCE WITH THE REQUIREMENTS OF THE ABOVE SPECIFICATION.

(ABX045001IAA)
SC20 1 A39

東日本製鉄所(京浜地区):〒210-0868神奈川県川崎市川崎区扇島1番地1 East Japan Works(Keihin):1-1, OHGISHIMA, KAWASAKI 210-0868 JAPAN

T. Yamazaki
東日本製鉄所(京浜地区)品質保証室
Quality Assurance Section
East Japan Works(Keihin)

This Inspection Certificate is printed with special forgery proof technology.
—このミルシートは特殊偽造防止技術を使用しております—

鋼材検査証明書
INSPECTION CERTIFICATE

証明書番号
Certificate No.: H17- 5041(01)
品名
Commodity : FLAT BAR
需要家
Customer : FURUSATO KOGYO K.K.
商社
Supplier : 105-6ZE
MM&KENZAI CORPORATION

JIS表示認証番号
JIS CERTIFICATION NO. QA0507045

日付
Date : 23 MAY 2017
契約番号
Contract No.: 307486
規格
Specification : JIS G 3136 SN490B

	Charge No.	Mfg. No.	Dimension	Length	Pieces	Mass (kg)	Control No.
1	U70655		9 X 25	6000	458	4,855	
2							
3							
4							
5							
6							
7							
8							
			-TOTAL-		458	4,855	

Application

※1 : Bend Test G : Good
※2 : Ultrasonic Test A : Acceptable

	Chemical Composition (%)														Ceq (%)	Pcm (%)	Tensile Test						Bend Test	Impact Test	Hard-ness	Ultrasonic Test	Remarks
	C	Si	Mn	P	S	Cu	Ni	Cr	Mo	V	Sn	B					G.L.	Y.P.	T.S.	Y.R.	EL.	R.A.					
	×100			×1000		×100					×1000				×100		mm	N/mm²		%	%	%		0℃			
Min																		325	490		17			27			
Max	18	55	165	30	15										44	29			610				※1			※2	
1	12	23	119	15	13	7	5	8	2	2	6	TR			35	20		365	509		28			---			
2																											
3																											
4																											
5																											
6																											
7																											
8																											

上記鋼材は、検査の結果、ご指定の規格または仕様に合格している事を証明致します。 We Hereby certify that the material described herein has been tested and inspected satisfactorily in accordance with the requirements of the above specification.

新関西製鐵株式会社
SHINKANSAI STEEL CORPORATION

星田工場
HOSHIDA WORKS
交野市星田北４丁目26番１号 〒576-0017
4-26-1 Hoshidakita, Katano, Osaka Japan
Tel.072-891-0624 Fax.072-893-1319

Masahiko Yamamoto
MASAHIKO YAMAMOTO
Manager of Quality Control Group

INSPECTION CERTIFICATE
検 査 証 明 書

Customer
(需要家) 株式会社 瀧上工作所 殿

Certificate No.
(証明書番号) 1706954V
Date (発行日) 平成29年6月5日

Trade Designation (銘柄)	Size mm (寸法)	Manuf.No. (製造番号)	Heat No. (製鋼番号)	Weight kg (数量)	Remark (備考)
NSSW YM-26	1.2	7W55230098	SF68980	-	JIS Z 3312 YGW11

Chemical Composition of Wire (ワイヤの化学成分%)

C	Si	Mn	P	S	Cu	Ti+Zr						
0.06	0.77	1.60	0.014	0.011	0.30	0.24						

We hereby certify that above welding materials satisfy
the requirements of the applicable specification.

上記溶接材料は、適用規格の要求事項を満足していることを証明します。

Group manager, Quality Control Dept.
Nippon Steel & Sumikin Welding Co., Ltd.
Hikari Plant
日鐵住金溶接工業株式会社
光工場 品質管理グループ長
4-2-1, ASAE, HIKARI-SHI, YAMAGUCHI-KEN, JAPAN
山口県光市浅江4丁目2番1号 TEL 0833(71)3390 FAX 0833(71)3394

名古屋大学　試験体

溶接施工記録

（先　行　分）

平成 29 年　6 月

㈱瀧上工作所

目　　次

母材部、溶接部(WELD, HAZ)
各15本採取×3セット

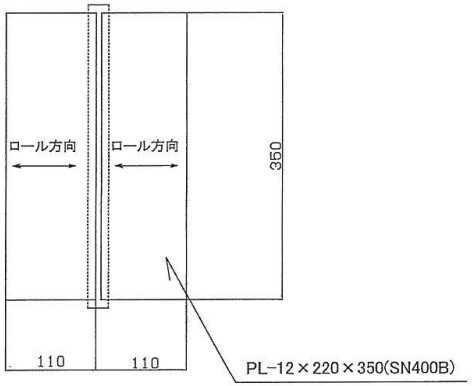

6体・・・・・今回試験
12体・・・・・次回試験
計 18体

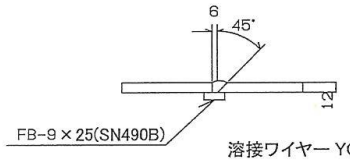

溶接ワイヤー YGW-11

素材引張試験材
(計 3 体)

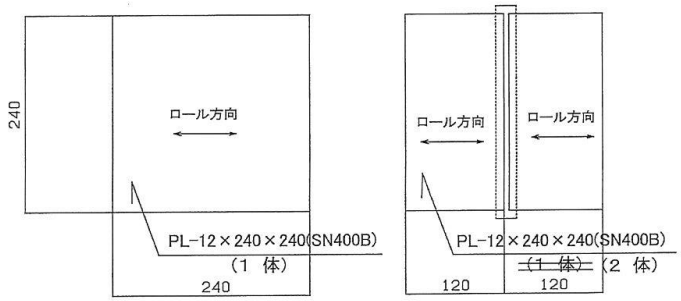

<注 記>
全ての鋼材は、同ロット材とする。

版数	改正年月日	改正箇所及び改正内容	ボルト記号			材質表示	
			径	HTB	中BOLT	無印 —— SS400 STK400	□ ——
1			M24(S10T)	⊕	⊕		□ ——
1			M22(S10T)	+	⊕		○ ——
1			M20(S10T)	※	⊕		○ ——
1			M16(S10T)	※	⊕		
1							
1							

縮尺	作成	工事名	図番	工事番号	Rev.
	H29.6.1	名古屋大学試験体		29-05	△
承認 浅井	審査 浅井	作成 栗野	図名 試験体図	株式会社 誼上工作所	

溶接施工記録

溶接方法	炭酸ガス半自動溶接	工事番号	29－05
電流・電圧	直流	工事名称	名古屋大学試験体
溶接長(mm)	350	記号	S－1
板厚	12	溶接技能者	市来原良行
溶接ワイヤ(銘柄)	YM－26(YGW－11)	溶接管理者	河合光国
ワイヤサイズ(φmm)	1.2	溶接施工日	平成29年6月21日
シールドガス	Co2	開先	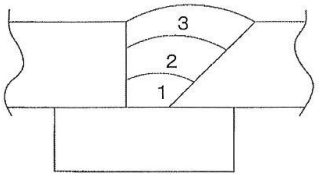
ガス流量(L/min)	25		
予熱温度(℃)	——		
上限パス(層)間温度(℃)	350		
下限パス(層)間温度(℃)	20		
基準入熱量(KJ/CM)	40		
アークタイム(秒)	283		
総パス数	3		

パス数	溶接時間	溶接電流	溶接電圧	溶接速度	パス間温度	入熱量	備考
	(秒)	(A)	(V)	(cm/min)	(℃)	(kJ/cm)	
1	73	300	40	28.77	24.6	25	
2	93	280	40	22.58	176	29.7	溶接後清掃
3	117	280	40	17.95	285	37.4	

コメント

溶 接 施 工 記 録

溶接方法	炭酸ガス半自動溶接	工事番号	29－05
電流・電圧	直 流	工事名称	名古屋大学試験体
溶接長(mm)	350	記 号	S－2
板厚	12	溶接技能者	市来原良行
溶接ワイヤ(銘柄)	YM－26(YGW－11)	溶接管理者	河合光国
ワイヤサイズ(φmm)	1.2	溶接施工日	平成29年6月21日
シールドガス	Co2	開 先	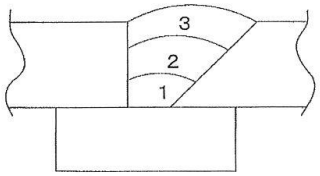
ガス流量(L/min)	25		
予熱温度(℃)	——		
上限パス(層)間温度(℃)	350		
下限パス(層)間温度(℃)	20		
基準入熱量(KJ/CM)	40		
アークタイム(秒)	283		
総パス数	3		

パス数	溶接時間	溶接電流	溶接電圧	溶接速度	パス間温度	入熱量	備 考
	(秒)	(A)	(V)	(cm/min)	(℃)	(kJ/cm)	
1	71	300	38	29.57	23.8	23.1	
2	94	300	38	22.34	153	30.6	溶接後清掃
3	118	300	38	17.79	278	38.4	

コメント

溶接施工記録

溶接方法	炭酸ガス半自動溶接	工事番号	29－05
電流・電圧	直流	工事名称	名古屋大学試験体
溶接長(mm)	350	記号	S－3
板厚	12	溶接技能者	市来原良行
溶接ワイヤ(銘柄)	YM－26(YGW－11)	溶接管理者	河合光国
ワイヤサイズ(φmm)	1.2	溶接施工日	平成29年6月21日
シールドガス	Co2	開先	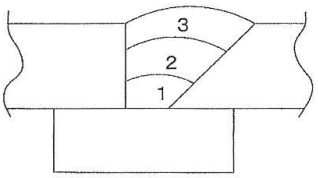
ガス流量(L/min)	25		
予熱温度(℃)	——		
上限パス(層)間温度(℃)	350		
下限パス(層)間温度(℃)	20		
基準入熱量(KJ/CM)	40		
アークタイム(秒)	301		
総パス数	3		

パス数	溶接時間	溶接電流	溶接電圧	溶接速度	パス間温度	入熱量	備考
	(秒)	(A)	(V)	(cm/min)	(℃)	(kJ/cm)	
1	84	300	38	25	24	27.36	
2	99	300	38	21.21	163	32.24	溶接後清掃
3	118	300	38	17.8	289	38.43	

コメント

溶接施工記録

溶接方法	炭酸ガス半自動溶接	工事番号	29−05
電流・電圧	直流	工事名称	名古屋大学試験体
溶接長(mm)	350	記号	S−4
板厚	12	溶接技能者	市来原良行
溶接ワイヤ(銘柄)	YM−26(YGW−11)	溶接管理者	河合光国
ワイヤサイズ(φmm)	1.2	溶接施工日	平成29年6月21日
シールドガス	Co2	開先	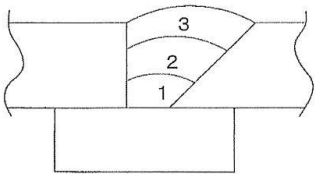
ガス流量(L/min)	25		
予熱温度(℃)	——		
上限パス(層)間温度(℃)	350		
下限パス(層)間温度(℃)	20		
基準入熱量(KJ/CM)	40		
アークタイム(秒)	293		
総パス数	3		

パス数	溶接時間	溶接電流	溶接電圧	溶接速度	パス間温度	入熱量	備考
	(秒)	(A)	(V)	(cm/min)	(℃)	(kJ/cm)	
1	78	300	38	26.92	23.7	25.4	
2	100	300	38	21	166	32.57	溶接後清掃
3	115	280	38	18.26	270	34.96	

コメント

溶接施工記録

溶接方法	炭酸ガス半自動溶接	工事番号	29－05
電流・電圧	直流	工事名称	名古屋大学試験体
溶接長(mm)	350	記号	S－5
板厚	12	溶接技能者	市来原良行
溶接ワイヤ(銘柄)	YM－26(YGW－11)	溶接管理者	河合光国
ワイヤサイズ(φmm)	1.2	溶接施工日	平成29年6月21日
シールドガス	Co2	開先	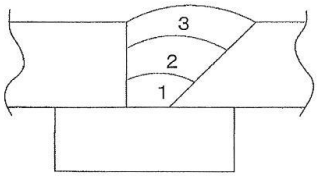
ガス流量(L/min)	25		
予熱温度(℃)	——		
上限パス(層)間温度(℃)	350		
下限パス(層)間温度(℃)	20		
基準入熱量(KJ/CM)	40		
アークタイム(秒)	308		
総パス数	3		

パス数	溶接時間	溶接電流	溶接電圧	溶接速度	パス間温度	入熱量	備考
	(秒)	(A)	(V)	(cm/min)	(℃)	(kJ/cm)	
1	75	280	38	27.99	23.4	22.8	
2	110	300	38	19.09	158	35.83	溶接後清掃
3	123	280	38	17.07	268	37.39	

コメント

溶接施工記録

溶接方法	炭酸ガス半自動溶接	工事番号	29−05
電流・電圧	直流	工事名称	名古屋大学試験体
溶接長(mm)	350	記号	S−6
板厚	12	溶接技能者	市来原良行
溶接ワイヤ(銘柄)	YM−26(YGW−11)	溶接管理者	河合光国
ワイヤサイズ(φmm)	1.2	溶接施工日	平成29年6月21日
シールドガス	Co2	開先	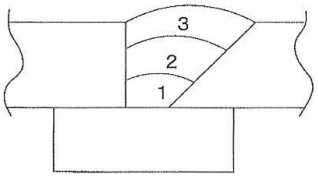
ガス流量(L/min)	25		
予熱温度(℃)	——		
上限パス(層)間温度(℃)	350		
下限パス(層)間温度(℃)	20		
基準入熱量(KJ/CM)	40		
アークタイム(秒)	308		
総パス数	3		

パス数	溶接時間	溶接電流	溶接電圧	溶接速度	パス間温度	入熱量	備考
	(秒)	(A)	(V)	(cm/min)	(℃)	(kJ/cm)	
1	73	300	38	28.76	24	23.78	
2	98	300	38	21.42	13	31.93	溶接後清掃
3	112	280	38	18.75	28.7	34.04	

コメント

溶 接 施 工 記 録

溶接方法	炭酸ガス半自動溶接	工事番号	29－05
電流・電圧	直 流	工事名称	名古屋大学試験体
溶接長(mm)	240	記 号	T－1
板厚	12	溶接技能者	市来原良行
溶接ワイヤ(銘柄)	YM－26(YGW－11)	溶接管理者	河合光国
ワイヤサイズ(φmm)	1.2	溶接施工日	平成29年6月21日
シールドガス	Co2	開 先	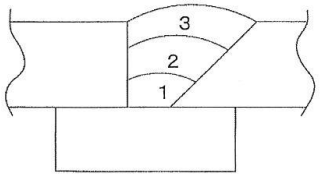
ガス流量(L/min)	25		
予熱温度(℃)	——		
上限パス(層)間温度(℃)	350		
下限パス(層)間温度(℃)	20		
基準入熱量(KJ/CM)	40		
アークタイム(秒)	212		
総パス数	3		

パス数	溶接時間	溶接電流	溶接電圧	溶接速度	パス間温度	入熱量	備 考
	(秒)	(A)	(V)	(cm/min)	(℃)	(kJ/cm)	
1	52	300	38	27.69	25.6	24.7	
2	74	300	38	19.45	190	35.16	溶接後清掃
3	86	280	38	16.74	274	38.13	

コメント

溶接施工記録

溶接方法	炭酸ガス半自動溶接	工事番号	29−05
電流・電圧	直流	工事名称	名古屋大学試験体
溶接長(mm)	240	記号	T−2
板厚	12	溶接技能者	市来原良行
溶接ワイヤ(銘柄)	YM−26(YGW−11)	溶接管理者	河合光国
ワイヤサイズ(φmm)	1.2	溶接施工日	平成29年6月21日
シールドガス	Co2	開先	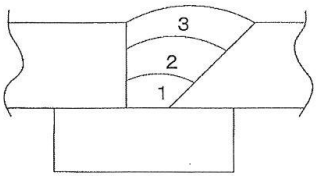
ガス流量(L/min)	25		
予熱温度(℃)	——		
上限パス(層)間温度(℃)	350		
下限パス(層)間温度(℃)	20		
基準入熱量(KJ/CM)	40		
アークタイム(秒)	214		
総パス数	3		

パス数	溶接時間	溶接電流	溶接電圧	溶接速度	パス間温度	入熱量	備考
	(秒)	(A)	(V)	(cm/min)	(℃)	(kJ/cm)	
1	52	300	38	27.69	26	24.7	
2	76	280	38	18.94	175	33.7	溶接後清掃
3	87	280	38	16.55	268	38.57	

コメント

INSPECTION CERTIFICATE
検 査 証 明 書

Customer
(需要家) 株式会社 瀧上工作所 殿

Certificate No.
(証明書番号) 1706954V
Date (発行日) 平成29年6月5日

Trade Designation (銘柄)	Size mm (寸法)	Manuf.No. (製造番号)	Heat No. (製鋼番号)	Weight kg (数量)	Remark (備考)
NSSW YM-26	1.2	7W55230098	SF68980	-	JIS Z 3312 YGW11

Chemical Composition of Wire (ワイヤの化学成分%)

C	Si	Mn	P	S	Cu	Ti+Zr						
0.06	0.77	1.60	0.014	0.011	0.30	0.24						

We hereby certify that above welding materials satisfy
the requirements of the applicable specification.

上記溶接材料は、適用規格の要求事項を満足していることを証明します。

Group manager, Quality Control Dept.
Nippon Steel & Sumikin Welding Co., Ltd.
Hikari Plant
日鐵住金溶接工業株式会社
光工場 品質管理グループ長
4-2-1, ASAE, HIKARI-SHI, YAMAGUCHI-KEN, JAPAN
山口県光市浅江4丁目2番1号 TEL 0833(71)3390 FAX 0833(71)3394

検査証明書
INSPECTION CERTIFICATE

JFE スチール 株式会社 東日本製鉄所(京浜地区)
JFE Steel Corporation East Japan Works(Keihin)

JFE

証明書番号 Certificate No.	:161121-ASH -8980
日付 Date	:2016-11-21
船番 Ship No.	:
工事番号 Construction No.	:
注文番号 Order No.	:6GR5062

需要家 Customer :MARUSADA SANGYO
需要家管理番号 Customer's Control No. :
注文者 Shipper :MM&KENZAI CORPORATION
注文者照合番号 Reference No. :8ZE -6B70040
品名 Commodity & 規格 Specification : HOT ROLLED STEEL PLATE JIS G3136 SN400B

製品番号 #1 Roll No. / 鋼番 Heat No.	行番 Item No.	需要家管理番号 Customer's Control No. / 寸法 Size T X W X L (MM)	員数 Quantity	質量 Mass (CAL)	化学成分 Chemical Composition (%) #3 C X100	Si	Mn X1000	P	S	NI MO V CR X100	X1000	X10	CEQ2 X100	引張試験 Tensile Test 降伏点/耐力 Y.P./Y.S. #4 N/MM2	引張強さ T.S.	伸び El % #5	降伏比 YR %	曲げ BT	UST
SPECIFIED VALUE (STANDARD) LADLE :				MIN.										235	400	18	-		
				MAX.										355	510	-	80		
				MIN.	-	-	60	-	-				-						
				MAX.	20	35	150	30	15				36						
定 KK72901 09798	001	12 X 2100 X 12500	1	2547	12	20	64	11	4	2	1	0	25	TC 284	421	32	67 A		
		TOTAL	1	2547	KG														
VISUAL & DIMENSIONS : GOOD																			

(注) (Notes) #1 原板製品番号の表示方法, Indication of Plate Roll Number
:上5桁:圧延番号, 2 letters&the 1st 3 figures:mother Plate Numbers
:下2桁:分割番号, the last 2 figures:divided Plate Numbers
#2 DG:脱ガス, Degassed
#4 位置, Position T:頭部, Top M:中部, Middle B:底部, Bottom
方向, Direction L:縦, Longitudinal C:横, Transverse Z:厚, Through-thickness
衝撃試験片寸法, Size of Impact Test Specimen 1:10X10mm 2:7.5X10mm 3:2/3X10mm 4:5X10mm 5:1/3X10mm 6:2.5X10mm 7:ThicknessX10mm
衝撃試験値特性単位, Unit of Impact Test Property
吸収エネルギー, Absorbed Energy:K:kgf.m C:kgf.m/cm² J:Joule, U:J/cm², F:ft.lbf, L:ft.lbf/cm²
破面率, Fracture; S:延性, Shear B:脆性, Brittle
横膨出量, Lateral Expansion; M:mm I:mil
#5 標点距離, Gauge Length A:200mm (■) D:50mm (■) E:50mm (●) H:8" (■) J:2" (●) K:5D (●) M:5.65√A (●) P:5.65√A (■) R:4D (●) S:80mm (■) U:100mm (■) Y:2" (■) T:70mm (●)
#6 BT :曲げ試験, Bend Test UST:超音波探傷, Ultrasonic Examination G :合格, Good

定 印のみ有効

#3 CEQ2=C+MN/6+SI/24+NI/40+CR/5+MO/4+V/14

丸定産業株式会社

発行責任者 谷川善計 印

上記商品は検査の結果指定の規格に合格していることを証明いたします。
WE HEREBY CERTIFY THAT THE MATERIAL DESCRIBED HEREIN HAS BEEN TESTED AND INSPECTED WITH SATISFACTORY RESULTS IN ACCORDANCE WITH THE REQUIREMENTS OF THE ABOVE SPECIFICATION.

(ABX045001IAA)
SC20 1 A39

P-14

東日本製鉄所(京浜地区):〒210-0868神奈川県川崎市川崎区扇島1番地1 East Japan Works(Keihin):1-1, OHGISHIMA, KAWASAKI 210-0868 JAPAN

T. Yamazaki

東日本製鉄所(京浜地区)品質保証室
Quality Assurance Section
East Japan Works(Keihin)

This Inspection Certificate is printed with special forgery proof technology.
---このミルシートは特殊偽造防止技術を使用しております---

証明書番号
Certificate No.: H17- 5041(01)

鋼材検査証明書
INSPECTION CERTIFICATE

日付
Date :23 MAY 2017

品名
Commodity :FLAT BAR

契約番号
Contract No.:307486

需要家
Customer :FURUSATO KOGYO K.K.

商社 105-6ZE
Supplier :MM&KENZAI CORPORATION

JIS表示認証番号
JIS CERTIFICATION NO. QA0507045

規格
Specification :JIS G 3136 SN490B

	Charge No.	Mfg. No.	Dimension	Length	Pieces	Mass (kg)	Control No.
1	U70655		9 X 25	6000	458	4,855	
2							
3							
4							
5							
6							
7							
8							
			-TOTAL-		458	4,855	

Application

※1 : Bend Test G : Good
※2 : Ultrasonic Test A : Acceptable

	Chemical Composition (%)													Ceq (%)	Pcm (%)	Tensile Test						Bend Test	Impact Test	Hard-ness	Ultrasonic Test	Remarks
	C	Si	Mn	P	S	Cu	Ni	Cr	Mo	V	Sn	B				G.L.	Y.P.	T.S.	Y.R.	EL.	R.A.					
	×100			×1000		×100					×1000			×100		mm	N/mm²		%	%	%		0℃			
Min																	325	490		17		※1	27		※2	
Max	18	55	165	30	15									44	29			610								
1	12	23	119	15	13	7	5	8	2	2	6	TR		35	20		365	509		28			---			
2																										
3																										
4																										
5																										
6																										
7																										
8																										

上記鋼材は、検査の結果、ご指定の規格または仕様に合格している事を証明致します。 We Hereby certify that the material described herein has been tested and inspected satisfactorily in accordance with the requirements of the above specification.

新関西製鐵株式会社
SHINKANSAI STEEL CORPORATION

星田工場
HOSHIDA WORKS
交野市星田北４丁目26番１号 〒576-0017
4-26-1 Hoshidakita, Katano, Osaka Japan
Tel.072-891-0624 Fax.072-893-1319

Masahiko Yamamoto
MASAHIKO YAMAMOTO
Manager of Quality Control Group

名古屋大学　試験体

溶 接 施 工 記 録

（12 体　分）

平成 29 年　10 月

㈱瀧 上 工 作 所

母材部、溶接部（WELD, HAZ）
各15本採取×3セット

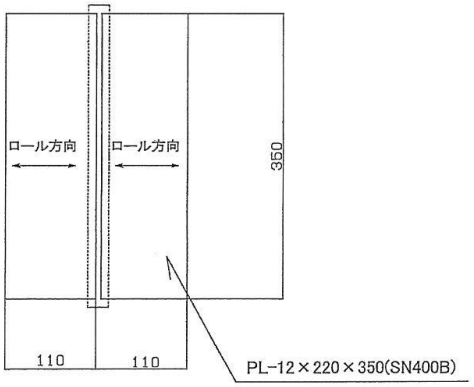

~~6体・・・・・今回試験~~
12体・・・・・次回試験
計 18体

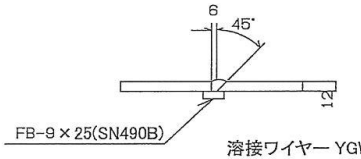

溶接ワイヤー YGW−11

素材引張試験材
（ 計 3 体 ）

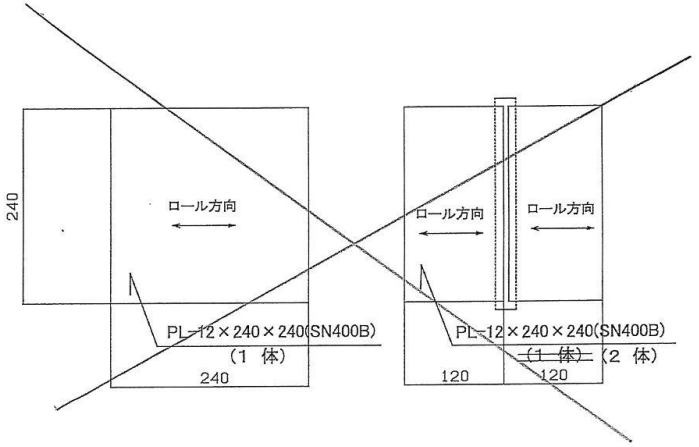

<注 記>
全ての鋼材は、同ロット材とする。

図面	改正年月日	改正箇所及び改正内容	ボルト記号			対象表示	
			記	HTB	中DLT	鋼 種 SS400 STK400	□
			H24(S10T)	◆	◆		□
			H22(S10T)	＋	◆		○
			H20(S10T)	＊	◆		○
			M16(S10T)	※	◆		

縮尺	作成	工事名	図番	工事番号	Rev.
	H29.6.1	名古屋大学試験体		29-05	△

承認	審査	作成	図名	株式会社遊上工作所
浅井	浅井	栗野	試 験 体 図	

目　　次

溶 接 施 工 記 録

溶接方法	炭酸ガス半自動溶接	工事番号	29−05
電流・電圧	直 流	工事名称	名古屋大学試験体
溶接長(mm)	350	記 号	S−7
板厚	12	溶接技能者	市来原良行
溶接ワイヤ(銘柄)	YM−26(YGW−11)	溶接管理者	河合光国
ワイヤサイズ(φmm)	1.2	溶接施工日	平成29年10月10日
シールドガス	Co2	開 先	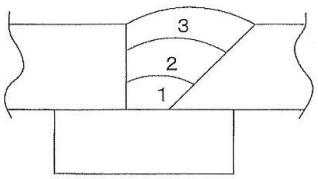
ガス流量(L/min)	25		
予熱温度(℃)	——		
上限パス(層)間温度(℃)	350		
下限パス(層)間温度(℃)	20		
基準入熱量(KJ/CM)	40		
アークタイム(秒)	308		
総パス数	3		

パス数	溶接時間	溶接電流	溶接電圧	溶接速度	パス間温度	入熱量	備 考
	(秒)	(A)	(V)	(cm/min)	(℃)	(kJ/cm)	
1	77	300	38	27.27	26.9	25.08	
2	111	300	38	18091	180	36.17	溶接後清掃
3	120	280	38	17.5	280	36.48	

コメント

溶接施工記録

溶接方法	炭酸ガス半自動溶接	工事番号	29－05
電流・電圧	直流	工事名称	名古屋大学試験体
溶接長(mm)	350	記号	S－8
板厚	12	溶接技能者	市来原良行
溶接ワイヤ(銘柄)	YM－26(YGW－11)	溶接管理者	河合光国
ワイヤサイズ(φmm)	1.2	溶接施工日	平成29年10月10日
シールドガス	Co2	開先	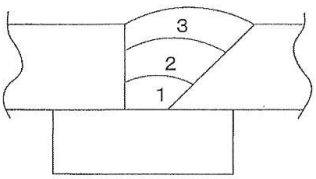
ガス流量(L/min)	25		
予熱温度(℃)	——		
上限パス(層)間温度(℃)	350		
下限パス(層)間温度(℃)	20		
基準入熱量(KJ/CM)	40		
アークタイム(秒)	303		
総パス数	3		

パス数	溶接時間	溶接電流	溶接電圧	溶接速度	パス間温度	入熱量	備考
	(秒)	(A)	(V)	(cm/min)	(℃)	(kJ/cm)	
1	79	300	38	26.58	28.5	25.73	
2	104	300	38	20.19	198	33.87	溶接後清掃
3	120	280	38	17.4	274	37.99	

コメント

溶接施工記録

溶接方法	炭酸ガス半自動溶接	工事番号	29−05
電流・電圧	直流	工事名称	名古屋大学試験体
溶接長(mm)	350	記号	S−9
板厚	12	溶接技能者	市来原良行
溶接ワイヤ(銘柄)	YM−26(YGW−11)	溶接管理者	河合光国
ワイヤサイズ(φmm)	1.2	溶接施工日	平成29年10月10日
シールドガス	Co2	開先	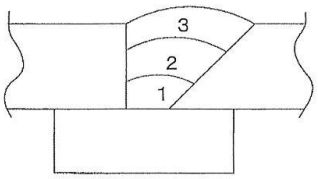
ガス流量(L/min)	25		
予熱温度(℃)	——		
上限パス(層)間温度(℃)	350		
下限パス(層)間温度(℃)	20		
基準入熱量(KJ/CM)	40		
アークタイム(秒)	298		
総パス数	3		

パス数	溶接時間	溶接電流	溶接電圧	溶接速度	パス間温度	入熱量	備考
	(秒)	(A)	(V)	(cm/min)	(℃)	(kJ/cm)	
1	75	300	38	27.99	27.8	24.43	
2	105	300	38	19.99	165	34.21	溶接後清掃
3	118	300	38	17.79	285	38.4	

コメント

溶接施工記録

溶接方法	炭酸ガス半自動溶接	工事番号	29−05
電流・電圧	直流	工事名称	名古屋大学試験体
溶接長(mm)	350	記号	S−10
板厚	12	溶接技能者	市来原良行
溶接ワイヤ(銘柄)	YM−26(YGW−11)	溶接管理者	河合光国
ワイヤサイズ(φmm)	1.2	溶接施工日	平成29年10月10日
シールドガス	Co2	開先	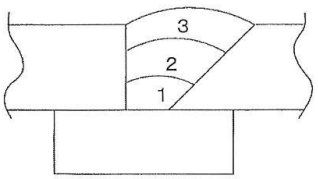
ガス流量(L/min)	25		
予熱温度(℃)	——		
上限パス(層)間温度(℃)	350		
下限パス(層)間温度(℃)	20		
基準入熱量(KJ/CM)	40		
アークタイム(秒)	304		
総パス数	3		

パス数	溶接時間	溶接電流	溶接電圧	溶接速度	パス間温度	入熱量	備考
	(秒)	(A)	(V)	(cm/min)	(℃)	(kJ/cm)	
1	76	300	38	27.63	25.8	24.75	
2	104	300	38	20.19	162	33.87	溶接後清掃
3	124	280	38	16.93	295	37.7	

コメント

溶接施工記録

溶接方法	炭酸ガス半自動溶接	工事番号	29−05
電流・電圧	直流	工事名称	名古屋大学試験体
溶接長(mm)	350	記号	S−11
板厚	12	溶接技能者	市来原良行
溶接ワイヤ(銘柄)	YM−26(YGW−11)	溶接管理者	河合光国
ワイヤサイズ(φmm)	1.2	溶接施工日	平成29年10月10日
シールドガス	Co2	開先	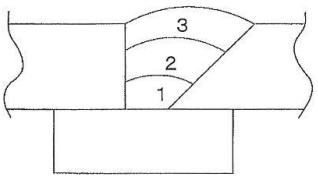
ガス流量(L/min)	25		
予熱温度(℃)	——		
上限パス(層)間温度(℃)	350		
下限パス(層)間温度(℃)	20		
基準入熱量(KJ/CM)	40		
アークタイム(秒)	287		
総パス数	3		

パス数	溶接時間	溶接電流	溶接電圧	溶接速度	パス間温度	入熱量	備考
	(秒)	(A)	(V)	(cm/min)	(℃)	(kJ/cm)	
1	74	300	38	28.37	26.1	24.1	
2	102	300	38	20.58	147	33.23	溶接後清掃
3	111	300	38	18.92	270	36.15	

コメント

溶 接 施 工 記 録

溶接方法	炭酸ガス半自動溶接	工事番号	29－05
電流・電圧	直 流	工事名称	名古屋大学試験体
溶接長(mm)	350	記 号	S－12
板厚	12	溶接技能者	市来原良行
溶接ワイヤ(銘柄)	YM－26(YGW－11)	溶接管理者	河合光国
ワイヤサイズ(φmm)	1.2	溶接施工日	平成29年10月10日
シールドガス	Co2	開 先	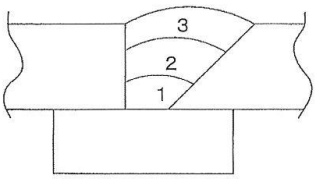
ガス流量(L/min)	25		
予熱温度(℃)	——		
上限パス(層)間温度(℃)	350		
下限パス(層)間温度(℃)	20		
基準入熱量(KJ/CM)	40		
アークタイム(秒)	297		
総パス数	3		

パス数	溶接時間	溶接電流	溶接電圧	溶接速度	パス間温度	入熱量	備 考
	(秒)	(A)	(V)	(cm/min)	(℃)	(kJ/cm)	
1	78	300	38	26.92	25.9	25.4	
2	109	300	38	19.26	174	35.51	溶接後清掃
3	110	300	38	19.09	282	35.83	

コメント

溶 接 施 工 記 録

溶接方法	炭酸ガス半自動溶接	工事番号	29−05
電流・電圧	直 流	工事名称	名古屋大学試験体
溶接長(mm)	350	記 号	S−13
板厚	12	溶接技能者	市来原良行
溶接ワイヤ(銘柄)	YM−26(YGW−11)	溶接管理者	河合光国
ワイヤサイズ(φmm)	1.2	溶接施工日	平成29年10月10日
シールドガス	Co2	開 先	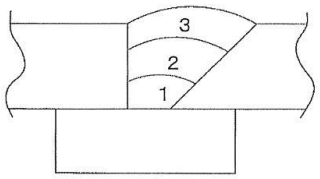
ガス流量(L/min)	25		
予熱温度(℃)	——		
上限パス(層)間温度(℃)	350		
下限パス(層)間温度(℃)	20		
基準入熱量(KJ/CM)	40		
アークタイム(秒)	288		
総パス数	3		

パス数	溶接時間	溶接電流	溶接電圧	溶接速度	パス間温度	入熱量	備 考
	(秒)	(A)	(V)	(cm/min)	(℃)	(kJ/cm)	
1	78	280	38	26.92	27	23.71	
2	103	300	38	20.8	173	33.56	溶接後清掃
3	107	300	38	19.62	289	34.86	

コメント

溶接施工記録

溶接方法	炭酸ガス半自動溶接	工事番号	29−05
電流・電圧	直流	工事名称	名古屋大学試験体
溶接長(mm)	350	記号	S−14
板厚	12	溶接技能者	市来原良行
溶接ワイヤ(銘柄)	YM−26(YGW−11)	溶接管理者	河合光国
ワイヤサイズ(φmm)	1.2	溶接施工日	平成29年10月10日
シールドガス	Co2	開先	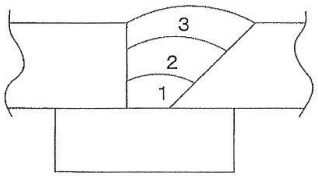
ガス流量(L/min)	25		
予熱温度(℃)	——		
上限パス(層)間温度(℃)	350		
下限パス(層)間温度(℃)	20		
基準入熱量(KJ/CM)	40		
アークタイム(秒)	296		
総パス数	3		

パス数	溶接時間	溶接電流	溶接電圧	溶接速度	パス間温度	入熱量	備考
	(秒)	(A)	(V)	(cm/min)	(℃)	(kJ/cm)	
1	77	300	38	27.27	26.4	25.08	
2	103	300	38	20.38	176	33.56	溶接後清掃
3	116	280	38	18.1	268	35.27	

コメント

溶接施工記録

溶接方法	炭酸ガス半自動溶接	工事番号	29−05
電流・電圧	直流	工事名称	名古屋大学試験体
溶接長(mm)	350	記号	S−15
板厚	12	溶接技能者	市来原良行
溶接ワイヤ(銘柄)	YM−26(YGW−11)	溶接管理者	河合光国
ワイヤサイズ(φmm)	1.2	溶接施工日	平成29年10月10日
シールドガス	Co2	開先	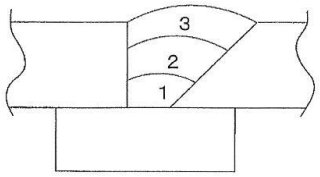
ガス流量(L/min)	25		
予熱温度(℃)	——		
上限パス(層)間温度(℃)	350		
下限パス(層)間温度(℃)	20		
基準入熱量(KJ/CM)	40		
アークタイム(秒)	304		
総パス数	3		

パス数	溶接時間	溶接電流	溶接電圧	溶接速度	パス間温度	入熱量	備考
	(秒)	(A)	(V)	(cm/min)	(℃)	(kJ/cm)	
1	73	300	38	28.76	26.4	23.78	
2	109	300	38	19.26	175	35.51	溶接後清掃
3	122	280	38	17.21	287	37.09	

コメント

溶接施工記録

溶接方法	炭酸ガス半自動溶接	工事番号	29−05
電流・電圧	直流	工事名称	名古屋大学試験体
溶接長(mm)	350	記号	S−16
板厚	12	溶接技能者	市来原良行
溶接ワイヤ(銘柄)	YM−26(YGW−11)	溶接管理者	河合光国
ワイヤサイズ(φmm)	1.2	溶接施工日	平成29年10月10日
シールドガス	Co2	開先	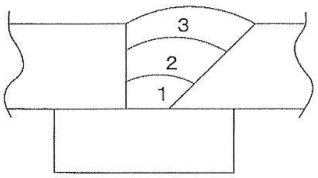
ガス流量(L/min)	25		
予熱温度(℃)	——		
上限パス(層)間温度(℃)	350		
下限パス(層)間温度(℃)	20		
基準入熱量(KJ/CM)	40		
アークタイム(秒)	304		
総パス数	3		

パス数	溶接時間	溶接電流	溶接電圧	溶接速度	パス間温度	入熱量	備考
	(秒)	(A)	(V)	(cm/min)	(℃)	(kJ/cm)	
1	73	300	38	28.76	28.2	23.78	
2	107	300	38	19.62	165	34.86	溶接後清掃
3	124	280	38	16.93	265	37.7	

コメント

溶 接 施 工 記 録

溶接方法	炭酸ガス半自動溶接	工事番号	29−05
電流・電圧	直 流	工事名称	名古屋大学試験体
溶接長(mm)	350	記 号	S−17
板厚	12	溶接技能者	市来原良行
溶接ワイヤ(銘柄)	YM−26(YGW−11)	溶接管理者	河合光国
ワイヤサイズ(φmm)	1.2	溶接施工日	平成29年10月10日
シールドガス	Co2	開 先	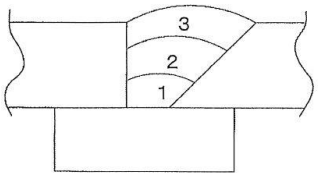
ガス流量(L/min)	25		
予熱温度(℃)	——		
上限パス(層)間温度(℃)	350		
下限パス(層)間温度(℃)	20		
基準入熱量(KJ/CM)	40		
アークタイム(秒)	292		
総パス数	3		

パス数	溶接時間	溶接電流	溶接電圧	溶接速度	パス間温度	入熱量	備 考
	(秒)	(A)	(V)	(cm/min)	(℃)	(kJ/cm)	
1	78	300	38	26.92	26.8	25.4	
2	101	300	38	20.79	189	32.9	溶接後清掃
3	113	280	38	18.58	280	34.35	

コメント

溶 接 施 工 記 録

溶接方法	炭酸ガス半自動溶接	工事番号	29－05
電流・電圧	直 流	工事名称	名古屋大学試験体
溶接長(mm)	350	記 号	S－18
板厚	12	溶接技能者	市来原良行
溶接ワイヤ(銘柄)	YM－26(YGW－11)	溶接管理者	河合光国
ワイヤサイズ(φmm)	1.2	溶接施工日	平成29年10月10日
シールドガス	Co2	開 先	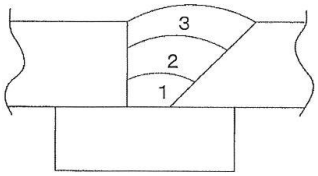
ガス流量(L/min)	25		
予熱温度(℃)	——		
上限パス(層)間温度(℃)	350		
下限パス(層)間温度(℃)	20		
基準入熱量(KJ/CM)	40		
アークタイム(秒)	305		
総パス数	3		

パス数	溶接時間	溶接電流	溶接電圧	溶接速度	パス間温度	入熱量	備 考
	(秒)	(A)	(V)	(cm/min)	(℃)	(kJ/cm)	
1	71	300	38	29.57	27.2	23.13	
2	112	300	38	18.75	176	36.48	溶接後清掃
3	122	280	38	17.21	260	37.09	

コメント

試験体

セット前単品部材

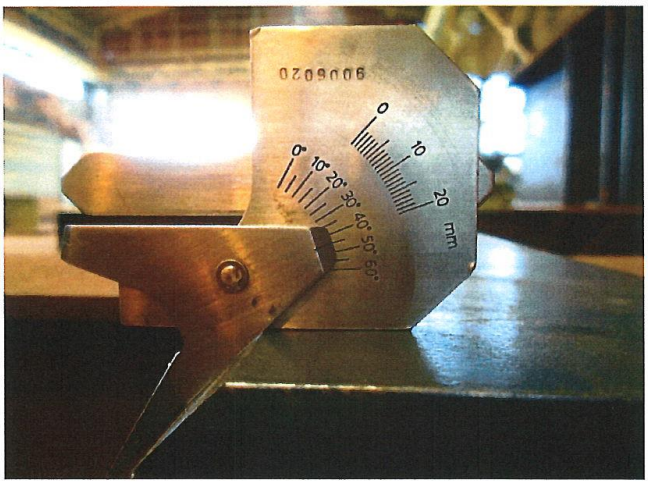

試験体

開先角度：４５°

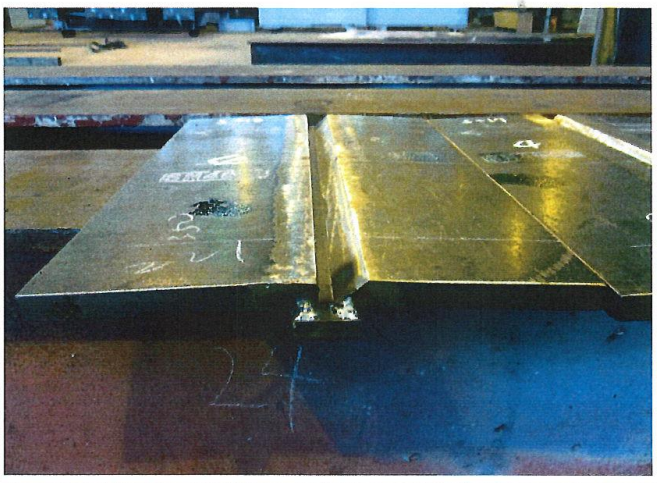

試験体

組立完了

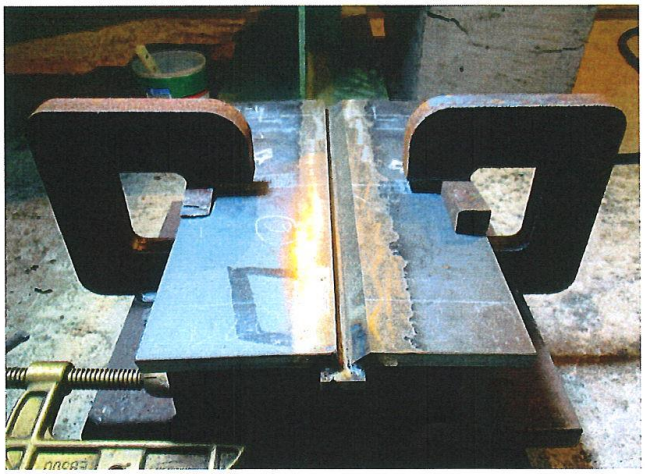

試験体

溶接前治具セット

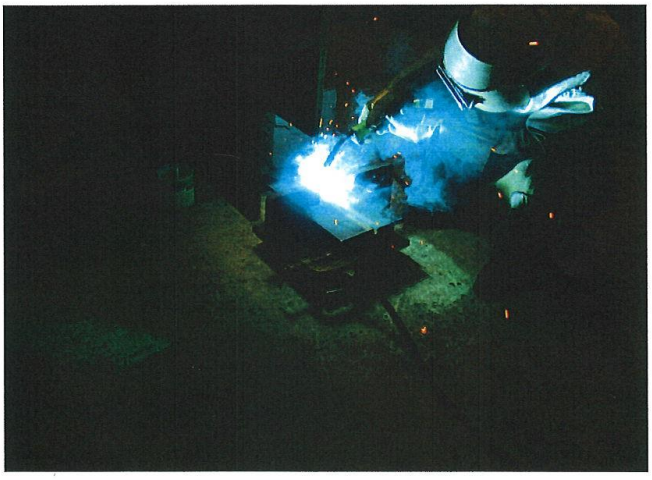

試験体

溶接作業状況
半自動溶接

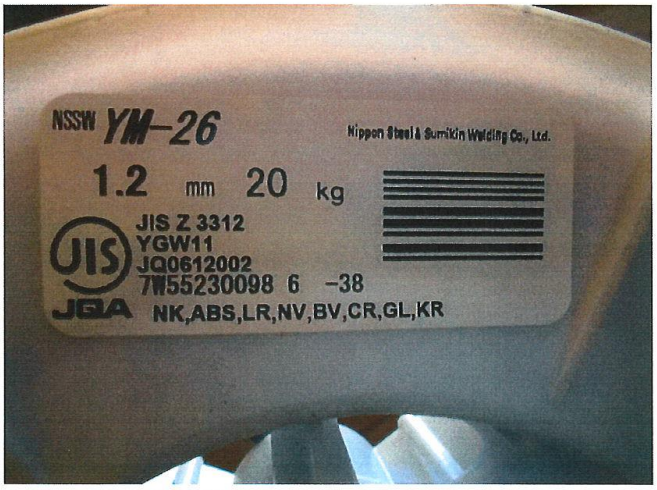

溶接ワイヤ

ＹＧＷ１１（ＹＭ－２６）
1.2φ

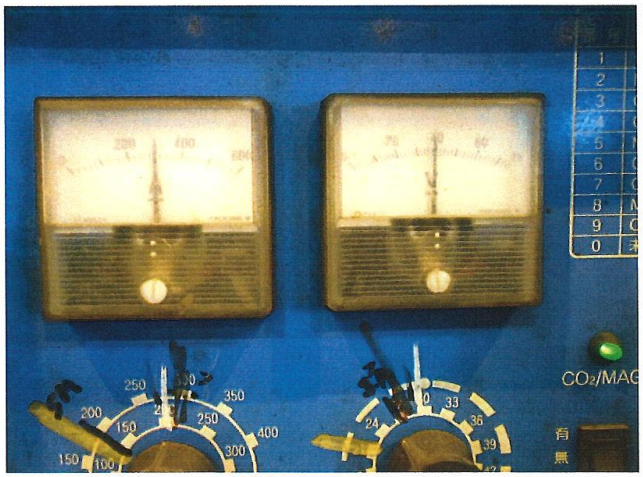

電流・電圧

電流：３００Ａ
電圧：４０Ｖ

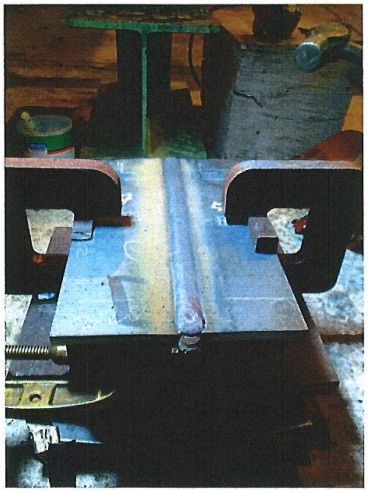

試験体

溶接完了

試験体

溶接検査

超音波探傷検査

試験体

衝撃試験用試験体完了

12×220×350(SN400B)
先行分１２体完了

Appendix C: Material records for BCR295 column steel

(1)証明書番号
3-01435　001

検査証明書

下記注文品は検査の結果御指定の規格に合格したことを証明します。

■日鐵住金建材株式会社

広畑製造所　管理グループ長
久保田 勝

(3)ミルシート宛先
中川鋼管　御中

(5)発行年月日
2018-03-18

(4)出荷年月日
2018-03-17

(6)注文番号
8-N1-A22-1-2-5803

(6)注文者
伊藤忠丸紅鉄鋼㈱　御中

(7)顧客コード
001

(8)照合番号

(9)品種
角形鋼管

(10)規格	(11)部材記号 断面・寸法 長さ(mm)	(12)員数	(13)質量(Kg)	(14)製鋼番号 製造番号	(15)引張試験 降伏点又は耐力(N/mm²)	引張強さ(N/mm²)	伸び(%)	降伏比(%)	(16)吸収エネルギー 0℃(J)	(17)曲げ試験	(18)偏平試験	(19)化学成分(%) C×100	Si×100	Mn×100	P×1000	S×1000	*5 Cu Mo	*5 Ni V	*7 Cr B	*1 *5 N	*2 *5 Ceq.	(20)*0*5*9 Pcm	(21)備考
BCR295	ロコラムBCR 16.0X250X250 12,000	2	2,664	NJ8418 712-063	372	446	40	83	304			7	1	55	11	6	14 0	11 0	6 1	23	18	11	

名古屋市港区当知1丁目701番地
中川鋼管㈱名古屋支店

(22)規格値

BCR295	板厚区分 管径区分	6 ≦ t < 12	最大値	−	550	−	−	−			20	35	140	30	15				60	36	26	
			最小値	295	400	*3	−	−			−	−	−	−	−				−	−	−	
BCR295	板厚区分 管径区分	t = 12	最大値	445	550	−	90	−			20	35	140	30	15				60	36	26	
			最小値	295	400	*3	−	−			−	−	−	−	−				−	−	−	
BCR295	板厚区分 管径区分	12 < t ≦ 16	最大値	445	550	−	90	−			20	35	140	30	15				60	36	26	
			最小値	295	400	*3	−	27			−	−	−	−	−				−	−	−	
BCR295	板厚区分 管径区分	16 < t ≦ 25	最大値	445	550	−	90	−			20	35	140	30	15				60	36	26	
			最小値	295	400	*3	−	27			−	−	−	−	−				−	−	−	

(23)備考
*0: Pcm =C+Si/30+Mn/20+Cu/20+Ni/60+Cr/20+Mo/15+V/10+5B
*1: Nはトータル N量　*5: x100　*6: x10000　*7: Cr=x100, B=xPPM
*2: Ceq. =C+Mn/6+Si/24+Ni/40+Cr/5+Mo/4+V/14　*9: 特別な要求がない場合はCeqで保証
*3: 伸びは板厚6mm: 19%以上、8mm, 9mm: 22%以上、12mm: 24%以上、14mm, 16mm: 27%以上、19mm: 29%以上、22mm: 31%以上、25mm: 33%以上

(2,664)
2,664 kg

P.1/1

Appendix D: Material records for JIS STKR400 column steel

(1)証明書番号
6-00426　001

検査証明書

下記注文品は検査の結果御指定の
規格に合格したことを証明します。

日鉄建材株式会社
広畑製造所　管理グループ長
遠藤 誠

(2)ミルシート提要家
中川鋼管　御中

(3)発行年月日
2021-06-04

(4)出荷年月日
2021-06-03

(5)注文番号
1-N1-A22-I-4-3011

(6)注文者
伊藤忠丸紅鉄鋼㈱　御中

(7)店部長コード
001

(8)照合番号

(9)品名
角形鋼管

(10) 規格	(11) 部材記号 断面・寸法	長さ (mm)	(12) 員数	(13) 質量 (Kg)	(14) 製鋼番号 製造番号	(15) 引張試験 降伏点又は耐力 (N/mm²)	引張強さ (N/mm²)	伸び (%)	(16)	(17) 曲げ試験	(18) 偏平試験	(19) 化学成分 (%) C × 100	Si × 100	Mn × 100	P × 1000	S × 1000	(20) めっき付着量 (g/m²)	(21) 備考
結束ラベル番号 105-003-A-01-001-0																		
JISG3466 STKR400	カクパイプ 1.6X50X50	6,000	80	1,144	ZC1794 105-003	358	456	34				15	2	43	14	6		
JISG3466 STKR400	(22) 規格値 板厚区分 管径区分	1.6 ≦ t ≦ 2.0			最大値 最小値	245	400	14				25			40	40		池田
	規格値 板厚区分 管径区分				最大値 最小値													
	規格値 板厚区分 管径区分				最大値 最小値													
	規格値 板厚区分 管径区分				最大値 最小値													

中川鋼管㈱名古屋支店

(23) 備考

(1,144)
1,144 kg

検　査　証　明　書
INSPECTION CERTIFICATE

契約番号 Contract No.:
注文者 Shipper:
需要家 Customer: 中川鋼管株式会社様
品名 Commodity: 一般構造用角形鋼管
規格 Specification: JIS G 3466 STKR400
本数 No. of Pieces: 160
重量 Mass: 4320KG

証明書番号 Certificate No.: F-21-05615
発行年月日 Date: 2021年 7月 2日
納品年月日 Invoice Date: 2021年 7月 2日
納品書番号 Invoice No.: 1F2100233

東洋電業株式会社
本社 千葉県船橋市栄町1丁目25番1号（〒273-0018）
TOYO DENGYO CO., LTD.
25-1 SAKAE-CHO-1 FUNABASHI-SHI
CHIBA-KEN. JAPAN (〒273-0018)

工番 Roll No	種別 Classify	製品寸法 Dimensions	コイル番号 Coil Number	化学成分 Chemical Composition % C ×100	Si ×100	Mn	P ×1000	S ×1000	Cu ×100	Ni ×100	Cr	Mo ×1000	V ×1000	Al	引張試験 Tensile Test 引張強さ T.S. N/mm²	降伏点 Y.P. MIN	伸び E.L. %MIN	試験片 Test Piece №
				MAX 25			MAX 40	40							400	245	17	5
1621838	B	50×50×3.2 × 6,000	C27780	16	Tr	43	17	3							431	339	39	5

中川鋼管(株)名古屋支店

へん平試験 Flattening Test	押し拡げ試験 Flaring Test	外観検査 Visual Inspection	寸法検査 Tolerance 外径 Outside Diameter		厚さ※1 Wall Thickness	長さ Length	記事 Note
			+1.50 -1.50	+1.50 -1.50	+0.32 -0.32	+ - 0	
		GOOD	GOOD		GOOD	GOOD	

※1 STKMについては母材部厚さ

上記製品は検査の結果、御指定の規格に合格している事を証明いたします。

WE HEREBY CERTIFY THAT THE MATERIAL DESCRIBED HEREIN HAS BEEN TESTED AND INSPECTED WITH SATISFACTORY RESULTS IN ACCORDANCE WITH THE REQUIREMENTS OF THE ABOVE SPECIFICATION.

品質管理部 次長 根本 克明
QUALITY CONTROL SEC

Publications

Journals

1. **Kai YE**, and Fuminobu OZAKI, Impact fracture energy of steel welded connections in fire and post-fire. J. Const.Ste.Res. 170(2020), pp.106-120.

2. **Kai YE**, Fuminobu OZAKI, and Markus KNOBLOCH, Impact fracture energy of cold-formed steel square hollow section in/after fire. J. Const.Ste.Res. 183(2021) 106740

3. **Kai YE**, and Fuminobu OZAKI, Post-fire mechanical properties and buckling strength of cold-formed steel square hollow section columns. J. Const.Ste.Res. 184(2021) 106806

4. Seok-Hyeon HAN, **Kai YE**, Fuminobu OZAKI, Kei KIMURA, SIMPLE TEMPERATURE EVALUATION METHODS FOR AN UNPROTECTED STEEL BEAM PLACED INSIDE DRY WALL ASSEMBLIES IN CASE OF FIRE. AIJ J. Technol. Des. Vol. 28, No.68, 239-244, Feb, 2022. (in Japanese)

5. Fuminobu OZAKI, Ying Liu, and **Kai YE**, Tensile and shear-strength for a self-drilling screw and transition of failure-modes and shear-strengths for self-drilling screwed connections at elevated temperature. J. Structural Fire Engineering, 15 Dec, 2021.

Proceedings of International Conference

1. **Kai YE**, and Fuminobu. OZAKI, Post-fire mechanical properties and buckling strength of cold-formed steel square hollow section columns. 12th Asia-Oceania Symposium on Fire Science and Technology, 7th Dec. 2021. (Accepted 07/12/2021)
2. **Kai YE**, and Fuminobu OZAKI：Estimation of Charpy Impact Values for Cold-formed Square Hollow Section Steel at High Temperature and after Heating and Cooling Processes, 12th Pacific Structural Steel Conference, pp.7-6-2, Nov.

2019.

3. **Kai YE**, and Fuminobu OZAKI：ESTIMATION OF CHARPY VALUES FOR STEEL WELDED CONNECTIONS AT HIG TEMPERATURE AND AFTER HEATING AND COOLING PROCESSES, Proceedings of 12th ISAIA, pp.1065-1070, Oct. 2018.

4. **Kai YE**, and Fuminobu OZAKI：ESTIMATION OF CHARPY IMPACT VALUES FOR STEEL WELDED CONNECTIONS AT HIGH TEMPERATURE AND AFTER HEATING AND COOLING PROCESSES，Conference proceedings of 10th International Conference on Structures in Fire, steel structures, pp.671-678, June. 2018.

Proceedings of National Conference

1. **Kai YE**, Yukina IWAI, and Fuminobu OZAKI: Experimental evaluation of redundancy of steel frames at fires Part 2 Validity examination of numerical analyses, Architectural Institute of Japan, Summaries of technical papers of annual meeting, Architectural Institute of Japan, fire protection, pp.197-198, SEP, 2021

2. Yahui DONG, Yukina IWAI, and Fuminobu OZAKI, **Kai YE**: Experimental evaluation of redundancy of steel frames at fires Part 2 Validity examination of numerical analyses, Proceedings of JAFSE Annual Symposium 2021, Japan Association for Fire science and Engineering, steel structure I, pp.78-79, MAY, 2021

3. **Kai YE**, and Fuminobu OZAKI：Experimental investigations of buckling behaviours of cold-formed steel square hollow section columns after fires, Architectural Institute of Japan, Summaries of technical papers of annual meeting, Architectural Institute of Japan, fire protection, pp.105-106, SEP, 2020

4. Seok-Hyeon HAN, **Kai YE**, Fuminobu OZAKI, Kei KIMURA：Studies on estimation of temperature of an unprotected steel beam in dry fire compartment wall - Part II Developments of a simple calculation method on the steel temperatures, Architectural Institute of Japan, Summaries of technical papers of annual meeting, Architectural Institute of Japan, fire protection, pp.115-116, SEP, 2020

5. Seok-Hyeon HAN, **Kai YE**, Fuminobu OZAKI, Kei KIMURA：Studies on estimation of temperature of an unprotected steel beam in dry fire compartment wall - Part II Developments of a simple calculation method on the steel temperatures, Proceedings of JAFSE Annual Symposium 2020, Japan Association for Fire science and Engineering, structure/fire safety IV, pp.111-112, MAY, 2020

6. **Kai YE**, Seok-Hyeon HAN, Fuminobu OZAKI, Kei KIMURA：Studies on estimation of temperature of an unprotected steel beam in dry fire compartment wall - Part 1, those experiments, Proceedings of JAFSE Annual Symposium 2020, Japan Association for Fire science and Engineering, structure/fire safety IV, pp.109-110, MAY, 2020

7. **Kai YE**, and Fuminobu OZAKI：ESTIMATION OF CHARPY IMPACT VALUES FOR STEEL WELDED CONNECTIONS AT HIGH TEMPERATURE AND AFTER HEATING AND COOLING PROCESSES, Summaries of technical papers of annual meeting, Architectural Institute of Japan, fire protection, pp.75-76, SEP, 2019

8. **Kai YE**, and Fuminobu OZAKI：ESTIMATION OF CHARPY IMPACT VALUES FOR BCR295 STEEL AT HIGH TEMPERATURE AND AFTER HEATING AND COOLING PROCESSES, Proceedings of JAFSE Annual Symposium 2019, Japan Association for Fire science and Engineering, structure fire safety III, pp.120-121, MAY, 2019

9. **Kai YE**, and Fuminobu OZAKI：ESTIMATION OF CHARPY IMPACT VALUES FOR STEEL WELDED CONNECTIONS AT HIGH TEMPERATURE, AIJ Tokai Chapter Architectural Research Meeting, Vol. 57, structure, pp,217-220, Feb. 2019

10. **Kai YE**, and Fuminobu OZAKI：ESTIMATION OF CHARPY IMPACT VALUES FOR STEEL WELDED CONNECTIONS AT HIGH TEMPERATURE AND AFTER HEATING AND COOLING PROCESSES, Summaries of technical papers of annual meeting, Architectural Institute of Japan, fire protection, pp.289-290, SEP, 2018

11. **Kai YE**, and Fuminobu OZAKI：ESTIMATION OF CHARPY IMPACT VALUES FOR STEEL WELDED CONNECTIONS AT HIGH TEMPERATURE AND AFTER HEATING AND COOLING, Proceedings of JAFSE Annual Symposium 2018, Japan Association for Fire science and Engineering, structure fire safety I, pp.108-109, MAY, 2018

12. **Kai YE**, and Fuminobu OZAKI：ESTIMATION OF CHARPY IMPACT VALUES FOR STEEL WELDED CONNECTIONS AT HIGH TEMPERATURE，AIJ Tokai Chapter Architectural Research Meeting, Vol. 56, structure, pp.145-148, Feb. 2018

13. **Kai YE**, Fuminobu OZAKI, and Kei KIMURA：Temperature Evaluation of Steel Beams without Fire Proofing Materials inside Partition Walls under a Standard Fire Heating Curve, Architectural Institute of Japan, Summaries of technical papers of annual meeting, Architectural Institute of Japan, fire protection, pp.143-144, SEP, 2017

Acknowledgements

This PhD thesis, as you can see, is my most important research result and my most precious work. It has been a tough mission and cost so many people' expectation, energy, endeavor as well as time. Therefore, here I would like to extend my sincere gratitude to all those who have helped me complete this thesis.

My instructor, Associate professor Fuminobu OZAKI, led me into this field of research when I was most confused. He taught me how to make a complete plan, how to complete effective research, how to organize the research results into a meaningful thesis, how to present the results in front of others, and how to make them easily understand my research report. He even taught me how to apply knowledge outside my major to my own research, how to guide my juniors in research, how to communicate frankly with people around me in a foreign country, and how to conduct collaborative research with foreign companies. His guidance is very important to the completion of this thesis. Without him, you may not be able to see the thesis I am showing you here.

The professor in our lab, Professor Yasuhiro MORI, is a gentle professor. He always kindly guides me and offers suggestions for the problems encountered in my research and the knowledge points that I do not understand in the study. In completing such a paper in a foreign country, he has also provided a great help.

Associate review professors, Professor Yoshikazu ARAKI, should also be thanked for taking the time out of their busy schedule to review this paper and give me a lot of precious opinions. It is due to their help that I can improve on the deficiencies in the paper and finally finish it in the end.

My parents not only gave birth to me, but also gave me their best resources, allowing me to receive a high-quality education. At the same time, they have also established an important outlook on life for me. They have been gentle and strict to me since I was young, so that I don't make unnecessary mistakes in my life. My father, Jing-yu YE, regards me as his pride and has spent most of his life working to ensure my comfortable life. He not only gives me financial support, but also gives me spiritual support. He tolerates my willfulness and supports my ideals. Even when I failed to study abroad for the first time, he still supported my second study abroad in Japan; although his body is getting frail, he still serves as my strongest backing and supports me to finish my studies. My mother, Pin XIE, although retired at home very early, has been silently supporting me. She said: "As a parent, if your children have dreams to pursue, you can't hold them back anyway." Only because of parents like them, I can show you the results of my research here.

My girlfriend, Wen-ting YU, spent five years of her youth supporting me silently and comforted me when I failed, rekindled my fighting spirit when I was depressed, and relieved me when I was uncomfortable. It is with her help that I can maintain a stable mental state and finish this doctoral dissertation.

AEON 1% Club Foundation fully supported my life during my master's study, reduced the burden on my parents, and allowed me to complete my research in a more immersive manner without having to do a part-time job.

NIPPON STEEL CORPORATION did not show any distrust to me because I am a foreigner, and let me

participate in their R&D projects completely, so that I could accumulate valuable project experience.

The Japan Iron and Steel Federation provided a lot of financial support for my research so that I could perfectly achieve my research goals, and provided a lot of data support for this paper.

This work was supported by JST SPRING，Grant number JPMJSPRD191027.

There are also many schoolmates in the lab and experts in the seminar that have made indelible contributions to this paper. Therefore, I would like to express my sincere thanks to all the above-mentioned people and groups.

Kai YE

January 2021